# Numerical Simulation of Steady/Unsteady MHD Flow over a Non-linear Stretching/Shrinking Sheet with Variable Liquid Characteristics

## Muhammad Irfan

Regn # NUST201590318PSNS7115F

A thesis submitted to the National University of Science and Technology, Islamabad

in partial fulfillment of the requirements for the degree of

## Doctor of Philosophy in

## Mathematics

Thesis Supervisor : Dr. Muhammad Asif Farooq

Department of Mathematics

School of Natural Sciences

National University of Sciences and Technology (NUST)

H-12, Islamabad, Pakistan

# THESIS ACCEPTANCE CERTIFICATE

Certified that final copy of PhD thesis written by **Muhammad Irfan**, (Registration No. **NUST201590318PSNS7115F)**, of **School of Natural Sciences** has been vetted by undersigned, found complete in all respects as per NUST statutes/regulations/PhD policy, is free of plagiarism, errors, and mistakes and is accepted as partial fulfillment for award of PhD degree. It is further certified that necessary amendments as pointed out by GEC members and foreign/local evaluators of the scholar have also been incorporated in the said thesis.

Signature: _____

Name of Supervisor: Dr. Muhammad Asif Farooq

Date: ___09/09/2021___

Signature (HoD): _____

Date: ___14/09/2021___

Signature (Dean/Principal): _____

Date: ___15. 09. 2021___

# National University of Sciences & Technology
## REPORT OF DOCTORAL THESIS DEFENCE

Name:  Muhammad Irfan                    NUST Regn No: NUST201590318PSNS7115F

School/College/Centre:     NUST – SCHOOL OF NATURAL SCIENCES (SNS)

## DOCTORAL DEFENCE COMMITTEE

Doctoral Defence held on **09 Sep, 2021 (Thursday) at 1000 hrs**

| | QUALIFIED | NOT QUALIFIED | SIGNATURE |
|---|---|---|---|
| GEC Member-1: Dr. Mujeeb ur Rehman | ✓ | | |
| GEC Member-2: Dr. Umer Saeed | ✓ | | |
| GEC Member-3: | | | |
| GEC Member (External): Dr. Adnan Maqsood | ✓ | | |
| Supervisor: Dr. Muhammad Asif Farooq | ✓ | | |
| Co-Supervisor (if appointed): | | | |
| External Evaluator-1: Dr. Sohail Nadeem (Local Expert) | ✓ | | |
| External Evaluator-2: Dr. Tariq Javed (Local Expert) | ✓ | | |
| External Evaluator-3: Dr. Anuar Mohd Ishak (Foreign Expert) | | | |
| External Evaluator-4: Dr. Lihao Zhao (Foreign Expert) | | | |

## FINAL RESULT OF THE DOCTORAL DEFENCE
### (Appropriate box to be signed by HOD)

| | PASS | | FAIL |
|---|---|---|---|
| | | | |

The student Muhammad Irfan Regn No NUST201590318PSNS7115F is / is NOT accepted for Doctor of Philosophy Degree.

Dated: 15.09.2021

Dean/Commandant/Principal/DG

Distribution:
1 x copy each for Registrar, Exam Branch, Dir R&D, Dir Acad Jat HQ NUST, HoD, Supervisor, Co-Supervisor (if appointed), one for student's dossier at the School/College/Centre and copy each for members of GEC.

Note:
* Decision of External Evaluators (Foreign Experts) will be sought through video conference, if possible, on the same date and their decision will be intimated (on paper) to HQ NUST at a later date.

# CERTIFICATE OF APPROVAL

This is to certify that the research work presented in this thesis entitled **"Numerical Simulation of Steady/Unsteady MHD Flow over a Non-linear Stretching/Shrinking Sheet with Variable Liquid Characteristics"** was conducted by **Muhammad Irfan** under the supervision of **Dr. Muhammad Asif Farooq**.
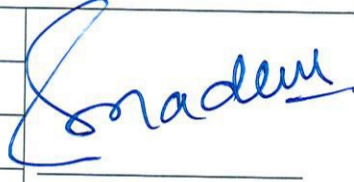
No part of this thesis has been submitted anywhere else for any degree. This thesis is submitted to the **School of Natural Sciences** in partial fulfillment of the requirements for the degree of Doctor of Philosophy in Field of **Mathematics** Department of **Mathematics, School of Natural Sciences (SNS)** University of **National University of Sciences and Technology, Islamabad, Pakistan.**

Student Name: **Muhammad Irfan**          Signature:

**Examination Committee:**

| a) | **External Examiner:** | | |
|---|---|---|---|
| | Name | Dr. Sohail Nadeem | |
| | Designation | Professor | |
| | Official Address | Department of Mathematics, Quaid-i-Azam University, Islamabad | Signature |

| b) | **External Examiner:** | | |
|---|---|---|---|
| | Name | Dr. Tariq Javed | |
| | Designation | Professor | |
| | Official Address | Department of Mathematics and Statistics, International Islamic University, Islamabad | Signature |

| c) | **Internal Examiner:** | | |
|---|---|---|---|
| | Name | Dr. Mujeeb ur Rehman | |
| | Designation | Associate Professor | |
| | Official Address | NUST-SNS | Signature |

Supervisor Name: **Dr. Muhammad Asif Farooq**          Signature:

Name of HOD : **Dr. Meraj Mustafa Hashmi**          Signature:

# AUTHOR'S DECLARATION

I, **Muhammad Irfan** hereby state that my PhD thesis titled **Numerical Simulation of Steady/Unsteady MHD Flow over a Non-linear Stretching/Shrinking Sheet with Variable Liquid Characteristics** is my own work and has not been submitted previously by me for taking any degree from this University

## "National University of Sciences and Technology"

Or anywhere else in the country / world.

At any time if my statement is found to be incorrect even after my Graduation the university has the right to withdraw my PhD degree.

Name of Student: ___Muhammad Irfan___

Signature: _(M).Irfan_

Date: ___9/09/2024___

# PLAGIARISM UNDERTAKING

I solemnly declare that research work presented in the thesis titled **"Numerical Simulation of Steady/Unsteady MHD Flow over a Non-linear Stretching/Shrinking Sheet with Variable Liquid Characteristics"** is solely my research work with no significant contribution from any other person. Small contribution/help wherever taken has been duly acknowledged and that complete thesis has been written by me.

I understand the zero tolerance policy of the HEC and University

**"National University of Sciences and Technology"**

towards plagiarism. Therefore I as an Author of the above titled thesis declare that no portion of my thesis has been plagiarized and any material used as reference is properly referred/cited.

I undertake that if I am found guilty of any formal plagiarism in the above titled thesis even after award of PhD degree, the University reserves the rights to withdraw/revoke my PhD degree and that HEC and the University has the right to publish my name on the HEC/University Website on which names of students are placed who submitted plagiarized thesis.

Student / Author Signature: _(M). Irfan_

Name: _____ **Muhammad Irfan** _____

<div align="center">

Dedicated

to

My Beloved Parents

Brothers and Sisters

My Wife, Especially My Sons

Muhammad Raahim and Muhammad Sudais

thanks to all for being there every single hour when I needed them.

</div>

# Acknowledgments

> Read: In the name of your Lord who created. Who created man from a clinging entity. Read! Your Lord is the most Noble, Who taught by the pen. Who taught man what he did not know. (Qur'an 96:1-5)

I thank Almighty Allah, the most Gracious and Merciful, for all the blessings in my life and without the help of Whom nothing could be achieved.

I consider myself lucky for getting a chance to collaborate and work with many great people all of whose contributions in assorted ways to my thesis and my experience in general made my time special. It is pleasure to convey my gratitude to all of them in my humble acknowledgments. First, I want to pay sincere thanks to my supervisor Dr. Muhammad Asif Farooq. I am much indebted to him for all the valuable discussions and precious time that he spent on me. I cannot thank him enough for his constant support throughout the tenure of this study. He also taught me many things other than science and mathematics that are necessary in life. I would also like to thank the GEC members Dr. Mujeeb ur Rehman (SNS), Dr. Umer Saeed (NICE) and Dr. Adnan Maqsood (RCMS) for guiding me from time to time in completion of this project. I am also thankful to SNS staff which was very helpful and supportive.

Last but not least, I would cordially like to express my extreme gratitude and thanks to all my family members especially my parents. My parents always encouraged me to achieve this milestone, Without their unbelievable support, prayers and care it would have been impossible for me to finish this work. Also special and profound thanks to my brothers and sisters who offered spiritual support to me. Without their prayers, I could not be able to complete this distinction.

# Contents

# Abstract

This dissertation is divided into two parts. The first part describes the work on magnetohydrodynamics boundary layer flow past a non-linear stretching surface in the presence of variable fluid characteristics. The second part is associated with the study of unsteady magnetohydrodynamics (MHD) stagnation point flow of bio-nanofluid near a shrinking/stretching surface. We use the relevant similarity transformation to convert the partial differential equations (PDEs) of the concerned problem into ordinary differential equation (ODEs). The shooting method has been used to obtain the numerical results of reduced coupled ODEs of the concerned problem. The acquired results from shooting method are compared with the *bvp4c* MATLAB solver. We also present a new numerical technique, namely, simplified finite difference method (SFDM) in our study and present some useful results by using it. Graphs are plotted to perceive the influence of several pertinent parameters on the fluid flow field while considering constant and variable fluid properties together. The current analysis of the first part describes the boundary layer flow with variable liquid properties past a non-linear stretching surface. Most of the studies were given on constant fluid properties. Whereas very few discuss the variable fluid properties in their study. To bridge this gap between constant and variable liquid properties. The comparison of constant and variable fluid characteristics is made in our study. The obtained results of constant and variable fluid properties are compared through graphs and tables. It is determined that the obtained results are different for variable and constant fluid characteristics. The heat and mass transfer rates in constant fluid properties are higher than the variable fluid properties. The wall resistance coefficient rises for changeable liquid characteristics when compare to constant liquid characteristics. It is also noted that width of boundary layer in Case B (variable fluid properties) is different compared to Case A (constant fluid properties). In the second part of the thesis, we investigate the

unsteady MHD stagnation point bio-nanofluid flow past a shrinking/stretching surface. The flow modeled PDEs are first reduced to non-linear coupled ODEs by appropriate transformation. The numerical outcomes of the reduced coupled ODEs are obtained through shooting and *bvp4c* method. We noticed an excellent resemblance between the present numerical results and the published results in the literature. It is found that boundary layer thickness is different in stretching sheet case when compared to shrinking sheet case also density of motile microorganism declines for raising values of $Nb$, $Lb$ and $Pe$.

# Preface

Studying basic physics of fluid flow due to a stretching surface is very significant as it has several practical and industrial applications. A production of sheeting materials takes place in a number of industrial manufacturing procedures and involves sheets of metal and polymer, such as cooling an infinite metal plate in a cooling bath, the boundary layer along material handling conveyors, aerodynamic extrusion of plastic sheets, the boundary layer along a liquid film in a condensation process, glass blowing, paper production, drawing plastic films and metal spinning.

Constant fluid properties of Newtonian and non-Newtonian fluids have been found in most of the published literature. Variable fluid properties analysis is uncommon with exponential and variable thickness stretching sheets. We analyzed the constant and variable fluid properties, to find difference between these two studies.Furthermore, we introduce a new numerical procedure name simplified finite difference method (SFDM) to find solution of the ODEs.

The arrangement of the dissertation is as follows:
Chapter 1 is an introduction to the dissertation. It describes the problem statement, research objectives, basic definitions, conservation laws and literature review. Details regarding the shooting method, *bvp4c* and SFDM is also appended to this chapter.

In Chapter 2, magnetohydrodynamic free stream and heat transfer of nanofluid flow over an exponentially radiating stretching sheet with variable fluid properties is investigated. First we transform the PDEs into set of coupled ODEs by using appropriate transformation and then obtained the numerical results of reduced ODEs by using shooting method and MATLAB

built in solver *bvp4c*. The outcomes of physical parameters namely, magnetic parameter $M$, viscosity parameter $\theta_r$, Brownian motion parameter $Nb$, small thermal conductivity parameter $\epsilon$, thermophoresis parameter $Nt$, Prandtl number $Pr_o$, Lewis number $Le$ and radiation parameter $Rd$ are conveyed through graphs. A complete analysis of the acquired results is also incorporated. The content of this chapter is published in **Frontier in Physics available from 15 November 2019.**

Thermophoretic MHD free stream flow with variable internal heat generation/absorption and variable liquid characteristics in a permeable medium past a radiative exponentially stretching surface is presented in chapter 3. The governing equations and boundary conditions of the problem are modified into dimensionless form by utilizing the suitable similarity transformation and then solved the resulting dimensionless ODEs by using shooting and bvp4c method. The acquired numerical results are displayed in the form of tables and figures against pertinent physical parameters. The comparison of the study with published data is also included in the chapter. The interpretation of the chapter is also presented at the end. The investigation of this work is published in **Journal of Materials Research and Technology available from (2020), 9(3), pp. 4855-4866**.

Chapter 4 is concerned with the study of a new computational technique design for EMHD nanofluid flow over a variable thicked surface with variable liquid characteristics. The governing PDEs reduced to non-linear ODEs by incorporating suitable transformation. The modeled ODEs are solved by employing SFDM and *bvp4c*. The influences of relevant physical parameters namely, electric field parameter, porosity parameter, viscosity parameter, wall thickness parameter, radiation parameter, Prandtl number, Biot number, Eckert number, Brownian motion parameter, thermophoresis parameter and Lewis number are analyzed through plots. The comparison of the study with published results is also made and is presented in the chapter. Finally, the conclusion of the Chapter is presented. The outcomes of the current chapter is published in **Frontier in Physics available from 8th April 2020.**

Chapter 5 predicts the effects of SFDM for EMHD Powell-Eyring nanofluid flow featuring

variable thickness surface and variable fluid Characteristics. The governing PDEs reduced to ODEs by suitable similarity transformation. SFDM and *bvp4c* method are employed to solve the developed non-linear ODEs. The numerical results of the chapter in the form of graphs and tables are presented. To see the accuracy of the developed numerical scheme SFDM, comparison has been made with published results. Present results developed with SFDM shows good resemblance with the already published results. The conclusion is also discussed at the end of the chapter. The observation of this chapter is published in **Mathematical Problem in Engineering**.

Chapter 6 reports the modeling and analysis of unsteady MHD stagnation point flow of bio-nanofluid along with internal heat generation/absorption and thermal radiation near a stretching/shrinking sheet. The modeled PDEs converted to dimensionless system of non-linear ODEs by applying appropriate transformation. The transformed coupled ODEs then solved by shooting and *bvp4c* method to obtain the numerical results. The numerical results are discussed through graphs and tables. To check the validity of the present results, comparison with the published literature has been made. The outcomes are discussed at the end of this chapter. This work is published in **Mathematical Problem in Engineering**.

A theoretical model for bio-nanofluid with variable fluid characteristics over a slippery sheet is analyzed in Chapter 7. The PDEs involve temperature dependent quantities have been transformed into ODES by applying relevant transformation. The shooting method and *bvp4c* have been used to find the numerical solution of modeled problem. To figure out the impact, graphs are plotted against pertinent parameters. The obtained data of the skin friction coefficient, the local Nusselt number, the local Sherwood number and the local density of motile organisms is tabulated against various parameters. The data obtained for physical parameters have a close agreement with the already published literature. The conclusion is presented at the end of the chapter. This work is published in **Mathematical Problem in Engineering**.

Chapter 8 contains the conclusions and outlook of the thesis.

# List of publications from the thesis

**Article 1:**

"Magnetohydrodynamic free stream and heat transfer of nanofluid flow Over an exponentially radiating stretching sheet with variable fluid properties, Frontier in Physics, 7(2019),186."

**Article 2:**

"Thermophoretic MHD free stream flow with variable internal heat generation/absorption and variable liquid characteristics in a permeable medium over a radiative exponentially stretching sheet, Journal of Materials Research and Technology (2020), 9(3), pp. 4855-4866."

**Article 3:**

"A new computational technique design for EMHD nanofluid flow over a variable thicked surface with variable liquid characteristics, Frontier in Physics, 8(2020),66."

**Article 4:**

"A simplified finite difference method (SFDM) for EMHD Powell-Eyring nanofluid flow featuring variable thickness surface and variable fluid characteristics, Mathematical Problems in Engineering (2020), volume (2020)."

**Article 5:**

"Unsteady MHD Bionanofluid Flow in a Porous Medium with Thermal Radiation near a Stretching/Shrinking Sheet, Mathematical Problems in Engineering (2020), volume (2020)."

**Article 6:**

"Magnetohydrodynamic time-dependent bio-nanofluid flow in a porous medium with variable thermo-physical properties, Mathematical Problems in Engineering (2021), volume (2021)."

# Chapter 1

# Introduction

The fundamental definitions of fluid dynamics is presented in this chapter. A detailed literature survey on the topic under investigation is also provided in this chapter.

## 1.1 Literature Review

A study of fluid past a stretching sheet is essential as it has many practical and industrial applications. In a number of industrial and manufacturing processes, material production occurs and involves sheets of metal, and polymer. For instance, cooling an infinite metal plate in a cooling bath, the boundary layer along material handling conveyors, plastic sheet aerodynamic extrusion, the boundary layer along a liquid film in condensation procedures, paper manufacturing, glass blowing, steel spinning and plastic film drawing. The flow over a flat stretching surface was first investigated by Crane [1]. Magyari and Keller [2] discussed the boundary layer flow of heat and mass transfer due to an exponentially stretching continuous surface. A new dimension is added to this investigation by Elbashbeshy [3] who discussed the flow and heat transfer characteristics due to an exponentially stretching permeable sheet. MHD stagnation point flow and heat transfer over an exponentially stretching sheet was discussed by Rajendar et al. [4]. Many researchers have extended the work for different flow model. But most of those studies have been focusing on constant fluid properties. The analysis of free stream boundary layer flow over a flat plate while variable fluid properties taking into consideration was investigated by Bachok et al. [5]. The magnetic field influence on a third grade fluid with

chemically reactive species has been put forward in Hayat et al. [6]. Pramanik [7] studied the impact of thermal radiation on Casson fluid flow and heat transfer past an exponentially porous stretching surface. Umar et al. [8] discussed the effect of thermo-diffusion on MHD nanofluid flow over a stretching surface. Suzilliana et al. [9] made the analysis on the impact of magnetohydrodynamics fluid flow with slip condition over a radiating exponentially surface. Mabood et al. [10] discussed the non-Darcian MHD convective flow and claimed that temperature rise depends on Eckert number. From the context of a stretching sheet for variable thickness, Fang et al. [11] has tackled the boundary layer flow and analyzed multiple solutions. Reddy et al. [12] investigated the MHD flow and heat transfer of Williamson nanofluid over variable thickness sheet with variable thermal conductivity and identified that the velocity profile decreases with wall thickness parameter when $m < 1$.

Magnetohydrodynamics (MHD) is the study of the flow of electrically conducting fluids in an electro-magnetic-fields. MHD flow research is of significant concern in contemporary processes of metallurgy and metalworking. The study of MHD flow is of considerable interest in modern metallurgical and metal-working process. Mukhopadhyay [13] discussed the slip effects on MHD flow over a radiating exponentially stretching sheet with suction/blowing. Mabood et al. [14] investigated heat transfer of nanofluid flow towards a nonlinear stretching surface. Reddy et al. [15] studied the MHD boundary layer flow of nanofluid and heat transfer over a porous exponentially stretching sheet in presence of thermal radiation and chemical reaction with suction. The effect of heat and mass transfer in magnetohydrodynamic Casson fluid over an exponentially permeable stretching surface was reported by Raju et al. [16]. The influence of MHD stagnation point flow of nanofluid over a stretching sheet with convective boundary condition was studied by Ibrahim and Rizwan [17]. Noreen et al. [18] examined the magnetohydrodynamic flow of tangent hyperbolic fluid over a stretching surface. They showed that the local skin friction coefficient rises with an increment in magnetic parameter $M$. Mukhopadhyay et al. [19] conducted the study to assess the effects of fluid flow with constant and changeable viscosity on heated surface. They noticed that the decrease in viscosity makes the velocity decrease with increasing distance of the stretching sheet. Nadeem et al. [20] examined MHD three-dimensional Casson fluid flow through a porous linear stretching plate and concluded that the stretching parameter resulted in decreasing behavior of velocity pro-

file. Zhang et al. [21] discussed the MHD and heat transfer of nanofluid while taking porous media, chemical reaction and variable surface into account. They examined three types of nanoparticles. Sheikholeslami et al. [22] discussed the convective heat transfer of nanofluid flow and showed that heat transfer rises with Hartmann number. Patel [23] studied the effects of heat generation, thermal radiation and hall current on hydro magnetic Casson fluid flow towards an osculating plate. They stated that the Hall current boosts mobility in both directions. Farooq et al. [24] discussed the MHD flow of Maxwell fluid with nanomaterials due to an exponentially stretching surface. The role of thermophoresis parameter is negligible on the temperature distribution. Magnetohydrodynamic (MHD) boundary layer flow past a wedge with heat transfer and viscous effects of nanofluid embedded in porous media was investigated by Ibrahim and Tulu [25]. They discover that the boundary layer thickness is influenced by the pressure gradient. The impact of 3D Maxwell nanofluid heat and mass transfer evaluation onto an exponentially stretching surface was explored by Ali et al. [26]. They showed that the skin friction coefficient decrease with Deborah number.

The thermal radiation plays an important role in industrial and engineering processes. Thermal radiation is a phenomenon in which energy is transported through indirect contact. Most activities exist at higher temperatures in manufacturing environments, so experience of radiative heat transfer of heat is very necessary when constructing equipment. Raptis et al. [27] reported the effect of thermal radiation on the MHD flow of a viscous fluid past a semi-infinite stationary plate. Devi et al. [28] presented analysis of the radiation and heat source effects on MHD flow over an exponentially stretching surface. Mukhopadhyay [29] discussed the MHD flow with slip effects over a radiating stretching surface. The influence of radiation effect over an exponentially stretching sheet was studied by Ishak [30] and Mabood et al. [31]. Bidin and Nazar [32] carried out a numerical study to investigate the impact of radiation on boundary layer flow due to an exponentially stretching surface. Poornima and Reddy [33] scrutinized an analysis of MHD free convective heat transfer flow of nanofluid over a nonlinear radiative stretching surface. Khalili et al. [34] examined the MHD flow with radiation effect and heat source past an exponentially stretching surface. Izadi et al. [35] discussed thermal radiation in a micropolar nanoliquid in a porous chamber. They applied Galerkin finite element method to compute numerical solution. Daniel et al. [36] presented theory on entropy analysis

for EMHD nanofluids considering thermal radiation and viscous dissipation. Muhammad et al. [37] obtained numerical solution via shooting method and *bvp4c* for the significant rule nonlinear thermal radiation played in 3D eyring-Powell nanofluid. Sohail et al. [38] described entropy analysis of Maxwell nanofluid in gyrotactic microorganism with thermal radiation. Gireesha et al. [39] provides hybrid nanofluid flow across a permeable longitudinal moving fin with thermal radiation.

Because of the unique physical and chemical properties of nanometer-sized products, nanofluids have many applications in the industrial sector. Nanofluids are composite of solid-liquid materials, typically 1-100 nm, consisting of powerful nanoparticles or liquid-suspended nanofibers. The term nanofluid was suggested by Choi [40]. He revealed that supplying a tiny quantity of nanoparticles to base fluids improved the thermal conductivity of the fluid by approximately two times. Nield and Kuznestov [41] studied convected heat transfer flow of nanofluid in a permeable medium. They considered natural convection past a vertical flat plate. Khan et al. [42] analyzed non-aligned hydro magnetic stagnation point nanofluid flow with changeable viscosity over a stretching surface along with radiation effect. They found that non-alignment of the reattachment point decreases with an increase in magnetic parameter M. Bachok et al. [43] discussed stagnation-point nanofluid flow and heat transfer analysis due to an exponentially shrinking/stretching surface. They discovered that the solution obtained for shrinking sheet is not unique. Nada et al. [44] examined the effects of nanofluid while variable properties are taken into account. Malik et al. [45] studied Casson nanofluid's boundary layer flow over a cylinder that stretches exponentially and found solution numerically. Eid [46] addressed the impact of chemical reaction towards an exponentially stretching surface on the MHD flow of two-phase nanofluid. They investigated that thermal boundary layer is dependent on the reaction and source parameter. Gangaiah et al. [47] examined the MHD nanofluid flow in the presence of viscous dissipation over an exponentially stretching surface. They showed that thermal boundary layer depends on viscous dissipation parameter. The effect of different variables like changeable viscosity, buoyancy and changeable thermal conductivity on mixed convective heat transfer towards a stretching sheet was discussed by Abel et al. [48]. They obtained solution numerically. In Yousaf et al. [49] and Ellahi et al. [50], they have discussed MHD Carreau and non-Newtonian nanofluid flow over an exponentially

4

and slippery walls, respectively. Unsteady flow with CNT-based MHD nanofluid, variable viscosity and a permeable shrinking surface have been discussed in Ahmed et al. [51]. See also Thoi et al. [52] for a different fluid flow aspects in a Y-shaped fin.

Thermophoresis arises when small particles transported from the sheet to the fluid. This phenomena is important in many industrial applications including filters, combustion and turbine blades. Many investigation connected to heat and mass transfer include Dufour and Soret impacts with thermophoretic. These type of effects arises when density difference is present in the flow system. Soret and Dufour impacts are useful in fields like as geosciences, petrology, hydrology etc. Hayat et al. [53] discussed Soret and Dufour effects in 3D flow with chemical reaction and convective condition in Maxwell fluid. Ramzan et al. [54] examined 3D boundary layer flow of a viscoelastic nanofluid with Soret and Dufour effects. MHD slip flow with Soret-Dufour effects in an exponentially stretching surface was discussed by Sravanthi [55]. Zaidi et al. [56] explored the study of Soret and Dufour effects of wall jet MHD flow with suction/injection. The study of thermophoretic MHD flow and non-linear radiative convective heat transfer over a non-linearly stretching sheet was investigated by Jain and Choudhar [57]. Muhaimin et al. [58] studied the impact of thermophoresis particle deposition and chemical reaction on unsteady non-Darcy mixed convective flow over a porous wedge in the presence of temperature-dependent viscosity. Makinde et al. [59] found stagnation point flow in chemically reacting nanofluid with slip conditions. Rehman et al. [60] have also addressed stagnation point flow but on the inclined surface. They noticed that nanoparticles concentration improves with thermophoresis parameter. Nonaligned stagnation point flow with changeable viscosity over a surface have been discussed in Khan et al. [61]. They indicated that reattachment point in nonalignment reduces with magnetic field strength. Ibrahim and Makinde [62] explored convective heat transfer of Casson nanofluid with slip conditions. They recorded the decline of the local Nusselt and Sherwood numbers with Casson parameter. In yet another work, Ibrahim and Makinde [63] discussed power-law nanofluid with slip conditions. They stated that skin friction falls with slip parameter and increases with power-law index. Bhatti et al. [64] computed numerical solution of Hall current in peristaltic flow. Thoi [65] et al. studied NEPCM solidifying heat storage unit in a Y-shaped fin. Tlili et al. [66] discussed convection in magnetic hybrid nanofluid. They ended-up finding that the radiation parameter

boosts the local Nusselt number. Bhatti et al. [67] used shooting method for finding solution of non-Newtonian hyperbolic tangent nanofluid with Hall current. They noticed that the Hall parameter raised the fluid velocity dramatically. Sheikholeslami [68] found computational results for energy under Lorentz force. Sheikholeslami et al. [69] did experimental study to find ways in enhancing boiling heat transfer. Sheikholeslami [70] discussed nanofluid transportation inside a permeable medium. They noticed that radiation causes the temperature gradient to decrease. Nanofluids have been in demand because of its use in energy efficient devices due to its high performance contribution in thermal conductivity compared to a traditional fluid [71], [72], [73]. Nanofluids have recently been used in detergent, vehicle coolant, sensing in microelectromechanical systems (MEMS), thermal energy storage [74]. Thus, it can be used in heating and electronic devices to make it more cost effective by minimization of energy lost in heat transfer process. There are a number of applications where nanofluid have been used such as in biomedical engineering, fluid power, mechanical and manufacturing industry, hydraulics etc. The nanofluids are a composite solution containing nanoparticles and the base fluid [75]. The scope of nanofluid has been further enlarged by coalescing nanoparticles with blood to cultivate comprehension of biological sciences as well. Such a fluid is ordinarily known as bionanofluid. The bionanofluid has instigated research in cancer therapy, nanotechnology and medical devices etc.

Bioconvection is a process in which microorganisms convection occur in the fluid [76]. Khan and Makinde [77] investigated nanofluids in motile gyrotactic microorganisms. In [78] found analytical solution of bioconvection of oxytactic bacteria. Winifred and Makinde [79] discussed hydromagnetic bioconvection due to microorganisms and solution is obtained numerically. Recently, Naganthran et al. [80] applied extrapolation technique in time dependent bionanofluid. Zaimi et al. [81] discussed stagnation point flow not only containing nanoparticles but also gyrotactic microogranisms. Ali and Zaib [82] discussed time dependent Eyring-Powell nanofluid flow. Zeng and Pedley [83] discussed gyrotactic micro-organisms in complex three dimensional flow. Shah et al. [84] have developed a fractional model in discussing a natural convection of bio-nanofluids between two vertical plates. Amiersom et al. [85] have discussed melting bioconvection nanofluid with second order slip with thermal physical properties. Khader et al. [86] performed experimental study to determine the thermal and electrical conductivity to develop a new correlation in bio-nanofluid. For other details in this direc-

tion [87], [88], [89], [90], [91], [92].

There exists a very extensive literature with and without nanofluid on the topic of a constant fluid properties. But not many studies were dedicated to explore the impacts of changeable liquid characteristics on nanofluid flow. To bridge that gap, the present research focuses on the influences of changeable viscosity and changeable thermal conductivity on the boundary layer nanofluid flow. The investigation on the unsteady bionanofluid over a stretching and shrinking sheet is also discussed.

## 1.2   Problem Statement

The present study is carried to cover a gap between constant and variable fluid properties of Newtonian and non-Newtonian fluid flow over a stretching sheet. The comparison of both constant and variable liquid characteristics is made to see the difference between both the studies. The current study also discussed the MHD bio-nanofluid flow past an unsteady stretching sheet considering constant and variable thermophysical properties. It comes to conclude that the use of variable properties offers distinct effects on fluid flow motion.

## 1.3   Research Questions

1. What are the impacts of variable viscosity and variable thermal conductivity on nanofluid flow past an exponentially stretching sheet?

2. What are the impacts of variable viscosity and variable thermal conductivity on Powell-Eyring nanofluid flow past a variable thickness stretching surface?

3. What are the impacts of MHD unsteady stretching/shrinking sheet on bio-nanofluid?

4. What are the impacts of MHD unsteady stretching sheets considering variable thermophysical properties on bio-nanofluid.?

## 1.4 Objectives and Scope

The objectives of this dissertations are:

1. To find the numerical solution of MHD flow of nanofluid with variable fluid properties over an exponentially stretching sheet.

2. To find the numerical solution by applying the SFDM on Newtonian and non-Newtonian fluid flow over a variable thickness stretching sheet while considering varying liquid characteristics.

3. To solve unsteady MHD flow of bio-nanofluid over a stretching/shrinking sheet numerically.

4. To find the numerical solution of unsteady MHD flow of bio-nanofluid with variable thermophysical properties by using shooting method.

## 1.5 Fluid

A fluid is a material which continuously deforms under the action of applied shearing forces. Types of fluids, are characterized into liquids and gases.
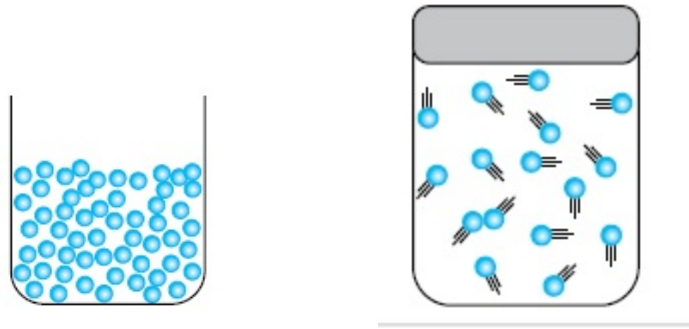


Figure 1.1: Molecular activity in liquid and gas (Source: Internet).

## 1.6 Nanofluid

The nanofluids are a composite solution containing nanometer sized particle and the base fluid. The nanoparticles usually consists of metals, carbides or oxides. Water, oil and ethylene gly-

col are some examples of the base fluid. There are a number of applications where nanofluids have been used such as in biomedical engineering, fluid power, mechanical and manufacturing industry, hydraulics, etc.
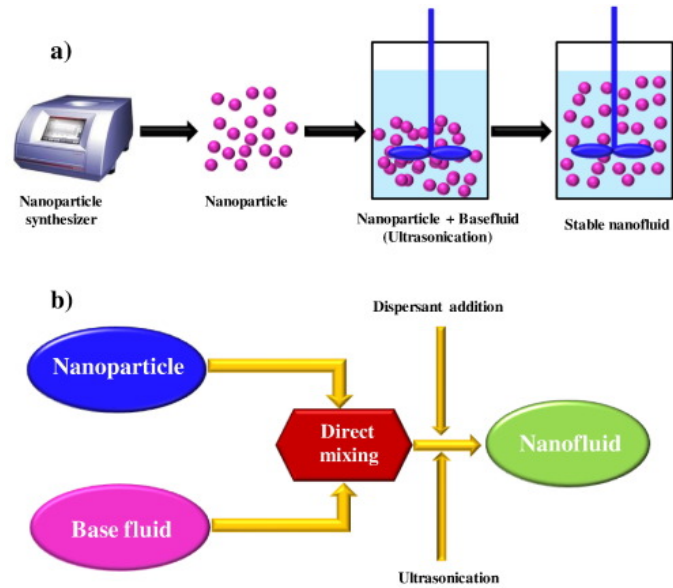


Figure 1.2: Nanofluid (Source: Internet).

## 1.7   Stress

The ratio of force to area is called stress. Mathematically stress expressed as,

$$\tau_1 = \frac{F_1}{A_1},$$

(1.1)

Where $F_1$ is the force applied on area $A_1$.



9
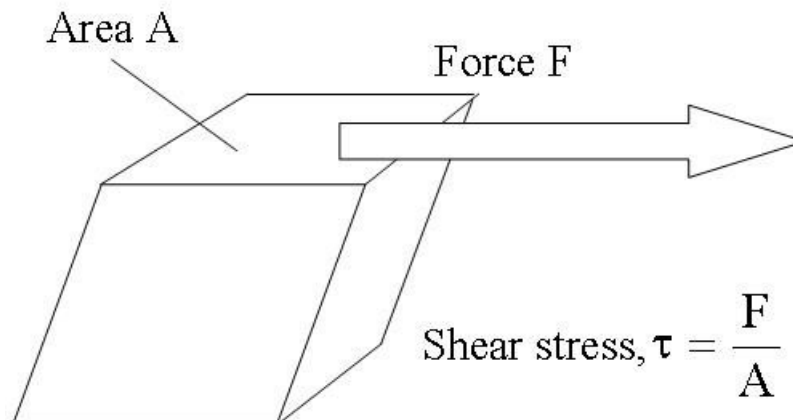
Figure 1.3: Stress (Source: Internet).

## 1.8   Dynamic Viscosity

A ratio of shear stress to strain rate is called dynamic viscosity. It is denoted by $\mu_1$.

$$\mu_1 = \frac{\text{shear stress}}{\text{strain rate}}. \tag{1.2}$$

$\frac{kg}{ms}$ is a unit of dynamic viscosity.

Table 1.1: Water as a function of temperature (White [101])

| $T_1(C)$ | $\rho_1(\frac{kg}{m^3})$ | $\mu_1 \times 10^{-3}\frac{Ns}{m^2}$ |
|---|---|---|
| 0 | 1000 | 1.788 |
| 10 | 1000 | 1.307 |
| 20 | 998 | 1.003 |
| 30 | 996 | 0.799 |
| 40 | 992 | 0.657 |
| 50 | 988 | 0.548 |
| 60 | 983 | 0.467 |
| 70 | 978 | 0.405 |
| 80 | 972 | 0.355 |
| 90 | 965 | 0.316 |
| 100 | 958 | 0.283 |

### 1.8.1   Newton's Law of Viscosity

According to Newton's law of viscosity shear stress $\tau_1$ is directly proportional to the shear rate. Mathematically,

$$\tau_1 = \mu_1 \frac{du_1}{dy_1}, \tag{1.3}$$

where $\mu_1$ is coefficient of viscosity.

10

### 1.8.2 Kinematic Viscosity

The fraction of dynamic viscosity $\mu_1$ to the density of fluid $\rho_1$ is called kinematic viscosity. It is defined by,

$$\nu_1 = \frac{\mu_1}{\rho_1}. \tag{1.4}$$

The unit of $\nu_1$ is $m^2/s$.

## 1.9 Types of Flows

Some key types of fluids are described given below.

### 1.9.1 Steady vs Unsteady Flow

Flow is steady, if the velocity of fluid flow remains constant function of time. Whereas flow is unsteady, if the velocity of fluid is variable with respect to time.
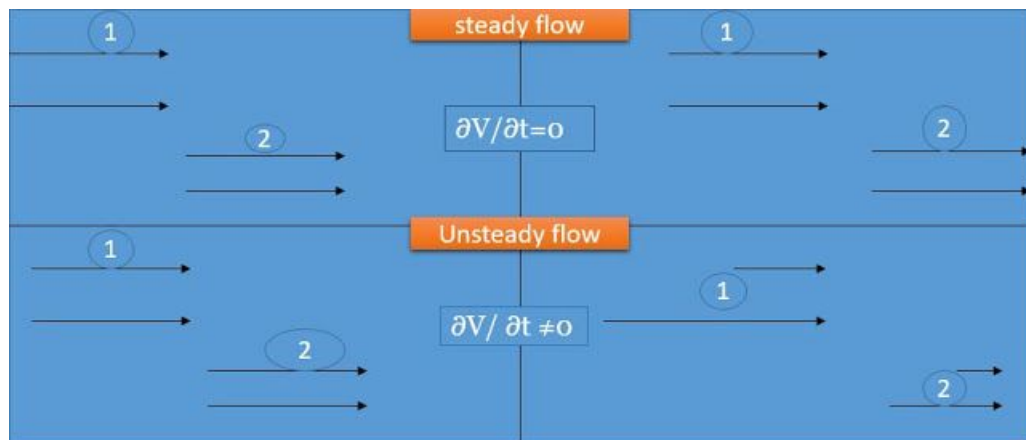


Figure 1.4: Steady vs Unsteady Flow (Source: Internet).

### 1.9.2 Laminar Flow and Turbulent Flow

If the velocity of the fluid flow is not changing with respect to time then flow is laminar . On the other hand if the velocity of flow is variable with time then flow is turbulent.
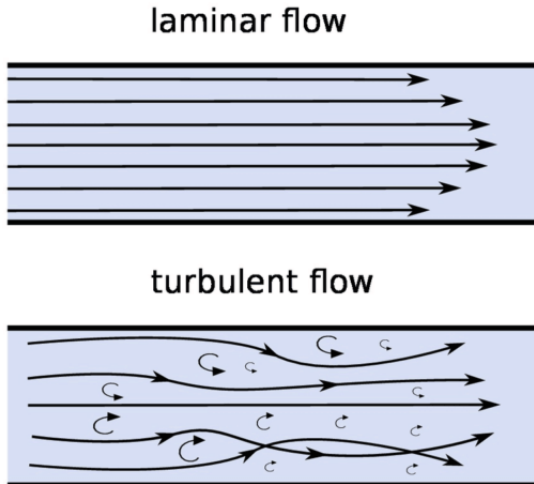
Figure 1.5: Laminar vs Turbulent Flow (Source: Internet).

### 1.9.3 Viscous Flow

In viscous flows, effects of fluid friction is significant.

### 1.9.4 Inviscid Flow

If there is no viscosity effect ($\mu_1 = 0$) on the fluid flow then flow is called inviscid flow.

### 1.9.5 Newtonian and Non-newtonian Fluid

Those real or viscous fluids which follow the Newton's law of viscosity are known as Newtonian fluids. Water and air are the examples of newtonian fluids. While on the other hand Non-Newtonian fluids do not obey the Newton's law of viscosity. Mathematically,

$$\tau_1 = \mu_1 \left(\frac{du_1}{dy_1}\right)^n, \text{where} \qquad n \neq 1. \tag{1.5}$$
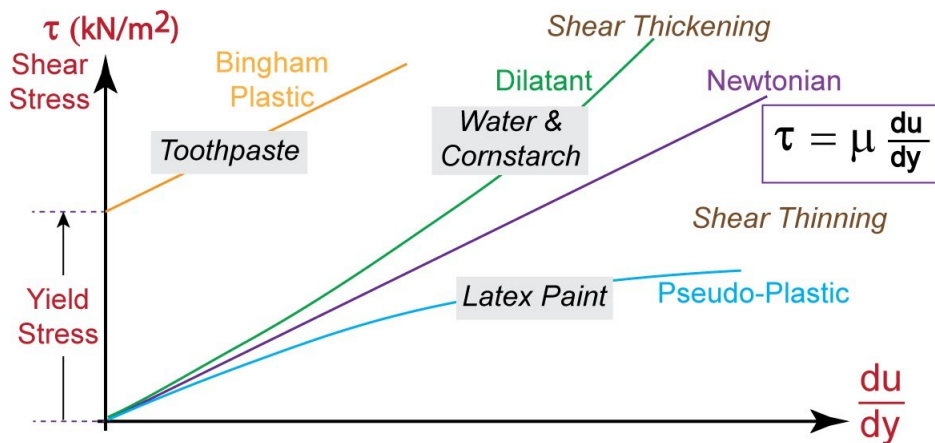
Figure 1.6: Newtonian and Non-Newtonian Fluids (Source: Internet).

## 1.9.6 Incompressible and Compressible Flow

If the density $\rho_1$ is constant function of time then the fluid flow is incompressible. Mathematically,

$$\frac{d\rho_1}{dt_1} = 0. \tag{1.6}$$

Whereas if the density $\rho_1$ changes with time then the fluid flow is compressible.
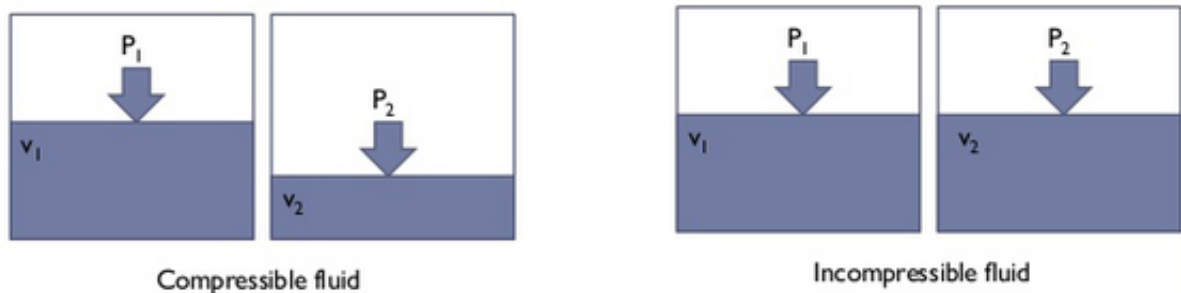


Figure 1.7: (Source: Internet).

Figure 1.8: Ranges of Mach number (Source: Internet).

## 1.10 Some Basic Laws

### 1.10.1 Law of Conservation of Mass (Continuity Equation)

The mathematical form of continuity equation is,

$$\frac{\partial \rho_1}{\partial t_1} + \nabla.(\rho_1.V) = 0, \tag{1.7}$$

where $V$ indicates the fluid flow velocity and $\rho_1$ denotes fluid density. The above equation for incompressible flow reduces to,

$$\nabla.\mathbf{V} = 0. \tag{1.8}$$

In cartesian coordinate three dimensional continuity equation can be expressed as,

$$\frac{\partial u_1}{\partial x_1} + \frac{\partial v_1}{\partial y_1} + \frac{\partial w_1}{\partial z_1} = 0. \tag{1.9}$$

### 1.10.2 Law of Conservation of Momentum

According to conservation of momentum, the quantity called linear momentum, of an isolated system remains unchanged. In vector form, it can be written as

$$\rho_1 \frac{d\mathbf{V}}{dt_1} = \nabla.\tau_1 + \rho_1\mathbf{b}. \tag{1.10}$$

14

The inertial force is represented on the L.H.S, whereas on R.H.S the first term is surface force and second term is body force. $\rho$ denotes density, $V$ is the velocity field, $b$ the body force and $\frac{d}{dt_1}$ material time. Cauchy stress tensor is $\tau_1 = -p_1 I_1 + S_1$. Here $p_1$, $I_1$ and $S_1$ represent pressure, identity tensor and extra stress tensor respectively. In Cartesian coordinates and considering the velocity field $V = [u_1(x_1, y_1, t_1), v_1(x_1, y_1, t_1), w_1(x_1, y_1, t_1)]$ and momentum equation gives

$$\rho_1\left(\frac{\partial u_1}{\partial t_1} + u_1\frac{\partial u_1}{\partial x_1} + v_1\frac{\partial u_1}{\partial y_1} + w_1\frac{\partial u_1}{\partial z_1}\right) = \frac{\partial \tau_{1xx}}{\partial x_1} + \frac{\partial \tau_{1xy}}{\partial y_1} + \frac{\partial \tau_{1xz}}{\partial z_1} + \rho_1 b_{x_1}, \tag{1.11}$$

$$\rho_1\left(\frac{\partial v_1}{\partial t_1} + u_1\frac{\partial v_1}{\partial x_1} + v_1\frac{\partial v_1}{\partial y_1} + w_1\frac{\partial v_1}{\partial z_1}\right) = \frac{\partial \tau_{1yx}}{\partial x_1} + \frac{\partial \tau_{1yy}}{\partial y_1} + \frac{\partial \tau_{1yz}}{\partial z_1} + \rho_1 b_{y_1}, \tag{1.12}$$

$$\rho_1\left(\frac{\partial w_1}{\partial t_1} + u_1\frac{\partial w_1}{\partial x_1} + v_1\frac{\partial w_1}{\partial y_1} + w_1\frac{\partial w_1}{\partial z_1}\right) = \frac{\partial \tau_{1zx}}{\partial x_1} + \frac{\partial \tau_{1zy}}{\partial y_1} + \frac{\partial \tau_{1zz}}{\partial z_1} + \rho_1 b_{z_1}. \tag{1.13}$$

### 1.10.3 Navier-Stokes Equation

The Navier-Stokes equation, in component form is:

$$\rho\frac{Du_i}{Dt_1} = -\frac{\partial \rho_1}{\partial x_i} + \rho_1 g_i + \frac{\partial}{\partial x_j}[2\mu_1 e_{ij} - \frac{2}{3}\mu_1(\nabla.\mathbf{V})\delta_{ij}], \tag{1.14}$$

where $\mu_1$ is the dynamic viscosity, $p_1$ is the hydrostatic pressure, g is the gravity and $\delta_{ij}$ is the Kronecker delta, defined by

$$\delta_{ij} = \begin{cases} 1 & , \quad \text{if } i = j \\ 0 & , \quad \text{if } i \neq j \end{cases} \tag{1.15}$$

and

$$e_{ij} = \frac{1}{2}\left(\frac{\partial u_i}{\partial x_j} + \frac{\partial u_j}{\partial x_i}\right), \tag{1.16}$$

if $\mu_1$ is constant then it can be taken outside and Eq. (1.14) takes the form

$$\rho_1\frac{Du_i}{Dt} = -\frac{\partial \rho_1}{\partial x_i} + \rho_1 g_i + 2\mu_1\frac{\partial e_{ij}}{\partial x_j} - \frac{2}{3}\mu_1\frac{\partial}{\partial x_i}(\nabla.\mathbf{V}), \tag{1.17}$$

$$= -\frac{\partial \rho}{\partial x_i} + \rho g_i + \mu_1[\nabla^2 u_i + \frac{1}{3}\frac{\partial}{\partial x_i}(\nabla.\mathbf{V})], \tag{1.18}$$

15

where

$$\nabla^2 u_i = \frac{\partial^2 u_i}{\partial x_j \partial x_i} = \frac{\partial^2 u_i}{\partial x_1^2} + \frac{\partial^2 u_i}{\partial x_2^2} + \frac{\partial^2 u_i}{\partial x_3^2}, \tag{1.19}$$

is Laplacian of $u_i$. For incompressible fluids $\nabla.\mathbf{V} = 0$ and using vector notation, the Navier-Stokes equation is

$$\rho_1 \frac{D\mathbf{V}}{Dt_1} = -\nabla P + \rho_1 \mathbf{g} + \mu_1 \nabla^2 \mathbf{V}. \tag{1.20}$$

Above equation is valid only for incompressible fluid. If viscous effects are negligible then

$$\rho_1 \frac{D\mathbf{V}}{Dt_1} = -\nabla P + \rho_1 \mathbf{g}. \tag{1.21}$$

which are the Euler equations of motion.

### 1.10.4   Prandtl Boundary Layer Equation

The deduction of the boundary layer equations was one of the most important advances in fluid dynamics. Using an order of magnitude analysis, the well-known governing Navier Stokes equations of viscous fluid flow can be greatly simplified within the boundary layer. The two dimensional Navier Stokes for steady incompressible flow in cartesian coordinates is given as:

$$u_1 \frac{\partial u_1}{\partial x_1} + v_1 \frac{\partial u_1}{\partial y_1} = \frac{-1}{\rho_1} \frac{\partial p_1}{\partial x_1} + \nu_1 \left( \frac{\partial^2 u_1}{\partial x_1^2} + \frac{\partial^2 u_1}{\partial y_1^2} \right), \tag{1.22}$$

Prandtl deducted that boundary layer near the surface must be extremely thin and applied following order of magnitude assumptions.

| Variables | Order of magnitude |
|-----------|--------------------|
| $u_1$ | 1 |
| $v_1$ | $\delta$ |
| $\frac{\partial u_1}{\partial x_1}$ | $\frac{1}{1} = 1$ |
| $\frac{\partial u_1}{\partial y_1}$ | $\frac{1}{\delta}$ |
| $p_1$ | 1 |

An inertia term in Navier Stokes equation in cartesian coordinates is $\rho_1 u_1 \frac{\partial u_1}{\partial x_1}$ and a viscous term $\mu_1 \frac{\partial^2 u_1}{\partial y_1^2}$. We can estimate the order of magnitude for each term of sheet having length $L$ as follows:

$$\rho_1 u_1 \frac{\partial u_1}{\partial x_1} \sim \frac{\rho_1 U_\infty}{L},$$

$$\mu_1 \frac{\partial^2 u_1}{\partial y_1^2} \sim \frac{\mu_1 U_\infty}{\delta^2},$$

As the viscous force in the boundary layer is comparable order to inertial force,

$$\frac{\rho_1 U_\infty}{L} \sim \frac{\mu_1 U_\infty}{\delta^2}.$$

After some simplification, we have $\delta^2 \sim \frac{\nu_1 L}{U_\infty} = \frac{1}{\sqrt{Re_L}}$

Now, apply the order of magnitude on equation (1.22),

$$u_1 \frac{\partial u_1}{\partial x_1} + v_1 \frac{\partial u_1}{\partial y_1} = \frac{-1}{\rho_1} \frac{\partial p_1}{\partial x_1} + \frac{1}{\sqrt{Re_L}} \left( \frac{\partial^2 u_1}{\partial x_1^2} + \frac{\partial^2 u_1}{\partial y_1^2} \right). \tag{1.23}$$

$$1 \quad 1+ \quad \delta \ \tfrac{1}{\delta} = \qquad\qquad\qquad \delta^2 \qquad \left(1 + \tfrac{1}{\delta^2}\right)$$

As, clearly we can see that $\frac{\partial^2 u_1}{\partial x_1^2} \sim o(\delta^2)$, which is very small and can be neglected.

## 1.10.5 Energy Conservation

First law of thermodynamics we have,

$$\rho_1 c_p \frac{dT_1}{dt_1} = -div.\overrightarrow{q_1} + h_p \nabla.\tilde{j}_p, \tag{1.24}$$

where $c_p$ denotes specific heat of fluid, $T_1$ temperature, $h_p$ the enthalpy for nanoparticles, $\overrightarrow{q_1}$ energy flux and nanoparticles diffusion mass flux $\tilde{j}_p$. Energy flux $\overrightarrow{q_1}$ and nanoparticles diffusion mass flux $\tilde{j}_p$ are given by

$$\overrightarrow{q_1} = -k_1 \nabla T_1 + h_p \tilde{j}_p, \tag{1.25}$$

$$\tilde{j}_p = -\rho_1 D_B \nabla C_1 - \rho_1 p D_t \frac{\nabla T_1}{T_\infty}. \tag{1.26}$$

Here $\rho_1 p$ , $k_1$, $D_B$, $D_T$ and $C_1$ are nanoparticle mass density, thermal conductivity, Brownian motion parameter, thermophoretic diffusion coefficient nanoparticle volume fraction respectively. In view of Eqs. (1.24) and (1.25) Eq. (1.26) becomes

$$\rho_1 c_p \frac{dT_1}{dt_1} = -k_1 \nabla^2 T_1 + \rho_1 p c_p \left[ D_B \nabla C_1.\nabla T_1 - D_T \frac{\nabla T_1.\nabla T_1}{T_\infty} \right]. \tag{1.27}$$

### 1.10.6 Concentration Law

The concentration equation for nanofluid is

$$\frac{\partial C_1}{\partial t_1} + V.\nabla C_1 = \frac{-1}{\rho_1 p}\nabla.\tilde{j}_p, \tag{1.28}$$

after insertion of Eq. (1.26) into Eq. (1.28),

$$\frac{\partial C_1}{\partial t_1} + V.\nabla C_1 = D_B\nabla^2 C_1 + D_T\frac{\nabla^2 T_1}{T_\infty}. \tag{1.29}$$

# 1.11 Some Common Useful Non-Dimensional Parameters

## 1.11.1 Reynolds Number

The ratio of inertial to viscous force is called Reynolds number($Re$). Mathematically, it is defined by,

$$Re = \frac{\text{inertial force}}{\text{viscous force}} = \frac{\rho_1 u_1 L}{\mu_1}. \tag{1.30}$$

## 1.11.2 Prandtl Number

The fraction of momentum to heat diffusivity is called Prandtl number. Mathematically,

$$Pr = \frac{\text{momentum diffusivity}}{\text{heat diffusivity}} = \frac{\nu_1}{\alpha_1} = \frac{c_p\mu_1}{k_1}. \tag{1.31}$$

## 1.11.3 Grashof Number

The Grashof is a dimensionless parameter that arise in heat transfer analysis of fluid dynamics to examine the velocity and temperature profiles in the mixed and free convection flows. The fraction of buoyancy to viscous forces is called Grashof nuumber. Mathematically, $Gr$ is defined by

$$Gr = \frac{g\beta\Delta T_1 l^3}{\nu_1^2}. \tag{1.32}$$

Where $l$ is the vertical length.

### 1.11.4 Eckert Number

The Eckert number is defined as the fraction of kinetic energy to enthalpy. Mathematically,

$$E_c = \frac{V_1^2}{c_p \Delta T_1}. \tag{1.33}$$

### 1.11.5 Schmidt Number

The Schmidt number is a dimensionless number defined as the ratio of kinematic viscosity (momentum diffusivity) and mass diffusivity, and is used to characterize fluid flows in which there are simultaneous momentum and mass diffusion convection processes. The Schmidt number describes the mass momentum transfer, and the equations can be seen below:

$$Sc = \frac{\nu_1}{D} = \frac{\text{viscous diffusion rate}}{\text{mass diffusion rate}}. \tag{1.34}$$

### 1.11.6 Lewis Number

The Lewis number is a dimensionless number defined as the ratio of thermal diffusivity to mass diffusivity.

$$Le = \frac{\alpha_1}{D}. \tag{1.35}$$

### 1.11.7 Biot Number

The fraction of heat transfer resistances inside and at the surface of a body is called Biot number (Bi).

$$B_i = \frac{hL}{k_1} = \frac{\text{convective heat transfer}}{\text{thermal conductivity}}. \tag{1.36}$$

### 1.11.8 Nusselt Number

The Nusselt number is a fraction of convective to conductive heat transfer. Mathematically,

$$Nu_L = \frac{h_1 L_1}{k_1}. \tag{1.37}$$

### 1.11.9   Sherwood Number

The Sherwood number is a fraction of convective to diffusive mass transfer. Mathematically,

$$Sh = \frac{K_1 L_1}{D} = \frac{\text{convective mass transfer coefficient}}{\text{diffusive mass transfer coefficient}}. \tag{1.38}$$

## 1.12   Boundary Layer

A layer of fluid close to a solid surface of wall where the impacts of viscosity are significant.
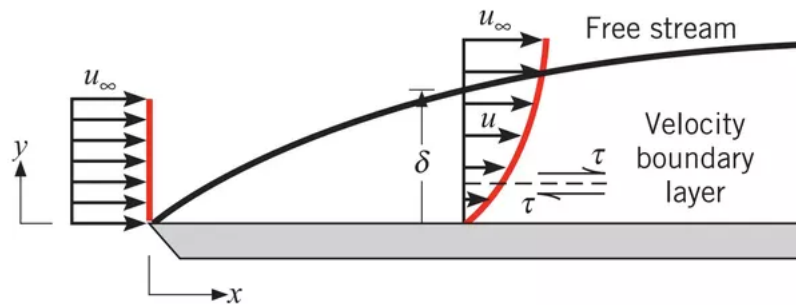


Figure 1.9: Velocity Boundary Layer(Source: Internet).

Where $\delta$ is a boundary layer thickness.

## 1.13   Numerical Techniques

### 1.13.1   Shooting Method for 2nd order Non-Linear Differential Equation

The shooting method is explained through the following second order ODE,

$$z'' = h(x, z, z'), \qquad \alpha_1 \leq x \leq \beta_1 \tag{1.39}$$

along with the boundary conditions,

$$z(\alpha_1) = a_1, \qquad z(\beta_1) = b_1. \tag{1.40}$$

In 1st step we turn down the BVP Into the IVP,

$$z'' = g(x, z, z') \quad \text{for} \quad \alpha_1 \leq x \leq \beta_1$$

with

$$z(\alpha_1) = a_1, \quad z'(\alpha_1) = u \text{ (unknown)}.$$

where $u$ is an unknown which needs to be find out.

$$\lim_{t \longrightarrow \infty} z(\beta_1, u_t) = z(\beta_1) = b_1. \tag{1.41}$$

Use $u_o$ as an initial approximation to generate $u_1$, $u_2$,....

The process of finding $u$ must be stop when

$$z(\beta_1, u) - b_1 = 0. \tag{1.42}$$

Above equation is nonlinear in u. We apply Newton Raphson method to create the sequence $u_t$ . We required only an initial guess $u_o$ in Newton's method and can find the remaining terms by

$$u_t = u_{t-1} - \frac{(z(\beta_1, u_{t-1}) - b_1)}{\frac{dz}{du}(b_1, u_{t-1})}. \tag{1.43}$$

For multi variables the Newton's method is,

$$u_t = u_{t-1} - \frac{(z(\beta_1, u_{t-1}) - b_1)}{|J_1|}. \tag{1.44}$$

where $J_1$ is the Jacobian matrix.
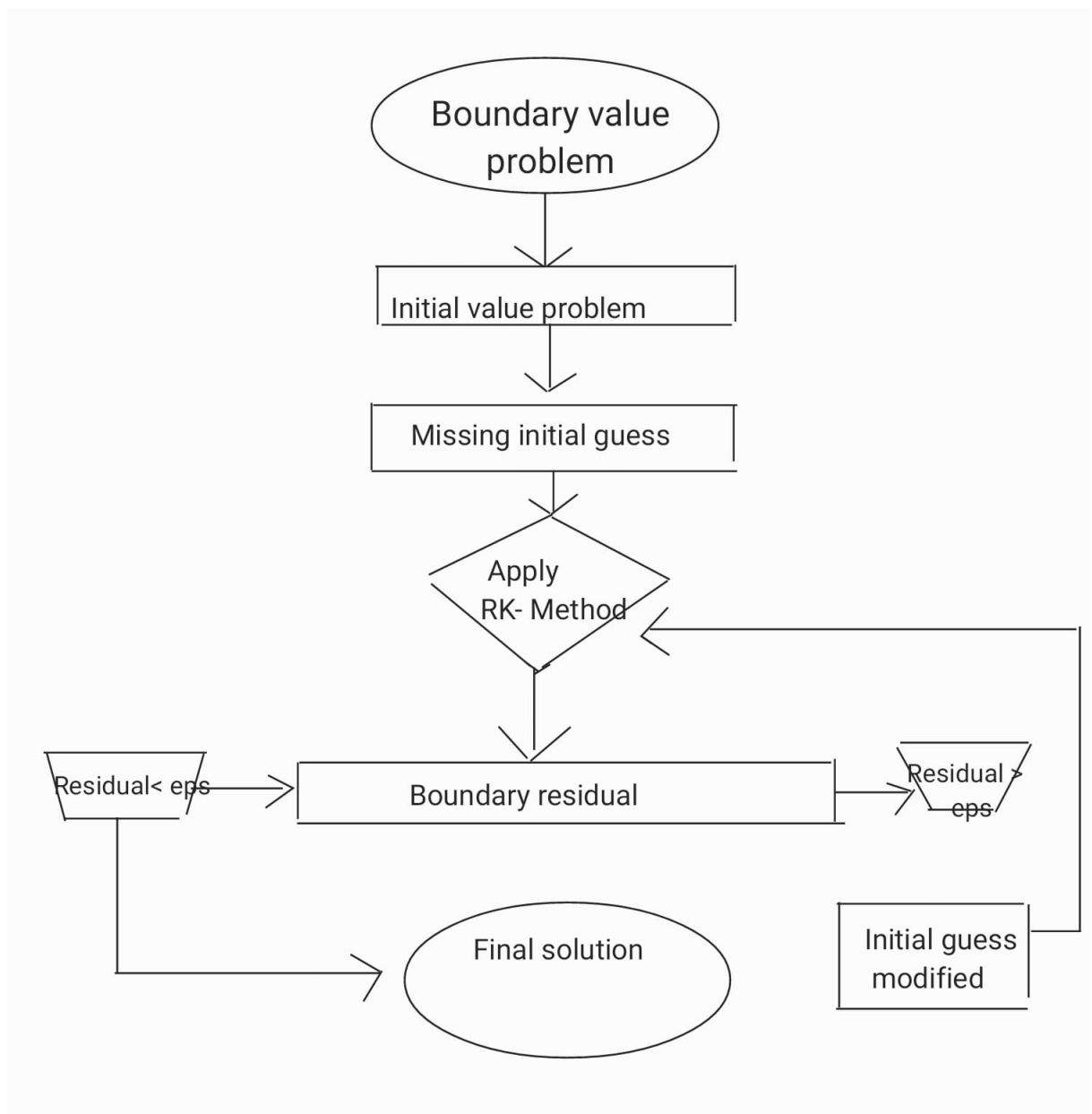
Figure 1.10: Flow chart of shooting method.

### 1.13.2 bvp4c

BVP can also be solved by using MATLAB solver *bvp4c*. *bvp4c* algorithm utilize the collocation approach in the background. To find solution of BVP by using *bvp4c* algorithm, we need initial guess, domain size and the number of points. Please see reference [95] for more detail and examples.
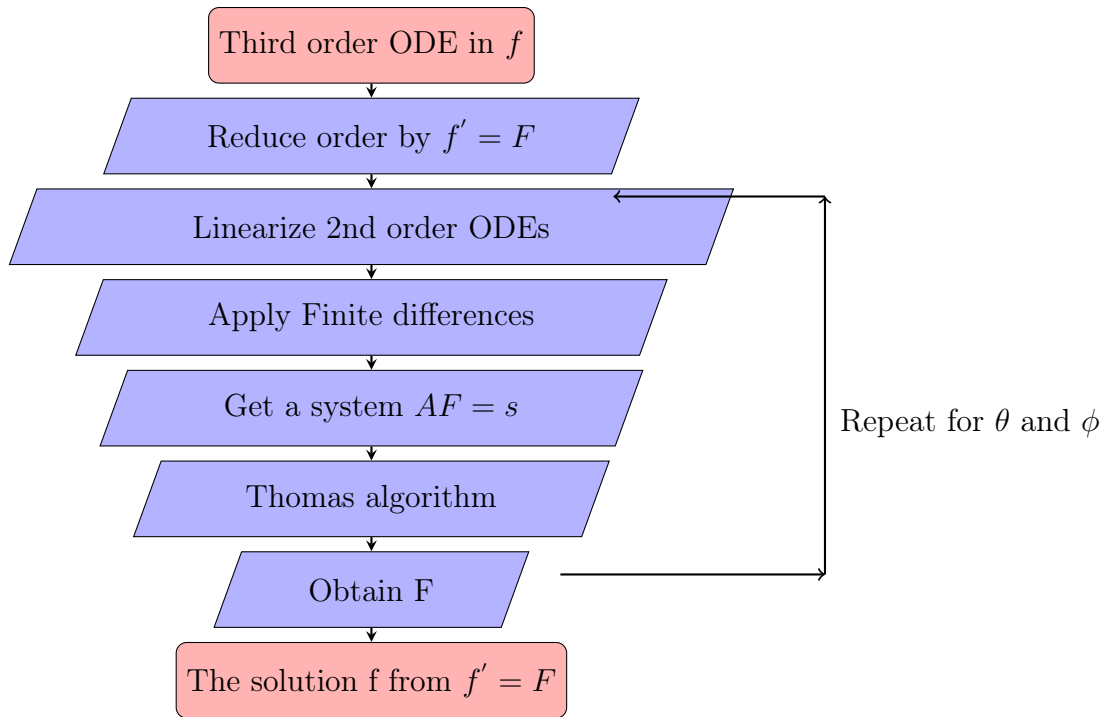
Figure 1.11: Flow Chart of SFDM

### 1.13.3 Simplified Finite Difference Scheme (SFDM)

The solution of non-linear coupled ODEs can also be found through simplified finite difference scheme (SFDM). The simplified finite difference scheme is explained through the following necessary steps.

1. First we bring down the third order ODE into a system of first and second order ODEs. This reduction of order simplify the process of finite difference approximation. The ODE already written in second order cannot be reduced.

2. Further, the set of non-linear ODEs is linearized by using Taylor series.

3. The finite difference approximation formulas is used in place of derivatives of ODEs.

4. In the end, we obtain system of algebraic equations that can be solved by Thomas algorithm.

5. The process will be repeated for energy and concentration equations.

## 1.13.4 Simplified Finite Difference Scheme for Linear Differential Equation

Consider the second order ODE,

$$\frac{d^2u}{dv^2} + A(v)\frac{du}{dv} + B(v)u = C(v). \tag{1.45}$$

Subject to the boundary constraints,

$$u(0) = \alpha_1, \qquad u(L_1) = \beta_1. \tag{1.46}$$

Grid points are taken as,

$$v_0 = 0, \qquad\qquad v_n = v_{n-1} + h, \qquad\qquad n = 1, 2, 3, , , , N.$$

The variable $u$ and its derivatives at $v_n$ are taken as,

$$u = u_n, \qquad \frac{du}{dv} = \frac{u_{n+1} - u_{n-1}}{2h}, \qquad \frac{d^2u}{dv^2} = \frac{u_{n+1} - 2u_n + u_{n-1}}{h^2} \tag{1.47}$$

Insert Eq.(1.47) into Eq.(1.45), Eq.(1.45) reduces to,

$$\frac{1}{h^2}(u_{n+1} - 2u_n + u_{n-1}) + \frac{A(v)}{2h}(u_{n+1} - u_{n-1}) + B(v)u_n = C(v) \tag{1.48}$$

Eq. (1.48) can also be written as,

$$a_n y_{n-1} + b_n y_n + c_n y_{n+1} = r_n \tag{1.49}$$

Where,

$$a_n = 1 - \frac{1}{2}hA(v_n), \quad b_n = h^2 B(v_n) - 2, \quad c_n = 1 + \frac{1}{2}hA(v_n), \quad r_n = h^2 C(v_n) \tag{1.50}$$

The boundary condition are taken as,

$$u_o = \alpha_1, \qquad\qquad u_N = \beta_1 \tag{1.51}$$

In matrix form Eq. (1.49) and Eq. (1.50) can be written as,

$$AU = S \tag{1.52}$$

Where,
$$
U = \begin{pmatrix} u_1 \\ u_2 \\ - \\ - \\ - \\ u_N \end{pmatrix}, \qquad
S = \begin{pmatrix} s_1 \\ s_2 \\ - \\ - \\ - \\ s_N \end{pmatrix} = \begin{pmatrix} r_1 - \alpha_1 a_1 \\ r_2 \\ - \\ - \\ - \\ r_{N-1} - \beta_1 r_{N-1} \end{pmatrix},
$$

$$
A = \begin{pmatrix}
b_1 & c_1 & - & - & & & \\
a_2 & b_2 & c_2 & & & & \\
 & & - & - & & & \\
 & & & - & - & & \\
 & & & & a_{N-2} & b_{N-2} & C_{N-2} \\
 & & & & & a_{N-1} & b_{N-1}
\end{pmatrix}
$$

In the end, we will apply the Thomas algorithm to obtain the solution of system of algebraic equations. Further we have discussed the detailed process of simplified finite difference method for non-linear coupled ODEs in Chapter 4 and 5.

# Chapter 2

# MHD Flow of Nanofluid over an Exponentially Stretching Sheet with Varying Fluid Properties

In this chapter we investigates the study of nanofluid and heat transfer flow of the MHD free stream over an exponentially radiating stretching sheet accompanied by constant and variable fluid characteristics together. The underlying governing PDEs have been translated into nonlinear ODEs by incorporating adequate transformations.The corresponding ODEs are effectively solved by using the shooting technique and the MATLAB algorithm *bvp4c*. The impact on the skin resistance coefficient (quantifying resistance), the local Nusselt number $Nu_{x_1}$ (heat transfer rate) and the local Sherwood number $Sh_{x_1}$ (mass transfer rate) on the surface due to the flow field variables have been computed against various parameters. To study the impact of pertinent parameters on momentum, thermal and concentration distributions, graphs are also plotted. It has been noted by raising the value of $\epsilon$, the heat transfer rate reduces for variable fluid properties. On the other hand, raising $Pr_o$ increases the heat transfer rate.

The arrangement of this chapter is given below.
The introduction of the chapter is presented in Section 2.1. The theoretical model and the governing equations of the chapter are described in Section 2.2. Section 2.3 consists on the

fluid properties. We discuss the numerical procedures in Section 2.4. Section 2.5 covers the results and discussion of the chapter with the help of graphs and tables. We draw a conclusion of this chapter in Section 2.6.

## 2.1   Introduction

Andersson and Aarseth [112] investigated the properties of fluid under the influence of temperature. The impact of thermal radiation on steady MHD flow over a stretching surface considering variable thermal conductivity and mass transfer was discussed by Ibrahim and Suneetha [113]. Makinde et al. [114] examined the MHD flow of nanofluid considering viscosity as variable towards a stretching surface. Mukhopadhyay et al. The influence of temperature on viscosity during heating surface was investigated by Elbashbeshay and Bazid [115].The effect of hydro-magnetic flow with variable liquid characteristic towards a nonlinearly stretching surface was discussed by Popley et al. [116]. The influence of MHD free stream and heat transfer flow with temperature-dependent fluid properties past a nonlinearly stretching surface was studied by Prasad et al. [117]. Sharif et al. [118]examined the study of nanofluid while considering changeable liquid properties. The influence of heat generation and radiation on nanofluid over an exponentially stretching sheet was reported by Murugesan et al. [119]. They sorted out two types of nanofluid in their study. There exists very extensive literature with and without nanofluid on the topic of a constant fluid properties. But not many studies were dedicated to explore the effects of variable fluid properties on nanofluid. To fill that gap, the present work focuses the impacts of variable viscosity and variable thermal conductivity on nanofluid over an exponentially radiating sheet.

## 2.2   Theoretical Model

We consider a laminar, MHD, radiative heat transfer of nanofluid flow due to an exponentially stretching surface. The sheet is situated at $y_1 = 0$. A changeable magnetic field $B_1(x_1) = B_o e^{\frac{x_1}{2L}}$ has been implemented normal to the surface. Fig. 2.1 is the geometry of the flow, in which $x_1$-axis is along and $y_1$-axis is taken as normal to the sheet.

$u_1 \to U_\infty, T_1 \to T_\infty, C_1 \to C_\infty, y_1 \to \infty$

Concentration boundary layer

Thermal boundary layer

Momentum boundary layer

$y_1$ axis

$x_1$ axis

$B_1(x_1) = B_0 e^{x_1/2L}$

Stretching sheet

$y_1 = 0$

$U_w$     $T_w,$     $C_w$
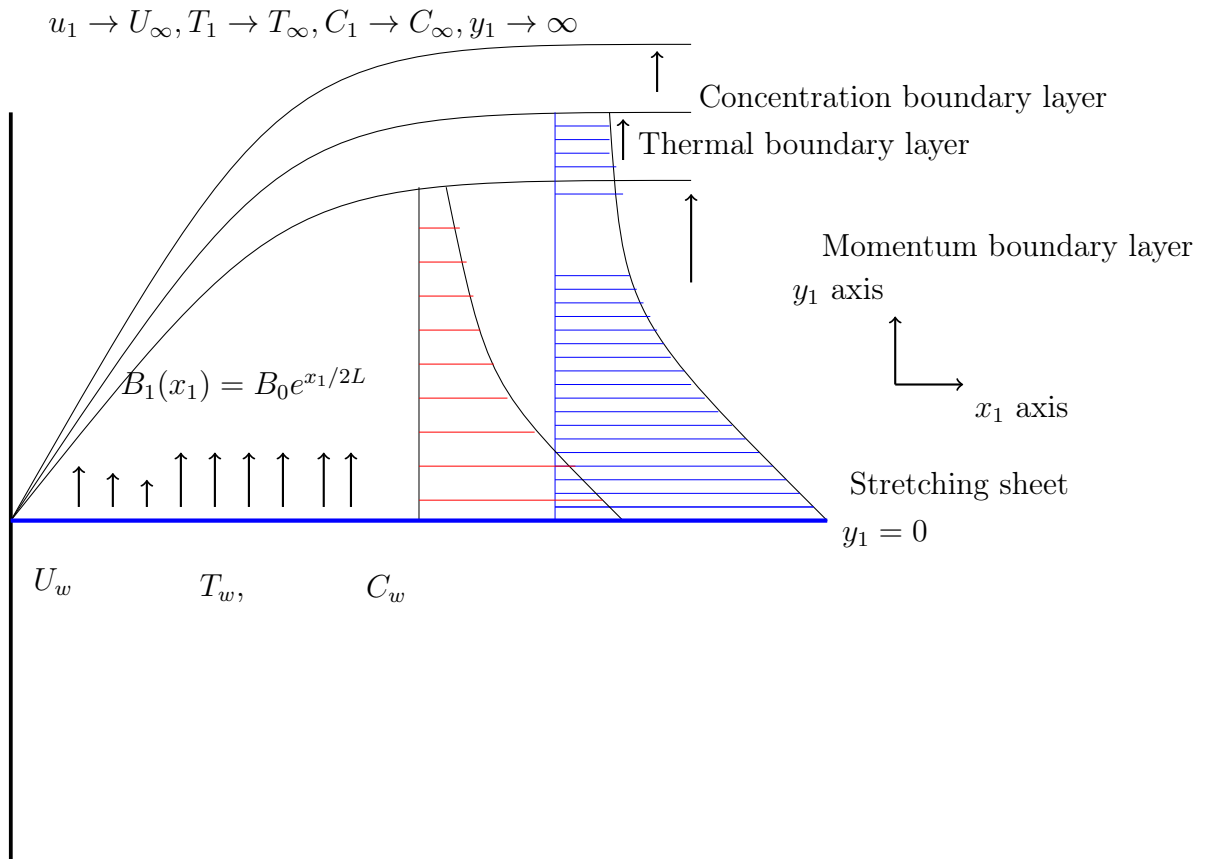
Figure 2.1: Geometry of the problem.

Let $u_w = ae^{\frac{x_1}{L}}$ is the wall velocity, whereas $u_\infty = be^{\frac{x_1}{L}}$ is a free stream velocity, in which stretching parameters $a, b > 0$. The sheet has been kept at constant wall temperature $T_w$ whereas $T_\infty$ point out the ambient temperature. The boundary layer equations with Buongiorno model [96], Popley et al. [116] and Khalili et al. [34] which regulate the above flow are

$$\frac{\partial u_1}{\partial x_1} + \frac{\partial v_1}{\partial y_1} = 0, \tag{2.1}$$

$$u_1 \frac{\partial u_1}{\partial x_1} + v_1 \frac{\partial v_1}{\partial y_1} = u_\infty \frac{du_\infty}{dx_1} + \frac{1}{\rho_1} \frac{\partial}{\partial y_1} \left( \frac{\mu_1 \partial u_1}{\partial y_1} \right) - \frac{\sigma B_1^2}{\rho_1} (u_1 - u_\infty), \tag{2.2}$$

$$u_1 \frac{\partial T_1}{\partial x_1} + v_1 \frac{\partial T_1}{\partial y_1} = \frac{1}{\rho_1 c_p} \frac{\partial}{\partial y_1} \left( \frac{k_1 \partial T_1}{\partial y_1} \right) +$$
$$\tau_1 \left( D_B \frac{\partial T_1}{\partial y_1} \frac{\partial C_1}{\partial y_1} + \frac{D_T}{T_\infty} (\frac{\partial T_1}{\partial y_1})^2 \right) - \frac{1}{\rho_1 c_p} \frac{\partial q_r}{\partial y_1}, \tag{2.3}$$

$$u_1 \frac{\partial C_1}{\partial x_1} + v_1 \frac{\partial C_1}{\partial y_1} = D_B \frac{\partial^2 C_1}{\partial y_1^2} + \frac{D_T}{T_\infty} \frac{\partial^2 T_1}{\partial y_1^2}, \tag{2.4}$$

where the coordinates of velocities $(u_1, v_1)$ are along $x_1-$ and $y_1-$ axes, respectively. $\mu_1$ is a fluid viscosity coefficient, $B_1(x_1)$ is a variable magnetic field along the $y_1-$ axis. Here $T_1$ is the temperature, $C_1$ is the nanoparticles concentration. The parameters $D_T$ and $D_B$ are characterized as thermophoretic diffusion and Brownian diffusion coefficients respectively. In $\tau_1 = \frac{(\rho_1 c)_p}{(\rho_1 c)_f}$, $(\rho_1 c)_p$ is the effective heat capacity of the nanoparticle and $(\rho_1 c)_f$ is the effective heat capacity of the fluid and $q_r$ represents the radiative heat flux.

Appropriate boundary conditions complete the above system by

$$u_1 = u_w(x_1) = ae^{\frac{x_1}{L}}, \quad v_1 = 0, u_1 \longrightarrow u_\infty(x_1) = be^{\frac{x_1}{L}}, \quad T_1 \longrightarrow T_\infty,$$

$$T_1 = T_w, \quad C_1 = C_w \quad at \quad y_1 = 0, \qquad C_1 \longrightarrow C_\infty \quad as \quad y_1 \longrightarrow \infty. \tag{2.5}$$

Using the following similarity transformation defined in khalili et al. [34] as:

$$\eta = \sqrt{\frac{a}{2\nu_1 L}} e^{\frac{x_1}{2L}} y_1, \quad \psi = \sqrt{2a\nu_1 L} e^{\frac{x_1}{2L}} f(\eta), \quad \theta = \frac{T_1 - T_\infty}{T_w - T_\infty},$$

$$u_1 = ae^{\frac{x_1}{L}} f'(\eta), \quad v_1 = -\sqrt{\frac{\nu_1 a}{2L}} e^{\frac{x_1}{2L}} (f(\eta) + \eta f'(\eta)). \tag{2.6}$$

Eq. (2.1) is identically satisfied. Moreover, when above similarity variables used in Eqs. (2.2), (2.3) and (2.4) which yields:

$$\left(\frac{\mu_1}{\mu_o}f''(\eta)\right)' + 2(\lambda^2 - (f'(\eta))^2) + f(\eta)f''(\eta) - M(f'(\eta) - \lambda) = 0, \quad (2.7)$$

$$\left(1 + \frac{4}{3}Rd\right)\left(\frac{k_1}{k_o}\theta'(\eta)\right)' + Pr_o(f\theta'(\eta) - f'(\eta)\theta(\eta) + Nb\theta'(\eta)\phi'(\eta) + Nt(\theta'(\eta))^2) = 0, \quad (2.8)$$

$$\phi''(\eta) + \frac{N_t}{N_b}\theta''(\eta) + Le(f\phi'(\eta) - f'(\eta)\phi(\eta)) = 0. \quad (2.9)$$

The boundary conditions transformed into:

$$f(\eta) = 0, \quad f'(\eta) = 1, \quad \theta(\eta) = 1, \quad \phi(\eta) = 1, \quad \text{at } \eta = 0,$$

$$f'(\eta) = \lambda, \quad \theta(\eta) = 0, \quad \phi(\eta) = 0, \quad \text{as } \eta \longrightarrow \infty. \quad (2.10)$$

where $M = \frac{2\sigma B_0^2 L}{\rho_1 a}$ represents a magnetic parameter. $Pr_o = \frac{\mu_o c_{p_o}}{k_o}$ represents the ambient Prandtl number. The parameters $Nb = \frac{\tau_1 D_B(C_w - C_\infty)}{\nu_1}$ and $Nt = \frac{\tau_1 D_T(T_w - T_\infty)}{T_\infty \nu_1}$ are characterized as Brownian motion and thermophoresis diffusion coefficients respectively. The parameter $\lambda = \frac{b}{a}$ is characterized as free stream velocity. $Rd = \frac{4\sigma^* T_\infty^3}{k_0 k^*}$ denotes the radiation parameter and $Le = \frac{\nu_1}{D_B}$ is the Lewis number.

## 2.3 Analysis on Fluid Properties

This section comprises of two subsections. Firstly, an overview of the constant fluid properties will be presented followed by the discussion on variable fluid properties.

### 2.3.1 Case A: Constant Fluid Properties

For this case, Eqs. (2.7), (2.8) and (2.9) can be adjusted as follows to incorporate constant fluid properties:

$$f'''(\eta) + 2(\lambda^2 - (f'(\eta))^2) + f(\eta)f''(\eta) - M(f'(\eta) - \lambda) = 0, \quad (2.11)$$

$$\left(1 + \frac{4}{3}Rd\right)\theta''(\eta) + Pr_o(f(\eta)\theta'(\eta) - f'(\eta)\theta(\eta) + Nb\theta'(\eta)\phi'(\eta) + Nt(\theta'(\eta))^2) = 0, \quad (2.12)$$

$$\phi''(\eta) + \frac{Nt}{Nb}\theta''(\eta) + Le(f(\eta)\phi'(\eta) - f'(\eta)\phi(\eta)) = 0. \quad (2.13)$$

## 2.3.2 Case B: Variable Fluid Properties

For this case, viscosity and thermal conductivity in Eqs. (2.7) and (2.8) is considered variable and taken as a function of a temperature. For viscosity we write

$$\mu_1(T) = \frac{\mu_{ref}}{1 + \gamma(T_1 - T_{ref})}, \tag{2.14}$$

where we follow Andersson and Aarseth [112] and reference within to write above expression (2.14). In above $\gamma_1$ is a fluid property. If $T_o \approx T_{ref}$ then above formula (2.14) becomes,

$$\mu_1 = \frac{\mu_o}{1 - \frac{T_1 - T_o}{\theta_r(T_w - T_o)}} = \frac{\mu_o}{1 - \frac{\theta(\eta)}{\theta_r}}, \tag{2.15}$$

here $\theta_r = \frac{-1}{\gamma_1(T_w - T_o)}$. If the above viscosity relation is incorporated in the Eq. (2.7), then it can be rewritten as

$$\frac{\theta_r}{(\theta_r - \theta(\eta))} f'''(\eta) + \frac{f''(\eta)\theta'(\eta)\theta_r}{(\theta_r - \theta(\eta))^2} + 2(\lambda^2 - (f'(\eta))^2) + f(\eta)f''(\eta) - M(f'(\eta) - \lambda) = 0. \tag{2.16}$$

The variable thermal conductivity is expressed in terms of temperature by following Prasad et al. [117] as,

$$k_1(T) = k_o(1 + \epsilon\theta), \tag{2.17}$$

Under this above relation the mathematical form of Eq. (2.8) can be described as

$$(1 + \frac{4}{3}Rd)((1 + \epsilon\theta(\eta))\theta''(\eta) + \epsilon(\theta'(\eta))^2) + Pr_o(f(\eta)\theta'(\eta) - f'(\eta)\theta(\eta) + Nb\theta'(\eta)\phi'(\eta) + Nt(\theta'(\eta))^2) = 0. \tag{2.18}$$

To measure the roughness, heat and mass transport rates onto the sheet, we calculate the $C_{fx_1}$ ( skin friction coefficient ), $Nu_{x_1}$ (the local Nusselt number ) and the $Sh_{x_1}$ (local Sherwood number ) respectively, i.e.

$$C_{fx_1} = \frac{\tau_w}{\rho_1 u_w^2} = \frac{f''(0)}{\sqrt{2Re_{x_1}}}, \tag{2.19}$$

$$Nu_{x_1} = -\frac{x_1 q_w}{T_w - T_\infty} = -\sqrt{\frac{x_1 Re_{x_1}}{2L}}\theta'(0), \tag{2.20}$$

$$Sh_{x_1} = -\frac{x_1 j_w}{C_w - C_\infty} = -\sqrt{\frac{x_1 Re_{x_1}}{2L}}\phi'(0). \tag{2.21}$$

## 2.4 Numerical Procedure

### 2.4.1 Shooting Method

To apply the shooting technique to Cases A and B together with the boundary conditions, we transformed BVP into an IVP and convert higher order ODEs into a set of first order ODEs. The Newton-Raphson technique was used to locate the root. After that, the order five Runge-Kutta method was implemented to determine the IVP solution. The shooting method is implemented in MATLAB. For Cases A and B, the system of first order ODEs are written as,

(a) Case A:

$$f = z_1, f^{'} = z_2, f^{''} = z_3, f^{'''} = z_3^{'} = -2(\lambda^2 - z_2^2) - z_1 z_3 + M(z_2 - \lambda),$$

$$z_4 = \theta, z_5 = \theta^{'}, \theta^{''} = z_5^{'} = -\frac{Pr_o}{(1 + \frac{4}{3})R_d}(z_1 z_5 - z_2 z_4 + N_b z_5 z_7 + N_t z_5^2),$$

$$z_6 = \phi, z_7 = \phi^{'}, \phi^{''} = z_7^{'} = -L_e(z_1 z_7 - z_2 z_6) - \frac{N_t}{N_b} z_5^{'}.$$

(b) Case B:

$$f = z_1, f^{'} = z_2, f^{''} = z_3, f^{'''} = z_3^{'} = \frac{(z_3 z_5)}{(z_4 - \theta_r)} + \frac{(z_4 - \theta_r)}{\theta_r}(2(\lambda^2 - z_2^2) + z_1 y_3 - M(z_2 - \lambda)),$$

$$z_4 = \theta, z_5 = \theta^{'}, \theta^{''} = z_5^{'} = \frac{-\epsilon z_5^2}{1 + \epsilon z_4} - \frac{Pr_o}{(1 + \epsilon z_4)(1 + \frac{4}{3}Rd)}(z_1 z_5 - z_2 z_4 + Nb z_5 z_7 + Nt z_5^2),$$

$$z_6 = \phi, z_7 = \phi^{'}, \phi^{''} = z_7^{'} = -Le(z_1 z_7 - z_2 z_6) - \frac{Nt}{Nb} z_5^{'}.$$

### 2.4.2 bvp4c

Using MATLAB *bvp4c* algorithm, BVP can even be solved. *bvp4c* solver employs the collocation technique in the background. It manages to find a solution after supplying initial guess, domain size and the number of points. Please see reference [95] for more detail and examples. The bvp4c scheme for table 2.1-2.4 is described below.

The system of first order ODEs for Cases A and B are written as,

(a) Case A:

$$f = z_1, f' = z_2, f'' = z_3, f''' = z_3' = -2(\lambda^2 - z_2^2) - z_1 z_3 + M(z_2 - \lambda),$$

$$z_4 = \theta, z_5 = \theta', \theta'' = z_5' = -\frac{Pr_o}{(1 + \frac{4}{3})R_d}(z_1 z_5 - z_2 z_4 + N_b z_5 z_7 + N_t z_5^2),$$

$$z_6 = \phi, z_7 = \phi', \phi'' = z_7' = -L_e(z_1 z_7 - z_2 z_6) - \frac{N_t}{N_b} z_5'.$$

(b) Case B:

$$f = z_1, f' = z_2, f'' = z_3, f''' = z_3' = \frac{(z_3 z_5)}{(z_4 - \theta_r)} + \frac{(z_4 - \theta_r)}{\theta_r}(2(\lambda^2 - z_2^2) + z_1 y_3 - M(z_2 - \lambda)),$$

$$z_4 = \theta, z_5 = \theta', \theta'' = z_5' = \frac{-\epsilon z_5^2}{1 + \epsilon z_4} - \frac{Pr_o}{(1 + \epsilon z_4)(1 + \frac{4}{3}Rd)}(z_1 z_5 - z_2 z_4 + Nb z_5 z_7 + Nt z_5^2),$$

$$z_6 = \phi, z_7 = \phi', \phi'' = z_7' = -Le(z_1 z_7 - z_2 z_6) - \frac{Nt}{Nb} z_5'.$$

The boundary conditions implemented in MATLAB are as follows:

$$z_1(0) = 0, z_2(0) = 1, z_4(0) = 1, z_6(0) = 1, y_2(\infty) = \lambda, z_4(\infty) = 0, z_6(\infty) = 0.$$

## 2.5    Results and Discussion

In Table 2.1, we compute the local Nusselt number and compared its values with published results for distinct parameters Prandtl number $Pr_0$, radiation parameter $Rd$ and magnetic parameter $M$.

Table 2.2 illustrates that $C_{fx_1}$ is not significantly changed whereas $Nu_{x_1}$ drops for $\epsilon$ and increases for the values of $\lambda$. The local Sherwood number grows with the rise of $\lambda$ and $\epsilon$. It is observed in Table 2.3 that $Nu_{x_1}$ and $Sh_{x_1}$ rises with a rise of $\lambda$ but $C_{fx_1}$ held opposite behavior. For fixed values of $\lambda = 0, 0.5$ and an increase in $\theta_r$ brings the increasing change in the $C_{fx_1}$ but $Nu_{x_1}$ and $Sh_{x_1}$ has revealed decreasing behavior. Table 2.4 demonstrates that as $Pr_o$ and $R_d$ rises, there is a negligible change in $C_{fx_1}$. But $Nu_{x_1}$ decreases and $Sh_{x_1}$ increases for increasing values of $R_d$. Moreover, the $Nu_{x_1}$ enhances by enhancing Prandtl number but $Sh_{x_1}$ decreases for increasing values of $Pr_o$.

Fig. 2.2 shows that the width of velocity distribution is reduced by enhancing $M$. It happens because of a transverse magnetic field as it opposes the phenomenon of transport.

Table 2.1: (**For Case A**)Resemblance of $-\theta'(0)$ against various values of $M$, $Rd$ and $Pr_0$, when $\lambda = Nb = Nt = Le = 0$.

| $Rd$ | M | $Pr_0$ | Magyari and Keller [2] | Ishak [30] | Mukhopadhay [13] | Mabood et al. [31] | Present results |
|------|---|--------|------------------------|------------|------------------|--------------------|-----------------|
| 0 | 0 | 1 | 0.9548 | 0.9548 | 0.9548 | 0.95478 | 0.9548 |
| | | 2 | - | - | 1.4715 | 1.47151 | 1.4715 |
| | | 3 | 1.8691 | 1.8691 | 1.8691 | 1.86909 | 1.8691 |
| | | 5 | 2.5001 | 2.5001 | 2.5001 | 2.50012 | 2.5001 |
| | | 10 | 3.6604 | 3.6604 | 3.6604 | 3.66039 | 3.6603 |
| 1 | 0 | 1 | - | - | 0.5312 | 0.53121 | 0.5312 |
| 0 | 1 | 1 | - | - | 0.8611 | 0.86113 | 0.8611 |
| 0.5 | 0 | 2 | - | 1.0735 | 1.0735 | 1.07352 | 1.0735 |
| | | 3 | - | 1.3807 | - | 1.38075 | 1.3808 |
| 1 | | | - | 1.1214 | - | 1.12142 | 1.1214 |
| | 1 | 1 | - | - | 0.4505 | 0.45052 | 0.4505 |

The Lorentz force generates resistance to the fluid flow with a rise of $M$ and slows down the velocity.

In Fig. 2.3, we observe that by rising $\theta_r$, a momentum boundary layer thins. Fig. 2.4 shows that there is a rise in temperature distribution for increasing values of $\epsilon$.

Fig. 2.5 and Fig. 2.6 are plotted for several values of $N_b$ and we observe that by increasing $N_b$ temperature distribution rises while concentration distribution decreases by increasing $N_b$.

As seen in Figs. 2.7 and 2.8 that by increasing $N_t$, temperature and concentration profiles increases.

Fig. 2.9 indicates that by increasing $Pr_o$ the thermal boundary layer thickness decreases. This is because, when $Pr_o$ increases, the thermal diffusivity decreases and thus the heat is diffused away from the heated surface more slowly and in consequence increase the temperature gradient at surface.

Fig. 2.10 shows that temperature and thermal boundary layer thickness increases when the radiation parameter intensifies.

Table 2.2: (**For Case B**)Comparison of $-f''(0)$ , $-\theta'(0)$ and $-\phi'(0)$ for distinct values of $\epsilon$ and $\lambda$ when $Rd = M = 0, Pr_0 = 1, \theta_r = -5, Le = 1.3$.

| $\lambda$ | $\epsilon$ | $-f''(0)$ | $-f''(0)$ | $-\theta'(0)$ | $-\theta'(0)$ | $-\phi'(0)$ | $-\phi'(0)$ |
|---|---|---|---|---|---|---|---|
| | | bvp4c method | Shooting technique | bvp4c method | Shooting technique | bvp4c | Shooting Method |
| 0 | 0 | 1.4218 | 1.4218 | 0.6162 | 0.6162 | 0.8951 | 0.8951 |
| 0 | 0.2 | 1.4204 | 1.4204 | 0.5604 | 0.5604 | 0.9188 | 0.9188 |
| 0 | 0.4 | 1.4193 | 1.4192 | 0.5163 | 0.5163 | 0.9367 | 0.9367 |
| 0.5 | 0 | 0.9771 | 0.9771 | 0.6898 | 0.6898 | 1.1075 | 1.1075 |
| 0.5 | 0.2 | 0.9762 | 0.9762 | 0.6383 | 0.6383 | 1.1292 | 1.1292 |
| 0.5 | 0.4 | 0.9755 | 0.9755 | 0.5975 | 0.5975 | 1.1455 | 1.1455 |
| 2 | 0 | -3.0187 | -3.0188 | 0.9261 | 0.9261 | 1.6143 | 1.6143 |
| 2 | 0.2 | -3.0163 | -3.0165 | 0.8716 | 0.8716 | 1.6337 | 1.6337 |
| 2 | 0.4 | -3.0143 | -3.0145 | 0.8274 | 0.8274 | 1.6482 | 1.6483 |

Fig. 2.11 describe the influence of $Le$ on concentration profile. We observe that by increasing $Le$ there is decrease in concentration profile. Lewis number is the ratio of Prandtl number and Schmidt number, so with the increase in Lewis number $Le$, molecular diffusivity decreases. As a result, increase in $Le$ the nanoparticle fraction is lowered.

Fig. 2.12 and Fig. 2.13 shows the impact of $N_b$ on thermal and concentration boundary layers respectively. The temperature distribution rises while concentration distribution reduces for increasing values of $N_b$.

Fig 2.14 and Fig. 2.15 predicts the influence of $N_t$ on temperature and concentration profiles respectively. By raising the values of $N_t$, both thermal and concentration boundary layers thickness increases.

Fig. 2.16 presents the effect of $\epsilon$ on temperature profile. It is noted that by raising $\epsilon$, temperature distribution increases.

Fig. 2.17 depicts the influence of $Le$ on concentration profile. It is observed that concen-

Table 2.3: (**For Case B**)Comparison of $-f''(0)$, $-\theta'(0)$ and $-\phi'(0)$ for different values of $\theta_r$ and $\lambda$ when $M = 0, Pr_0 = 10, \epsilon = 0$.

| $\lambda$ | $\theta_r$ | $-f''(0)$ | $-f''(0)$ | $-\theta'(0)$ | $-\theta'(0)$ | $-\phi'(0)$ | $-\phi'(0)$ |
|---|---|---|---|---|---|---|---|
| | | bvp4c method | Shooting technique | bvp4c method | Shooting technique | bvp4c method | Shooting technique |
| 0 | -10 | 1.3539 | 1.3539 | 0.6223 | 0.6223 | 0.9082 | 0.9081 |
| 0 | -1 | 1.8658 | 1.8657 | 0.5753 | 0.5753 | 0.8085 | 0.8085 |
| 0 | -0.5 | 2.2863 | 2.2863 | 0.5360 | 0.5360 | 0.7281 | 0.7281 |
| 0.5 | -10 | 0.9299 | 0.9299 | 0.6923 | 0.6923 | 1.1119 | 1.1119 |
| 0.5 | -1 | 1.2869 | 1.2868 | 0.6744 | 0.6744 | 1.0814 | 1.0814 |
| 0.5 | -0.5 | 1.5816 | 1.5810 | 0.6220 | 0.6620 | 1.0611 | 1.0611 |
| 2 | -10 | -2.8719 | -2.8720 | 0.9227 | 0.9227 | 1.6088 | 1.6088 |
| 2 | -1 | -3.9846 | -3.9848 | 0.9459 | 0.9459 | 1.6457 | 1.6457 |
| 2 | -0.5 | -4.9021 | -4.9026 | 0.9611 | 0.9611 | 1.6692 | 1.6692 |

tration boundary layer decreases for rising values of $Le$.

Fig. 2.18 depicts the skin friction coefficient against the magnetic parameter $M$ with variations in $\theta_r$. The skin friction coefficient increases with increase in $Kp$ and $\theta_r$.

Fig. 2.19 portrays the effects of $\epsilon$ and $\theta_r$ on local Nusselt number. The local Nusselt number reduces for elevating values of $\epsilon$ and $Rd$.

Fig. 2.20 is drawn to see the impacts of $Le$ and $Nt$ on Sherwood number. It is analyzed that Sherwood number elevates for higher values of $Le$ and $Nt$.

Table 2.4: (**For Case B**)Comparison of $-f''(0)$, $\theta'(0)$ and $\phi'(0)$ for different values of $Rd$ and $Pr_0$ when $M = \lambda = \epsilon = 0, \theta_r = -5, Nb = 0.8, Nt = 0.5, Le = 1.3$

| $Rd$ | $Pr_o$ | $-f''(0)$ | $-f''(0)$ | $-\theta'(0)$ | $-\theta'(0)$ | $-\phi'(0)$ | $-\phi'(0)$ |
|------|--------|-----------|-----------|---------------|---------------|-------------|-------------|
|      |        | bvp4c method | Shooting technique | bvp4c method | Shooting technique | bvp4c method | Shooting technique |
| 0    | 1      | 1.4218    | 1.4218    | 0.6162        | 0.6162        | 0.8951      | 0.8951      |
|      | 2      | 1.4264    | 1.4263    | 0.7611        | 0.7610        | 0.8452      | 0.8452      |
|      | 3      | 1.4285    | 1.4285    | 0.8193        | 0.8193        | 0.8274      | 0.8274      |
|      | 5      | 1.4304    | 1.4304    | 0.8608        | 0.8608        | 0.8186      | 0.8186      |
|      | 10     | 1.4319    | 1.4319    | 0.8805        | 0.8805        | 0.8196      | 0.8196      |
| 0.5  | 1      | 1.4181    | 1.4181    | 0.4910        | 0.4910        | 0.9396      | 0.9396      |
|      | 2      | 1.4231    | 1.4231    | 0.6585        | 0.6585        | 0.8802      | 0.8802      |
|      | 3      | 1.4257    | 1.4257    | 0.7423        | 0.7423        | 0.8514      | 0.8514      |
|      | 5      | 1.4285    | 1.4285    | 0.8193        | 0.8193        | 0.8274      | 0.8274      |
|      | 10     | 1.4309    | 1.4309    | 0.8687        | 0.8687        | 0.8182      | 0.8182      |
| 1    | 1      | 1.4158    | 1.4158    | 0.4162        | 0.4163        | 0.9689      | 0.9689      |
|      | 2      | 1.4207    | 1.4207    | 0.5790        | 0.5790        | 0.9082      | 0.9082      |
|      | 3      | 1.4235    | 1.4235    | 0.6738        | 0.6738        | 0.8749      | 0.8749      |
|      | 5      | 1.4268    | 1.4268    | 0.7726        | 0.7726        | 0.8415      | 0.8415      |
|      | 10     | 1.4299    | 1.4299    | 0.8517        | 0.8517        | 0.8199      | 0.8199      |
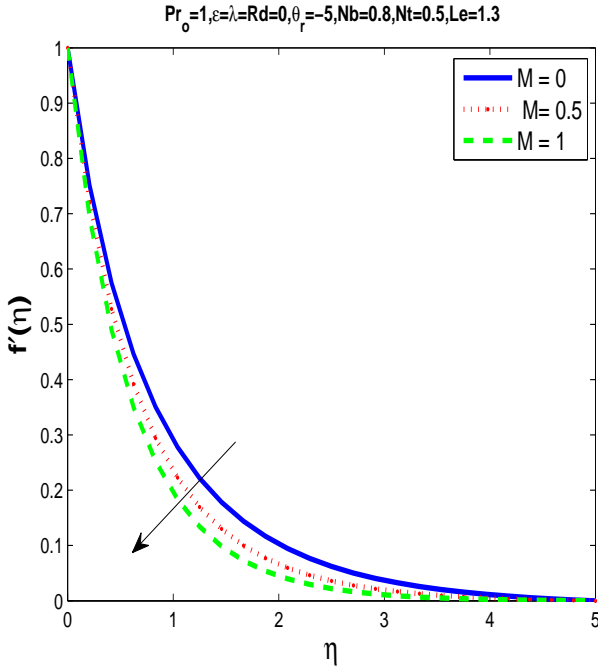


Figure 2.2: Velocity profile $f'(\eta)$ for different $M$ (**For Case B**).
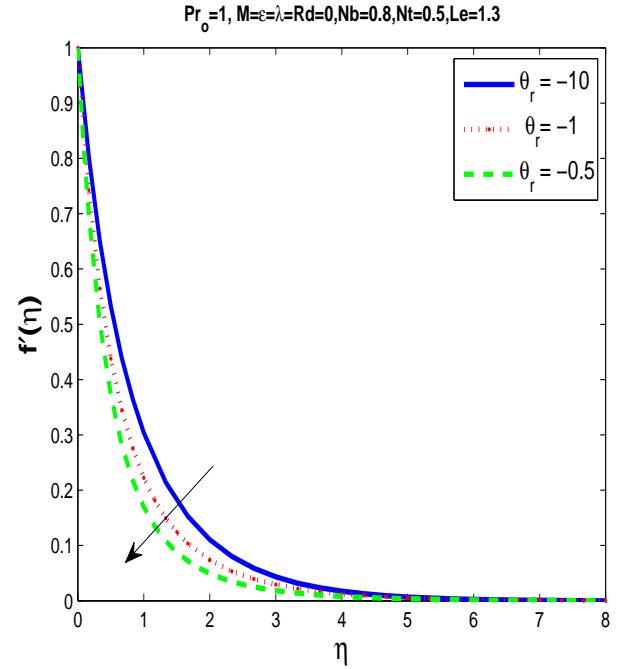


Figure 2.3: Velocity profile $f'(\eta)$ for different $\theta_r$ (**For Case B**).

Figure 2.4: Temperature profile $\theta(\eta)$ for different $\epsilon$ (**For Case B**).
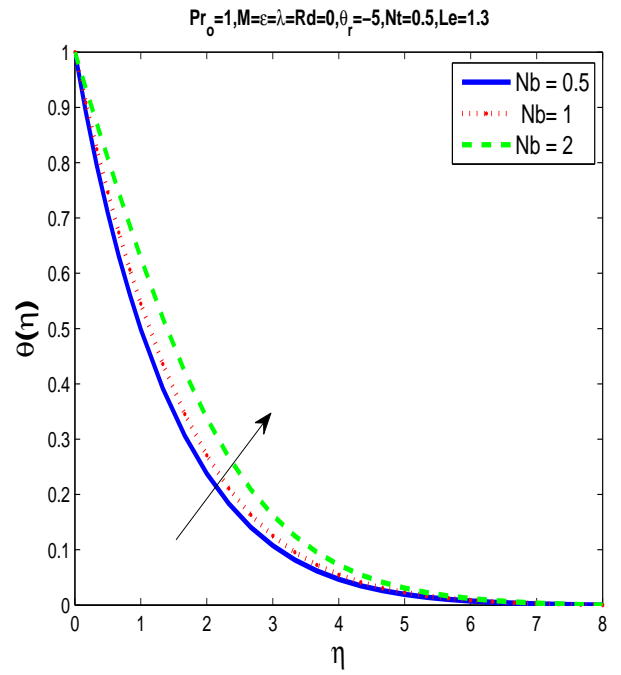


Figure 2.5: Temperature profile $\theta(\eta)$ for different $N_b$ (**For Case B**).



Figure 2.6: The concentration profile $\phi(\eta)$ for different $N_b$ (**For Case B**).



Figure 2.7: Temperature profile $\theta(\eta)$ for different $N_t$ (**For Case B**).

Figure 2.8: Concentration profile $\phi(\eta)$ for different $N_t$ (**For Case B**).
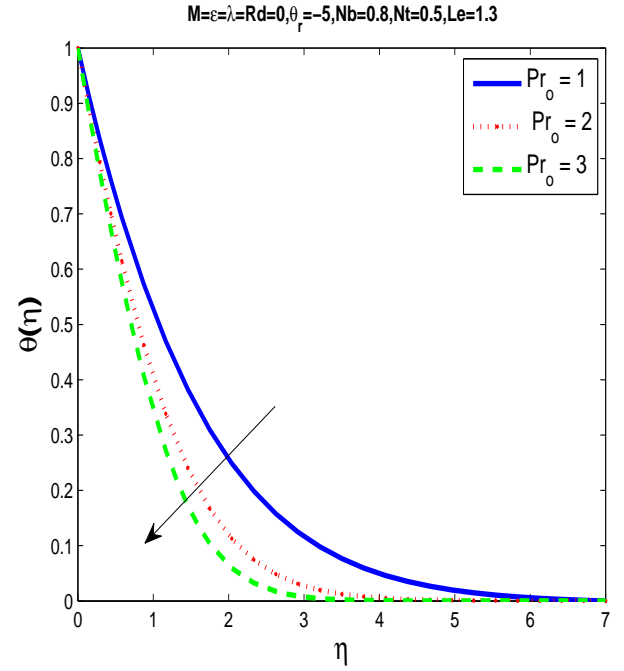


Figure 2.9: Temperature profile $\theta(\eta)$ for different $Pr_o$ (**For Case B**).
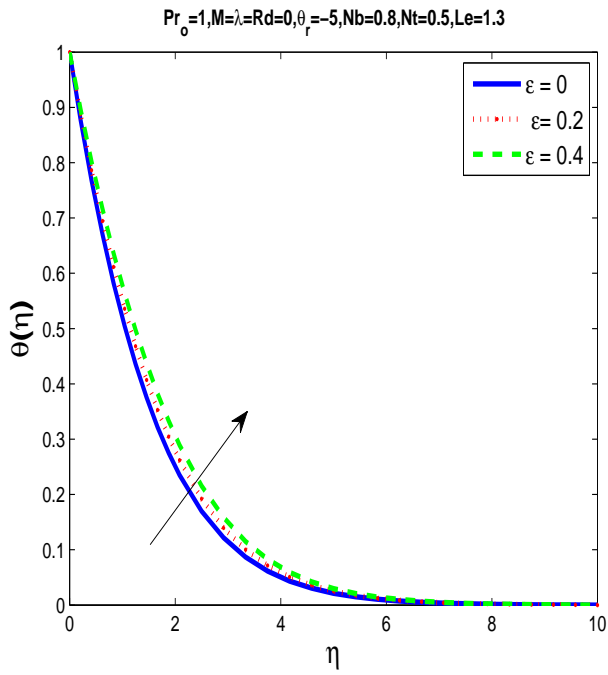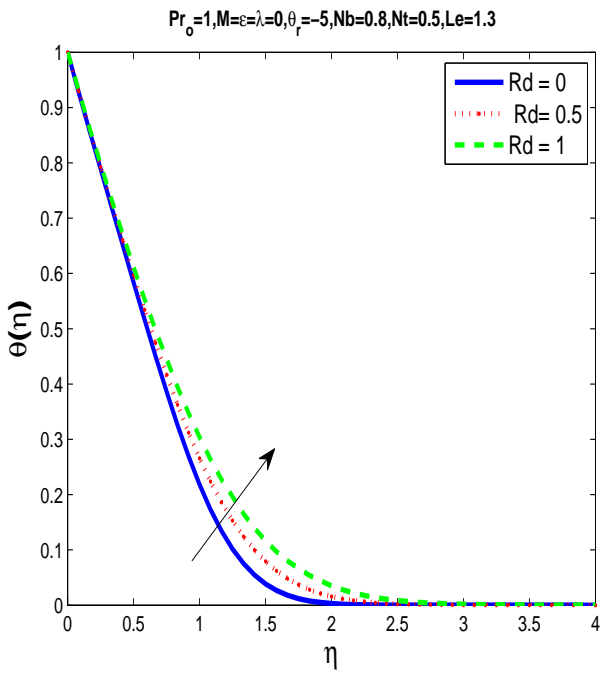


Figure 2.10: Temperature profile $\theta(\eta)$ for different $Rd$ (**For Case B**).
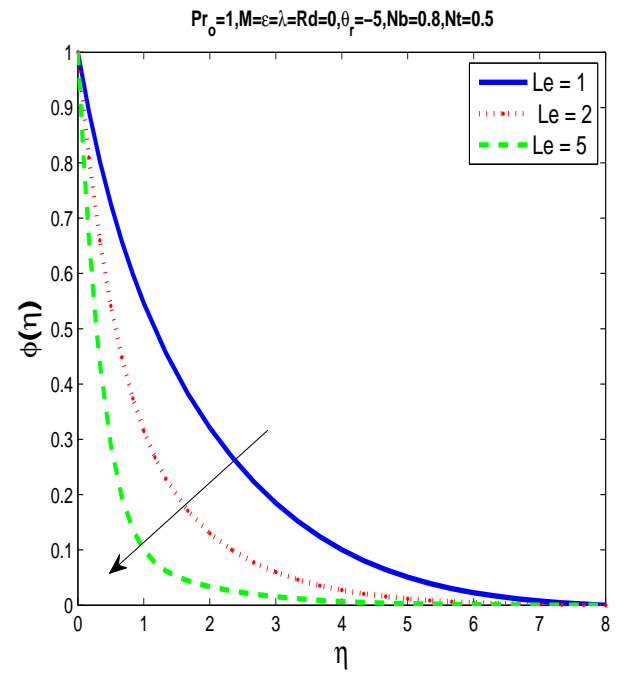


Figure 2.11: Concentration profile $\phi(\eta)$ for different $Le$ (**For Case B**).

Table 2.5: (**For Case B**)Comparison of $-f''(0)$ , $-\theta'(0)$ and $-\phi'(0)$ for distinct values of $\epsilon$ and $\lambda$ when $Rd = M = 0, Pr_0 = 6.8, \theta_r = -5, Le = 1.3$.

| $\lambda$ | $\epsilon$ | $-f''(0)$ | $-\theta'(0)$ | $-\phi'(0)$ |
|---|---|---|---|---|
| | | bvp4c method | bvp4c method | bvp4c method |
| 0 | 0 | 1.4312 | 0.8726 | 0.8183 |
| 0 | 0.2 | 1.4305 | 0.8493 | 0.8282 |
| 0 | 0.4 | 1.4299 | 0.8279 | 0.8371 |
| 0.5 | 0 | 0.9808 | 0.7861 | 1.1090 |
| 0.5 | 0.2 | 0.9805 | 0.7750 | 1.1126 |
| 0.5 | 0.4 | 0.9802 | 0.7641 | 1.1160 |
| 2 | 0 | -3.0219 | 0.7244 | 1.8063 |
| 2 | 0.2 | -3.0217 | 0.7406 | 1.7933 |
| 2 | 0.4 | -3.0213 | 0.7529 | 1.7826 |
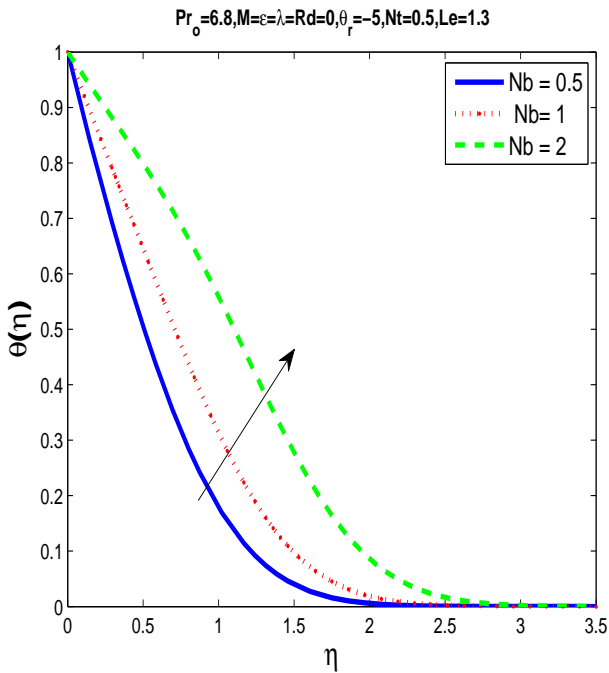


Figure 2.12: Temperature profile $\theta(\eta)$ for different $Nb$ (**For Case B**).
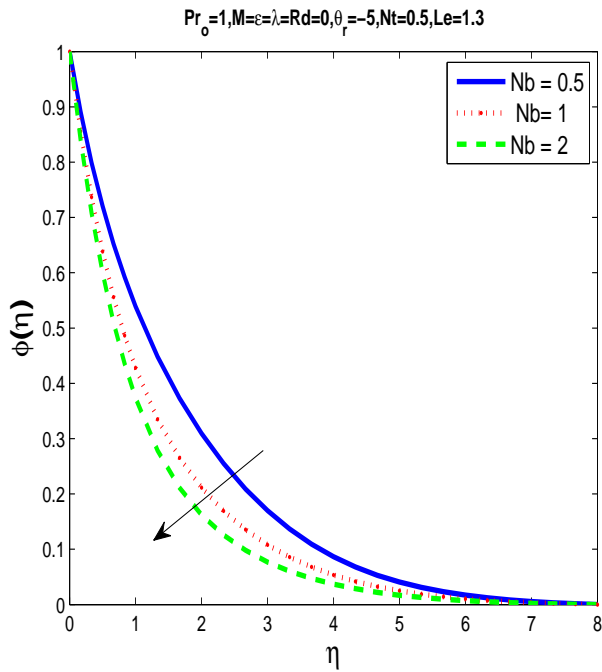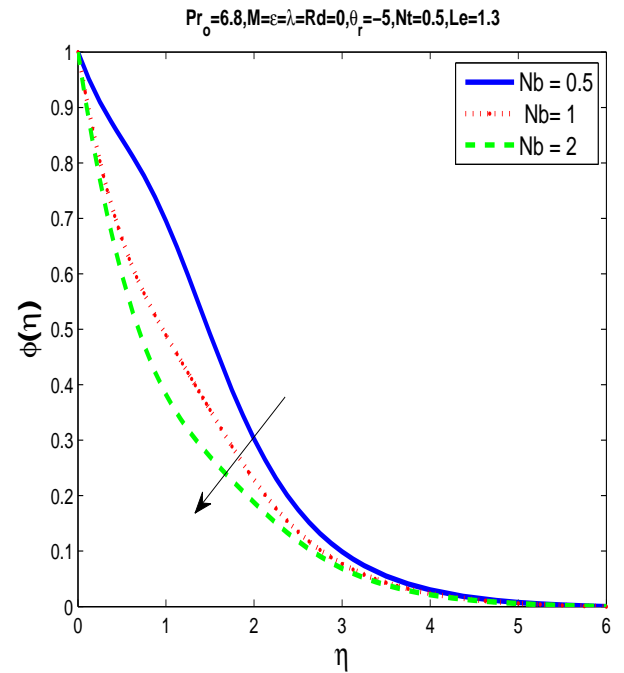


Figure 2.13: Concentration profile $\phi(\eta)$ for different $Nb$ (**For Case B**).
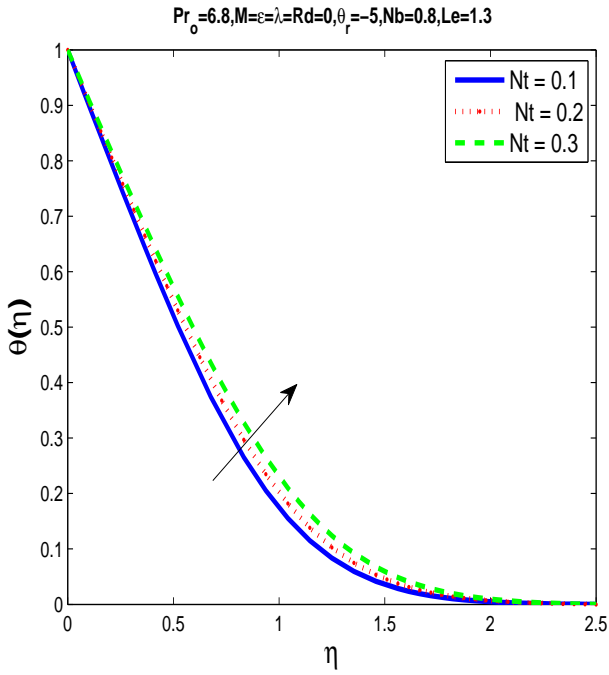
Figure 2.14: Temperature profile $\theta(\eta)$ for different $Nt$ (**For Case B**).
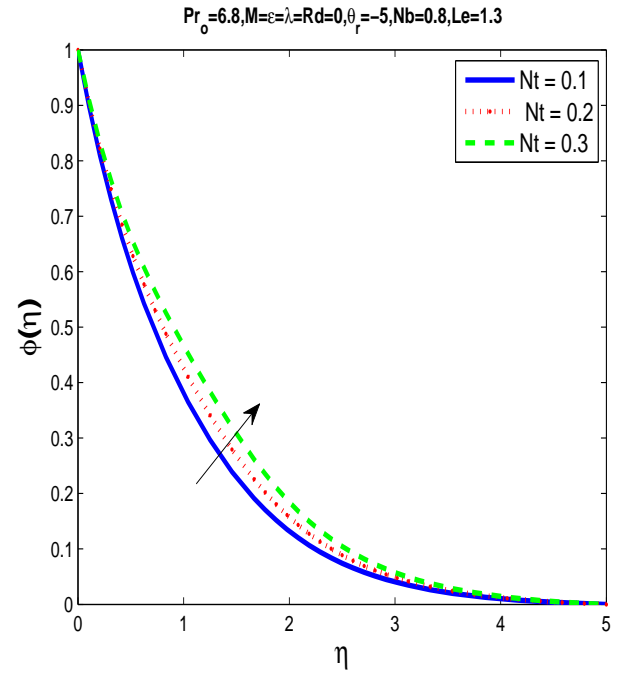


Figure 2.15: Concentration profile $\phi(\eta)$ for different $Nt$ (**For Case B**).
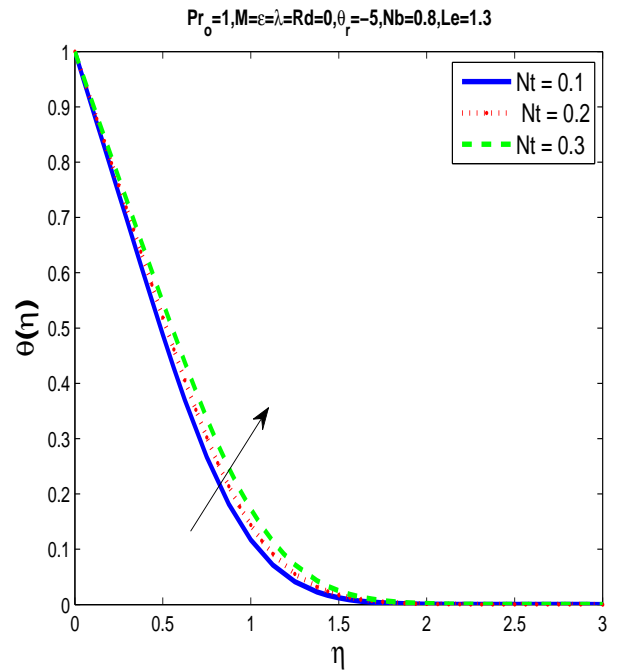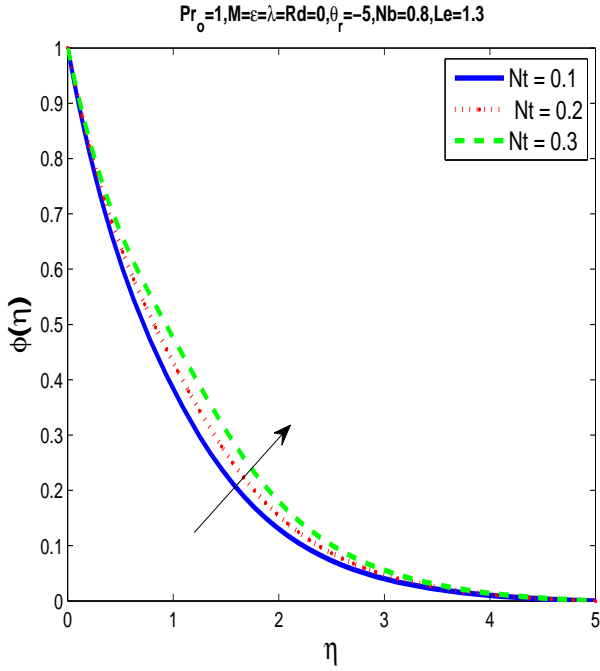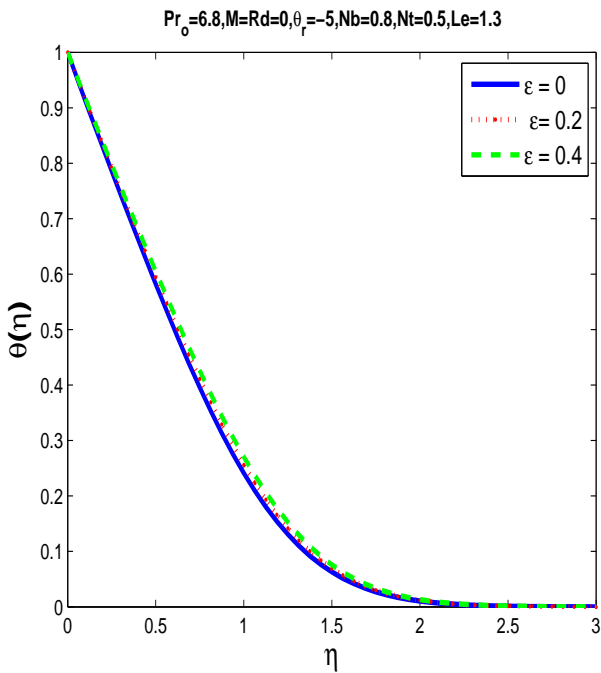


Figure 2.16: Temperature profile $\theta(\eta)$ for different $\epsilon$ (**For Case B**).
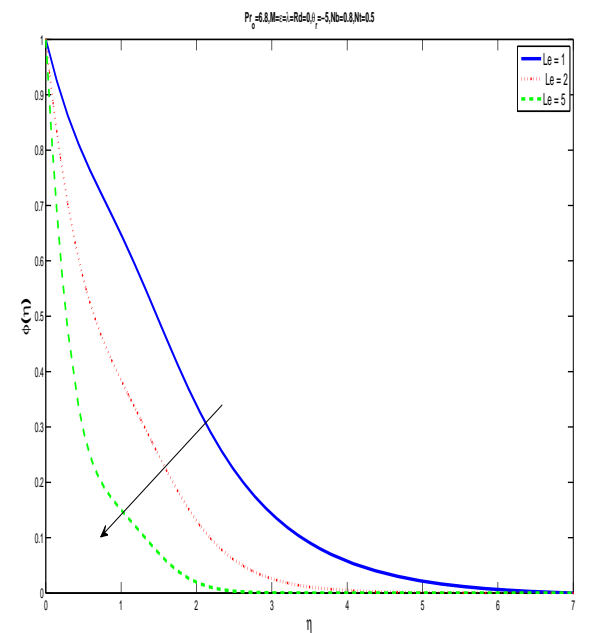


Figure 2.17: Concentration profile $\phi(\eta)$ for different $Le$ (**For Case B**).
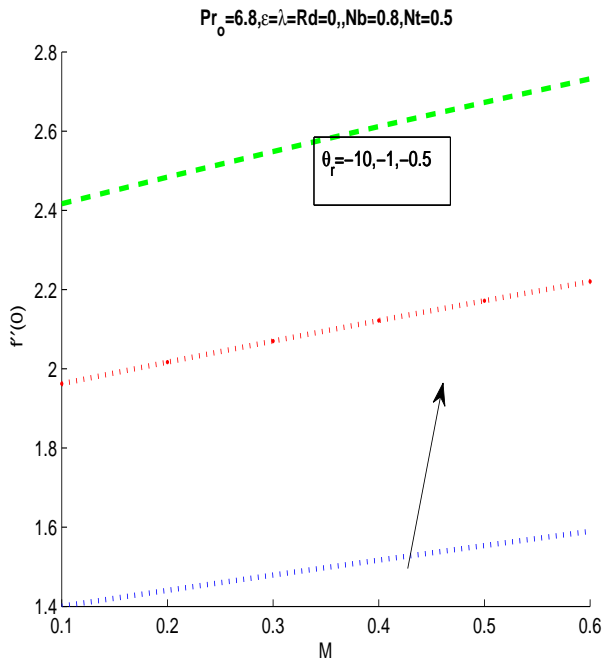
Figure 2.18: The skin friction coefficient with variations of $M$ and $\theta_r$ (**For Case B).**
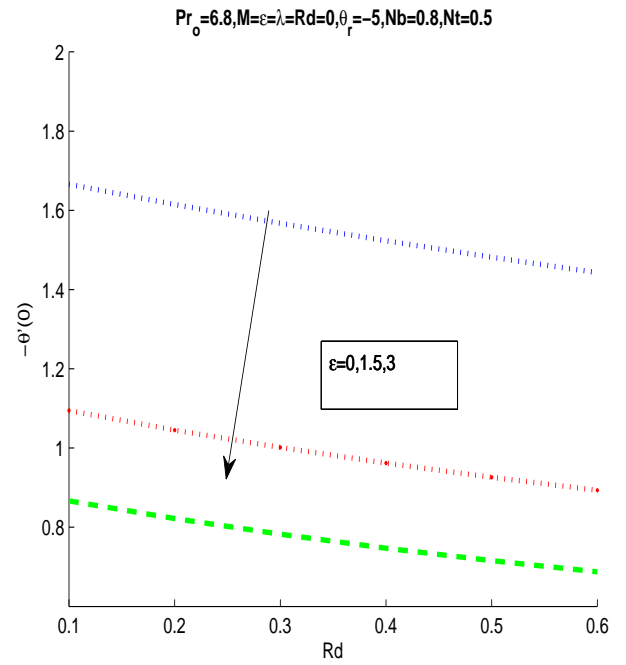


Figure 2.19: The reduced Nusselt number with variations of $\epsilon$ and $Rd$ (**For Case B).**
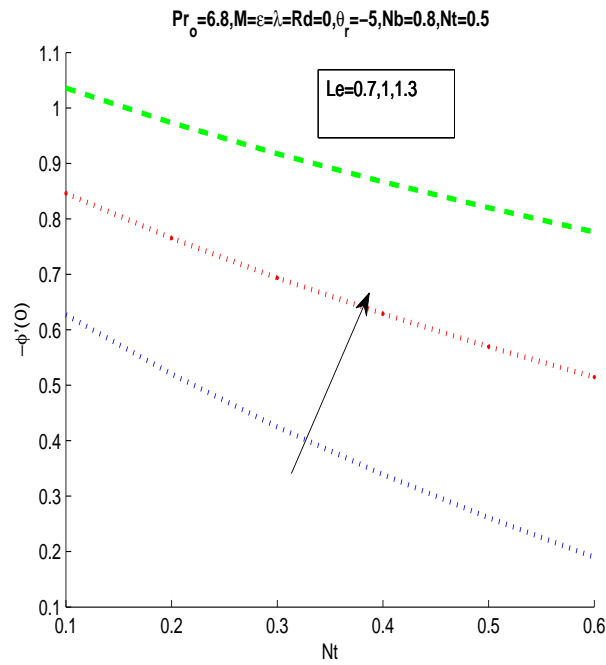


Figure 2.20: The reduced Sherwood number with variations of $Nt$ and $Le$ (**For Case B).**

## 2.6 Conclusions

The current study offers the findings of a two-dimensional, incompressible, MHD flow through an exponentially stretched surface whereas treating viscosity and thermal conductivity constant in Case A and variable for Case B. The significance of distinct pertinent parameters on velocity, temperature and concentration distributions are examined. The study's main results for Case B are as follows:

- Momentum boundary layer thickness decrease by increasing $\theta_r$ and $M$.

- Thermal boundary layer thickness increases by increasing $\epsilon$, $N_b$ and $N_t$.

- Thermal boundary layer thickness decreases by increasing $Pr_0$ whereas increases for $Rd$.

- Thickness of concentration boundary layer stretches by rising $N_t$ whereas decreases by increasing $N_b$ and $Le$.

# Chapter 3

# Thermophoretic MHD Flow with Variable Fluid Properties over a Radiative Exponentially Stretching Sheet

This chapter analyzed the impact of changeable viscosity and thermal conductivity due to an exponentially stretching surface in MHD radiating free stream Newtonian fluid through porous media along with internal heat generation/absorption. The underlying problem consists of mass, momentum and energy equations, which are transformed by implying appropriate similarity transformations into ODEs. Employing the shooting technique, the reduced nonlinear ODEs has been solved numerically and tested with MATLAB built-in solver *bvp4c*. The numerical data produced for $c_{fx_1}$, $Nu_{x_1}$ and $Sh_{x_1}$ are matched with the published literature,the produced results shows close agreement. In addition, the profiles of momentum, thermal, and concentration are discussed through graphically. It is noted that $C_{fx_1}$ enhances for enhancing values of $\theta_r$, $M$ and $Kp$ which causes reduction in velocity of the fluid flow. On the other $Nu_{x_1}$ and $Sh_{x_1}$ decreases for higher values of $\theta_r$ and $\epsilon$. Heat transfer rate is higher for constant fluid properties when compared with variable fluid properties.

Structuring of this chapter is given below.

Introductory part of this chapter is described in section 3.1. Theoretical model of the chapter is discussed in section 3.2. The study regrading fluid properties is presented in section 3.3.

We explore the numerical procedures in Section 3.4. The results and discussion part of the chapter is described in section 3.5 through graph and tables. The conclusion of the chapter is drawn in Section 3.6.

## 3.1   Introduction

The effect of thermophoresis, viscous dissipation and Joule heating on MHD flow was discussed by Reddy [120]. Swain et al. [121] analyzed the impact of heat and mass transfer MHD flow with changeable liquid characteristics in porous medium. Ali et al. [122]discussed the thermophoresis effect of MHD thin film fluid flow with variable fluid characteristics. The effect of thermophoretic diffusion and Brownian motion while considering variable fluid properties was analyzed by irfan [123]. He reported the aspects of chemical reaction and heat source sink. Ogunseye et al. [124] examined the influence of thermophoresis on powell-eyring nanofluid flow with chemical reaction and changeable thermal conductivity. Khan et al. [125] explored non-Newtonian fluid flow considering variable fluid properties past an unsteady stretching sheet. The study of thermophoresis and thermal radiation for second grade fluid over a stretching surface with variable fluid properties was investigated by Khan et al. [126]. All previous studies mostly considered constant fluid properties. Nonetheless addressing variable fluid properties is equally important. For deeper understanding, the objective of this work is to present constant and variable physical effects together so that comparison between two is easier.

## 3.2   Problem Formulation

We examine MHD thermophoretic, steady, laminar flow through an exponentially stretched surface along with thermal radiation, variable viscosity, variable thermal conductivity, variable heat generation and variable permeability. The sheet is taken at $y_1 = 0$. A constant magnetic field $B_o$ has also been applied normal to the surface. Flow geometry is displayed in Fig. 3.1 where $x_1$ and $y_1$ axes are along and perpendicular to the surface respectively.

The velocity of stretching surface and free stream are designated as $U_w = ae^{\frac{x_1}{L}}$, $U_\infty = be^{\frac{x_1}{L}}$ respectively $(a, b > 0)$. A changeable magnetic field $B(x_1) = B_o e^{\frac{x_1}{2L}}$ has been implemented normal to the sheet. $T_w$ and $C_w$ are the temperature and concentration at the surface of the

$u_1 \to U_\infty, T_1 \to T_\infty, C_1 \to C_\infty, y_1 \to \infty$

Concentration boundary layer

Thermal boundary layer

Momentum boundary layer

$y_1$ axis

MHD

$x_1$ axis

Stretching sheet

$y_1 = 0$

$U_w$      $T_w,$      $C_w$
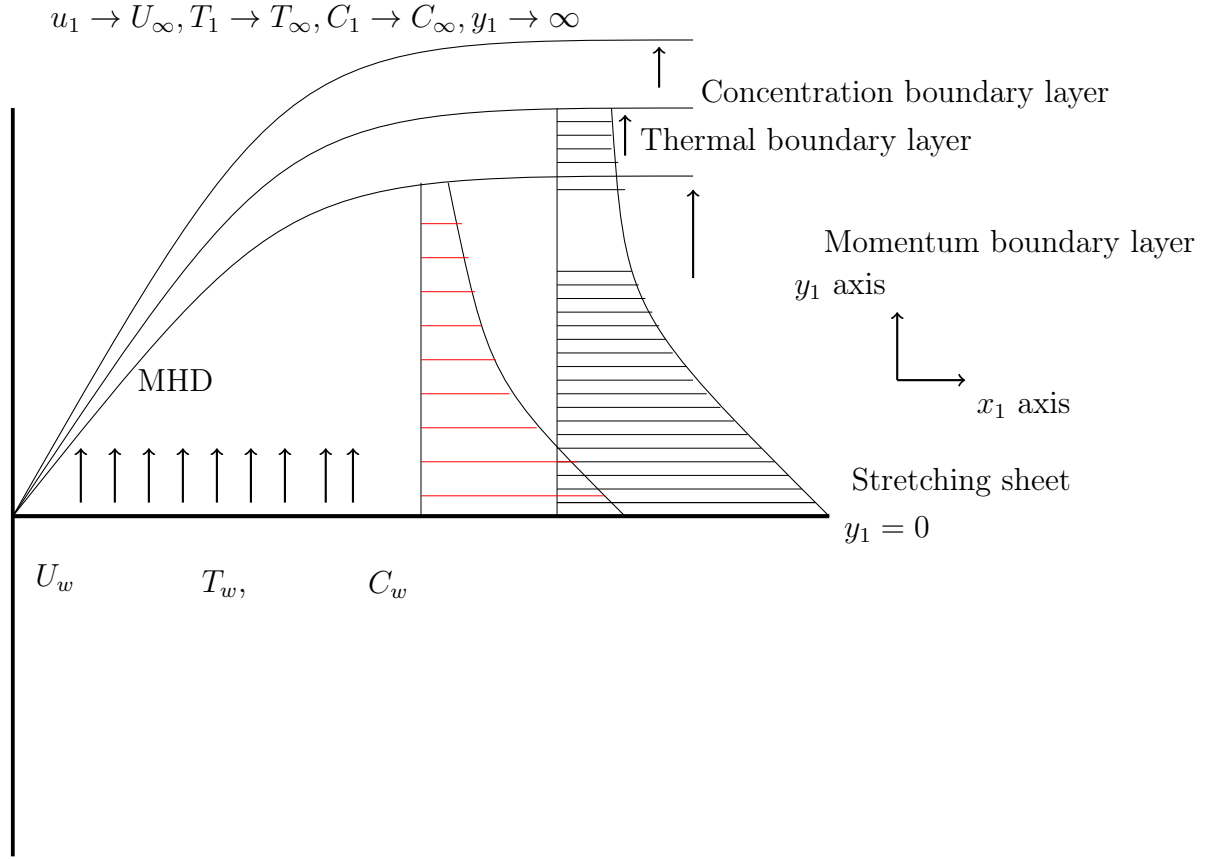
Figure 3.1: Geometry of the problem.

sheet respectively. $T_\infty$ and $C_\infty$ are designated as ambient temperature and concentration, respectively. The two dimensional magnetohydrodynamic flow equations are given as Swain et al. [121] and Reddy [120],

$$\frac{\partial u_1}{\partial x_1} + \frac{\partial v_1}{\partial y_1} = 0, \tag{3.1}$$

$$u_1 \frac{\partial u_1}{\partial x_1} + v_1 \frac{\partial u_1}{\partial y_1} = u_\infty \frac{du_\infty}{dx_1} + \frac{1}{\rho_1} \frac{\partial}{\partial y_1}\left(\frac{\mu_1 \partial u_1}{\partial y_1}\right) - \frac{\sigma B_o^2}{\rho_1}(u_1 - u_\infty) - \frac{\mu_1}{\rho_1 K p^*(x)}(u_1 - u_\infty), \tag{3.2}$$

$$u_1 \frac{\partial T_1}{\partial x_1} + v_1 \frac{\partial T_1}{\partial y_1} = \frac{1}{\rho_1 c_p} \frac{\partial}{\partial y_1}\left(\frac{k_1 \partial T_1}{\partial y_1}\right) - \frac{1}{\rho_1 c_p} \frac{\partial q_r}{\partial y_1} + \frac{\mu_1}{\rho_1 c_p}\left(\frac{\partial u_1}{\partial y_1}\right)^2 + \frac{\sigma B_o^2}{\rho_1 c_p}(u_\infty - u_1)^2 +$$
$$\frac{\mu_1}{\rho_1 c_p K p^*(x_1)}(u_\infty - u_1)^2 + \frac{Q(x_1)}{\rho_1 c_p}(T_1 - T_\infty), \tag{3.3}$$

$$u_1 \frac{\partial C_1}{\partial x_1} + v_1 \frac{\partial C_1}{\partial y_1} = D_1 \frac{\partial^2 C_1}{\partial y_1^2} - \frac{\partial}{\partial y_1}(V_{T_1}(C_1 - C_\infty)), \tag{3.4}$$

where $V_{T_1} = \frac{-t_p \mu_1}{\rho_1 T_f} \frac{\partial T_1}{\partial y_1}$ is the thermophoretic velocity, $\mu_1$ is the coefficient of fluid viscosity, $\sigma$ is the electrical conductivity of fluid, $B_o$ is uniform magnetic field along positive $y_1$ direction, $u_1$ and $v_1$ are th components of velocity in $x_1-$ and $y_1-$ directions respectively. Here $T_1$

is the temperature, $C_1$ is the concentration of nanoparticles, $Kp^*(x) = Kp_o e^{\frac{-x_1}{L}}$ is permeability of the porous medium, $c_p$ is the specific heat constant, $D$ is the molecular diffusivity coefficient, $q_r$ is the radiative heat flux, and $Q(x_1) = Q_o e^{\frac{x_1}{L}}$ is the volumetric rate of heat generation/absorption.

The above system is completed with the following appropriate boundary conditions as Swain et al. [121],

$$u_1 = U_w(x_1) = ae^{\frac{x_1}{L}}, \quad v_1 = 0, \quad T_1 = T_w, \quad C_1 = C_w \quad at \quad y_1 = 0,$$

$$u_1 \longrightarrow U_\infty(x_1) = be^{\frac{x_1}{L}}, \quad T_1 \longrightarrow T_\infty, \quad C_1 \longrightarrow C_\infty \quad as \quad y_1 \longrightarrow \infty. \quad (3.5)$$

The non-dimensional similarity variables are presented as Ishak [30]:

$$\eta = \sqrt{\frac{a}{2\nu_1 L}}e^{\frac{x_1}{2L}}y_1, \qquad \psi = \sqrt{2a\nu_1 L}e^{\frac{x_1}{2L}}f(\eta), \qquad \theta(\eta) = \frac{T_1 - T_\infty}{T_w - T_\infty}, \qquad \phi(\eta) = \frac{C_1 - C_\infty}{C_w - C_\infty},$$

$$u_1 = ae^{\frac{x_1}{L}}f'(\eta), \quad v_1 = -\sqrt{\frac{\nu_1 a}{2L}}e^{\frac{x_1}{2L}}(f(\eta) + \eta f'(\eta)).$$

$$(3.6)$$

After employing non-dimensional variables stated in Eq. (3.6) into (3.1)-(3.4). We acquired the transformed ODEs as:

$$\left(\frac{\mu_1}{\mu_o}f''\right)' + 2(\lambda^2 - f'^2) + ff'' - (M + Kp\frac{\mu_1}{\mu_o})(f' - \lambda) = 0, \quad (3.7)$$

$$(1 + \frac{4}{3}Rd)(\frac{k_1}{k_o}\theta')' + Pr_o(f\theta' - f'\theta + Ec(M + Kp\frac{\mu_1}{\mu_o})(f' - \lambda)^2 + Ec\frac{\mu_1}{\mu_o}f''^2 + s\theta) = 0, \quad (3.8)$$

$$\phi'' + Sc(f\phi' - f'\phi) - \tau Sc(\frac{\mu_1}{\mu_o}\theta'\phi' + \phi(\frac{\mu_1}{\mu_o}\theta')') = 0. \quad (3.9)$$

The transformed boundary conditions corresponding to above non-dimensional variable is presented as:

$$f(\eta) = 0, \quad f'(\eta) = 1, \quad \theta(\eta) = 1, \quad \phi(\eta) = 1 \quad at \quad \eta = 0,$$

$$f'(\eta) = \lambda, \quad \theta(\eta) = 0, \quad \phi(\eta) = 0, \quad and \quad \eta \to \infty. \quad (3.10)$$

where local magnetic field constant is designated as $M = \frac{2\sigma B_0^2 L}{\rho a}$ ,$Kp = \frac{2\nu L}{aKp_o}$ is the porosity parameter, $Rd = \frac{4\sigma T_\infty^3}{k_o k^*}$ denotes the radiative heat transfer parameter, Eckert number is denoted by $Ec = \frac{U_w^2}{(T_w - T_\infty)c_p}$ (Rao et al. [160]), $s = \frac{2LQ_o}{a\rho_1 c_p}$ local heat source/sink parameter, $\tau = \frac{-t_p(T_w - T_\infty)}{T_f}$ is thermal diffusion coefficient,$Pr_o = \frac{\mu_o c_p}{k_o}$ denotes the ambient Prandtl number and $Sc = \frac{\nu_1}{D}$ is Schmidt number.

## 3.3 Analysis on Fluid Properties

In this section, we illustrate the main theme of this work in the following two subsections.

### 3.3.1 Constant Fluid Properties

For this case we rewrite Eqs. (3.7), (3.8) and (3.9) into the set of ODEs as,

$$f''' + 2(\lambda^2 - f'^2) + ff'' - (M + Kp)(f' - \lambda) = 0, \tag{3.11}$$

$$(1 + \frac{4}{3}Rd)\theta'' + Pr_o(f\theta' - f'\theta + Ec(M + Kp)(\lambda - f')^2 + Ecf''^2 + s\theta) = 0, \tag{3.12}$$

$$\phi'' + Sc(f\phi' - f'\phi) - \tau Sc(\phi'\theta' + \phi\theta'') = 0. \tag{3.13}$$

### 3.3.2 Variable Fluid properties

In this case we write viscosity and thermal conductivity as defined below,

$$\mu_1(T_1) = \frac{\mu_{ref}}{1 + \gamma_1(T_1 - T_{ref})}. \tag{3.14}$$

We follow Andersson and Aarseth [112] to write above expression (3.14) in which the $\gamma$ is a fluid property. If $T_\infty \approx T_{ref}$ the above formula becomes,

$$\mu_1 = \frac{\mu_o}{1 - \frac{T_1 - T_\infty}{\theta_r(T_w - T_\infty)}} = \frac{\mu_o}{1 - \frac{\theta(\eta)}{\theta_r}}, \tag{3.15}$$

here $\theta_r = \frac{-1}{\gamma_1(T_w - T_\infty)}$. If the above viscosity relation is incorporated in Eq. (3.7) and (3.9) then it can be rewritten as,

$$\frac{\theta_r}{(\theta r - \theta)}f''' + \frac{f''\theta'\theta_r}{(\theta_r - \theta)^2} + 2(\lambda^2 - f'^2) + ff'' - (M + Kp\frac{\theta_r}{\theta_r - \theta})(f' - \lambda) = 0, \tag{3.16}$$

$$\phi'' + Sc(f\phi' - f'\phi) - \tau Sc(\frac{\theta_r}{\theta_r - \theta})(\theta'\phi' + \theta''\phi + \frac{\theta'^2\phi}{\theta_r - \theta}) = 0. \tag{3.17}$$

The variable thermal conductivity is expressed in terms of temperature by following Prasad et al. [117] as,

$$k_1(T) = k_o(1 + \epsilon\theta). \tag{3.18}$$

Under this above relation the mathematical form of Eq. (3.8) can be described as

$$(1 + \frac{4}{3}R_d)((1 + \epsilon\theta)\theta'' + \epsilon\theta'^2) + Pr_o(f\theta' - f'\theta + Ec(M + (\frac{\theta_r}{\theta_r - \theta})Kp)(\lambda - f')^2 + Ec(\frac{\theta_r}{\theta_r - \theta})f''^2 + s\theta) = 0. \tag{3.19}$$

Expression for the skin resistance $C_{fx_1}$, local Nusselt number $Nu_{x_1}$ and local Sherwood number $Sh_{x_1}$, are indicated as,

$$C_{fx_1} = \frac{\tilde{\tau}_w}{\rho_1 u_w^2}, \quad Nu_{x_1} = -\frac{x_1 q_w}{k_o(T_w - T_\infty)} \quad \text{and} \quad Sh_{x_1} = -\frac{x_1 j_w}{C_w - C_\infty}, \quad (3.20)$$

where $q_w$ is heat flux, $\tilde{\tau}_w$ is wall shear stress and $j_w$ is mass flux.

$$\tilde{\tau}_w = \mu_1(\frac{\partial u_1}{\partial y_1})_{y_1=0}, \quad q_w = k_o(\frac{\partial T_1}{\partial y_1})_{y_1=0} \quad \text{and} \quad j_w = -D_B(\frac{\partial C_1}{\partial y_1})_{y_1=0}, \quad (3.21)$$

By inserting the values of Eq. (3.21) into Eq. (3.20) the $C_{fx_1}$, $Nu_{x_1}$ and $Sh_{x_1}$ are converted to

$$C_{fx_1} = \frac{\theta_r}{(\theta_r - 1)} \frac{1}{\sqrt{Re_{x_1}}} f''(0), \quad Nu_{x_1} = -(1 + \frac{4Rd}{3})\sqrt{\frac{x_1 Re_{x_1}}{2L}}\theta'(0) \quad \text{and} \quad Sh_{x_1} = -\sqrt{\frac{x Re_{x_1}}{2L}}\phi'(0).$$

$$(3.22)$$

## 3.4  Numerical Procedure

### 3.4.1  Shooting Method

The system of ODEs for Case A and Case B is solved by using shooting technique in MATLAB. To apply the shooting algorithm, we transformed the BVP into an IVP and reduce the higher order ODEs into a system of first order ODEs. We have applied Newton-Raphson method to locate the root. Finally, the Runge-Kutta method of order five was implemented to determine the solution of IVP. The transformed system of first order ODEs for Case A and Case B are written as,

(a) Case A:

$$f = z_1, f' = z_2, f'' = z_3, f''' = z_3' = -2(\lambda^2 - z_2^2) - z_1 z_3 + (M + Kp)(z_2 - \lambda),$$

$$z_4 = \theta, z_5 = \theta', \theta'' = z_5' = -\frac{Pr_o}{(1 + \frac{4}{3}Rd)}(z_1 z_5 - z_2 z_4 + Ec(M + Kp)(\lambda - z_2)^2 + Ec z_3^2 + s z_4),$$

$$z_6 = \phi, z_7 = \phi', \phi'' = z_7' = -Sc(z_1 z_7 - z_2 z_6) + \tau Sc(z_5 z_7 + z_6 z_5').$$

(b) Case B:

$$f = z_1, f' = z_2, f'' = z_3,$$

$$f''' = z_3' = \frac{(z_3 z_5)}{(z_4 - \theta_r)} + \frac{(z_4 - \theta_r)}{\theta_r}(2(\lambda^2 - z_2^2) + z_1 z_3 - (M + Kp(\frac{\theta_r}{\theta_r - z_4}))(z_2 - \lambda)),$$

$$z_4 = \theta, z_5 = \theta', \theta'' = z_5' = \frac{-\epsilon z_5^2}{1 + \epsilon z_4} - \frac{Pr_o}{(1 + \epsilon z_4)(1 + \frac{4}{3}Rd)}(z_1 z_5 - z_2 z_4 +$$

$$Ec(M + Kp(\frac{\theta_r}{\theta_r - z_4}))(\lambda - z_2)^2 + Ec(\frac{\theta_r}{\theta_r - z_4})z_3^2 + sz_4),$$

$$z_6 = \phi, z_7 = \phi', \phi'' = z_7' = -Sc(z_1 z_7 - z_2 z_6) + \tau Sc(\frac{\theta_r}{\theta_r - z_4})(z_6 z_5' + z_5 z_7 + \frac{z_5^2 z_6}{\theta_r - z_4}).$$

### 3.4.2 bvp4c

By bvp4c algorithm, we can solve the BVP for ODEs. The results obtained by shooting method is validated by using MATLAB built-in solver bvp4c, which uses collocation method in the background. It starts solution with an initial guess supplied at an initial mesh points and changes step-size (hence changes mesh) to get the specified accuracy.

## 3.5 Result and Discussion

For the verification of accuracy of the applied numerical scheme, comparisons of the present results corresponding to the values of $-\theta'(0)$ for separate values of $Pr_o$, $Rd$ and $M$ are made with the available published results and presented in Table 3.1. The obtained results are found in excellent agreement.

Effect of various governing parameters on $C_{fx_1}$, $Nu_{x_1}$ and $Sh_{x_1}$ for both constant and variable fluid properties cases are shown in Tables 3.2 and 3.3 respectively. It is observed that $C_{fx_1}$ is higher in Case B when compared to Case A for increasing values of $M$, $Kp$ and $\lambda$. It is observed that $Nu_{x_1}$ declines in Case B compared to Case A for distinct values of $M$, $Kp$, $Rd$, $s$, $\lambda$ and $Pr_o$. It is analyzed that the $Sh_{x_1}$ shows reduction in Case B as compared to Case A for the higher values of $\lambda$, $Pr_o$, $Sc$ and $\tau$, $M$, $Kp$, $Rd$ and $s$.

Table 3.1: Comparison of $-\theta'(0)$ for distinct values of $Pr_o$ and $Rd$, $M$ (Case A).

| $Rd$ | $M$ | $Pr_o$ | Mabood et al. [31] | Rajendar et al. [4] | Isa et al. [9] | Khalili et al. [34] | Current Results |
|---|---|---|---|---|---|---|---|
| 0 | 0 | 1 | 0.95478 | 0.954705 | 0.9548 | 0.954955 | 0.9548 |
| | | 2 | 1.47151 | 1.471551 | 1.4715 | 1.471421 | 1.4715 |
| | | 3 | 1.86909 | 1.86958 | 1.8691 | 1.869044 | 1.8691 |
| | | 5 | 2.50012 | 2.50221 | 2.5001 | 2.500109 | 2.5001 |
| | | 10 | 3.66039 | 3.670012 | 3.6604 | - | 3.6603 |
| 1 | 0 | 1 | 0.53121 | 0.53108 | 0.5313 | - | 0.5312 |
| 0 | 1 | 1 | 0.86113 | 0.86096 | 0.8615 | - | 0.8611 |
| 0.5 | 0 | 2 | 1.07352 | 1.073455 | 1.0735 | - | 1.0735 |
| | 0 | 3 | 1.38075 | 1.38078 | 1.3807 | - | 1.3808 |
| 1 | 0 | 3 | 1.12142 | 1.12137 | 1.1214 | - | 1.1214 |
| 1 | 1 | 1 | 0.45052 | 0.45045 | 0.4506 | - | 0.4505 |

Fig. 3.2 describes the velocity profile for different values of $\lambda$. It shows that the velocity rises by increasing free stream parameter $\lambda$ and we notice an inverted boundary layer structure for $\lambda > 1$. This inverted boundary layer is constructed, when the stretching surface velocity is lower than that of free stream velocity.

Fig. 3.3 presents the velocity profile for different $M$. It is observed that the presence of $M$ introduce Lorentz force in the flow. This Lorentz force produce a retarding force. Therefore, by increasing magnetic parameter the retarding force also increases due to which velocity profile decreases. Velocity has a higher value for Case A as compare to Case B.

Fig. 3.4 illustrates the influence of $\theta_r$ on velocity distribution. It is noticed that an enhancement in $\theta_r$ produce more friction, which lowers the velocity of flow field.

The effect of $Kp$ is depicted in Fig. 3.5. It can be recognized that velocity distribution decreases by increasing porosity parameter. The presence of $Kp$ causes higher diminution, which in turns decelerate the velocity of the flow field. Velocity has a higher value for Case A as compare to Case B.

Table 3.2: Comparison of $-f''(0)$, $-\theta'(0)$ and $-\phi'(0)$ for distinct $M$, $Kp$, $\lambda$, $Pr_o$, $Rd$, $s$, $\tau$, $Ec$ and $Sc$ (Case A).

| | | | | | | | | | bvp4c | S.M | bvp4c | S.M | bvp4c | S.M |
|---|---|---|---|---|---|---|---|---|---|---|---|---|---|---|
| M | Kp | $\lambda$ | $Pr_o$ | Rd | s | Ec | Sc | $\tau$ | $-f''(0)$ | $-f''(0)$ | $-\theta'(0)$ | $-\theta'(0)$ | $-\phi'(0)$ | $-\phi'(0)$ |
| 0 | 0.2 | 0.1 | 1 | 0.2 | 0.1 | 0.2 | 1 | 0.2 | 1.3169 | 1.3169 | 0.6841 | 0.6841 | 1.0631 | 1.0631 |
| 0.3 | | | | | | | | | 1.4065 | 1.4065 | 0.6480 | 0.6480 | 1.0403 | 1.0403 |
| 0.6 | | | | | | | | | 1.4906 | 1.4906 | 0.6153 | 0.6153 | 1.0195 | 1.0196 |
| 0.3 | 0 | 0.1 | 1 | 0.2 | 0.1 | 0.2 | 1 | 0.2 | 1.3475 | 1.3475 | 0.6716 | 0.6717 | 1.0552 | 1.0552 |
| | 0.5 | | | | | | | | 1.4906 | 1.4906 | 0.6153 | 0.6153 | 1.0195 | 1.0196 |
| | 1 | | | | | | | | 1.6211 | 1.6211 | 0.5667 | 0.5667 | 0.9889 | 0.9889 |
| 0.3 | 0.2 | 0 | 1 | 0.2 | 0.1 | 0.2 | 1 | 0.2 | 1.4665 | 1.4664 | 0.5423 | 0.5423 | 0.9842 | 0.9842 |
| | | 0.5 | | | | | | | 0.9480 | 0.9480 | 0.8816 | 0.8816 | 1.2152 | 1.2152 |
| | | 0.9 | | | | | | | 0.2177 | 0.2177 | 1.0473 | 1.0473 | 1.3644 | 1.3644 |
| 0.3 | 0.2 | 0.1 | 0.71 | 0.2 | 0.1 | 0.2 | 1 | 0.2 | 1.4065 | 1.4065 | 0.5170 | 0.5173 | 1.0204 | 1.0205 |
| | | | 1 | | | | | | 1.4065 | 1.4065 | 0.6480 | 0.6480 | 1.0403 | 1.0403 |
| | | | 2 | | | | | | 1.4065 | 1.4065 | 0.9963 | 0.9964 | 1.0951 | 1.0951 |
| 0.3 | 0.2 | 0.1 | 1 | 0 | 0.1 | 0.2 | 1 | 0.2 | 1.4065 | 1.4065 | 0.7535 | 0.7536 | 1.0566 | 1.0566 |
| | | | | 0.4 | | | | | 1.4065 | 1.4065 | 0.5719 | 0.5720 | 1.0287 | 1.0287 |
| | | | | 0.8 | | | | | 1.4065 | 1.4065 | 0.4682 | 0.4683 | 1.0132 | 1.0132 |
| 0.3 | 0.2 | 0.1 | 1 | 0.2 | 0 | 0.2 | 1 | 0.2 | 1.4065 | 1.4065 | 0.7172 | 0.7172 | 1.0511 | 1.0511 |
| | | | | | 0.1 | | | | 1.4065 | 1.4065 | 0.6480 | 0.6480 | 1.0403 | 1.0403 |
| | | | | | 0.2 | | | | 1.4065 | 1.4065 | 0.5652 | 0.5652 | 1.0275 | 1.0275 |
| 0.3 | 0.2 | 0.1 | 1 | 0.2 | 0.1 | 0.3 | 1 | 0.2 | 1.4065 | 1.4065 | 0.5981 | 0.5981 | 1.0315 | 1.0315 |
| | | | | | | 0.7 | | | 1.4065 | 1.4065 | 0.3986 | 0.3986 | 0.9965 | 0.9965 |
| | | | | | | 1 | | | 1.4065 | 1.4065 | 0.2490 | 0.2490 | 0.9702 | 0.9702 |
| 0.3 | 0.2 | 0.1 | 1 | 0.2 | 0.1 | 0.2 | 0.7 | 0.2 | 1.4065 | 1.4065 | 0.6480 | 0.6480 | 0.8209 | 0.8209 |
| | | | | | | | 1 | | 1.4065 | 1.4065 | 0.6480 | 0.6480 | 1.0403 | 1.0403 |
| | | | | | | | 1.3 | | 1.4065 | 1.4065 | 0.6480 | 0.6480 | 1.2350 | 1.2350 |
| 0.3 | 0.2 | 0.1 | 1 | 0.2 | 0.1 | 0.2 | 1 | 0 | 1.4065 | 1.4065 | 0.6480 | 0.6480 | 0.9475 | 0.9475 |
| | | | | | | | | 0.5 | 1.4065 | 1.4065 | 0.6480 | 0.6480 | 1.1831 | 1.1831 |
| | | | | | | | | 1 | 1.4065 | 1.4065 | 0.6480 | 0.6480 | 1.4301 | 1.4301 |

Table 3.3: Comparison of $-f''(0)$, $-\theta'(0)$ and $-\phi'(0)$ for various $M$, $Kp$, $\lambda$, $Pr$, $Rd$, $s$, $Ec$, $\tau$, $\theta_r$, $\epsilon$ and $Sc$ (Case B)

| M | Kp | λ | $Pr_o$ | Rd | s | Ec | Sc | τ | $\theta_r$ | $\epsilon$ | bvp4c $-f''(0)$ | S.M $-f''(0)$ | bvp4c $-\theta'(0)$ | S.M $-\theta'(0)$ | bvp4c $-\phi'(0)$ | S.M $-\phi'(0)$ |
|---|---|---|---|---|---|---|---|---|---|---|---|---|---|---|---|---|
| 0 | 0.2 | 0.1 | 1 | 0.2 | 0.1 | 0.2 | 1 | 0.2 | -5 | 0.2 | 1.4500 | 1.4500 | 0.5847 | 0.5847 | 1.0138 | 1.0138 |
| 0.3 | | | | | | | | | | | 1.5483 | 1.5483 | 0.5532 | 0.5532 | 0.9916 | 0.9916 |
| 0.6 | | | | | | | | | | | 1.6405 | 1.6405 | 0.5249 | 0.5249 | 0.9717 | 0.9717 |
| 0.3 | 0 | 0.1 | 1 | 0.2 | 0.1 | 0.2 | 1 | 0.2 | -5 | 0.2 | 1.4929 | 1.4929 | 0.5712 | 0.5712 | 1.0044 | 1.0044 |
| | 0.5 | | | | | | | | | | 1.6274 | 1.6274 | 0.5283 | 0.5283 | 0.9740 | 0.9740 |
| | 1 | | | | | | | | | | 1.7505 | 1.7506 | 0.4916 | 0.4922 | 0.9480 | 0.9481 |
| 0.3 | 0.2 | 0 | 1 | 0.2 | 0.1 | 0.2 | 1 | 0.2 | -5 | 0.2 | 1.6093 | 1.6093 | 0.4496 | 0.4496 | 0.9329 | 0.9329 |
| | | 0.5 | | | | | | | | | 1.0486 | 1.0486 | 0.7727 | 0.7727 | 1.1702 | 1.1702 |
| | | 0.9 | | | | | | | | | 0.2413 | 0.2413 | 0.9258 | 0.9258 | 1.3208 | 1.3208 |
| 0.3 | 0.2 | 0.1 | 0.71 | 0.2 | 0.1 | 0.2 | 1 | 0.2 | -5 | 0.2 | 1.5446 | 1.5446 | 0.4390 | 0.4390 | 0.9775 | 0.9775 |
| | | | 1 | | | | | | | | 1.5483 | 1.5483 | 0.5532 | 0.5532 | 0.9916 | 0.9916 |
| | | | 2 | | | | | | | | 1.5577 | 1.5577 | 0.8616 | 0.8616 | 1.0311 | 1.0311 |
| 0.3 | 0.2 | 0.1 | 1 | 0 | 0.1 | 0.2 | 1 | 0.2 | -5 | 0.2 | 1.5512 | 1.5512 | 0.6462 | 0.6461 | 1.0033 | 1.0033 |
| | | | | 0.4 | | | | | | | 1.5462 | 1.5462 | 0.4866 | 0.4866 | 0.9834 | 0.9834 |
| | | | | 0.8 | | | | | | | 1.5433 | 1.5433 | 0.3970 | 0.3970 | 0.9724 | 0.9724 |
| 0.3 | 0.2 | 0.1 | 1 | 0.2 | 0 | 0.2 | 1 | 0.2 | -5 | 0.2 | 1.5502 | 1.5502 | 0.6183 | 0.6183 | 0.9999 | 0.9999 |
| | | | | | 0.1 | | | | | | 1.5483 | 1.5483 | 0.5532 | 0.5532 | 0.9916 | 0.9916 |
| | | | | | 0.2 | | | | | | 1.5458 | 1.5458 | 0.4734 | 0.4734 | 0.9817 | 0.9817 |
| 0.3 | 0.2 | 0.1 | 1 | 0.2 | 0.1 | 0.3 | 1 | 0.2 | -5 | 0.2 | 1.5476 | 1.5476 | 0.5140 | 0.5140 | 0.9859 | 0.9859 |
| | | | | | | 0.7 | | | | | 1.5449 | 1.5449 | 0.3579 | 0.3579 | 0.9628 | 0.9628 |
| | | | | | | 1 | | | | | 1.5429 | 1.5429 | 0.2411 | 0.2411 | 0.9456 | 0.9456 |
| 0.3 | 0.2 | 0.1 | 1 | 0.2 | 0.1 | 0.2 | 0.7 | 0.2 | -5 | 0.2 | 1.5483 | 1.5483 | 0.5532 | 0.5532 | 0.7830 | 0.7830 |
| | | | | | | | 1 | | | | 1.5483 | 1.5483 | 0.5532 | 0.5532 | 0.9916 | 0.9916 |
| | | | | | | | 1.3 | | | | 1.5483 | 1.5483 | 0.5532 | 0.5532 | 1.1767 | 1.1767 |
| 0.3 | 0.2 | 0.1 | 1 | 0.2 | 0.1 | 0.2 | 1 | 0 | -5 | 0.2 | 1.5483 | 1.5483 | 0.5532 | 0.5532 | 0.9273 | 0.9273 |
| | | | | | | | | 0.5 | | | 1.5483 | 1.5483 | 0.5532 | 0.5532 | 1.0904 | 1.0904 |
| | | | | | | | | 1 | | | 1.5483 | 1.5483 | 0.5532 | 0.5532 | 1.2608 | 1.2608 |
| 0.3 | 0.2 | 0.1 | 1 | 0.2 | 0.1 | 0.2 | 1 | 0.2 | -10 | 0.2 | 1.4795 | 1.4795 | 0.5595 | 0.5595 | 1.0083 | 1.0083 |
| | | | | | | | | | -1 | | 2.0003 | 2.0003 | 0.5123 | 0.5123 | 0.9016 | 0.9016 |
| | | | | | | | | | -0.5 | | 2.4335 | 2.4334 | 0.4764 | 0.4764 | 0.8367 | 0.8366 |
| 0.3 | 0.2 | 0.1 | 1 | 0.2 | 0.1 | 0.2 | 1 | 0.2 | -5 | 0 | 1.5504 | 1.5504 | 0.6341 | 0.6341 | 1.0025 | 1.0025 |
| | | | | | | | | | | 0.5 | 1.5458 | 1.5458 | 0.4684 | 0.4683 | 0.9806 | 0.9806 |
| | | | | | | | | | | 1 | 1.5439 | 1.5439 | 0.3779 | 0.3779 | 0.9694 | 0.9694 |

Fig. 3.6 is plotted to perceive the effect of $\epsilon$ on temperature distribution. It is observed that temperature of the flow enhances for higher values of small thermal conductivity parameter.

Fig. 3.7 portrays the influence of $Rd$ on temperature distribution. It is noted that an increase in $Rd$ results an increment in thermal boundary layer thickness. The enhancement in $Rd$ provides more energy to the fluid which supply additional heat to the flow. Temperature has a higher value for Case B than Case A.

Fig. 3.8 illustrates the temperature profile for different values of $Pr_o$. It is shown that an increase in the Prandtl number results in lowering the thickness of thermal layer. The reason of this reduction is that smaller values of Prandtl number are equivalent to increasing the thermal conductivities. Therefore, heat is diffused away from the boundary more rapidly for higher values of $Pr_0$. Temperature has a higher value for Case B as compare to Case A.

Fig. 3.9 shows the effect of $s$ on temperature profile. It is analyzed that the temperature increases with an increase in $s$. The improve values of heat generation parameter provide more thermal energy to the fluid which results rises the temperature of flow. Temperature has a higher value for Case B as compare to Case A.

Fig. 3.10 depicts the impacts of $Sc$ on concentration distribution. We observe that by increasing $Sc$ there is a reduction in concentration profile. The Schmidt number is a quotient of the momentum and mass diffusivity, so with an increment in $Sc$ mass diffusivity decreases. As a result, increase in $Sc$ causes reduction in nanoparticle concentration. Concentration has a higher value for Case B as compare to Case A.

Fig. 3.11 demonstrates the variation of $\tau$ on concentration distribution. It is noted that for escalating values of $\tau$ concentration boundary layer thickness reduces. Concentration has a higher value for Case B as compare to Case A.

Fig. 3.12 and Fig. 3.13 depict the influences of $\theta_r$ on concentration distribution for $Pr_o = 1$ and $Pr_o = 6.2$. It is analyzed that nanoparticles concentration elevates in both figures for increasing values of $\theta_r$.

Fig. 3.14 is drawn to see the impacts of $Ec$ on temperature profile for $Pr_o = 6.2$. It is noticed that an increment in $Ec$ causes enhancement in temperature profile.

Fig. 3.15 is plotted to perceive the effects of $\epsilon$ on temperature profile for $Pr_o = 6.2$. It is analyzed that by raising $\epsilon$ temperature of the fluid increases.

Fig. 3.16 and 3.17 portray the impacts of $Rd$ and $s$ on temperature profile respectively. It is observed that the thickness of thermal boundary layer increases for increasing values of $Rd$ and $s$.

Fig. 3.18 presents the influence of $\tau$ on concentration profile. It is observed that concentration boundary layer rises for raising values of $\tau$.

Fig. 3.19 presents the influence of $Kp$ and $M$ on skin friction coefficient. It is reported that skin friction coefficient declines for incremental values of $Kp$ and $M$.

Fig. 3.20 categorizes the effects of $s$ and $Rd$ on local Nusselt number. It is inspected that an incremental values of $s$ and $Rd$ causes reduction in local Nusselt number.

Fig. 3.21 illustrates the impacts of $Sc$ and $\tau$ on local Sherwood number. An enhancement in $Sc$ and $\tau$ Shows intensification in local Sherwood number.
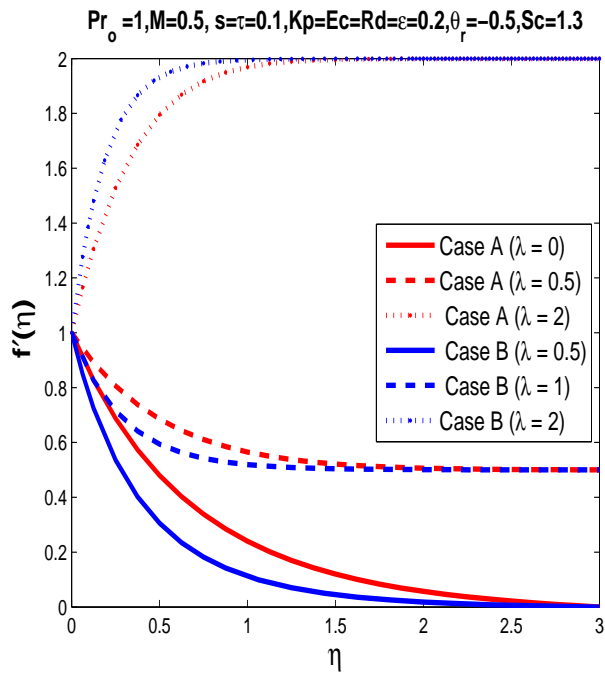
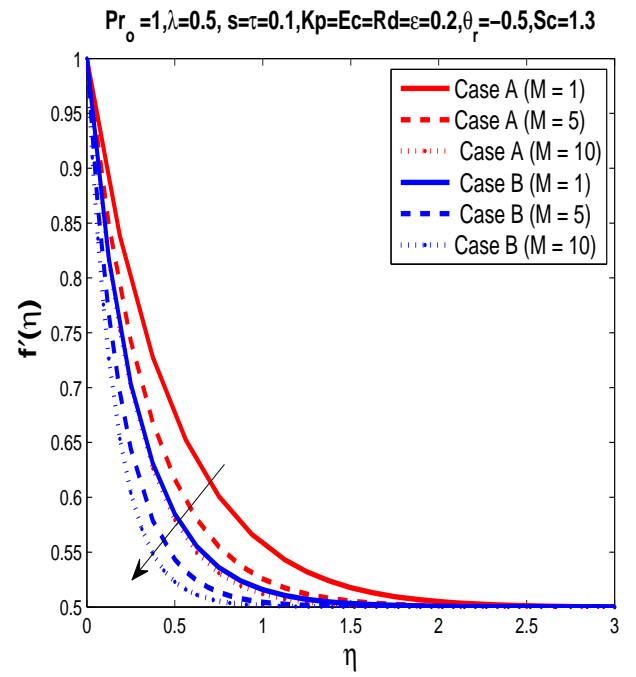Figure 3.2: Velocity profile $f\prime(\eta)$ for different $\lambda$.



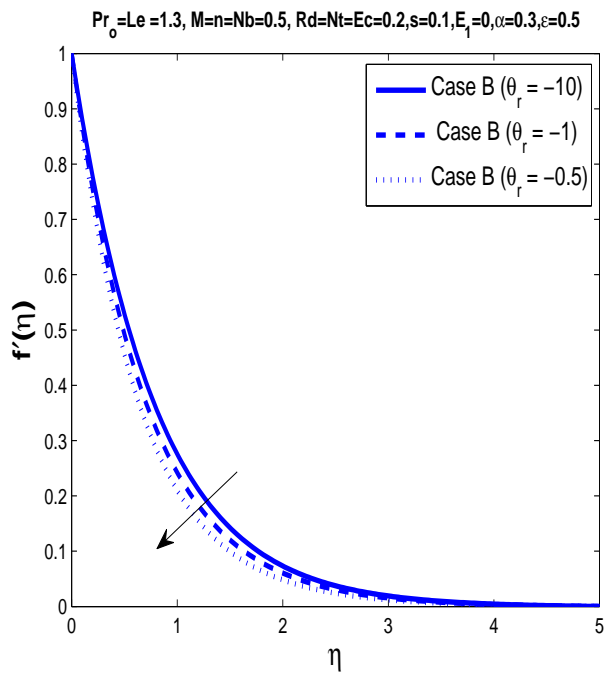Figure 3.3: Velocity profile $f\prime(\eta)$ for different $M$.



Figure 3.4: Velocity profile $f^{'}(\eta)$ for different $\theta_r$.
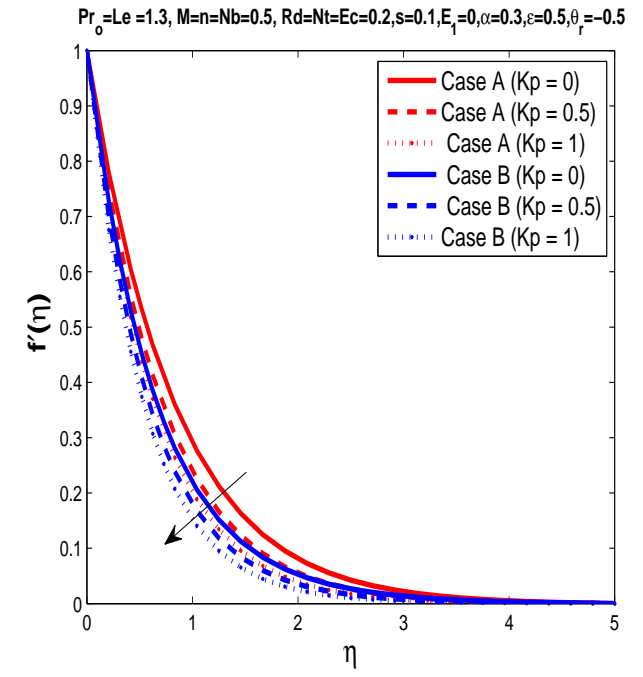


Figure 3.5: Velocity profile $f^{'}(\eta)$ for different $Kp$.

Figure 3.6: The temperature profile $\theta(\eta)$ for different $\epsilon$.
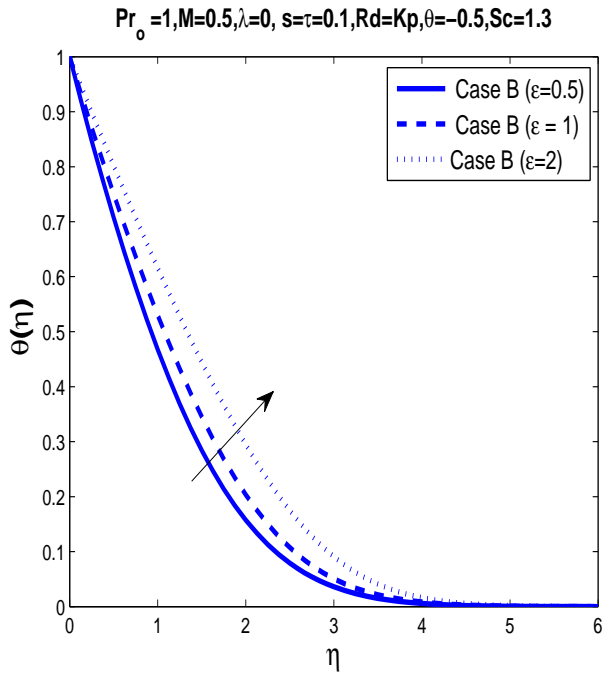


Figure 3.7: The temperature profile $\theta(\eta)$ for different $Rd$.



Figure 3.8: The temperature profile $\theta(\eta)$ for different $Pr$.



Figure 3.9: The temperature profile $\theta(\eta)$ for different $s$.

**Pr$_o$=1,M=0.5,λ=0.3, s=τ=0.1,Kp=Ec=Rd=ε=0.2,θ$_r$=−0.5**
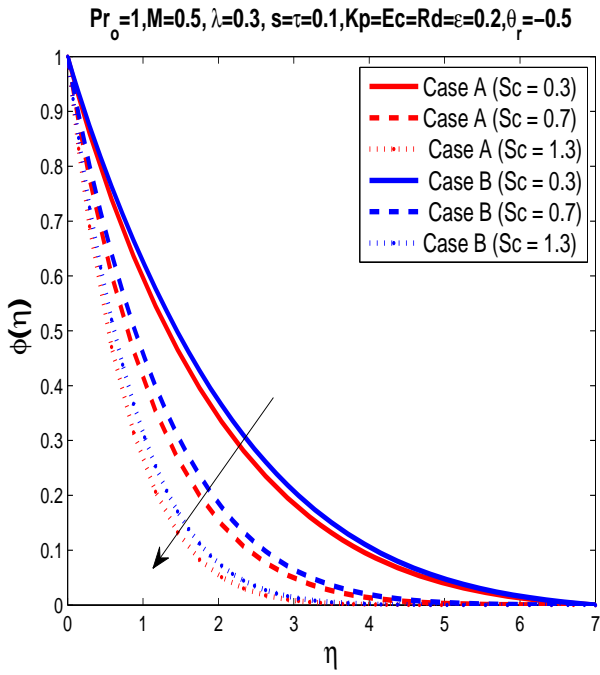
Figure 3.10: The concentration profile $\phi(\eta)$ for different $Sc$.



**Pr$_o$=1,M=λ=0.5, s=0.1,Kp=Ec=Rd=ε=0.2,θ$_r$=−0.5, Sc=1.3**

Figure 3.11: The concentration profile $\phi(\eta)$ for different $\tau$.



**Pr$_o$=1,M=0.5,λ=0, s=τ=0.1,Rd=Kp=ε=0.2,Sc=1.3**
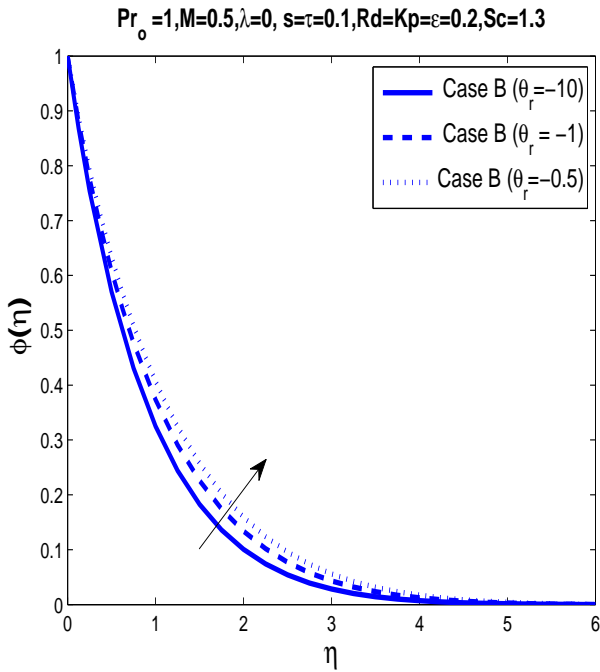
Figure 3.12: The concentration profile $\phi(\eta)$ for different $\theta_r$.



**Pr$_o$=6.2,M=0.5,λ=0, s=τ=0.1,Rd=Kp=ε=0.2,Sc=1.3**

Figure 3.13: The concentration profile $\phi(\eta)$ for different $\theta_r$.

Table 3.4: Comparison of $-f''(0)$, $-\theta'(0)$ and $-\phi'(0)$ for various $M$, $Kp$, $\lambda$, $Pr$, $Rd$, $s$, $Ec$, $\tau$, $\theta_r$, $\epsilon$ and $Sc$ (Case B)

| | | | | | | | | | | | bvp4c | bvp4c | bvp4c |
|---|---|---|---|---|---|---|---|---|---|---|---|---|---|
| M | Kp | $\lambda$ | $Pr_o$ | Rd | s | Ec | Sc | $\tau$ | $\theta_r$ | $\epsilon$ | $-f''(0)$ | $-\theta'(0)$ | $-\phi'(0)$ |
| 0 | 0.2 | 0.1 | 6.8 | 0.2 | 0.1 | 0.2 | 1 | 0.2 | -5 | 0.2 | 1.4808 | 1.8163 | 1.1821 |
| 0.3 | | | | | | | | | | | 1.5794 | 1.7179 | 1.1501 |
| 0.6 | | | | | | | | | | | 1.6717 | 1.6261 | 1.1208 |
| 0.3 | 0 | 0.1 | 6.8 | 0.2 | 0.1 | 0.2 | 1 | 0.2 | -5 | 0.2 | 1.5212 | 1.7769 | 1.1696 |
| | 0.5 | | | | | | | | | | 1.6619 | 1.6349 | 1.1231 |
| | 1 | | | | | | | | | | 1.7890 | 1.5073 | 1.0824 |
| 0.3 | 0.2 | 0 | 6.8 | 0.2 | 0.1 | 0.2 | 1 | 0.2 | -5 | 0.2 | 1.6443 | 1.6239 | 1.0942 |
| | | 0.5 | | | | | | | | | 1.0689 | 2.1291 | 1.3526 |
| | | 0.9 | | | | | | | | | 0.2459 | 2.4432 | 1.5232 |
| 0.3 | 0.2 | 0.1 | 5 | 0.2 | 0.1 | 0.2 | 1 | 0.2 | -5 | 0.2 | 1.5735 | 1.4590 | 1.1129 |
| | | | 6.8 | | | | | | | | 1.5794 | 1.7179 | 1.1501 |
| | | | 10 | | | | | | | | 1.5869 | 2.0925 | 1.2056 |
| 0.3 | 0.2 | 0.1 | 6.8 | 0 | 0.1 | 0.2 | 1 | 0.2 | -5 | 0.2 | 1.5840 | 1.9405 | 1.1829 |
| | | | | 0.4 | | | | | | | 1.5757 | 1.5532 | 1.1263 |
| | | | | 0.8 | | | | | | | 1.5701 | 1.3207 | 1.0934 |
| 0.3 | 0.2 | 0.1 | 6.8 | 0.2 | 0 | 0.2 | 1 | 0.2 | -5 | 0.2 | 1.5813 | 1.8342 | 1.1678 |
| | | | | | 0.1 | | | | | | 1.5794 | 1.7179 | 1.1501 |
| | | | | | 0.2 | | | | | | 1.5773 | 1.5933 | 1.1314 |
| 0.3 | 0.2 | 0.1 | 6.8 | 0.2 | 0.1 | 0.3 | 1 | 0.2 | -5 | 0.2 | 1.5765 | 1.5096 | 1.1181 |
| | | | | | | 0.7 | | | | | 1.5652 | 0.6818 | 0.9905 |
| | | | | | | 1 | | | | | 1.5571 | 0.0667 | 0.8956 |
| 0.3 | 0.2 | 0.1 | 6.8 | 0.2 | 0.1 | 0.2 | 0.7 | 0.2 | -5 | 0.2 | 1.5794 | 1.7179 | 0.8987 |
| | | | | | | | 1 | | | | 1.5794 | 1.7179 | 1.1501 |
| | | | | | | | 1.3 | | | | 1.5794 | 1.7179 | 1.3767 |
| 0.3 | 0.2 | 0.1 | 6.8 | 0.2 | 0.1 | 0.2 | 1 | 0 | -5 | 0.2 | 1.5794 | 1.7179 | 0.9303 |
| | | | | | | | | 0.5 | | | 1.5794 | 1.7179 | 1.4909 |
| | | | | | | | | 1 | | | 1.5794 | 1.7179 | 2.0846 |
| 0.3 | 0.2 | 0.1 | 6.8 | 0.2 | 0.1 | 0.2 | 1 | 0.2 | -10 | 0.2 | 1.4954 | 1.7259 | 1.1814 |
| | | | | | | | | | -1 | | 2.1250 | 1.6683 | 0.9989 |
| | | | | | | | | | -0.5 | | 2.6210 | 1.6247 | 0.9052 |
| 0.3 | 0.2 | 0.1 | 6.8 | 0.2 | 0.1 | 0.2 | 1 | 0.2 | -5 | 0 | 1.5824 | 1.9366 | 1.1839 |
| | | | | | | | | | | 0.5 | 1.5755 | 1.4877 | 1.1153 |
| | | | | | | | | | | 1 | 1.5705 | 1.2399 | 1.0789 |

Figure 3.14: The temperature profile $\theta(\eta)$ for different $Ec$.



Figure 3.15: The temperature profile $\theta(\eta)$ for different $\epsilon$.
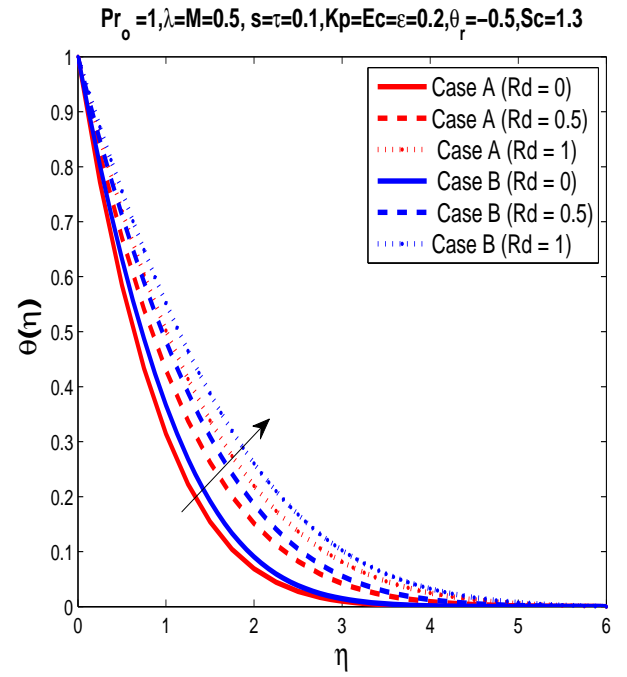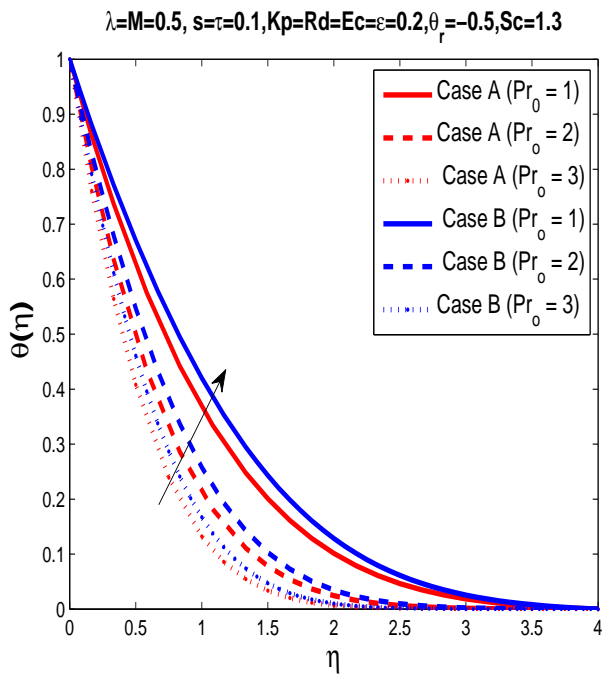


Figure 3.16: The temperature profile $\theta(\eta)$ for different $Rd$.



Figure 3.17: The temperature profile $\theta(\eta)$ for different $s$.

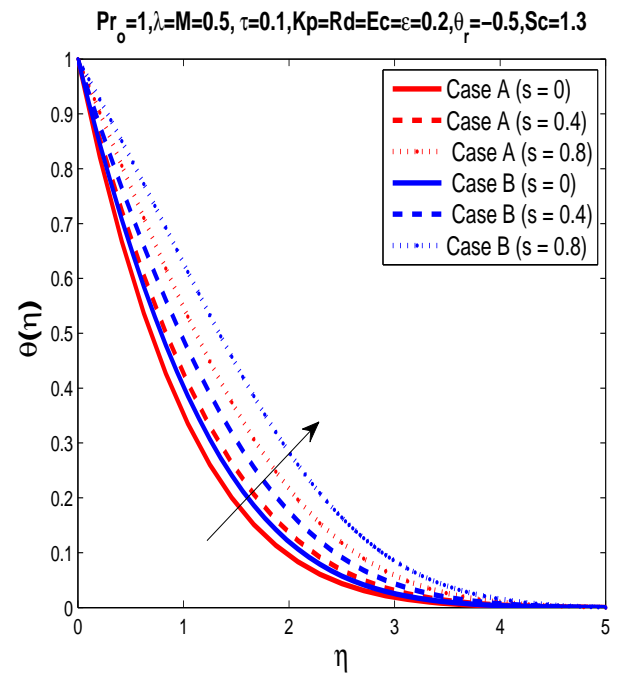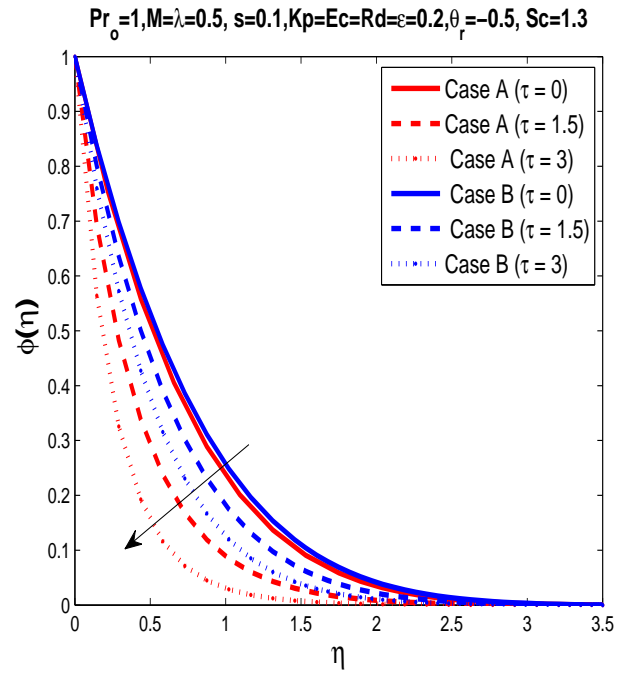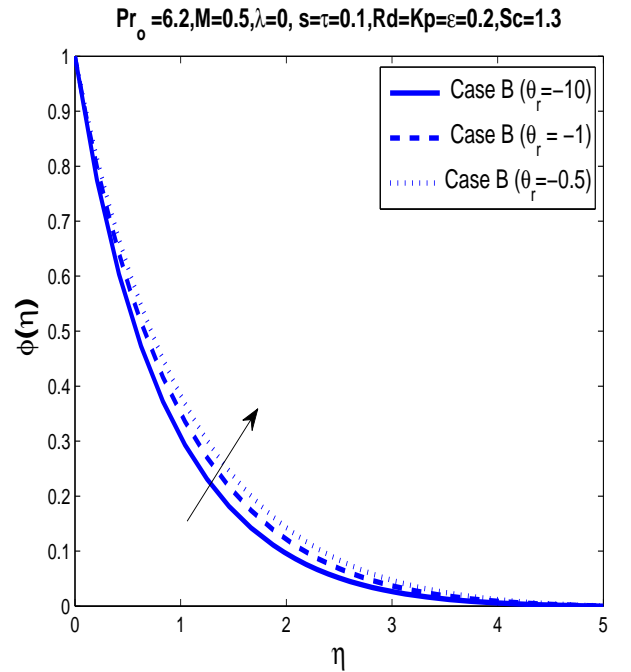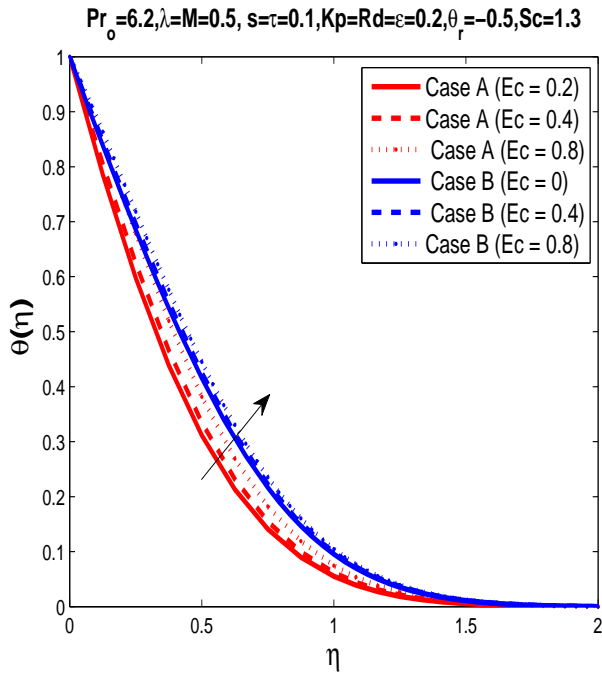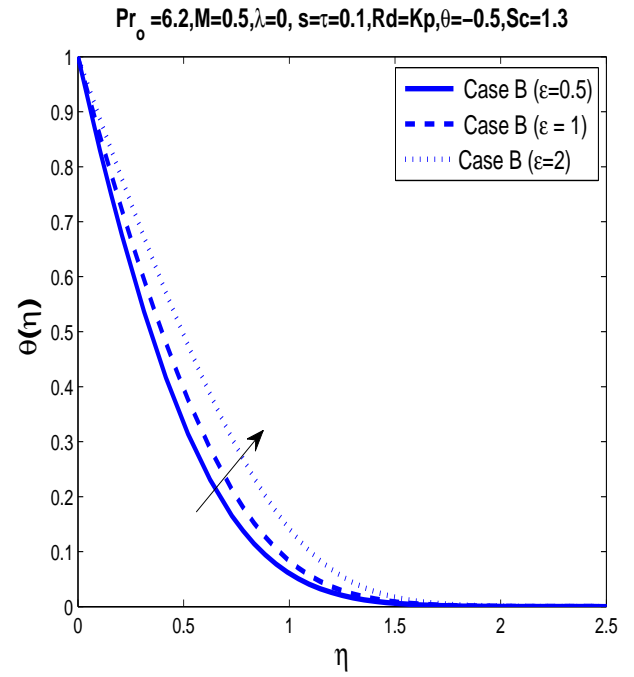Figure 3.18: The temperature profile $\theta(\eta)$ for different $\tau$.
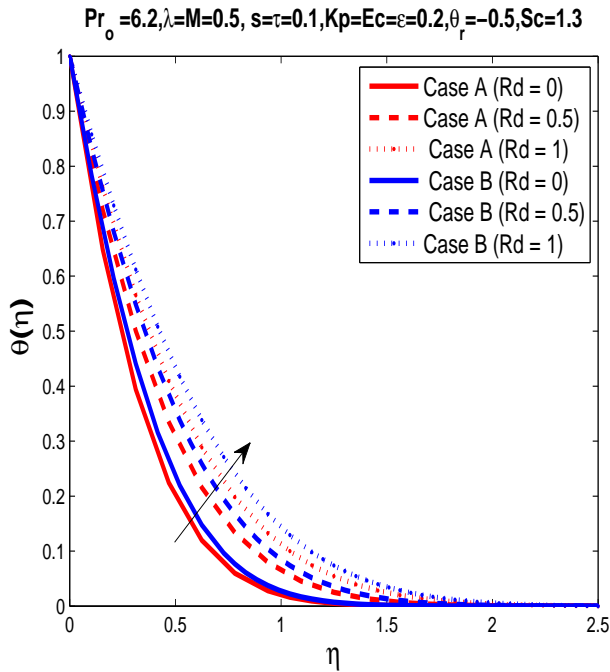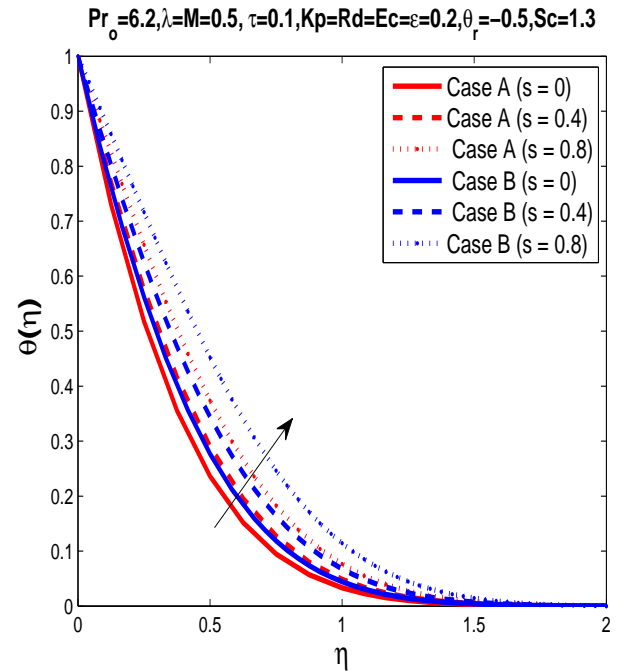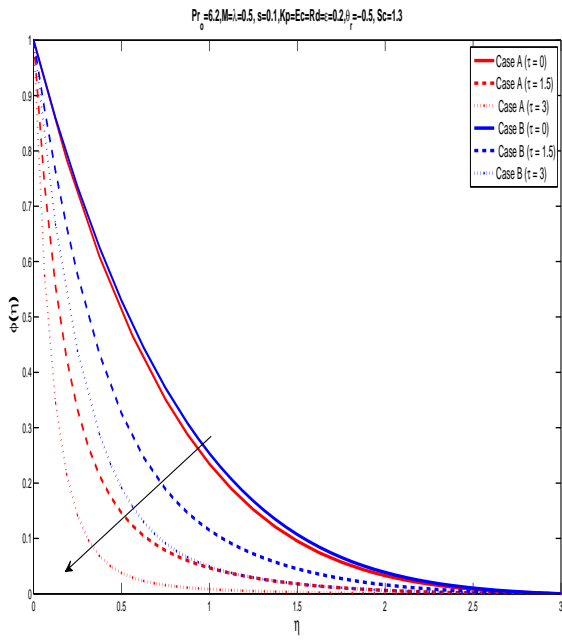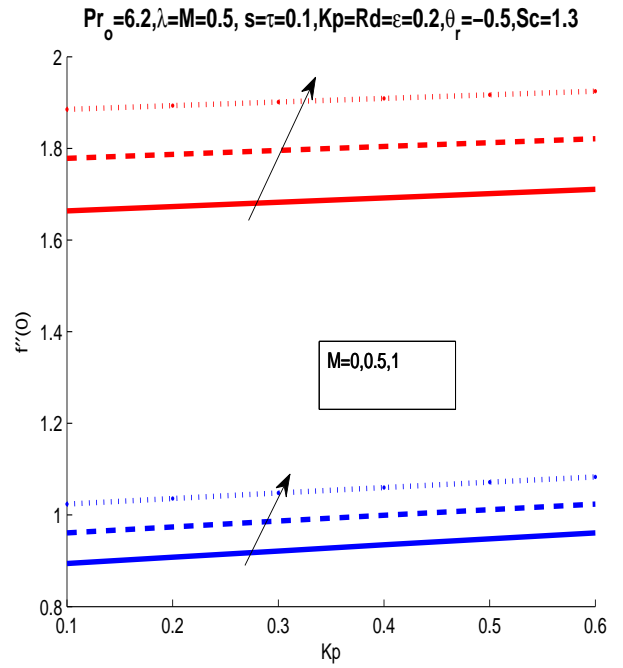


Figure 3.19: The skin friction coefficient with variations of $Kp$ and $M$.
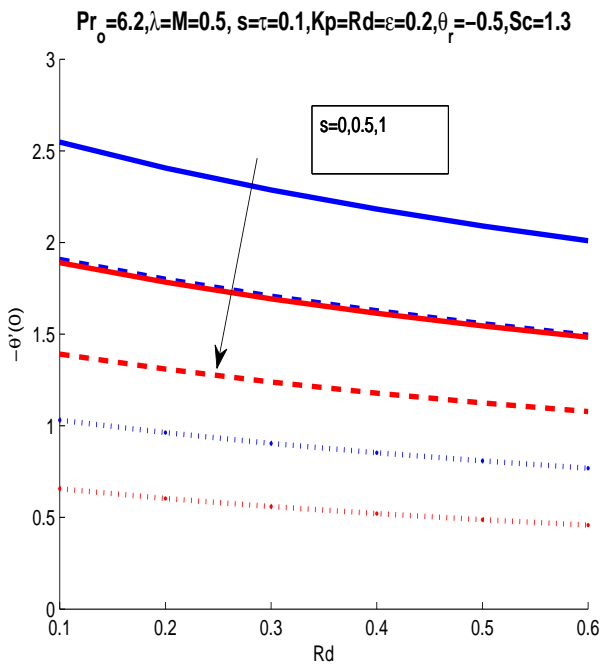


Figure 3.20: The reduced Nusselt number with variations of $s$ and $Rd$.
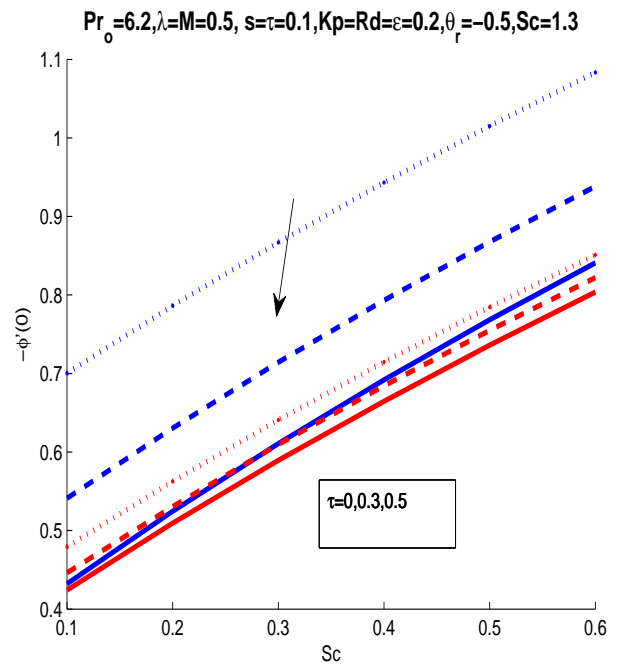


Figure 3.21: The Sherwood number with variations of $\tau$ and $Sc$.

## 3.6 Conclusions

The present study gives the results of two dimensional MHD thermophoretic, incompressible, free stream flow over an exponentially radiating stretched surface while taking heat generation/absorption, permeability, viscosity and thermal conductivity as a variable. The influence of distinct parameters have been studied on momentum, thermal and nanoparticles concentration profiles for constant and variable fluid properties. The key findings of the study for Cases A and B are as follows:

- Thermal boundary layer thickness increases for higher values of $\epsilon$, $Rd$ and $s$ while decrease for $Pr_0$.

- Momentum boundary layer thickness shows decrement for higher values of $\theta_r$, $M$ and $Kp$.

- Concentration boundary layer thickness shows increment for increasing values of $\theta_r$, whereas it lowers for $\tau$ and $Sc$.

- Momentum boundary layer thickness for Case A is higher when compared to Case B (except when $\lambda < 1$) while thermal boundary layer is higher in Case B as compared to Case A.

- Graphs shows that the numerical results of Case A and Case B are different.

# Chapter 4

# EMHD Flow of Nanofluid with Varying Fluid Properties over a Variably Thicked Stretching Sheet

The objective of this chapter comprises in two key points: descriptive mathematical model for constant and variable fluid flows over a variable thickness sheet by inducting applied electric and magnetic fields, porosity, radiative heat transfer, heat generation/absorption and seeking their solution by constructing a novel numerical method, the SFDM. We resort to similarity transformations to implicate PDEs into a set of ODEs. Optimal results for a pair of ODEs obtained from SFDM are assessed by drawing a comparison with *bvp4c* and existing literature values. SFDM has been implemented in MATLAB for both constant and variable fluid properties. Tabulated numerical values of $C_{fx_1}$, $Nu_{x_1}$ and $Sh_{x_1}$ are measured and scrutinized against different parameters. Influence of distinct parameters on velocity, temperature, and nanoparticles volume fraction have been explained in great detail via diagrams. The $C_{fx_1}$ for variable fluid properties is greater than the constant fluid properties. However, $Nu_{x_1}$ is less for variable fluid properties when compare with constant fluid properties. Surprisingly, the high precision computational results are achieved from the SFDM.

    This chapter is arranged as follows.
Section 4.1 gives the introduction of the chapter. In Sections 4.2 and 4.3 mathematical model

and the analysis on fluid properties are presented. In Section 4.4, we presents physical quantities. The numerical procedure is analyzed in Section 4.5. The results and discussion with the help of graphs and table is described in Section 4.6. In Section 4.7 conclusion of the chapter is given.

## 4.1 Introduction

Hayat et al. [127, 128] analyzed the consequences on fluid flow by Cattaneo-Christov heat flux and a temperature-dependent fluid thermal conductivity over a variable thickness sheet and showed that the variable conductivity enhances temperature distribution. They also maintained that temperature profile decrease with thermal relaxation paramter. Khader and Ahmed [129] have computed the numerical solution for variable sheet thickness with slip velocity and pointed out that the skin friction coefficient increases with wall thickness parameter. Daniel et al. [130] discussed the MHD radiative flow of nanofluid taking thermal radiation into account for variable thickness sheet. They submitted that the thermal stratification effect reduces temperature. Daniel et al. [131] examined the effect of electrical MHD nanofluid flow with thermal radiation towards a variable thickness surface and concluded that the thermal radiation did impact the nanofluid temperature. Seth and Mandal [132] presented the analysis on EMHD stagnation point flow of nanofluid past a variable thickness surface. They showed that intensification in electric field slows down the flow velocity. Qayyum et al. [133] studied the aspects of third grade nanofluid with chemical reaction over a variable thickness stretching sheet. They found that heat generation/ absorption decrease in the heat transfer rate. This analysis achieved two goals. Firstly, an assessment of distinctive features for constant and variable properties. Secondly, we adopted a new numerical process, the SFDM, to compute solutions and compared its accuracy with bvp4c.

## 4.2 Mathematical Model

We assume an electrical magnetohydrodynamics, steady, laminar nanofluid flow through a nonlinear variable thickness stretching surface. The variable magnetic field $B_1(x_1) = B_o(x_1 + b^*)^{\frac{n-1}{2}} (n \neq 1)$ and variable electrical field $E(x_1) = E_o(x_1 + b^*)^{\frac{n-1}{2}} (n \neq 1)$ is applied normal to
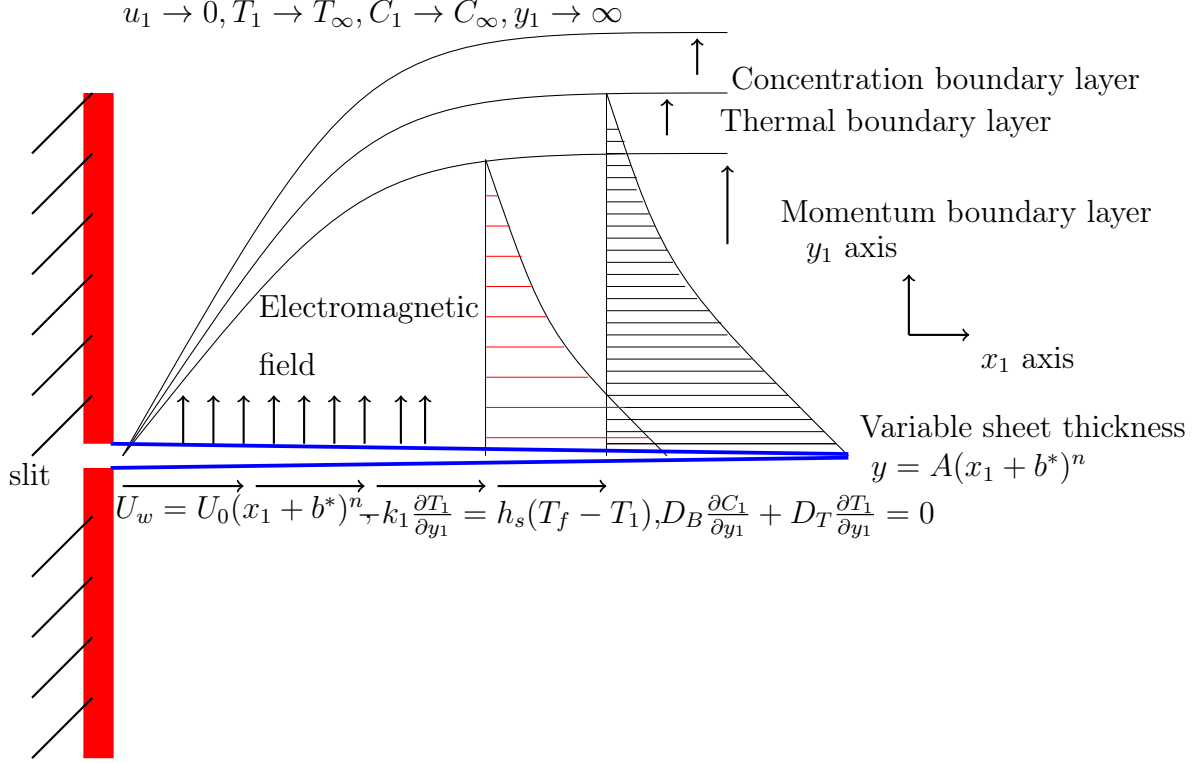
Figure 4.1: Schematic diagram of the problem.

the direction of flow. The sheet is stretching with non-linear velocity $U_w = U_o(x_1+b^*)^n (n \neq 1)$ where $b^*$ is the dimensional constant and $U_o$ is the reference velocity. Therefore, the surface is considered not to be flat and its thickness varies as $y = A(x_1 + b^*)^{\frac{1-n}{2}}(n \neq 1)$, where $A$ is a very small constant to hold the sheet thin enough. We also observed that for $n = 1$ the current problem reduce to a flat sheet. The geometry of the problem is shown in Figure 4.1 where $x_1$ and $y_1$ axes is taken along and normal to the stretching surface respectively.

The equations governing this flow are Daniel et al. [130, 131]

$$\frac{\partial u_1}{\partial x_1} + \frac{\partial v_1}{\partial y_1} = 0, \tag{4.1}$$

$$u_1\frac{\partial u_1}{\partial x_1} + v_1\frac{\partial u_1}{\partial y_1} = \frac{1}{\rho_1}\frac{\partial}{\partial y_1}\left(\frac{\mu_1 \partial u_1}{\partial y_1}\right) - \frac{\sigma}{\rho_1}(E(x_1)B_1(x_1) - B^2(x_1))u_1 - \frac{\mu_1}{\rho_1 K(x)}u_1, \tag{4.2}$$

$$u_1\frac{\partial T_1}{\partial x_1} + v_1\frac{\partial T_1}{\partial y_1} = \frac{1}{\rho_1 C_p}\frac{\partial}{\partial y_1}\left(\frac{k_1 \partial T_1}{\partial y_1}\right) + \tau_1\left(D_B\frac{\partial T_1}{\partial y_1}\frac{\partial C_1}{\partial y_1} + \frac{D_T}{T_\infty}\left(\frac{\partial T_1}{\partial y_1}\right)^2\right) - \frac{1}{\rho_1 C_p}\frac{\partial q_r}{\partial y_1} +$$

$$\frac{\sigma}{\rho_1 C_p}(u_1 B(x_1) - E(x_1))^2 + \frac{Q(x_1)}{\rho_1 C_p}(T_1 - T_\infty), \tag{4.3}$$

$$u_1\frac{\partial C_1}{\partial x_1} + v_1\frac{\partial C_1}{\partial y_1} = D_B\frac{\partial^2 C_1}{\partial y_1^2} + \frac{D_T}{T_\infty}\frac{\partial^2 T_1}{\partial y_1^2}, \tag{4.4}$$

65

here $u_1$ and $v_1$ are the velocity components parallel to $x_1-$ and $y_1-$ axis, respectively. Further, $\mu_1$ symbolizes the viscosity, $\rho_1$ denotes the density, $\nu_1$ is designated as kinematic viscosity, $C_p$ is the specific heat capacity, $B_1$ is the magnetic field. Temperature of fluid and nanoparticle fraction are symbolized as $T_1$ and $C_1$ respectively. The wall and ambient fluid temperatures are designated as $T_w$ and $T_\infty$ respectively. $Q(x_1) = Q_0(x_1 + b^*)^{\frac{n-1}{2}}$ is the volumetric rate of heat generation and $K(x_1) = K_0(x_1 + b^*)^{n-1}$ is a variable permeability.

The above system is completed with the following appropriate boundary conditions taking in view of [97] and [98]

$$u_1 = U_w(x_1) = U_o(x_1 + b^*)^n, \ v_1 = 0, \ -k_1\frac{\partial T_1}{\partial y_1} = h_s(T_f - T_1), \ D_B\frac{\partial C_1}{\partial y_1} + D_T\frac{\partial T_1}{\partial y_1} = 0$$

$$\text{at } y_1 = A(x_1 + b^*)^{\frac{1-n}{2}},$$

$$u_1 \longrightarrow 0, \quad T_1 \longrightarrow T_\infty, \quad C_1 \longrightarrow C_\infty \quad \text{as} \quad y_1 \longrightarrow \infty. \tag{4.5}$$

The following are the relevant transformations:

$$\psi = \sqrt{\frac{2}{n+1}\nu_1 U_o(x_1 + b^*)^{n+1}} f(\eta), \ \xi = y_1\sqrt{(\frac{n+1}{2})\frac{U_o(x_1 + b^*)^{n-1}}{\nu_1}}, \alpha = A\left(\frac{(n+1)U_0}{2\nu_1}\right)^{\frac{1}{2}},$$

$$\eta = \xi - \alpha = y_1\sqrt{(\frac{n+1}{2})\frac{U_o(x_1 + b^*)^{n-1}}{\nu_1}} - \alpha,$$

$$\theta = \frac{T_1 - T_\infty}{T_w - T_\infty}, \quad \phi = \frac{C_1 - C_\infty}{C_w - C_\infty}, \quad u_1 = U_o(x_1 + b^*)^n f'(\eta),$$

$$v_1 = -\sqrt{\frac{2}{n+1}\nu_1 U_o(x_1 + b^*)^{n-1}}(f(\eta) + \eta\frac{n-1}{n+1}f'(\eta)).$$

$$\tag{4.6}$$

Eq. (4.1) is identically satisfied. In addition, when above similarity variables applied to Eqs. (4.2), (4.3) and (4.4) yielding:

$$(\frac{\mu_1}{\mu_o}f''(\eta))' - \frac{2n}{n+1}f'^2(\eta) + f(\eta)f''(\eta) + M(E_1 - f'(\eta)) - Kp\frac{\mu_1}{\mu_o}f'(\eta) = 0, \tag{4.7}$$

$$(1 + \frac{4}{3}Rd)(\frac{k_1}{k_o}\theta'(\eta))' + Pr_o(f(\eta)\theta'(\eta) + Nb\theta'(\eta)\phi'(\eta) + Nt(\theta')^2(\eta) + MEc(f'(\eta) - E_1)^2$$

$$+ \frac{2}{n+1}s\theta(\eta)) = 0, \tag{4.8}$$

$$\phi''(\eta) + \frac{Nt}{Nb}\theta''(\eta) + LePr_o f(\eta)\phi'(\eta) = 0. \tag{4.9}$$

The equivalent boundary conditions in terms of similarity variables are specified as:

$$f(\eta) = \alpha(\frac{1-n}{1+n}), \ f'(\eta) = 1,, \ \theta'(\eta) = -B_i(1 - \theta(\eta)), \ Nb\phi'(\eta) + Nt\theta'(\eta) = 0, \ \text{at} \ \eta = 0,$$

$$f'(\eta) = 0, \qquad \theta(\eta) = 0, \qquad \phi(\eta) = 0, \qquad \text{as} \qquad \eta \to \infty.$$

$$(4.10)$$

where $M = \frac{2\sigma B_o^2}{\rho_1 U_o(n+1)}$ is a magnetic parameter, $\alpha$ is the wall thickness parameter, $E_1 = \frac{E_o}{B_o U_o(x_1+b^*)^n}$ (Daniel et al. [130, 131]) is the electric field, $Kp = \frac{2\nu_1}{K_o U_o(n+1)}$ is the permeability constant. $Pr_o = \frac{\mu_o C_p}{k_o}$ is the Prandtl number, $Nb = \frac{\tau_1 D_B(C_w - C_\infty)}{\nu_1}$ is the Brownian motion parameter, $Nt = \frac{\tau_1 D_T(T_w - T_\infty)}{T_\infty \nu_1}$ is the thermophoresis parameter, $Ec = \frac{U_w^2}{C_p(T_w - T_\infty)}$ (Daniel et al. [130, 131]) is the local Eckert number, $Rd = \frac{4\sigma^* T_\infty^3}{k_o k^*}$ denotes the radiation parameter, $s = \frac{Q_o(x_1+b^*)}{\rho_1 u_w C_p}$ (Hayat et al. [158]) is the heat source parameter, $B_i$ is the Biot number and $Le = \frac{\nu_1}{D_B}$ is Lewis number.

## 4.3    Fluid Properties Analysis

In this section, we illustrate the main theme of this work in the following two subsections.

### 4.3.1    Case A: Constant Fluid Characteristics

For this case, we rewrite Eqs. (4.7), (4.8) and (4.9) into the following set of equations:

$$f''' - \frac{2n}{n+1}f'^2 + ff'' + M(E_1 - f') - Kpf' = 0, \qquad (4.11)$$

$$(1 + \frac{4}{3}Rd)\theta'' + Pr_o(f\theta' + Nb\theta'\phi' + Nt(\theta')^2 + MEc(f' - E_1)^2 + \frac{2}{n+1}s\theta) = 0, \qquad (4.12)$$

$$\phi'' + \frac{Nt}{Nb}\theta'' + Pr_o Lef\phi' = 0. \qquad (4.13)$$

### 4.3.2    Case B: Variable Fluid properties

In this case, we write viscosity and thermal conductivity as a function of temperature Popley et al. [116]

$$\mu_1(T_1) = \frac{\mu_{ref}}{1 + \gamma_1(T_1 - T_{ref})}, \qquad (4.14)$$

Assuming $T_o \approx T_{ref}$ then we get,

$$\mu_1 = \frac{\mu_o}{1 - \frac{T_1 - T_o}{\theta_r (T_w - T_o)}} = \frac{\mu_o}{1 - \frac{\theta(\eta)}{\theta_r}}. \qquad (4.15)$$

here $\theta_r = \frac{-1}{\gamma_1 (T_w - T_o)}$. Inserting Eq. (4.15) in Eq. (4.7) we get

$$\frac{\theta_r}{(\theta r - \theta)} f''' + \frac{f'' \theta' \theta_r}{(\theta_r - \theta)^2} - \frac{2n}{n+1} f'^2 + ff'' + M(E_1 - f') - Kp \frac{\theta_r}{\theta_r - \theta} f' = 0. \qquad (4.16)$$

Following Hayat et al. [97] the changeable thermal conductivity is expressed as,

$$k_1(T) = k_o(1 + \epsilon \theta). \qquad (4.17)$$

Using Eq. (4.17) into Eq. (4.8) we get

$$(1 + \tfrac{4}{3} Rd)((1 + \epsilon \theta(\eta))\theta''(\eta) + \epsilon(\theta'(\eta))^2) + Pr_o(f(\eta)\theta'(\eta) + Nb\theta'(\eta)\phi'(\eta) + Nt(\theta'(\eta))^2$$

$$+ MEc(f'(\eta) - E_1)^2 + \tfrac{2}{n+1} s\theta(\eta)) = 0. \qquad (4.18)$$

## 4.4   Physical Quantities

The important physical parameters are defined as

### 4.4.1   The Skin Friction Coefficient

The wall resistance coefficient for case A and case B are defined as,

$$C_{fx_1} = \frac{\tau_w}{\rho_1 u_w^2} = \sqrt{\frac{1+n}{2Re_{x_1}}} f''(0).(\textbf{CASE A}) \qquad (4.19)$$

$$C_{fx_1} = \frac{\tau_w}{\rho_1 u_w^2} = \frac{\theta_r}{\theta_r - \theta_0} \sqrt{\frac{1+n}{2Re_{x_1}}} f''(0).(\textbf{CASE B}) \qquad (4.20)$$

### 4.4.2   The Local Nusselt Number

The local Nusselt number for Cases A and B are same and can be written as,

$$Nu_{x_1} = -\frac{(x_1 + b^*)q_w}{k_o(T_w - T_\infty)} = -(1 + \frac{4}{3} Rd)\sqrt{\frac{(1+n)Re_{x_1}}{2}} \theta'(0). \qquad (4.21)$$

### 4.4.3 The Local Sherwood Number

The local Sherwood number for Case A and Case B is,

$$Sh_{x_1} = -\frac{(x_1 + b^*)j_w}{C_w - C_\infty} = -\sqrt{\frac{(1+n)Re_{x_1}}{2}}\phi'(0). \tag{4.22}$$

## 4.5  Numerical Procedure

The system of ODEs for Case A and Case B are first modified into a system of first order ODEs. We use two numerical methods to find the solution of these ODEs. The first method is the SFDM [99] and the second is implemented through MATLAB built-in solver *bvp4c*. The details of the methods and its implications are described below.

### 4.5.1  Simplified Finite Difference Method (SFDM)

The algorithm with necessary details for the simplified SFDM are as follows:

1. We first reduce the third order ODE into a group of first and second order ODEs. This reduction of order simplify the process of finite difference approximation. The ODE already written in second order cannot be reduced.

2. For further simplification, we use Taylor series to linearize the system of nonlinear ODEs.

3. We replace the derivatives in linear ODEs with the corresponding finite difference approximation formulas.

4. In the end, we reach at algebraic system of equations that can be solved efficiently by Thomas algorithm.

5. The process will be repeated for energy and concentration equations.

The explanation of SFDM has been shown in the flowchart. Generally, we find the results when $N = 1000$ grid points in the $\eta$ direction. The domain to achieve steady state varies due

to effect of different parameters, however, the domain $\eta = 7$ seems enough for our results. To initiate we assume $f' = F$ in ((4.11)) then we get

$$\frac{d^2 F}{d\eta^2} = \frac{2n}{n+1} F^2 - f \frac{dF}{d\eta} - M(E_1 - F) + KpF \tag{4.23}$$

we can write this expression for the function $f$ as

$$\chi_1(\eta, F, F') = \frac{2n}{n+1} F^2 - f \frac{dF}{d\eta} - M(E_1 - F) + KpF \tag{4.24}$$

let us approximate $\frac{dF}{d\eta}$ in above equation by forward difference approximation

$$\chi_1(\eta, F, F') = \frac{2n}{n+1} F_i^2 - f_i \left( \frac{F_{i+1} - F_i}{h} \right) - M(E_1 - F_i) + KpF_i \tag{4.25}$$

The coefficients of second order ODE read as

$$A_n = -\frac{\partial \chi_1}{\partial F'} = -(-f) = f = f_i \tag{4.26}$$

$$B_n = -\frac{\partial \chi_1}{\partial F} = -\left( \frac{4n}{n+1} F + M + Kp \right) = -\left( \frac{4n}{n+1} F_i + M + Kp \right) \tag{4.27}$$

$$D_n = \chi_1(\eta, F, F') + B_n F_i + A_n \frac{F_{i+1} - F_i}{h} \tag{4.28}$$

After some manipulation (4.28) becomes

$$a_i F_{i-1} + b_i F_i + c_i F_{i+1} = r_i, \qquad i = 1, 2, 3...., N \tag{4.29}$$

where

$$a_i = 2 - hA_n, \quad b_i = 2h^2 B_n - 4, \quad c_i = 2 + hA_n, \quad r_i = 2h^2 D_n \tag{4.30}$$

In matrix-vector form it is written in compact as

$$AF = s \tag{4.31}$$

where

$$A = \begin{bmatrix} b_1 & c_1 & & & & \\ a_2 & b_2 & c_2 & & & \\ & & .... & & & \\ & & & a_{N-2} & b_{N-2} & c_{N-2} \\ & & & & a_{N-1} & b_{N-1} \end{bmatrix}$$

(4.32)

$$F = \begin{bmatrix} F_1 \\ F_2 \\ . \\ . \\ F_{N-1} \end{bmatrix} \qquad s = \begin{bmatrix} s_1 \\ s_2 \\ . \\ . \\ s_{N-1} \end{bmatrix}$$

(4.33)

The matrix $A$ is tridiagonal matrix and is written in LU-Factorization as [100]

$$A = LU$$

(4.34)

where

$$L = \begin{bmatrix} \beta_1 & & & & \\ a_2 & \beta_2 & & & \\ & & .... & & \\ & & & a_{N-2} & \beta_{N-2} \\ & & & & a_{N-1} & \beta_{N-1} \end{bmatrix}$$

(4.35)

and

$$U = \begin{bmatrix} 1 & \gamma_1 & & & \\ & 1 & \gamma_2 & & \\ & & .... & & \\ & & & 1 & \gamma_{N-2} \\ & & & & 1 \end{bmatrix}$$

(4.36)

where $L$ and $U$ are the lower and upper triangular matrices, respectively. Here the unknowns $(\beta_i, \gamma_i),\quad i = 1, 2, ..., N-1$ are to be related as [100]

$$\beta_1 = -1 - \frac{\lambda}{h}, \qquad \gamma_1 = \frac{\lambda}{\beta_1 h}$$

(4.37)

$$\beta_i = b_i - a_i\gamma_{i-1}, \quad i = 2, 3, ..., N - 1 \tag{4.38}$$

$$\beta_i\gamma_i = c_i, \quad i = 2, 3, ...., N - 2 \tag{4.39}$$

After defining these relations (4.34) becomes

$$LUF = s, \qquad UF = z, \qquad \text{and} \qquad Lz = s \tag{4.40}$$

we have

$$
\begin{bmatrix}
\beta_1 & & & & \\
a_2 & \beta_2 & & & \\
& & .... & & \\
& & a_{N-2} & \beta_{N-2} & \\
& & & a_{N-1} &
\end{bmatrix}
\begin{bmatrix}
z_1 \\ z_2 \\ z_3 \\ . \\ . \\ z_{N-2} \\ z_{N-1}
\end{bmatrix}
=
\begin{bmatrix}
s_1 \\ s_2 \\ s_3 \\ . \\ . \\ s_{N-2} \\ s_{N-1}
\end{bmatrix}
\tag{4.41}
$$

The unknown elements of z can be found by

$$z_1 = s_1/\beta_1, \; z_i = \frac{s_i - a_i z_{i-1}}{\beta_i}, i = 2, 3, ..., N - 1 \tag{4.42}$$

and

$$
\begin{bmatrix}
1 & \gamma_1 & & & \\
& 1 & \gamma_2 & & \\
& & .... & & \\
& & 1 & \gamma_{N-2} & \\
& & & 1 &
\end{bmatrix}
\begin{bmatrix}
F_1 \\ F_2 \\ . \\ . \\ . \\ F_{N-2} \\ F_{N-1}
\end{bmatrix}
=
\begin{bmatrix}
z_1 \\ z_2 \\ . \\ . \\ . \\ z_{N-2} \\ z_{N-1}
\end{bmatrix}
\tag{4.43}
$$

We then get

$$F_{i-1} = z_{i-1}, \qquad F_i = z_i - \gamma_i F_{i+1}, \qquad i = N - 2, N - 3, ..., 3, 2, 1 \tag{4.44}$$

which is a solution of (4.23). We can easily find f from $f' = F$ which in discretization form

$$\frac{f_{i+1} - f_i}{h} = F_i \tag{4.45}$$

gives a required solution of (4.11). A similar procedure can also opted for solutions $\theta$ and $\phi$. For the sake of brevity we only present coefficients for these ODEs and leave the details which follows on the same line as presented above. For example the energy equation(4.12) is

$$\frac{d^2\theta}{d\eta^2} = -\left(\frac{Pr_o}{(1 + \frac{4}{3}Rd)}(f\frac{d\theta}{d\eta} + Nb\frac{d\theta}{d\eta}\frac{d\phi}{d\eta} + Nt(\frac{d\theta}{d\eta})^2 + MEc(\frac{df}{d\eta} - E_1)^2 + \frac{2}{n+1}s\theta))\right)$$

$$\chi_2(\eta, \theta, \theta') = -\left(\frac{Pr_o}{(1 + \frac{4}{3}Rd)}(f_i(\frac{\theta_i - \theta_{i-1}}{h}) + Nb(\frac{\theta_i - \theta_{i-1}}{h})(\frac{\phi_i - \phi_{i-1}}{h})\right.$$
$$\left. + Nt(\frac{\theta_i - \theta_{i-1}}{h})^2 + MEc(F_i - E_1)^2 + \frac{2}{n+1}s\theta_i))\right) \tag{4.46}$$

$$A_{nn} = -\frac{\partial\chi}{\partial\theta'} = -\left(-\frac{Pr_o}{(1 + \frac{4}{3}Rd)}(f + Nb\phi' + 2Nt\theta'))\right) \tag{4.47}$$

$$A_{nn} = \frac{Pr_o}{(1 + \frac{4}{3}Rd)}(f_i + Nb(\frac{\phi_i - \phi_{i-1}}{h}) + 2N_t\frac{\theta_i - \theta_{i-1}}{h})) \tag{4.48}$$

$$B_{nn} = \frac{2Pr_o}{(n+1)(1 + 4/3Rd)}s \tag{4.49}$$

$$\frac{d^2\phi}{d\eta^2} = \frac{-Nt}{Nb}\frac{d^2\theta}{d\eta^2} - LePr_o f\phi' \tag{4.50}$$

$$\chi_3(\eta, \phi, \phi') = \frac{-Nt}{Nb}\frac{\theta_{i-1} - 2\theta_i + \theta_{i+1}}{h^2} - LePr_o(f_i\frac{\phi_i - \phi_{i-1}}{h}) \tag{4.51}$$

Similarly, the coefficients for (4.13) are written as

$$A_{nnn} = Pr_o Le f_i, \qquad B_{nnn} = 0 \tag{4.52}$$

Boundary conditions can easily be discretized by following the above procedure.

## 4.5.2 bvp4c

To solve the system of ODEs for Case A and Case B, we first transformed the system into a first order ODEs to compute the solution using *bvp4c*. For Case A it gives,

(a) Case A:

$$f = v_1, f' = v_2, f'' = v_3, f''' = v_3' = \frac{2n}{n+1}v_2^2 - v_1v_3 - M(E_1 - v_2) + Kpv_2,$$

$$v_4 = \theta, v_5 = \theta', \theta'' = v_5' = -\frac{Pr_o}{(1+\frac{4}{3})Rd}(v_1v_5 + Nbv_5v_7 + Ntv_5^2 + MEc(v_2 - E_1)^2 + \frac{2}{n+1}sv_4),$$

$$v_6 = \phi, v_7 = \phi', \phi'' = v_7' = -LePr_ov_1v_7 + \frac{Nt}{Nb}v_5'.$$

(b) Case B: The transformed ODEs for Case B are,

$$f = u_1, f' = u_2, f'' = u_3, f''' = u_3' = \frac{(u_3u_5)}{(u_4 - \theta_r)} + \frac{(u_4 - \theta_r)}{\theta_r}(-\frac{2n}{n+1}u_2^2 + u_1u_3 +$$

$$M(E_1 - u_2) - Kpu_2),$$

$$u_4 = \theta, u_5 = \theta', \theta'' = u_5' = \frac{-\epsilon u_5^2}{1 + \epsilon u_4} - \frac{Pr_o}{(1 + \epsilon u_4)(1 + \frac{4}{3}Rd)}(u_1u_5 +$$

$$NbNtu_5u_7 + Ntu_5^2 + MEc(u_2 - E_1)^2 + \frac{2}{n+1}su_4),$$

$$u_6 = \phi, u_7 = \phi', \phi'' = u_7' = -LePr_ou_1u_7 + \frac{Nt}{Nb}u_5'.$$

## 4.6 Results and Discussion

In this section, we present outcomes of our results both in tabulated and graphical forms.

In Table 4.1, we compare our results with literature for the $-f''(0)$ against distinct values of $n$ while fixing $\alpha = 0.25$ and $\alpha = 0.5$. The SFDM shows an excellent agreement when compared with *bvp4c* and the literature. In summary, the skin friction coefficient is higher for Case B and lower values for Case A.

In Table 4.2, $C_{fx_1}$ is measured for various parameters like $M$, $n$, $E_1$, $Kp$, $\alpha$ and $\theta_r$. Its value goes up by making change in $M$, $n$, $\alpha$, $Kp$ and $\theta_r$, while it gets lower by changing $E_1$.

Table 4.3 shared the heat and mass transfer rates for different parameters.

An electric field parameter $E_1$ enhances the velocity of the fluid as can be seen in Fig. 4.2. Lorentz force is responsible in increasing velocity due to the fact that $C_{fx_1}$ (as shown in Table 2) decreases.

In Fig.4.3, we noticed that momentum boundary layer thickness thins by increasing $Kp$. This decrease in velocity profile is due to increase in $C_{fx_1}$ for increasing values of $Kp$.

Fig. 4.4 describes influence of $\theta_r$ on momentum distribution. It is analyzed that momentum boundary later thins by escalating $\theta_r$. Relating to Table 2 where we can see that by increasing $\theta_r$, magnitude of $C_{fx_1}$ increases, which causes the reduction in velocity. By increasing viscosity provide more resistance to the fluid motion since high shear stress required to more viscous fluids.

The effect of $\alpha$ on temperature can be seen in Fig. 4.5. It is observed that only some energy is transmitted from the surface to that of the liquid when we raise the wall thickness parameter.

Fig. 4.6 is plotted to perceive the effect of $Rd$ on temperature profile. It is found that with the rise in $Rd$ the temperature of fluid enhances significantly as an increment in the $Rd$ provides more energy to the fluid which increases the thickness of the thermal boundary layer.

In Fig. 4.7, it is noticed that enhancement in $Pr_o$ causes the reduction in temperature profile. The reason for this decrease is that Prandtl number $Pr_0$'s smaller values are equivalent to increasing thermal conductivity. Since thermal conductivity of air is higher ultimately temperature is higher. However, for high Prandtl number corresponds to low thermal conductivity and lower temperature flow.

In Fig. 4.8, we illustrate the influence of Biot number $B_i$ on the temperature profile. It is seen that for higher values of $B_i$ the thermal boundary layer thickness increases. This increase in temperature profile is due to the heat transfer rate. Since the thermal conductivity

is dominant compare to convection, therefore, heat transport more as Biot number increases.

To examine the effects of $Ec$ on thermal profile we plot Fig. 4.9. For higher values of $Ec$, it is evaluated that somehow the temperature of the fluid rises and the thermal boundary layer gets thinner. Eckert number is the ratio of kinetic energy of fluid and enthalpy. For increasing values of Eckert number the kinetic energy increases which causes enhancement in fluid temperature.

Fig. 4.10 is plotted to perceive the effect of $Nb$ on concentration profile. It is concluded that higher values of $Nb$ causes reduction in nanoparticles concentration profile.

Fig. 4.11 is presented to characterize the behaviour of $Nt$ on concentration profile. It is noted that by increasing $Nt$, we find reduction of the nanoparticles in concentration profile.

In Figs.4.12 ($Pr_o = 1$) and 4.13($Pr_o = 6.8$), it is found that increase in $\epsilon$ enhances the temperature profile. Table 3 indicates that $Nu_{x_1}$ decreases with increasing $\epsilon$. Due to this heat transfer rate increases and hence temperature profile increases.

Fig. 4.14 and Fig. 4.15 is drawn to see the impacts of $Ec$ and $Rd$ on temperature distribution respectively. It is noted that temperature profile increases for increasing values of $Ec$ and $Rd$.

Fig. 4.16 shows the effects of $B_i$ on temperature profile. It is shown that an enhancement in $B_i$ causes enhancement in temperature distribution.

The effects of $Kp$ and $M$ on skin friction is presented in Fig. 4.17. It is examined that skin friction shows improvement for rising values of $Kp$ and $M$ for both cases A and B.//

Impacts of $Rd$ and $Ec$ on local Nusselt number are displayed in Fig. 4.18. The local Nusselt number shows enhancement for higher values of $Rd$ and $Ec$.

Fig. 4.19 is portrayed to see impacts of $Le$ and $Pr_o$ on local Sherwood number. It is interpreted that local sherwood number climbs up for incremental values of $Le$.

Table 4.1: Resemblance of $-f''(0)$ from literature for various $n$ values (**CASE A**)

| $n$ | $\alpha$ | Fang et al. [11] | Khader and Ahmed [129] | Present result (bvp4c) | Present Result (SFDM) |
|---|---|---|---|---|---|
| 10 | 0.25 | 1.1433 | 1.1433 | 1.1433 | 1.1433 |
| 9 | | 1.1404 | 1.1404 | 1.1404 | 1.1404 |
| 7 | | 1.1323 | 1.1322 | 1.1323 | 1.1323 |
| 5 | | 1.1186 | 1.1186 | 1.1186 | 1.1186 |
| 3 | | 1.0905 | 1.0904 | 1.0905 | 1.0905 |
| 1 | | 1.0000 | 1.0000 | 1.0000 | 1.0000 |
| 0.5 | | 0.9338 | 0.9337 | 0.9338 | 0.9338 |
| 0 | | 0.7843 | 0.7843 | 0.7843 | 0.7843 |
| -1/3 | | 0.5000 | 0.5000 | 0.5000 | 0.5025 |
| -0.5 | | 0.0833 | 0.0833 | 0.0833 | 0.0892 |
| 10 | 0.5 | 1.0603 | 1.0603 | 1.0603 | 1.0603 |
| 9 | | 1.0589 | 1.0588 | 1.0589 | 1.0589 |
| 7 | | 1.0550 | 1.0551 | 1.0551 | 1.0551 |
| 5 | | 1.0486 | 1.0486 | 1.0486 | 1.0486 |
| 3 | | 1.0359 | 1.0358 | 1.0359 | 1.0359 |
| 2 | | 1.0234 | 1.0234 | 1.0234 | 1.0234 |
| 1 | | 1.0000 | 1.0000 | 1.0000 | 1.0000 |
| 0.5 | | 0.9799 | 0.9798 | 0.9799 | 0.9798 |
| 0.00 | | 0.9576 | 0.9577 | 0.9576 | 0.9577 |
| -0.5 | | 1.1667 | 1.1667 | 1.1667 | 1.1661 |

Table 4.2: Resemblance of $-f''(0)$ for separate values of $M, n, \alpha, E_1$ and $\theta_r$.

| | | | | | | Case B | | Case A | |
|---|---|---|---|---|---|---|---|---|---|
| $M$ | $n$ | $\alpha$ | $E_1$ | $Kp$ | $\theta_r$ | $-f''(0)(bvp4c)$ | $-f''(0)$(SFDM) | $-f''(0)(bvp4c)$ | $-f''(0)$ (SFDM) |
| 0 | 0.5 | 0.3 | 0.1 | 0.1 | -5 | 1.075408 | 1.075408 | 0.996308 | 0.996308 |
| 0.3 | | | | | | 1.184031 | 1.184031 | 1.097247 | 1.097247 |
| 0.7 | | | | | | 1.335487 | 1.335487 | 1.236298 | 1.236298 |
| 0.1 | 0 | | | | | 0.983771 | 0.987475 | 0.907889 | 0.907889 |
| | 0.5 | | | | | 1.106245 | 1.106245 | 1.025923 | 1.025923 |
| | 1 | | | | | 1.160763 | 1.160763 | 1.078835 | 1.078835 |
| | 0.5 | 0.4 | | | | 1.125682 | 1.125682 | 1.043448 | 1.043448 |
| | | 0.7 | | | | 1.185376 | 1.185376 | 1.097515 | 1.097515 |
| | | 1 | | | | 1.247097 | 1.247097 | 1.153791 | 1.153791 |
| | | 0.3 | 0.5 | | | 1.025633 | 1.025633 | 0.954581 | 0.954581 |
| | | | 1 | | | 0.940761 | 0.940761 | 0.877466 | 0.877466 |
| | | | 1.5 | | | 0.864007 | 0.864007 | 0.807036 | 0.807036 |
| | | | 0.1 | 0.1 | | 1.106245 | 1.106245 | 1.025923 | 1.025923 |
| | | | | 0.3 | | 1.205899 | 1.205899 | 1.12657 | 1.12657 |
| | | | | 0.5 | | 1.294325 | 1.294325 | 1.216757 | 1.216757 |
| | | | | 0.1 | -10 | 1.066455 | 1.066455 | | |
| | | | | | -1 | 1.391356 | 1.391356 | | |
| | | | | | -0.5 | 1.703479 | 1.703479 | | |



$Pr_o$=Le =1.3, M=n=Nb=0.5, Rd=Nt=Ec=0.2,s=Kp=0.1,$\alpha$=0.3,$\varepsilon$=0.5,$\theta_r$=-0.5
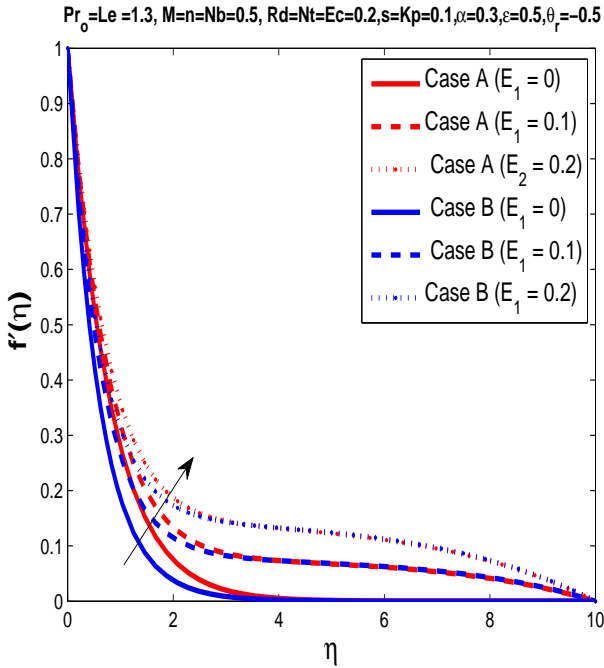
Figure 4.2: Velocity $f'(\eta)$ for different $E_1$.(danial et al. [130])



$Pr_o$=Le =1.3, M=n=Nb=0.5, Rd=Nt=Ec=0.2,s=0.1,$E_1$=0,$\alpha$=0.3,$\varepsilon$=0.5,$\theta_r$=-0.5
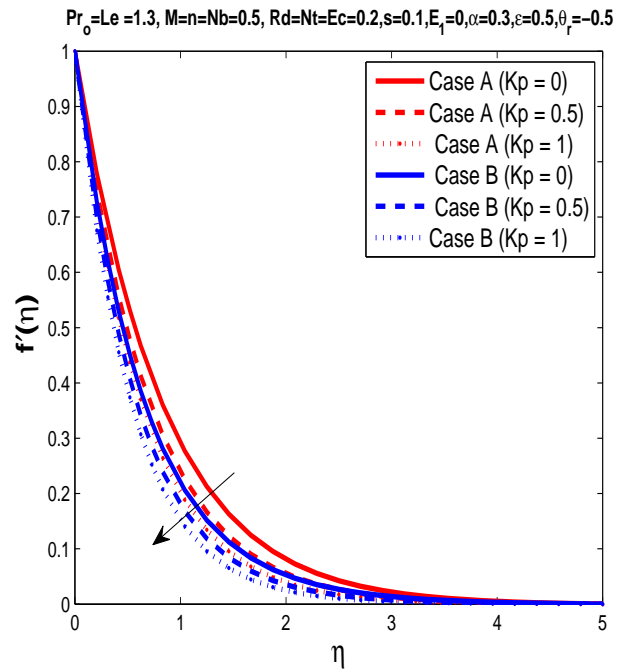
Figure 4.3: Velocity $f'(\eta)$ for different $Kp$.

Table 4.3: Comparison of $-\theta'(0)$ and $-\phi'(0)$ for $Rd$, $Ec$, $Le$, $Nb$, $Nt$, $n$, $Pr_o$, $s$, $\alpha$ and $\epsilon$ of Case B with Case A, respectively .

| | | | | | | | | | | Case B | | Case A | |
|---|---|---|---|---|---|---|---|---|---|---|---|---|---|
| $Rd$ | $Ec$ | $Le$ | $Nb$ | $Nt$ | $n$ | $Pr_o$ | $s$ | $\alpha$ | $\epsilon$ | $-\theta'(0)$ | $-\phi'(0)$ | $-\theta'(0)$ | $-\phi'(0)$ |
| 0.4 | 0.1 | 1 | 0.1 | 0.2 | 0.5 | 1 | 0.1 | 0.3 | 0.2 | 0.2125241 | -0.4250431 | 0.2477734 | -0.4955469 |
| 0.7 | | | | | | | | | | 0.1682977 | -0.3365954 | 0.2047175 | -0.409435 |
| 1 | | | | | | | | | | 0.1331988 | -0.2663976 | 0.1704 | -0.3407401 |
| 0.2 | 0.2 | | | | | | | | | 0.2450324 | -0.4900648 | 0.2790463 | -0.5580926 |
| | 0.6 | | | | | | | | | 0.2263721 | -0.4527441 | 0.2603162 | -0.5206325 |
| | 1 | | | | | | | | | 0.2077006 | -0.4154012 | 0.2415691 | -0.4831381 |
| | 0.1 | 0.7 | | | | | | | | 0.2507037 | -0.5014074 | 0.2847274 | -0.5694548 |
| | | 1 | | | | | | | | 0.2496957 | -0.4993915 | 0.2837261 | -0.5674523 |
| | | 1.3 | | | | | | | | 0.2489893 | -0.4979786 | 0.283001 | -0.566002 |
| | | 1 | 0.2 | | | | | | | 0.2496958 | -0.2496958 | 0.2837261 | -0.2837261 |
| | | | 0.5 | | | | | | | 0.2496958 | -0.0998783 | 0.2837261 | -0.1134905 |
| | | | 0.7 | | | | | | | 0.2496958 | -0.07134165 | 0.2837261 | -0.08106461 |
| | | | 0.1 | 0.1 | | | | | | 0.2532452 | -0.2532452 | 0.2869886 | - 0.2869886 |
| | | | | 0.2 | | | | | | 0.249657 | -0.4993915 | 0.2837261 | -0.5674523 |
| | | | | 0.4 | | | | | | 0.2424194 | -0.969777 | 0.2770397 | -1.108159 |
| | | | | 0.2 | 0 | | | | | 0.28097 | -0.5619401 | 0.3176236 | -0.6352471 |
| | | | | | 0.5 | | | | | 0.2496957 | -0.4993915 | 0.2837261 | -0.5674523 |
| | | | | | 1 | | | | | 0.236645 | -0.4732899 | 0.268578 | -0.5371561 |
| | | | | | 0.5 | 0.7 | | | | 0.1808165 | -0.361633 | 0.2169344 | -0.4338689 |
| | | | | | | 1 | | | | 0.2496957 | -0.4993915 | 0.2837261 | -0.5674523 |
| | | | | | | 1.3 | | | | 0.3014584 | -0.6029168 | 0.3334471 | -0.6668941 |
| | | | | | | 1 | 0 | | | 0.3226349 | -0.6452698 | 0.3492327 | -0.6984654 |
| | | | | | | | 0.1 | | | 0.2496957 | -0.4993915 | 0.2837261 | -0.5674523 |
| | | | | | | | 0.1 | 0.4 | | 0.2597021 | -0.5194042 | 0.2935494 | -0.5870988 |
| | | | | | | | | 0.7 | | 0.2886493 | -0.5772986 | 0.3219052 | -0.6438104 |
| | | | | | | | | 1 | | 0.3160671 | -0.6321342 | 0.3486554 | -0.6973109 |
| | | | | | | | | 0.3 | 0.3 | 0.2380814 | -0.4761629 | | |
| | | | | | | | | | 0.5 | 0.2168179 | -0.4336357 | | |
| | | | | | | | | | 0.8 | 0.1892523 | -0.3785047 | | |

**Pr$_o$=Le =1.3, M=n=Nb=0.5, Rd=Nt=Ec=0.2,s=0.1,E$_1$=0,α=0.3,ε=0.5**
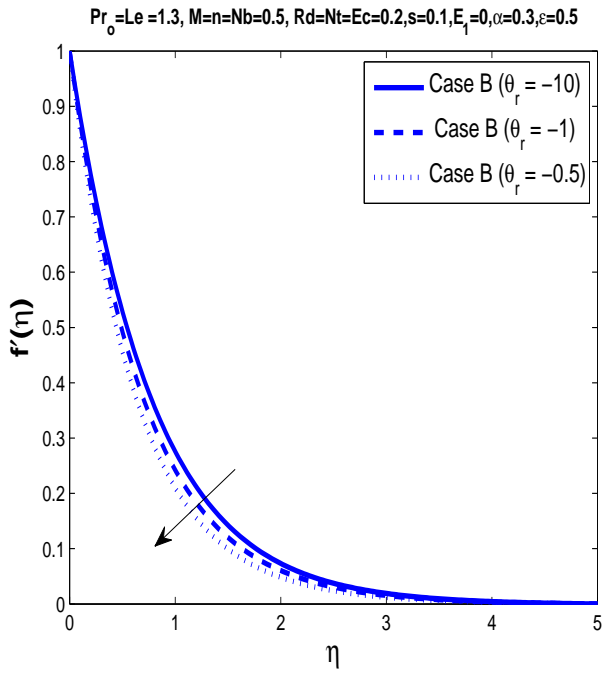
Figure 4.4: Velocity profile $f'(\eta)$ for different $\theta_r$.



**Pr$_o$=Le =1.3, M=n=Nb=0.5, Rd=Nt=Ec=0.2,s=Kp=0.1,E$_1$=0,ε=0.5,θ$_r$=−0.5**
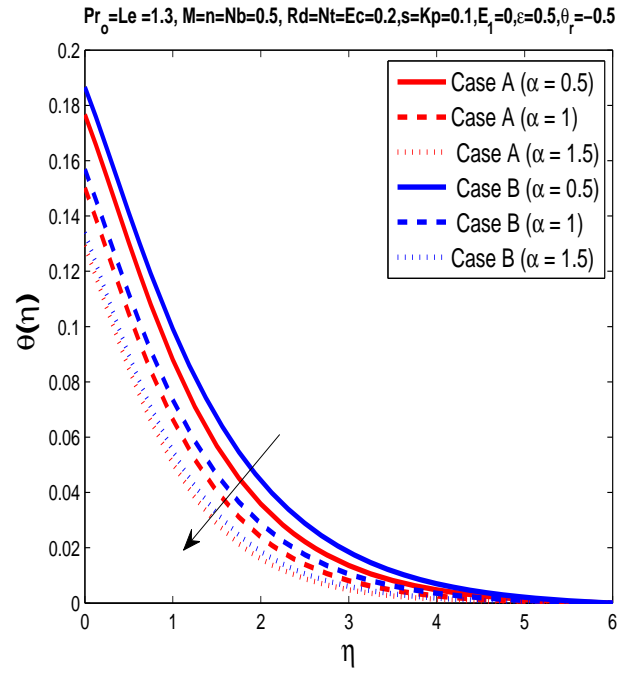
Figure 4.5: Temperature profile $\theta(\eta)$ for different $\alpha$ .



**Pr$_o$=Le =1.3, M=n=Nb=0.5, Nt=Ec=0.2,s=0,E$_1$=0,Kp=0.1,α=0.3,ε=0.5,θ$_r$=−0.5**
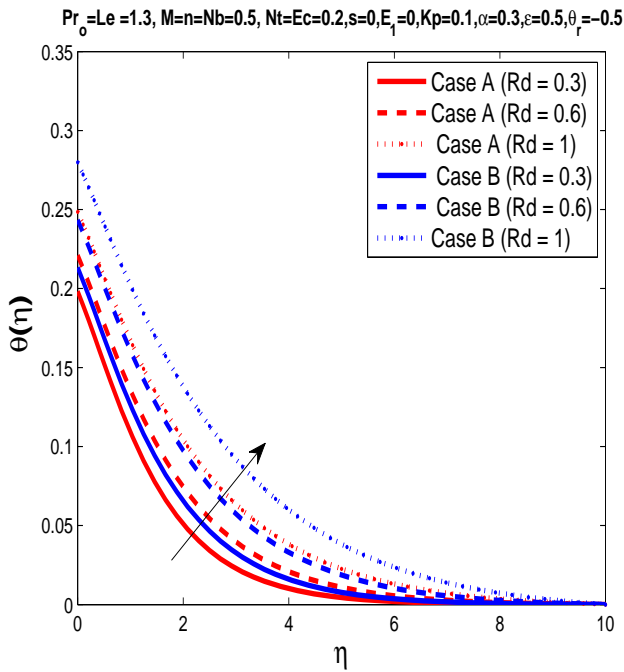
Figure 4.6: Temperature profile $\theta(\eta)$ for different $Rd$ .



**Le =1.3, M=n=Nb=0.5, Rd=Nt=Ec=0.2,s=0,E$_1$=0,Kp=0.1,α=0.3,ε=0.5,θ$_r$=−0.5**
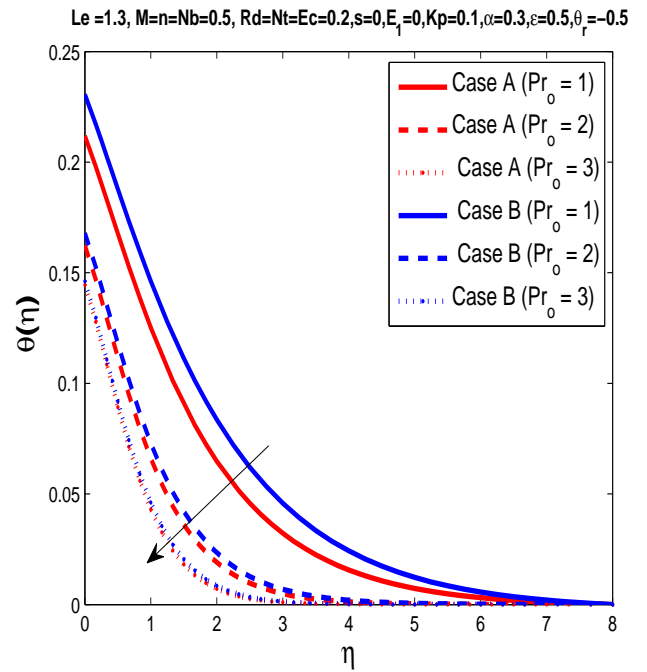
Figure 4.7: Temperature profile $\theta(\eta)$ for different $Pr_o$ .
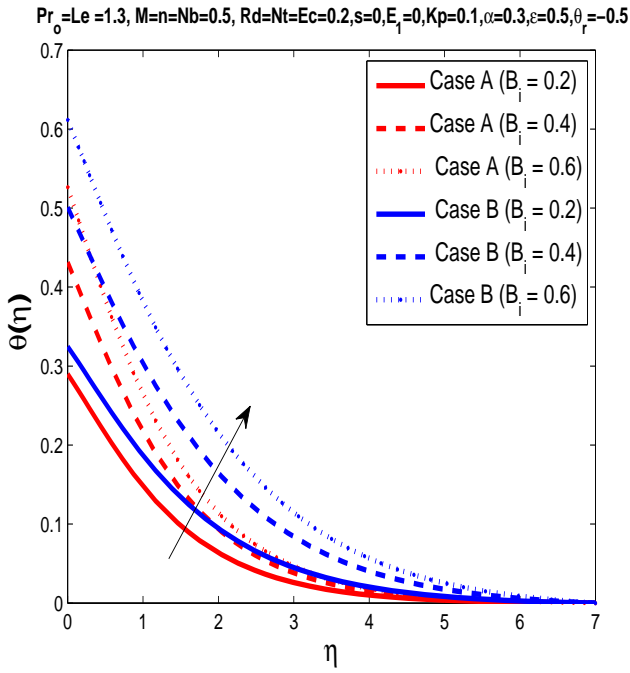
Figure 4.8: Temperature profile $\theta(\eta)$ for different $B_i$ .
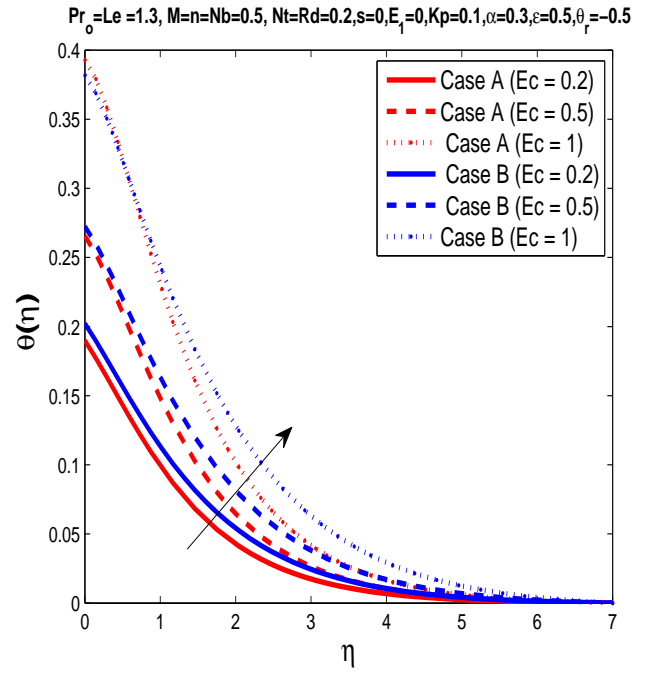


Figure 4.9: Temperature profile $\theta(\eta)$ for different $Ec$ .
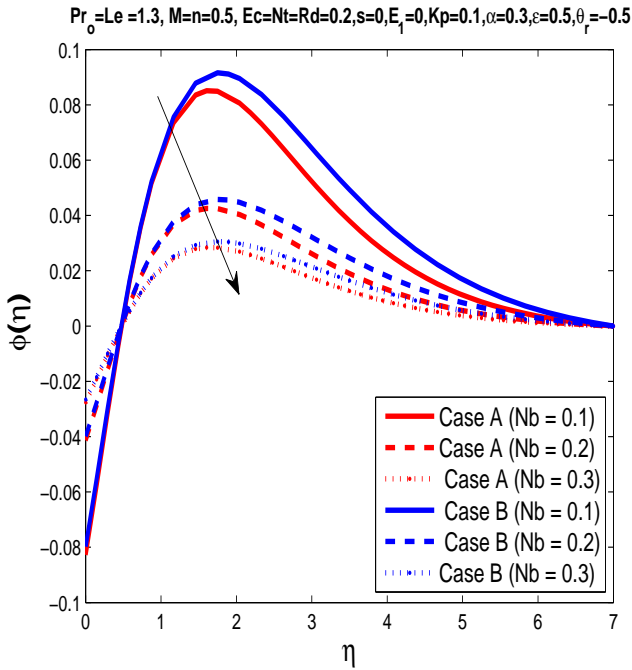


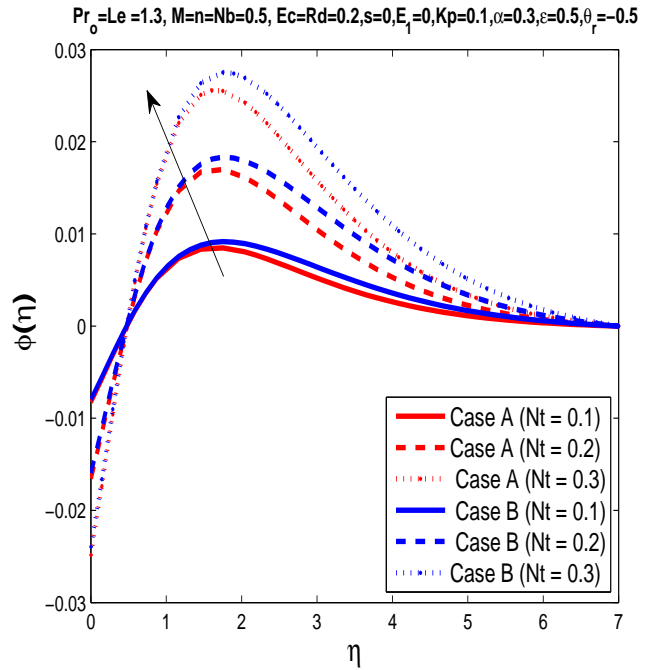Figure 4.10: Concentration profile $\phi(\eta)$ for different $Nb$ .



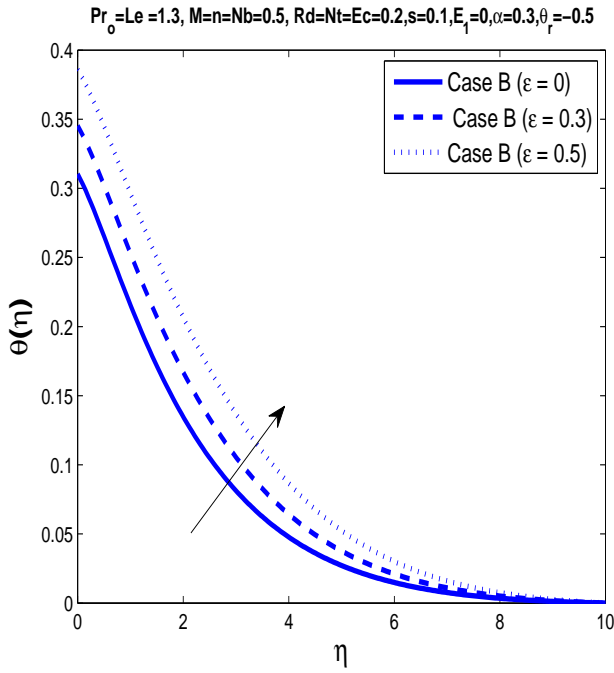Figure 4.11: Concentration profile $\phi(\eta)$ for different $Nt$.

81

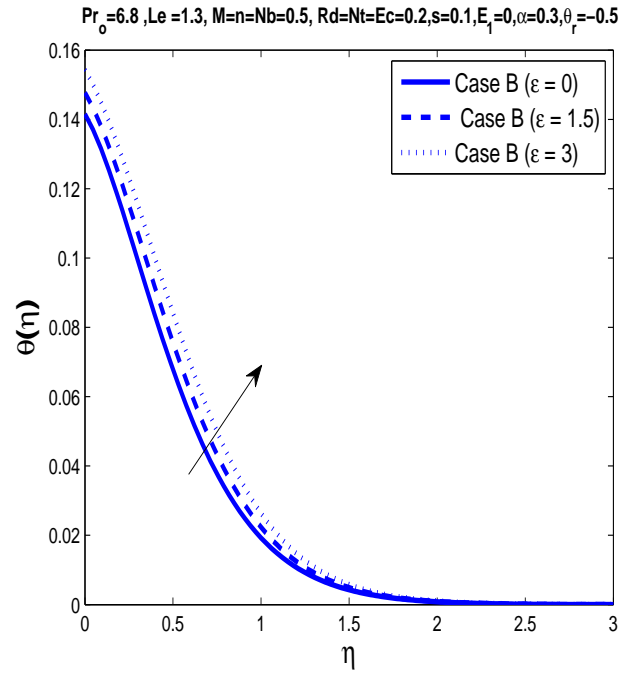Figure 4.12: Temperature profile $\theta(\eta)$ for different $\epsilon$ .



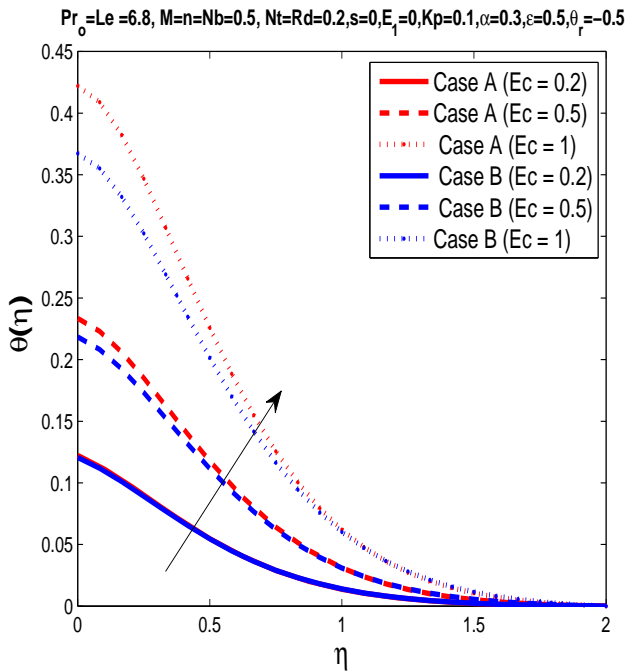Figure 4.13: Temperature profile $\theta(\eta)$ for different $\epsilon$.



Figure 4.14: temperature profile $\theta(\eta)$ for different $Ec$ .
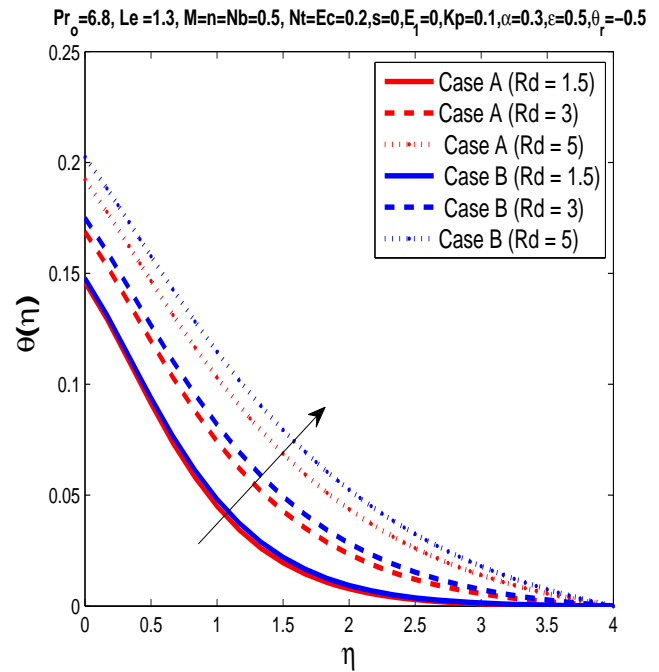


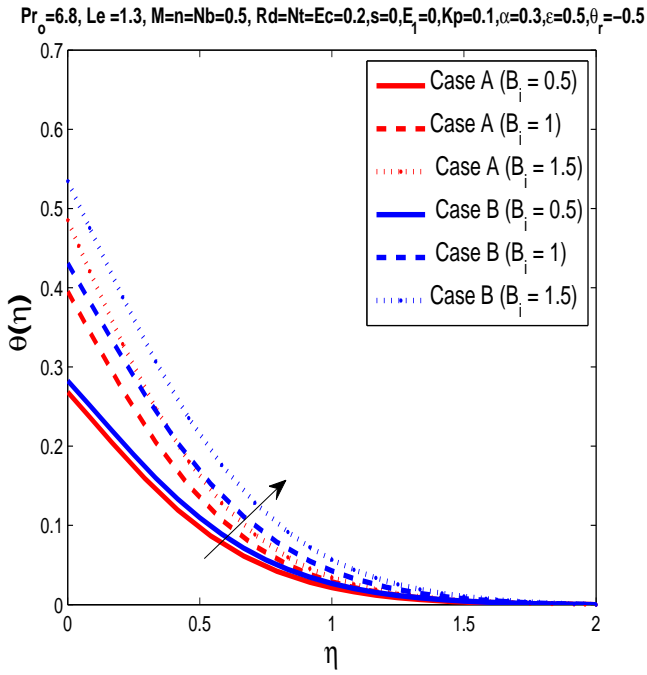Figure 4.15: Temperature profile $\theta(\eta)$ for different $Rd$.

Figure 4.16: The temperature profile $\theta(\eta)$ for different $B_i$.
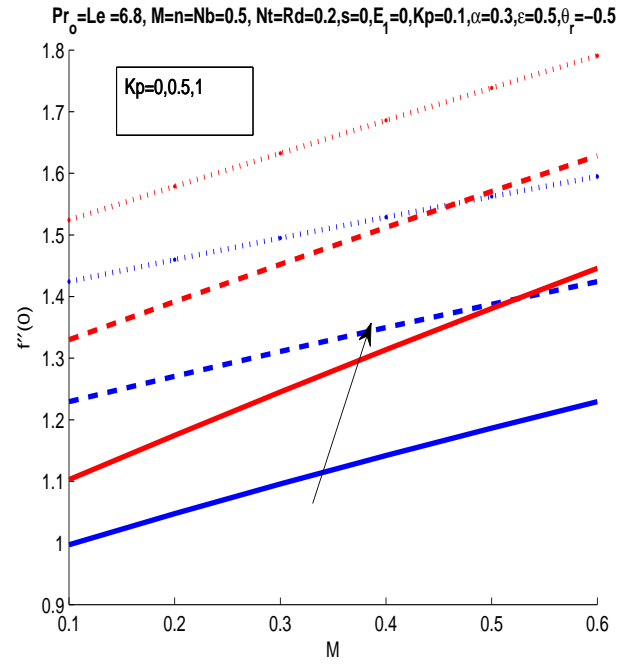


Figure 4.17: The skin friction coefficient with variations with in $Kp$ and $M$.
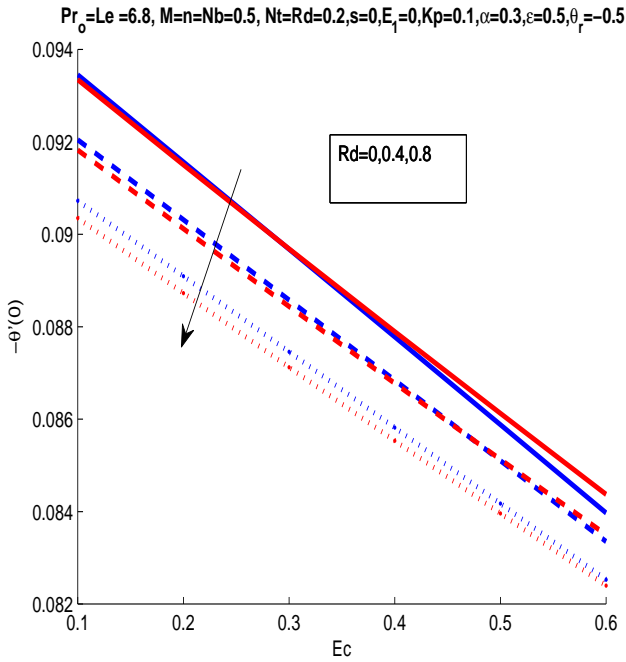


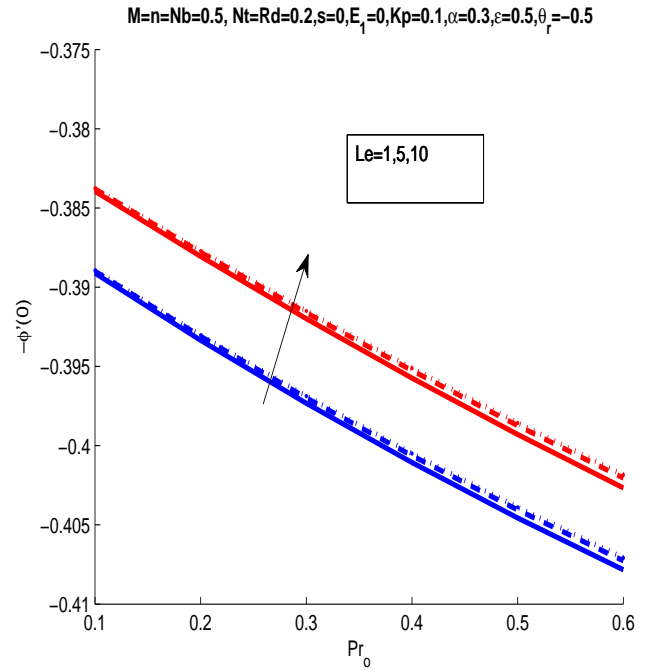Figure 4.18: The reduced Nusselt number with variations in $Ec$ and $Rd$.



Figure 4.19: The sherwood number with variations with $Le$ and $Pr_o$.

Table 4.4: Comparison of $-\theta'(0)$ and $-\phi'(0)$ for $Rd$, $Ec$, $Le$, $Nb$, $Nt$, $n$, $Pr_o$, $s$, $\alpha$ and $\epsilon$ of Case B with Case A, respectively .

| | | | | | | | | | | Case B | |
|------|-----|-----|-----|-----|-----|--------|-----|----------|------------|-------------|-------------|
| $Rd$ | $Ec$ | $Le$ | $Nb$ | $Nt$ | $n$ | $Pr_o$ | $s$ | $\alpha$ | $\epsilon$ | $-\theta'(0)$ | $-\phi'(0)$ |
| 0.4 | 0.1 | 1 | 0.1 | 0.2 | 0.5 | 6.8 | 0.1 | 0.3 | 0.2 | 0.5799 | -1.1598 |
| 0.7 | | | | | | | | | | 0.4610 | -1.0781 |
| 1 | | | | | | | | | | 0.5046 | -1.0092 |
| 0.2 | 0.2 | | | | | | | | | 0.6010 | -1.2019 |
| | 0.6 | | | | | | | | | 0.5561 | -1.1122 |
| | 1 | | | | | | | | | 0.5113 | -1.0225 |
| | 0.1 | 0.7 | | | | | | | | 0.6135 | -1.2269 |
| | | 1 | | | | | | | | 0.6122 | -1.2243 |
| | | 1.3 | | | | | | | | 0.6110 | -1.2219 |
| | | 1 | 0.2 | | | | | | | 0.6122 | -0.6122 |
| | | | 0.5 | | | | | | | 0.6122 | -0.2449 |
| | | | 0.7 | | | | | | | 0.6122 | -0.1749 |
| | | | 0.1 | 0.1 | | | | | | 0.6145 | -0.6145 |
| | | | | 0.2 | | | | | | 0.6122 | -1.2243 |
| | | | | 0.4 | | | | | | 0.6072 | -2.4289 |
| | | | | 0.2 | 0 | | | | | 0.6878 | -1.3756 |
| | | | | | 0.5 | | | | | 0.6122 | -1.2243 |
| | | | | | 1 | | | | | 0.5626 | -1.1252 |
| | | | | | 0.5 | 5 | | | | 0.5596 | -1.1192 |
| | | | | | | 6.8 | | | | 0.6122 | -1.2243 |
| | | | | | | 10 | | | | 0.6729 | -1.3458 |
| | | | | | | 6.8 | 0 | | | 0.6461 | -1.2921 |
| | | | | | | | 0.1 | | | 0.6122 | -1.2243 |
| | | | | | | | 0.1 | 0.4 | | 0.6296 | -1.2592 |
| | | | | | | | | 0.7 | | 0.6754 | -1.3508 |
| | | | | | | | | 1 | | 0.7129 | -1.4258 |
| | | | | | | | | 0.3 | 0.3 | 0.6053 | -1.2107 |
| | | | | | | | | | 0.5 | 0.5917 | -1.1834 |
| | | | | | | | | | 0.8 | 0.5714 | -1.1428 |

## 4.7 Conclusions

This analysis establishes two goals. Firstly, assessment on distinctive features for constant and variable properties has been done. Secondly, we adopted new numerical process, the SFDM, to compute solution and compared its accuracy with *bvp4c*. The notable results for both cases, Case A and B are as follows:

- The numerical technique, the SFDM, has produced excellent results with high accuracy as shown in Table 1 and 2.

- Momentum boundary layer thickness grows by increasing $E_1$ whereas it decreases with $K_p$ and $\theta_r$.

- Thermal boundary layer thickness raises by raising $R_d$, $B_i$, $Ec$, $\epsilon$ while decreases for higher values of $\alpha$ and $Pr_o$.

- Concentration boundary layer thickness decreases by increasing $Nb$ and increases by increasing $Nt$.

- It is shown that the results are different for constant and variable fluid properties. For variable fluid properties heat transfer and mass transfer rates are lower than the constant fluid properties. The skin friction coefficient increases for variable fluid properties compare to constant fluid properties.

# Chapter 5

# EMHD Flow of Powell-Eyring Nanofluid Featuring Variable Liquid Characteristic and Variable Thickness Stretching Surface

This chapter investigates the constant and variable fluid properties together to analyze their effect on electrical magnetohydrodynamics (EMHD) Powell-Eyring nanofluid flow with thermal radiation and heat generation over a variable thickness sheet. The similarity variables assist in having ODEs acquired from PDEs. A novel numerical procedure, the SFDM, is developed to calculate the physical solution. The SFDM described here is simple, efficient and accurate. To highlight its accuracy, results of the SFDM are compared with the literature. The results seems to indicate that the SFDM and the literature give a close agreed solutions. The velocity, temperature and concentration distributions, when drawn at the same time for constant and variable physical features, are observed to be affected against incremental values of the flow variables. Furthermore, the impact of contributing flow variables on the $C_{fx_1}$ (drag on the wall), $Nu_{x_1}$ (heat transfer rate on the wall) and $Sh_{x_1}$ (mass transfer on the wall) are illustrated by data distributed in tables. The non dimensional skin friction coefficient experience higher values for constant flow regimes especially in comparison with changing flow features.

This chapter is organized as follows.

Introduction of the chapter is presented in Section 5.1. In Sections 5.2 and 5.3 theoretical model and the analysis on fluid properties are explained. Section 5.4 illustrates SFDM. The result and discussion part of the chapter is presented in Section 5.5. Section 5.6 analyzed the conclusion of the chapter.

## 5.1   Introduction

Hayat et al. [134] discussed melting heat transfer for Powell-Eyring fluid. Jalil and Asghar [135] also used Powell-Eyring fluid for their analysis and found solution by Lie group method. Fluid flow with numerical and series solutions over an exponentially stretchable surface with Powell-Eyring model have been discussed in Mushtaq et al. [136]. In Javed et al. [137] the flow of Eyring-Powell non-Newtonian fluid have been discussed. Mustafa et al. [138] discussed MHD boundary layer nanofluid for second grade fluid. Motsumi et al. [139] discussed thermal radiation and viscous dissipation on boundary layer flow of nanofluids over a permeable moving flat plate. Hayat et al. [140] investigated the MHD eyring-Powell nanofluid flow past a variable thickness surface. They reported that impacts of thermophoresis parameter on temperature and concentration distributions are similar. The novelty of the current work lies in addressing the nanofluid of Powell-Eyring along with constant and variable fluid properties. A novel computational technique, the SFDM, has been tested for the PowellŰEyring nanofluids in addition to theoretical modeling of fluid flow. The SFDM is simple, accurate, and easy to implement in MATLAB.

## 5.2   Theoretical Model

Consider a magnetohydrodynamic (MHD) Powell-Eyring nanofluid due to an uneven stretching surface emerges from the narrow slit with variable fluid characteristics. Assume that varying magnetic field $B_1(x_1) = B_0(x_1+b^*)^{\frac{n-1}{2}}$ is directed perpendicular to the flow motion. In addition, variable electric field is chosen as $E_1^*(x_1) = E_0(x_1+b^*)^{\frac{n-1}{2}}$. Also $K(x_1) = K_0(x_1+b^*)^{1-n}$ is the variable permeability. The surface has a nonlinear stretching velocity $U_w = a_0(x_1+b^*)^n$. Furthermore, the thickness of the sheet is varying by the relation $y_1 = A(x_1+b^*)^{\frac{1-n}{2}}$, in which
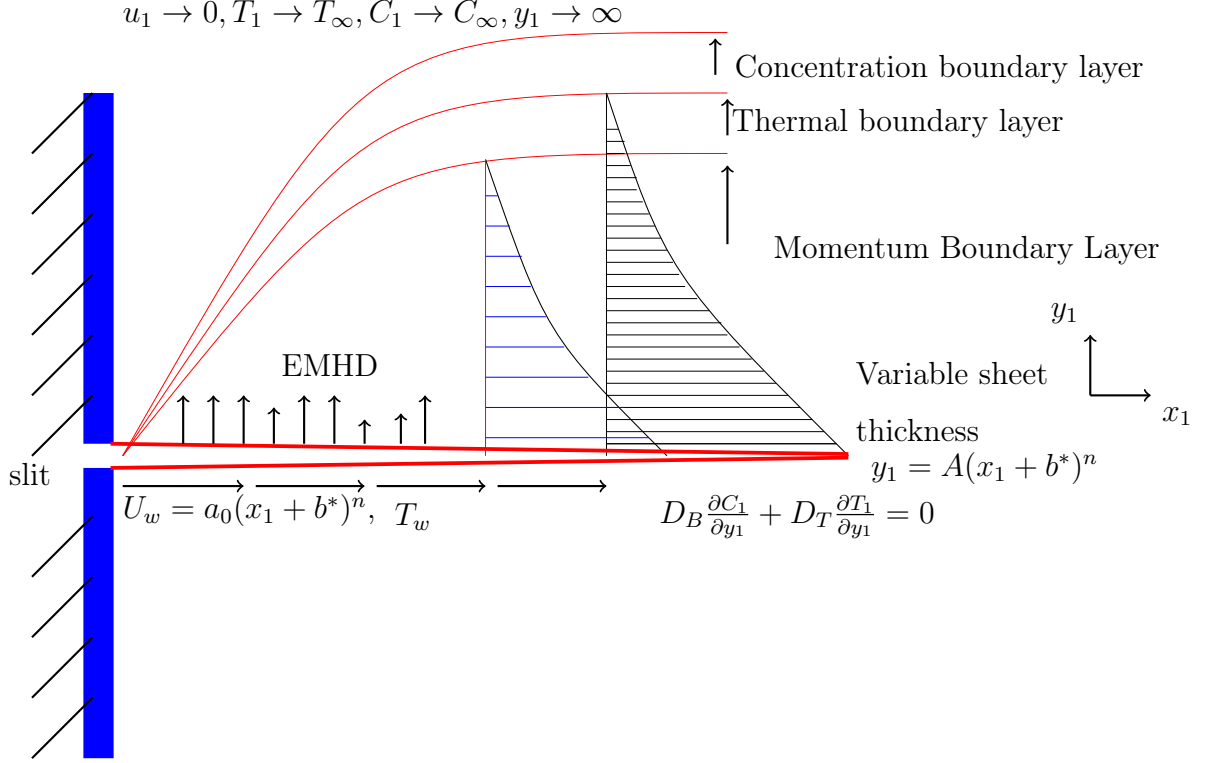
Figure 5.1: Geometry of the problem.

$A$ is a very small constant. Fluid flow configuration is illustrated in Fig. 5.1.

After incorporating aforementioned fluid flow assumptions, in view of Daniel et al. [131] and Hayat et al. [140], the following equations of motion we get:

$$\frac{\partial u_1}{\partial x_1} + \frac{\partial v_1}{\partial y_1} = 0,  \tag{5.1}$$

$$u_1 \frac{\partial u_1}{\partial x_1} + v_1 \frac{\partial u_1}{\partial y_1} = \frac{1}{\rho_1} \frac{\partial}{\partial y_1} \left( \mu_1(T_1) \frac{\partial u_1}{\partial y_1} \right) + \frac{1}{\rho_1 \beta_1 d} \frac{\partial^2 u_1}{\partial y_1^2} - \frac{1}{2\rho_1 \beta_1 d^3} \left( \frac{\partial u_1}{\partial y_1} \right)^2 \frac{\partial^2 u_1}{\partial y_1^2} +$$
$$\frac{\sigma}{\rho_1} \left( E_1^*(x_1) B_1(x_1) - B_1^2(x_1) u_1 \right) + g\beta(T_1 - T_\infty) - \frac{\mu_1 u_1}{\rho_1 K(x_1)},  \tag{5.2}$$

$$u_1 \frac{\partial T_1}{\partial x_1} + v_1 \frac{\partial T_1}{\partial y_1} = \frac{1}{\rho_1 C_p} \frac{\partial}{\partial y_1} \left( k_1(T_1) \frac{\partial T_1}{\partial y_1} \right) - \frac{1}{\rho_1 C_p} \frac{\partial q_r}{\partial y_1} + \frac{\sigma}{\rho_1 C_p} \left( u_1 B_1(x_1) - E_1^*(x_1) \right)^2 +$$
$$\frac{Q_1(x_1)}{\rho C_p}(T_1 - T_\infty) + \tau_1 \left( D_B \frac{\partial T_1}{\partial y_1} \frac{\partial C_1}{\partial y_1} + \frac{D_T}{T_\infty} \left( \frac{\partial T_1}{\partial y_1} \right)^2 \right),  \tag{5.3}$$

$$u_1 \frac{\partial C_1}{\partial x_1} + v_1 \frac{\partial C_1}{\partial y_1} = D_B \frac{\partial^2 C_1}{\partial y_1^2} + \frac{D_T}{T_\infty} \frac{\partial^2 T_1}{\partial y_1^2},  \tag{5.4}$$

Where $(u_1, v_1)$, $\mu_1$, $\rho_1$, $C_p$ are the velocity components, the dynamic viscosity, the density and the specific heat capacity, respectively. Moreover, $E_1^*(x_1)$, $B_1(x_1)$, $T_1$ and $C_1$ are the electric

field, the magnetic field, fluid temperature and nanoparticle concentration, respectively. Also, $T_w$ and $T_\infty$ are wall and free stream temperatures respectively. The parameters $D_B$ and $D_T$ are characterized as the Brownian diffusion and thermophoretic diffusion coefficients, respectively. In $\tau_1 = \frac{(\rho_1 c)_p}{(\rho_1 c)_f}$, $(\rho_1 c)_p$ is the effective heat capacity of the nanoparticle and $(\rho_1 c)_f$ is the heat capacity of the fluid. $q_r$ represents radiation due to heat flow and $Q_1(x_1)$ is heat generation/absorption parameter.

The boundary conditions needed to solve (5.1), (5.2), (5.3) and (5.4) are given by

$$u_1 = U_w(x_1) = a_o(x_1 + b)^n, \quad v_1 = 0, \quad T_1 = T_w, \quad D_B \frac{\partial C_1}{\partial y_1} + \frac{D_T}{T_\infty} \frac{\partial T_1}{\partial y_1} = 0 \quad at \quad y_1 = A(x_1 + b^*)^{\frac{1-n}{2}},$$

$$u_1 \longrightarrow 0, \quad T_1 \longrightarrow T_\infty, \quad C_1 \longrightarrow C_\infty \quad as \quad y_1 \longrightarrow \infty.$$

$$(5.5)$$

With the following transformations

$$\xi = \sqrt{\left(\frac{n+1}{2}\right) \frac{a_0(x_1 + b^*)^{n-1}}{\nu_0}} y_1, \psi = \sqrt{\frac{2}{n+1} \nu_0 a_0 (x_1 + b^*)^{n+1}} F(\xi), \alpha = A \left(\frac{(n+1)a_0}{2\nu_0}\right)^{\frac{1}{2}},$$

$$\eta = \xi - \alpha = y_1 \sqrt{\left(\frac{n+1}{2}\right) \frac{a_0(x_1 + b^*)^{n-1}}{\nu_0}} - \alpha. \tag{5.6}$$

$$\tilde{\Theta} = \frac{T_1 - T_\infty}{T_w - T_\infty}, \quad \tilde{\Phi} = \frac{C_1 - C_\infty}{C_w - C_\infty}, \quad u_1 = a_0(x_1 + b^*)^n \tilde{F}'(\xi),$$

$$v_1 = -\sqrt{\frac{n+1}{2} \nu_0 a_0 (x_1 + b^*)^{n-1}} \tilde{F}(\xi) - \xi \left(\frac{n-1}{n+1}\right) \tilde{F}'(\xi) \sqrt{\frac{n+1}{2} \nu_0 a_0 (x_1 + b^*)^{n-1}}. \tag{5.7}$$

Eq. (5.1) is satisfied through $\psi$. In above $\nu_0 = \frac{\mu_0}{\rho_1}$ is an ambient kinematic viscosity. By using above transformations Eqs. (5.2), (5.3) and (5.4) resulted into:

$$\left(\frac{\mu_1}{\mu_o} \tilde{F}''(\xi)\right)' + N\tilde{F}'''(\xi) - N\lambda \left(\frac{n+1}{2}\right) \tilde{F}''^2(\xi) \tilde{F}'''(\xi) - \frac{2n}{n+1} \tilde{F}'^2(\xi) + \tilde{F}(\xi)\tilde{F}''(\xi) + M\left(E - \tilde{F}'(\xi)\right)$$

$$- Kp \frac{\mu_1}{\mu_o} \tilde{F}'(\xi) + Gr\tilde{\Theta}(\xi) = 0, \tag{5.8}$$

$$(1 + \frac{4}{3}Rd)\left(\frac{k_1}{k_0} \tilde{\Theta}'(\xi)\right)' + Pr_0(\tilde{F}(\xi)\Theta'(\xi) + Nb\tilde{\Theta}'(\xi)\tilde{\Phi}'(\xi) + Nt(\tilde{\Theta}'(\xi))^2 + MEc\left(\tilde{F}'(\xi) - E\right)^2$$

$$+ \frac{2}{n+1} s\tilde{\Theta}(\xi) = 0, \tag{5.9}$$

$$\tilde{\Phi}''(\xi) + \frac{Nt}{Nb} \tilde{\Theta}''(\xi) + LePr_0\tilde{F}(\xi)\tilde{\Phi}'(\xi) = 0. \tag{5.10}$$

Boundary conditions of the current problem are modified as:

$$\tilde{F} = \alpha\left(\frac{1-n}{1+n}\right), \quad \tilde{F}' = 1, \quad Nb\tilde{\Phi}' + Nt\tilde{\Theta}' = 0, \quad \tilde{\Theta} = 1, \quad \text{at} \ \ \alpha = A\left(\frac{(n+1)a_0}{2\nu_0}\right)^{\frac{1}{2}},$$

$$\tilde{\Theta} = 0, \quad \tilde{F}' = 0, \quad \tilde{\Phi} = 0, \text{when} \ \ \xi \to \infty. \quad (5.11)$$

Assuming $\tilde{F}(\xi) = \tilde{f}(\xi - \alpha) = \tilde{f}(\eta)$ we get

$$(\frac{\mu_1}{\mu_o}\tilde{f}''(\eta))' + N\tilde{f}'''(\eta) - N\lambda(\frac{n+1}{2})\tilde{f}''^{2(\eta)}\tilde{f}'''(\eta) - \frac{2n}{n+1}\tilde{f}'^{2(\eta)} + \tilde{f}\tilde{f}''(\eta) + M(E - \tilde{f}'(\eta))$$

$$- Kp\frac{\mu_1}{\mu_o}\tilde{f}'(\eta) + Gr\theta(\tilde{\eta}) = 0, \quad (5.12)$$

$$(1 + \frac{4}{3}Rd)(\frac{k_1}{k_0}\tilde{\theta}'(\eta))' + Pr_0(\tilde{f}(\eta)\tilde{\theta}'(\eta) + Nb\tilde{\theta}'(\eta)\tilde{\phi}'(\eta) + Nt(\tilde{\theta}'(\eta))^2 + MEc(\tilde{f}'(\eta) - E)^2$$

$$+ \frac{2}{n+1}s\theta(\tilde{\eta})) = 0, \quad (5.13)$$

$$\tilde{\phi}''(\eta) + \frac{Nt}{Nb}\tilde{\theta}''(\eta) + LePr_0\tilde{f}(\eta)\tilde{\phi}'(\eta) = 0. \quad (5.14)$$

The transformed boundary conditions on the new domain are written as:

$$\tilde{f}(\eta) = \alpha(\frac{1-n}{1+n}), \quad \tilde{f}'(\eta) = 1, \quad Nb\tilde{\phi}'(\eta) + Nt\tilde{\theta}'(\eta) = 0, \quad \tilde{\theta}(\eta) = 1, \quad \text{at} \ \ \eta = 0,$$

$$\tilde{\theta}(\eta) = 0, \quad \tilde{f}'(\eta) = 0, \quad \tilde{\phi}(\eta) = 0, \text{when} \ \ \eta \to \infty. \quad (5.15)$$

The quantities appear above are grouped into:

$M = \frac{2\sigma B_o^2}{\rho_1 a_0(n+1)}, \ E = \frac{E_0}{B_0 a_0(x_1+b^*)^n}$(Daniel et al. [131]), $Kp = \frac{2\nu_o}{K_o a_0(n+1)}, \ N = \frac{1}{d\beta_1\mu_o}, \ \lambda_1 = \frac{a_0^3(x_1+b)^{3n-1}}{2d^2\nu_0}$ ( Hayat et al. [140]), $Pr_0 = \frac{\mu_0 C_p}{k_0}, \ Nb = \frac{\tau_1 D_B(C_w-C_\infty)}{\nu_0}, \ Nt = \frac{\tau_1 D_T(T_w-T_\infty)}{T_\infty\nu_0}, \ E_c = \frac{U_w^2}{C_p(T_w-T_\infty)}, \ Rd = \frac{4\sigma T_\infty^3}{k_o k^*}, \ s = \frac{Q_o}{\rho_1 a_0 C_p}, \ Gr = \frac{2g\beta(T_w-T_\infty)}{a_0^2(n+1)(x_1+b^*)^{2n-1}}, \ Le = \frac{\nu_0}{D_B}$

here $\alpha$ is the wall thickness parameter, $b^*$ is a positive constant, $a_0$ is a rate of stretching sheet, $Ec$ and $\epsilon$ symbolize the Eckert number and thermal conductivity parameter respectively, $M$ is a magnetic parameter, $s$ is a heat source parameter, $\sigma$ is an electrical conductivity, $Pr_0$ indicates an ambient Prandtl number, $Gr$ is the Grashof number and $B_0$ is applied magnetic field, The Lewis number is designated by $Le$, $Kp$ is a permeability parameter, $Nb$ and $Nt$ are symbols of the Brownian and thermophoresis diffusion coefficients, $Rd$ is a thermal radiation parameter.

## 5.3 Analysis on Fluid properties

First consider constant thermo-physical properties of liquids then followed by the variable physical properties.

### 5.3.1 Case A: Constant Fluid Features

In such scenario, Eqs. (5.12), (5.13) and (5.14) reduce into the following:

$$\tilde{f}''' + N\tilde{f}''' - N\lambda(\frac{n+1}{2})\tilde{f}''^2\tilde{f}''' - \frac{2n}{n+1}\tilde{f}'^2 + \tilde{f}\tilde{f}'' + M(E - \tilde{f}') - K_p\tilde{f}' + Gr\tilde{\theta} = 0, \quad (5.16)$$

$$(1 + \frac{4}{3}Rd)\tilde{\theta}'' + Pr_o\left(\tilde{f}\tilde{\theta}' + Nb\tilde{\theta}'\tilde{\phi}' + Nt(\tilde{\theta}')^2 + MEc(\tilde{f}' - E)^2 + \frac{2}{n+1}s\tilde{\theta}\right) = 0, \quad (5.17)$$

$$\tilde{\phi}'' + \frac{Nt}{Nb}\tilde{\theta}'' + Le\tilde{f}\tilde{\phi}' = 0. \quad (5.18)$$

Illustration of the skin friction coefficient in Table 1 reveals an outstanding alignment of the SFDM (discussed below) with Daniel et al. [130] and Fang et al. [11].

Table 5.1: Presenting $-\tilde{f}''(0)$ both for varying $n$ and specific $\alpha = 0.25$ (**Case A**).

| $n$ | Fang et al. [11] | Daniel et al. [130] | Present result (SFDM) |
|------|------------------|---------------------|------------------------|
| 10 | 1.1433 | 1.143316 | 1.143301 |
| 9 | 1.1404 | 1.140388 | 1.140431 |
| 7 | 1.1323 | 1.132281 | 1.132301 |
| 5 | 1.1186 | 1.118587 | 1.118602 |
| 3 | 1.0905 | 1.090490 | 1.090400 |
| 0.5 | 0.9338 | 0.933828 | 0.933796 |
| -1/3 | 0.5000 | 0.500000 | 0.502557 |
| -0.5 | 0.0833 | 0.083289 | 0.086736 |

### 5.3.2 Case B: Variable Fluid Features

The variation in viscosity for water due to change in temperature is illustrated in Table 5.2 ( see White [101]). The viscosity decreases by a factor of 6. However, less change is noted

in density. This motivates us to study the variable fluid properties. Therefore, viscosity and thermal conductivity vary accordingly with temperature [116]

$$\mu_1(T) = \frac{\mu_r}{1 + \gamma_1(T_1 - T_r)}, \tag{5.19}$$

where $\gamma_1$ is a fluid property. Hereafter, the subscript 'r' denotes reference value. When $T_o \approx T_r$ we obtain,

$$\mu_1 = \frac{\mu_o}{1 - \frac{T_1 - T_o}{\theta_r(T_w - T_o)}} = \frac{\mu_o}{1 - \frac{\tilde{\theta}(\eta)}{\theta_r}}. \tag{5.20}$$

here $\theta_r = \frac{-1}{\gamma_1(T_w - T_o)}$ is the fluid viscosity parameter. Including Eq. (5.20) into Eq. (5.12) we get

$$\frac{\theta_r}{(\theta r - \tilde{\theta})}\tilde{f}''' + \frac{\tilde{f}''\tilde{\theta}'\theta_r}{(\theta_r - \tilde{\theta})^2} + N\tilde{f}''' - N\lambda\left(\frac{n+1}{2}\right)\tilde{f}''^2\tilde{f}''' - \frac{2n}{n+1}\tilde{f}'^2 + \tilde{f}\tilde{f}'' + M(E - \tilde{f}') - K_p\frac{\theta_r}{\theta_r - \tilde{\theta}}\tilde{f}' + G_r\tilde{\theta} = 0. \tag{5.21}$$

Similarly, the variable thermal conductivity is articulated by varying temperature as [98],

$$k_1(T_1) = k_o(1 + \epsilon\tilde{\theta}), \tag{5.22}$$

Introducing Eq. (5.22) in Eq. (5.13) one obtains

$$(1 + \frac{4}{3}Rd)\left((1 + \epsilon\tilde{\theta})\tilde{\theta}'' + \epsilon(\tilde{\theta}')^2\right) + Pr_o\left(\tilde{f}\tilde{\theta}' + Nb\tilde{\theta}'\tilde{\phi}' + Nt(\tilde{\theta}')^2 + MEc(\tilde{f}' - E)^2 + \frac{2}{n+1}s\tilde{\theta}\right) = 0. \tag{5.23}$$

The skin friction coefficient $C_f$ is determined in the following manner:

$$C_{fx_1} = \frac{\tau_w}{\rho_1 U_w^2}, \tag{5.24}$$

in which $\tau_w$ is wall shear stress defined as

$$\tau_w = \left(\mu_1\frac{\partial u_1}{\partial y_1} + \frac{1}{\beta_1 d}\frac{\partial u_1}{\partial y_1} - \frac{1}{6\beta_1 d^3}(\frac{\partial u_1}{\partial y_1})^3\right). \tag{5.25}$$

Using Eq. (5.25) in Eq. (5.24), the skin friction coefficient in dimensionless form is defined in the following section.

### 5.3.3 The Skin Friction Coefficients (Cases A, B)

The skin friction coefficients for Cases A and B are written as:

$$\frac{C_{fx_1}\sqrt{Re_{x_1}}}{2} = \sqrt{\frac{n+1}{2}}\left((1 + N)\tilde{f}''(0) - \frac{n+1}{2}\frac{N\lambda}{3}(\tilde{f}''(0))^3\right), \tag{5.26}$$

92

$$\frac{C_{fx_1}\sqrt{Re_{x_1}}}{2} = \sqrt{\frac{n+1}{2}}\left(\left(\frac{\theta_r}{\theta_r - \theta(0)} + N\right)\tilde{f}''(0) - \frac{n+1}{2}\frac{N\lambda}{3}(\tilde{f}''(0))^3\right). \qquad (5.27)$$

Likewise, defining the local Nusselt and the Sherwood numbers in the following manners.

### 5.3.4  The Local Nusselt Number:

$$Nu_{x_1} = -\frac{(x_1+b)q_w}{k_o(T_w - T_\infty)} = -(1 + \frac{4}{3}Rd)\sqrt{\frac{(1+n)Re_{x_1}}{2}}\tilde{\theta}'(0). \qquad (5.28)$$

### 5.3.5  The Local Sherwood Number:

$$Sh_{x_1} = -\frac{x_1 j_w}{C_w - C_\infty} = -\sqrt{\frac{(1+n)Re_{x_1}}{2}}\tilde{\phi}'(0). \qquad (5.29)$$

Here $Re_{x_1}$ is local Reynolds number.

Table 5.2: Water as a function of temperature (White [101])

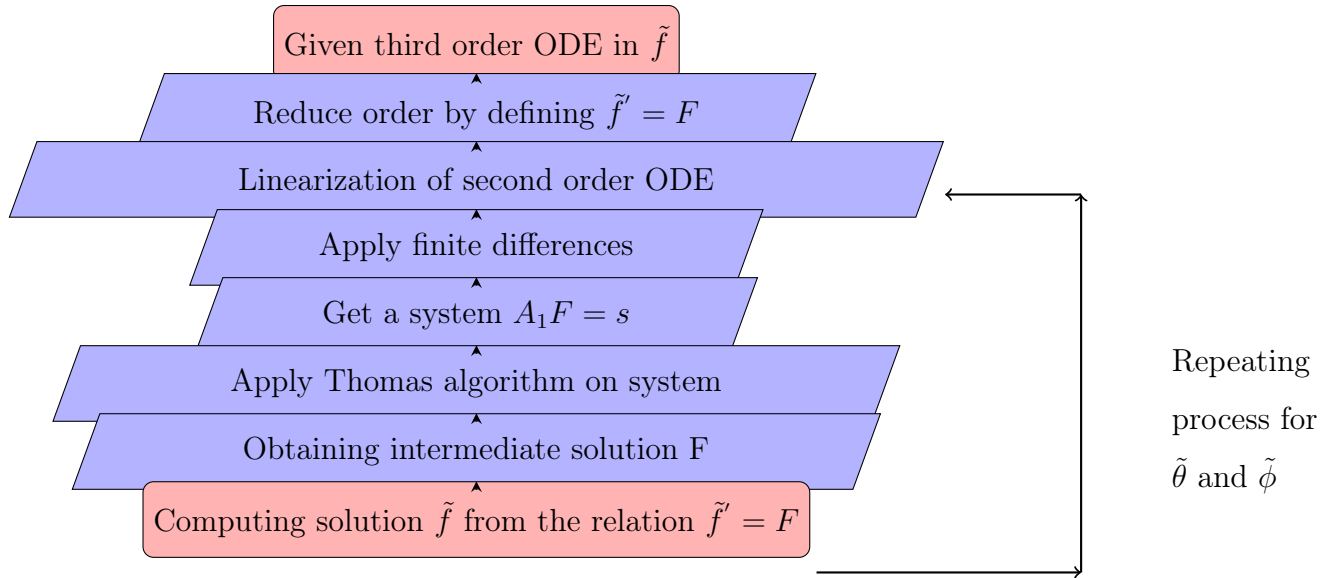| $T_1(C)$ | $\rho_1(\frac{kg}{m^3})$ | $\mu_1 \times 10^{-3}\frac{Ns}{m^2}$ |
|---|---|---|
| 0 | 1000 | 1.788 |
| 10 | 1000 | 1.307 |
| 20 | 998 | 1.003 |
| 30 | 996 | 0.799 |
| 40 | 992 | 0.657 |
| 50 | 988 | 0.548 |
| 60 | 983 | 0.467 |
| 70 | 978 | 0.405 |
| 80 | 972 | 0.355 |
| 90 | 965 | 0.316 |
| 100 | 958 | 0.283 |

Figure 5.2: Flow diagram of SFDM [102].

## 5.4 Simplified Finite Difference Method (SFDM)

The simplified finite difference method has been introduced in [102]. This scheme is motivated from the work by Na [103]. The algorithmic steps involved in the SFDM are:

1. Reduction of higher order ODE into a system of first and second order ODEs.

2. Linearization of nonlinear ODE through the use of Taylor series.

3. Use finite differences to discretize the linear second order ODE.

4. Finally, the obtained algebraic system is solved efficiently by LU-decomposition.

5. Repeating above procedure will produce solutions in $\tilde{\theta}$ and $\tilde{\phi}$

The summary of the involved steps in the SFDM is also shown in Fig. 5.2. The results are computed for N=1000 grid points in the $\eta$ direction. However, the number of grid points was varied in some calculations to achieve better accuracy, The iterative procedure has been done with tolerance of machine epsilon in MATLAB. Assuming $f' = F$ in equation (5.16), we may write

The results are computed for $N = 1000$ grid points in the $\eta$ direction. However, number of grid points varied in some calculations to achieve better accuracy. Assume $\tilde{f}' = F$ in Eq. (

5.16), we may write

$$\frac{d^2 F}{d\eta^2} = \left( \frac{1}{1 + N - N\lambda(\frac{n+1}{2})(\frac{dF}{d\eta})^2} \right) \left( \frac{2n}{n+1} F^2 - \tilde{f}\frac{dF}{d\eta} - M(E - F) + K_p F - G_r \theta \right). \quad (5.30)$$

Then writing this expression as

$$\chi(h, F, F') = \left( \frac{1}{1 + N - N\lambda(\frac{n+1}{2})(\frac{dF}{d\eta})^2} \right) \left( \frac{2n}{n+1} F^2 - \tilde{f}\frac{dF}{d\eta} - M(E - F) + K_p F - G_r \theta \right),$$

$$(5.31)$$

and replace $\frac{dF}{d\eta}$ by forward difference approximation

$$\chi(h, F, F') = (\frac{1}{1 + N - N\lambda(\frac{n+1}{2})(\frac{F_{j+1}-F_j}{h})^2}(\frac{2n}{n+1} F_j^2 - \tilde{f}_j(\frac{F_{j+1}-F_i}{h}) -$$

$$M(E - F_j) + K_p F_j) - Gr\theta). \quad (5.32)$$

The coefficients of second order ODE read

$$Q_n = -\frac{\partial \chi}{\partial F'} = \left( \frac{1}{(1 + N - N\lambda(\frac{n+1}{2})(\frac{dF}{d\eta})^2)^2} \right) [(\lambda N(n+1))(\frac{-2n}{n+1} F^2 +$$

$$\tilde{f}\frac{dF}{d\eta} + M(E - F) - K_p F + Gr\theta) - \tilde{f}\left( 1 + N - N\lambda(\frac{n+1}{2})(\frac{dF}{d\eta})^2 \right)] =$$

$$\left( \frac{1}{(1 + N - N\lambda(\frac{n+1}{2})(\frac{F_{j+1}-F_j}{h})^2)^2} \right) [\lambda N(n+1)(\frac{-2n}{n+1} F_j^2 + \quad (5.33)$$

$$\tilde{f}_j\frac{F_{j+1}-F_j}{h} + M(E - F) - K_p F_j + Gr\theta) - f_j\left( 1 + N - N\lambda(\frac{n+1}{2})(\frac{F_{j+1}-F_j}{h}) \right)],$$

$$R_n = -\frac{\partial \chi}{\partial F} = -\left( \frac{1}{1 + N - N\lambda(\frac{n+1}{2})(\frac{dF}{d\eta})^2} \right) \left( \frac{4n}{n+1} F + M + Kp \right)$$

$$= -\left( \frac{1}{1 + N - N\lambda(\frac{n+1}{2})(\frac{F_{j+1}-F_i}{h})^2} \right) \left( \frac{4n}{n+1} F_j + M + Kp \right), \quad (5.34)$$

$$S_n = \chi(h, F, F') + R_n F_j + Q_n \frac{F_{j+1}-F_j}{h}. \quad (5.35)$$

After manipulating Eqs. ( 5.30)-( 5.35) the linear algebraic system in $F$ are written as [102]

$$X_j F_{j-1} + Y_j F_j + Z_j F_{j+1} = W_j, \qquad j = 1, 2, 3...., N. \quad (5.36)$$

where the coefficients are defined by

$$X_j = 2 - hQ_n, \quad Y_j = 2h^2 R_n - 4, \quad Z_j = 2 + hQ_n, \quad W_j = 2h^2 S_n. \tag{5.37}$$

In matrix-vector format, it is

$$A_1 F = S, \tag{5.38}$$

where

$$A_1 = \begin{bmatrix} Y_1 & Z_1 & & & & \\ X_2 & Y_2 & Z_2 & & & \\ & & .... & & & \\ & & & X_{N-2} & Y_{N-2} & Z_{N-2} \\ & & & & X_{N-1} & Y_{N-1} \end{bmatrix}, \tag{5.39}$$

is a tridiagonal matrix. The column vectors $F$ and $s$ are

$$F = \begin{bmatrix} F_1 \\ F_2 \\ . \\ . \\ F_{N-1} \end{bmatrix} \quad , s = \begin{bmatrix} s_1 \\ s_2 \\ . \\ . \\ s_{N-1} \end{bmatrix}. \tag{5.40}$$

## 5.4.1 Thomas Algorithm

The Thomas algorithm [104] is implemented in MATLAB to compute the solution $F$. An LU-Factorization has been chosen for the matrix factorization of $A_1$ i.e.

$$A_1 = L_1 U_1, \tag{5.41}$$

where

$$L_1 = \begin{bmatrix} \Lambda_1 & & & & \\ X_2 & \Lambda_2 & & & \\ & & .... & & \\ & & & X_{N-2} & \Lambda_{N-2} \\ & & & & X_{N-1} & \Lambda_{N-1} \end{bmatrix}, \tag{5.42}$$

and

$$U_1 = \begin{bmatrix} 1 & \zeta_1 & & & \\ & 1 & \zeta_2 & & \\ & & .... & & \\ & & & 1 & \zeta_{N-2} \\ & & & & 1 \end{bmatrix}.$$ 

(5.43)

It is clear that $L_1$ and $U_1$ are the lower and unit upper triangular matrices, respectively. Variables $(\Lambda_j, \zeta_j)$, $j = 1, 2, ..., N - 1$ are related by

$$\Lambda_1 = -1 - \frac{\lambda}{h}, \quad \zeta_1 = \frac{\lambda}{\Lambda_1 h},$$ 

(5.44)

$$\Lambda_j = Y_j - X_j \zeta_{j-1}, \quad j = 2, 3, ..., N - 1,$$ 

(5.45)

$$\Lambda_j \zeta_j = z_j, \quad j = 2, 3, ...., N - 2.$$ 

(5.46)

After defining these relations, Eq. ( ) becomes

$$L_1 U_1 F = S, \quad U_1 F = z, \quad \text{and} \quad L_1 z = S,$$ 

(5.47)

we have

$$\begin{bmatrix} \Lambda_1 & & & & \\ X_2 & \Lambda_2 & & & \\ & & .... & & \\ & & X_{N-2} & \Lambda_{N-2} & \\ & & & X_{N-1} & \end{bmatrix} \begin{bmatrix} z_1 \\ z_2 \\ z_3 \\ . \\ . \\ . \\ z_{N-2} \\ z_{N-1} \end{bmatrix} = \begin{bmatrix} S_1 \\ S_2 \\ S_3 \\ . \\ . \\ . \\ S_{N-2} \\ S_{N-1} \end{bmatrix}.$$ 

(5.48)

The unknown elements $z$ is computed from

$$z_1 = S_1/\Lambda_1, z_j = \frac{S_j - X_j z_{j-1}}{\Lambda_j}, j = 2, 3, ..., N - 1,$$ 

(5.49)

and

$$
\begin{bmatrix}
1 & \zeta_1 & & & \\
& 1 & \zeta_2 & & \\
& & .... & & \\
& & & 1 & \zeta_{N-2} \\
& & & & 1
\end{bmatrix}
\begin{bmatrix}
F_1 \\
F_2 \\
. \\
. \\
. \\
F_{N-2} \\
F_{N-1}
\end{bmatrix}
=
\begin{bmatrix}
z_1 \\
z_2 \\
. \\
. \\
. \\
z_{N-2} \\
z_{N-1}
\end{bmatrix}.
\tag{5.50}
$$

We get

$$
F_{j-1} = z_{j-1}, \qquad F_j = z_j - \zeta_j F_{j+1}, \qquad j = N-2, N-3, ..., 3, 2, 1.
\tag{5.51}
$$

The above Eq. ( 5.51) is a solution of Eq. ( 5.30). Discretizing the relation $f' = F$ like

$$
\frac{\tilde{f}_{j+1} - \tilde{f}_j}{h} = F_j,
\tag{5.52}
$$

which gives a required solution of Eq. ( 5.16). Repeating above process one can easily get $\tilde{\theta}$ and $\tilde{\phi}$ appear in Eqs. ( 5.17) and ( 5.18). However, all the details for these variables have been omitted for brevity. The reader is referred to [102] for further details on the SFDM. Since the SFDM results for both constant and variable fluid properties have been discussed in detail in [102], thus in the current work only Table 2 is produced from the SFDM to compare accuracy with the literature. However, we obtain $-Re_{x_1}^{1/2}C_{fx_1}$ and $-Re_{x_1}^{-1/2}Nu_{x_1}$ for Case A and Case B (Table 5.3 and Table 5.4) by using MATLAB built-in solver $bvp4c$. [95].

## 5.5   Results and Discussion

The comparison of $-Re_{x_1}^{1/2}C_{fx_1}$ for Case A and Case B is given in Table 5.3. The surface resistance rises for higher values of $M$, $n$, $\alpha$, $n$ and $Kp$ while it decreases by increasing parameter $\lambda_1$, $Gr$ and $E$. The same phenomenon is noticed for the wall resistance coefficient in both Cases A and B. The surface resistance declines for larger values of $\theta_r$ in Case B. Table 5.4 shows the variation of $-Re_{x_1}^{-1/2}Nu_{x_1}$ for Cases A and B in relation to different pertinent parameter. Note that $-Re_{x_1}^{-1/2}Nu_{x_1}$ went up for larger values of $n$ and $\alpha$ while it went down

for $M$, $Pr_o$, $Nt$, $Rd$, $E$, and $s$. The $-Re_{x_1}^{-1/2}Nu_{x_1}$ for case B lowers for larger values of small thermal conductivity parameter $\epsilon$. In these tables, we can see the difference in values for $-Re_{x_1}^{1/2}C_{fx_1}$ and $-Re_{x_1}^{-1/2}Nu_{x_1}$. The wall resistance coefficient and local Nusselt numbers for the results of constant fluid properties have higher values when compared with the results obtained for variable fluid properties.

Fig. 5.3 describes the role of $\alpha$ in the fluid's velocity. Noting that the velocity profile diminishes significantly for both Cases A and B with a rise in the values of $\alpha$. Because it is observed that higher values of $\alpha$ corresponds to deformation due to stretching wall which results decline in velocity distribution. Fig. 5.4 is plotted to perceive the influence of $E$ on velocity distribution. It is shown that increase in electric field parameter enhance the velocity of nanofluid. Because the electrical force introduces accelerating body force which acts to the direction of the electrical force. The force, known as Lorentz force, accelerates the boundary layer flow and thickness the momentum boundary layer. Hence, it is resulted in a reduction in $C_{fx_1}$. Fig. 5.5 is presented the effect of $M$ on velocity profile. From Fig. (5.5) we conclude that a rise in $M$ causes reduction in the velocity of fluid. An increase in $M$ generates a resistive force called Lorentz force in the fluid layers. This resistive force causes the reduction in velocity profile. Fig. 5.6 is constructed to know the consequences of $n$ on momentum profile. It is analyzed that for higher values of $n$ velocity profile remains unchanged. Fig. 5.7 is reflecting the influence of $\theta_r$ has on the velocity. The larger values of $\theta_r$ intensifies the skin friction, which causes the reduction in the velocity profile. Fig. 5.8 demonstrates the effect of $N$ on the velocity distribution. It can be seen that velocity profile enhances for higher values of $N$. Fig. 5.9 is constructed to know the outcomes of $Gr$ on velocity distribution. The velocity goes down with larger values of $Gr$. Fig. 5.10 highlights effect of $Kp$ on velocity profiles. It is seen that velocity profile decreases with increase in $Kp$. Fig. 5.11 demonstrates the effect of $\alpha$ on thermal profile. It is observed that an enhancement in $\alpha$ reduce the thermal boundary layer. The behavior of $E$ on temperature distribution is portrayed in Fig. 5.12. It is noted that enhancement in $E$ decreases the thermal boundary layer thickness. Fig. 5.13 is presented to describe the influence of $\epsilon$ on temperature profile. It is examined that increment in $\epsilon$ causes enhancement in temperature profile. Fig. 5.14 is presented to examine the outcomes of $Pr_0$ on temperature distribution. It is noted that by increasing $Pr_0$ reduces thermal conductivity of fluid which decreases temperature profile. Fig. 5.15 demonstrates the impacts of $Rd$

on temperature profile. It is seen that small increment in $Rd$ intensifies the temperature profile. Because an increment in radiation parameter provides more heat to fluid that causes enhancement in the thermal boundary layer thickness. Fig. 5.16 displays the impacts of $s$ on temperature profile. It is observed that by increasing $s$ temperature of the fluid enhances and hence thermal boundary layer increases. Fig. 5.17 displays the influences of $n$ on temperature distribution. It is noted that by increasing $n$ increases the temperature profile. Figs. 5.18-5.19 show the effect of $Nb$ on the temperature and concentration profiles respectively. It is noticed that for higher values of $Nb$ there is no significant increase or decrease in temperature profile but by increasing $Nb$ concentration boundary layer thickness increase. Figs. 5.20-5-21 describes the effect of $Nt$ on temperature and concentration profile respectively. It is found that an increment in thermophoretic parameter enhance both temperature and concentration profiles. Fig. 5.22 depicts the influence of $Le$ on concentration profile. We have seen that for larger values of $Le$, the concentration boundary layer thickness is decreased. The reason is that by raising $Le$ reduces the diffusivity rate of concentration and hence concentration profile decreases. Fig. 5.23 and Fig. 5.24 are plotted to see the impacts of $\alpha$ and $Rd$ on temperature profile. It is examined that by raising the values of $\alpha$ causes decrement in thermal boundary layer thickness while thermal boundary thickness magnify for elevating values of $Rd$. In Fig. 5.25 we noticed that by enhancing $s$ temperature profile increases. Fig. 5.26 inspects the effects of $Le$ on concentration distribution. It is interpreted that concentration boundary layer thins for rising values of $Le$. Fig. 5.27 and Fig. 5.28 scrutinized the influence of $Nt$ on thermal and concentration boundary layer respectively. It is explored that thermal boundary layer width increases while concentration boundary layer width thins for incremental values of $Nt$. Fig. 5.29 shows the influences of $\theta_r$ and $Kp$ on skin friction coefficient. It is noted that skin friction coefficient rises for raising values of skin friction coefficient. Fig. 5.30 is plotted to perceive the effects of $Ec$ and $Pr_o$ on local Nusselt number. It is observed that by raising $Ec$ local Nusselt number increases. Fig. 5.31 presents the effects of $Le$ and $Nt$ on local Sherwood number. It is noticed that an increment in $Le$ shows enhancement in local Sherwood number.
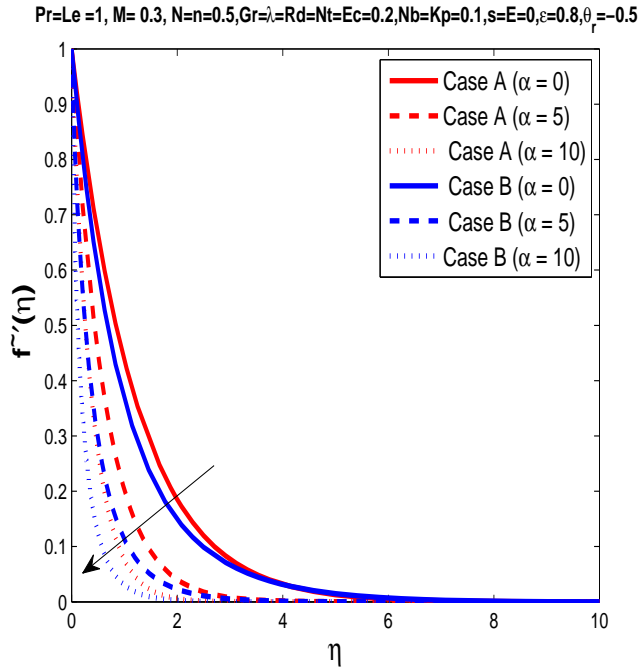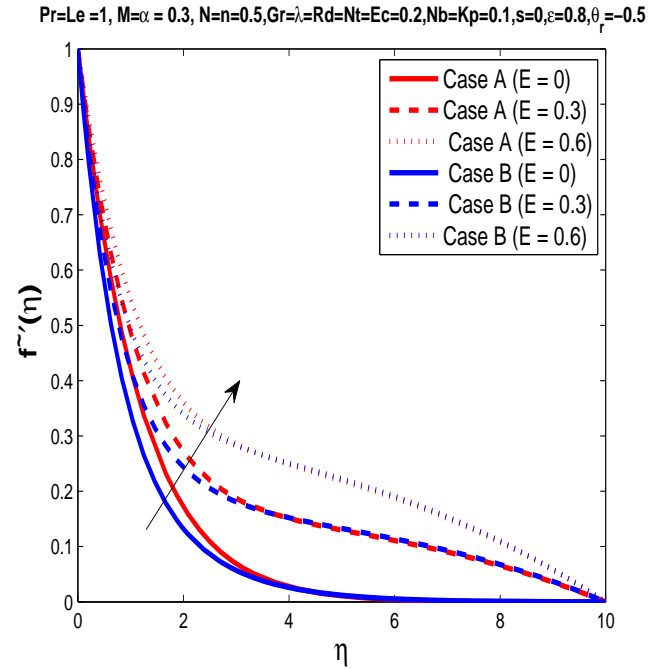
**Figure 5.3:** Velocity profile for different $\alpha$.



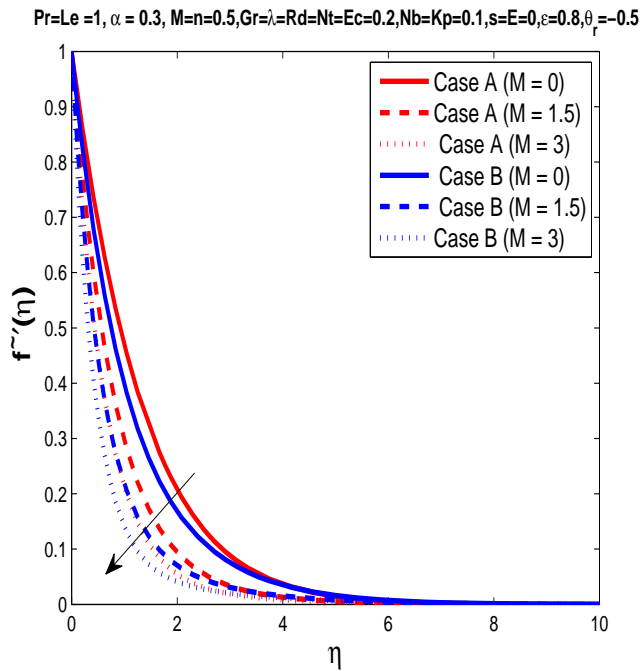**Figure 5.4:** Velocity profile for different $E$.



**Figure 5.5:** Velocity profile for different $M$.



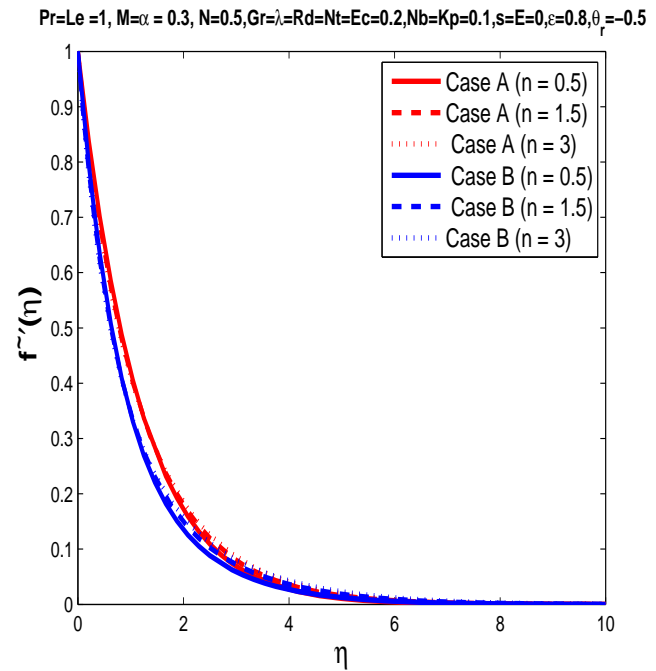**Figure 5.6:** Velocity profile for different $n$.

Table 5.3: Numerical values of $-C_{fx_1}Re_{x_1}^{1/2}$ for distinct involved parameter $\alpha$, $\lambda$, $M$, $N$ and $n$ when $Nb = s = 0.1$, $Pr_o = 1$, $Le = 1$, $Nt = Ec = Rd = 0.2$.

| | | | | | | | | | Case A | Case B |
|---|---|---|---|---|---|---|---|---|---|---|
| $M$ | n | $\lambda$ | $\alpha$ | $N$ | $Gr$ | $E$ | $K_p$ | $\theta_r$ | $-C_{fx_1}Re_{x_1}^{1/2}$ | $-C_{fx_1}Re_{x_1}^{1/2}$ |
| 0.0 | 0.5 | 0.2 | 0.3 | 0.5 | 0 | 0 | 0.2 | -10 | 2.1927 | 2.1231 |
| 0.4 | | | | | | | | | 2.5751 | 2.4938 |
| 0.6 | | | | | | | | | 2.7458 | 2.6588 |
| 0.3 | 0.4 | 0.2 | 0.3 | 0.5 | 0 | 0 | 0.2 | -10 | 2.3729 | 2.2989 |
| | 0.6 | | | | | | | | 2.5925 | 2.5097 |
| | 0.8 | | | | | | | | 2.7939 | 2.7033 |
| 0.3 | 0.5 | 0.0 | 0.3 | 0.5 | 0 | 0 | 0.2 | -10 | 2.4957 | 2.4183 |
| | | 0.3 | | | | | | | 2.4798 | 2.4008 |
| | | 0.6 | | | | | | | 2.4630 | 2.3821 |
| 0.3 | 0.5 | 0.2 | 0.0 | 0.5 | 0 | 0 | 0.2 | -10 | 2.3954 | 2.3154 |
| | | | 0.2 | | | | | | 2.4550 | 2.3760 |
| | | | 0.4 | | | | | | 2.5158 | 2.4379 |
| 0.3 | 0.5 | 0.2 | 0.3 | 0.0 | 0 | 0 | 0.2 | -10 | 2.0547 | 1.9586 |
| | | | | 0.3 | | | | | 2.3219 | 2.2378 |
| | | | | 0.5 | | | | | 2.4852 | 2.4068 |
| 0.3 | 0.5 | 0.2 | 0.3 | 0.5 | 0.2 | 0 | 0.2 | -10 | 2.2394 | 2.1527 |
| | | | | | 0.4 | | | | 2.0119 | 1.9198 |
| | | | | | 0.6 | | | | 1.7955 | 1.6989 |
| 0.3 | 0.5 | 0.2 | 0.3 | 0.5 | 0 | 0.2 | 0.2 | -10 | 2.3220 | 2.2484 |
| | | | | | | 0.4 | | | 2.1687 | 2.0984 |
| | | | | | | 0.7 | | | 1.9511 | 1.8844 |
| 0.3 | 0.5 | 0.2 | 0.3 | 0.5 | 0 | 0 | 0.5 | -10 | 2.7458 | 2.6403 |
| | | | | | | | 1 | | 3.1300 | 2.9840 |
| | | | | | | | 1.5 | | 3.4692 | 3.2834 |
| 0.3 | 0.5 | 0.2 | 0.3 | 0.5 | 0 | 0 | 0.2 | -5 | | 2.3380 |
| | | | | | | | | -3 | | 2.2586 |
| | | | | | | | | -1 | | 1.9935 |

Table 5.4: Numerical values of $-Nu_{x_1}Re_{x_1}^{-1/2}$ for involved parameter $n$, $M$, $\alpha$, $Nb$, $Nt$, $Pr_o$ and $Le$, where $Gr = 0$, $Kp = Ec = \lambda = 0.2$, $N = 0.5$, $\theta_r = -10$.

| | | | | | | | | | | | Case A | Case B |
|---|---|---|---|---|---|---|---|---|---|---|---|---|
| $M$ | $n$ | $Pr_o$ | $Le$ | $N_t$ | $N_b$ | $\alpha$ | $Rd$ | $E$ | $s$ | $\epsilon$ | $-Nu_{x_1}Re_{x_1}^{-1/2}$ | $-Nu_{x_1}Re_{x_1}^{-1/2}$ |
| 0.0 | 0.5 | 1 | 1 | 0.2 | 0.1 | 0.3 | 0.2 | 0 | 0.1 | 0.2 | 0.4801 | 0.4028 |
| 0.3 | | | | | | | | | | | 0.4158 | 0.3430 |
| 0.7 | | | | | | | | | | | 0.3365 | 0.2673 |
| 0.3 | 0.2 | 1 | 1 | 0.2 | 0.1 | 0.3 | 0.2 | 0 | 0.1 | 0.2 | 0.4055 | 0.3326 |
| | 0.5 | | | | | | | | | | 0.4157 | 0.3430 |
| | 1 | | | | | | | | | | 0.4427 | 0.3685 |
| 0.3 | 0.5 | 0.7 | 1 | 0.2 | 0.1 | 0.3 | 0.2 | 0 | 0.1 | 0.2 | 0.2742 | 0.2094 |
| | | 1 | | | | | | | | | 0.4157 | 0.3430 |
| | | 1.3 | | | | | | | | | 0.5268 | 0.4427 |
| 0.3 | 0.5 | 1 | 0.7 | | 0.1 | 0.3 | 0.2 | 0 | 0.1 | 0.2 | 0.4187 | 0.3453 |
| | | | 1.0 | | | | | | | | 0.4157 | 0.3430 |
| | | | 1.3 | | | | | | | | 0.4136 | 0.3413 |
| 0.3 | 0.5 | 1 | 1.0 | 0 | 0.1 | 0.3 | 0.2 | 0 | 0.1 | 0.2 | 0.4362 | 0.3610 |
| | | | | 0.2 | | | | | | | 0.4157 | 0.3430 |
| | | | | 0.4 | | | | | | | 0.3952 | 0.3250 |
| 0.3 | 0.5 | 1 | | 0.2 | 0.2 | 0.3 | 0.2 | 0 | 0.1 | 0.2 | 0.4157 | 0.3430 |
| | | | | | 0.5 | | | | | | 0.4157 | 0.3430 |
| | | | | | 0.7 | | | | | | 0.4157 | 0.3430 |
| 0.3 | 0.5 | 1 | 1.0 | 0.2 | 0.1 | 0.0 | 0.2 | 0 | 0.1 | 0.2 | 0.3469 | 0.2827 |
| | | | | | | 0.4 | | | | | 0.4385 | 0.3627 |
| | | | | | | 0.8 | | | | | 0.5301 | 0.4413 |
| 0.3 | 0.5 | 1 | 1.0 | 0.2 | 0.2 | 0.3 | 0.0 | 0 | 0.1 | 0.2 | 0.4092 | 0.3433 |
| | | | | | | | 0.5 | | | | 0.4142 | 0.3379 |
| | | | | | | | 0.8 | | | | 0.3890 | 0.2994 |
| 0.3 | 0.5 | 1 | 1.0 | 0.2 | 0.1 | 0.0 | 0.2 | 0.2 | 0.1 | 0.2 | 0.4930 | 0.4121 |
| | | | | | | 0.4 | | 0.4 | | | 0.4789 | 0.3942 |
| | | | | | | 0.8 | | 0.7 | | | 0.4285 | 0.3420 |
| 0.3 | 0.5 | 1 | 1.0 | 0.2 | | 0.3 | 0.2 | 0 | 0 | 0.2 | 0.5699 | 0.4892 |
| | | | | | | | | | 0.1 | | 0.4157 | 0.3430 |
| | | | | | | | | | 0.15 | | 0.2940 | 0.2127 |
| 0.3 | 0.5 | 1 | 1.0 | 0.2 | 0.1 | 0.3 | 0.2 | 0 | 0.1 | 0 | | 0.4069 |
| | | | | | | | | 0.4 | | 0.5 | | 0.2751 |
| | | | | | | | | 0.8 | | 1 | | 0.2003 |

Table 5.5: Numerical values of $-Nu_{x_1}Re_{x_1}^{-1/2}$ for involved parameter $n$, $M$, $\alpha$, $Nb$, $Nt$, $Pr_o$ and $Le$, where $Gr = 0$, $Kp = Ec = \lambda = 0.2$, $N = 0.5$, $\theta_r = -10$.

| $M$ | $n$ | $Pr_o$ | $Le$ | $N_t$ | $N_b$ | $\alpha$ | $Rd$ | $E$ | $s$ | $\epsilon$ | Case B $-Nu_{x_1}Re_{x_1}^{-1/2}$ |
|---|---|---|---|---|---|---|---|---|---|---|---|
| 0.0 | 0.5 | 1 | 1 | 0.2 | 0.1 | 0.3 | 0.2 | 0 | 0.1 | 0.2 | 1.4268 |
| 0.3 | | | | | | | | | | | 1.2922 |
| 0.7 | | | | | | | | | | | 1.1353 |
| 0.3 | 0.2 | 1 | 1 | 0.2 | 0.1 | 0.3 | 0.2 | 0 | 0.1 | 0.2 | 1.3653 |
| | 0.5 | | | | | | | | | | 1.2922 |
| | 1 | | | | | | | | | | 1.2492 |
| 0.3 | 0.5 | 0.7 | 1 | 0.2 | 0.1 | 0.3 | 0.2 | 0 | 0.1 | 0.2 | 1.1105 |
| | | 1 | | | | | | | | | 1.2922 |
| | | 1.3 | | | | | | | | | 1.5067 |
| 0.3 | 0.5 | 1 | 0.7 | | 0.1 | 0.3 | 0.2 | 0 | 0.1 | 0.2 | 1.3435 |
| | | | 1.0 | | | | | | | | 1.2922 |
| | | | 1.3 | | | | | | | | 1.2551 |
| 0.3 | 0.5 | 1 | 1.0 | 0 | 0.1 | 0.3 | 0.2 | 0 | 0.1 | 0.2 | 1.6044 |
| | | | | 0.2 | | | | | | | 1.2922 |
| | | | | 0.4 | | | | | | | 1.0159 |
| 0.3 | 0.5 | 1 | | 0.2 | 0.2 | 0.3 | 0.2 | 0 | 0.1 | 0.2 | 1.2922 |
| | | | | | 0.5 | | | | | | 1.2922 |
| | | | | | 0.7 | | | | | | 1.2922 |
| 0.3 | 0.5 | 1 | 1.0 | 0.2 | 0.1 | 0.0 | 0.2 | 0 | 0.1 | 0.2 | 1.0286 |
| | | | | | | 0.4 | | | | | 1.3836 |
| | | | | | | 0.8 | | | | | 1.7650 |
| 0.3 | 0.5 | 1 | 1.0 | 0.2 | 0.2 | 0.3 | 0.0 | 0 | 0.1 | 0.2 | 1.1648 |
| | | | | | | | 0.5 | | | | 1.4526 |
| | | | | | | | 0.8 | | | | 1.5860 |
| 0.3 | 0.5 | 1 | 1.0 | 0.2 | 0.1 | 0.0 | 0.2 | 0.2 | 0.1 | 0.2 | 1.2922 |
| | | | | | | 0.4 | | 0.4 | | | 1.3207 |
| | | | | | | 0.8 | | 0.7 | | | 1.2268 |
| 0.3 | 0.5 | 1 | 1.0 | 0.2 | | 0.3 | 0.2 | 0 | 0 | 0.2 | 1.5225 |
| | | | | | | | | | 0.1 | | 1.2922 |
| | | | | | | | | | 0.15 | | 1.1642 |
| 0.3 | 0.5 | 1 | 1.0 | 0.2 | 0.1 | 0.3 | 0.2 | 0 | 0.1 | 0 | 1.4759 |
| | | | | | | | | 0.4 | | 0.5 | 1.1025 |
| | | | | | | | | 0.8 | | 1 | 0.9032 |
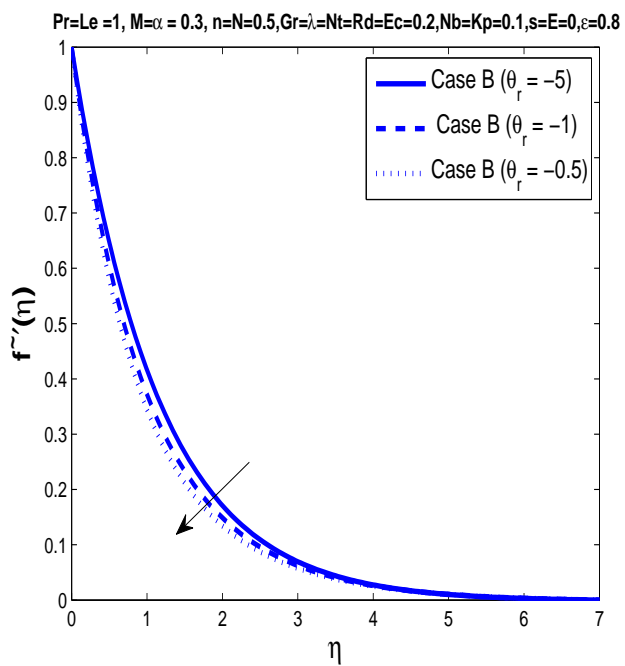
Figure 5.7: Velocity profile for different $\theta_r$.
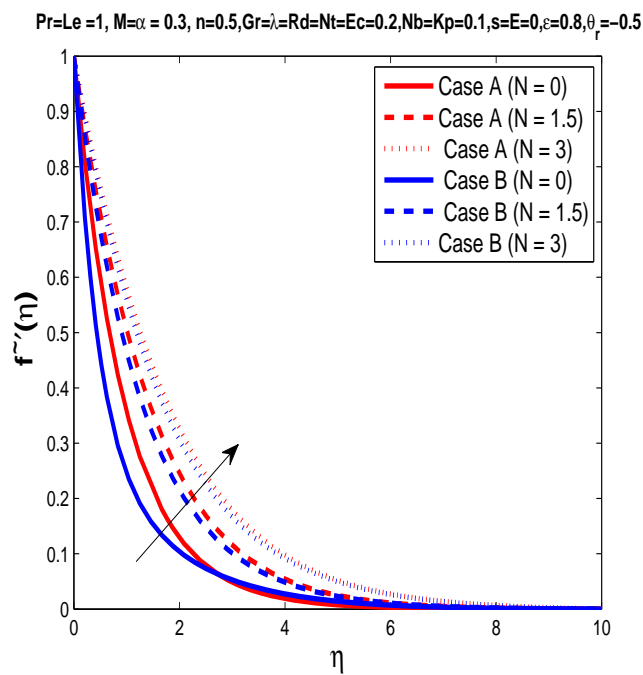


Figure 5.8: Velocity profile for different $N$.
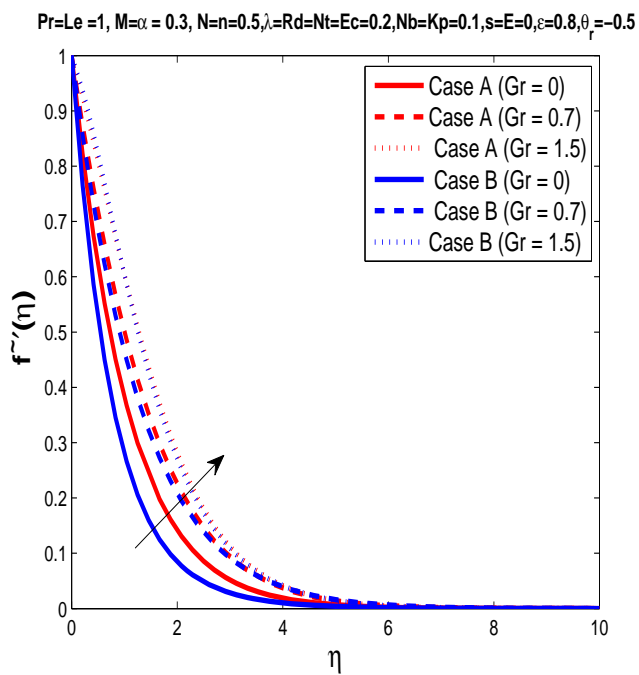


Figure 5.9: Velocity profile for different $Gr$.
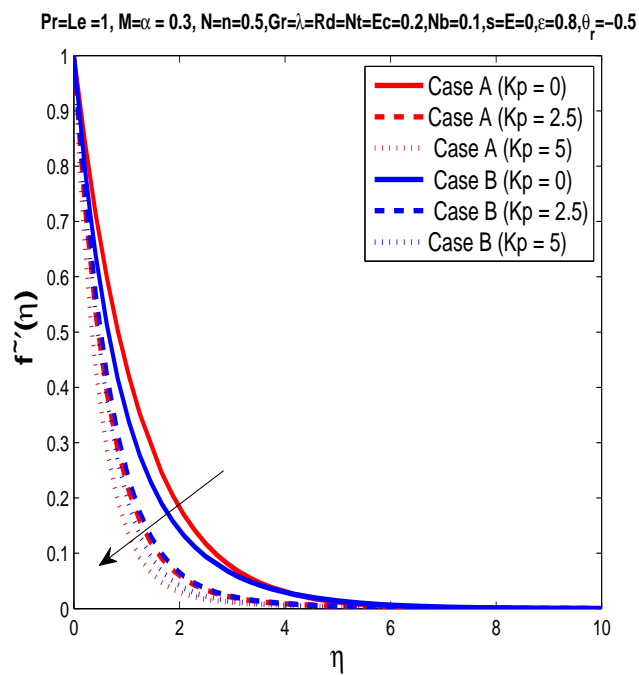


Figure 5.10: Velocity profile for different $Kp$.
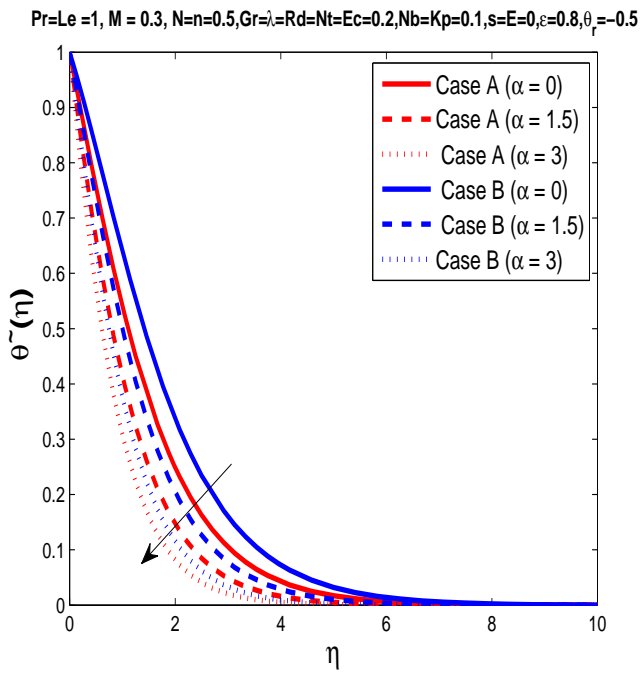
Figure 5.11: Temperature profile for different $\alpha$.
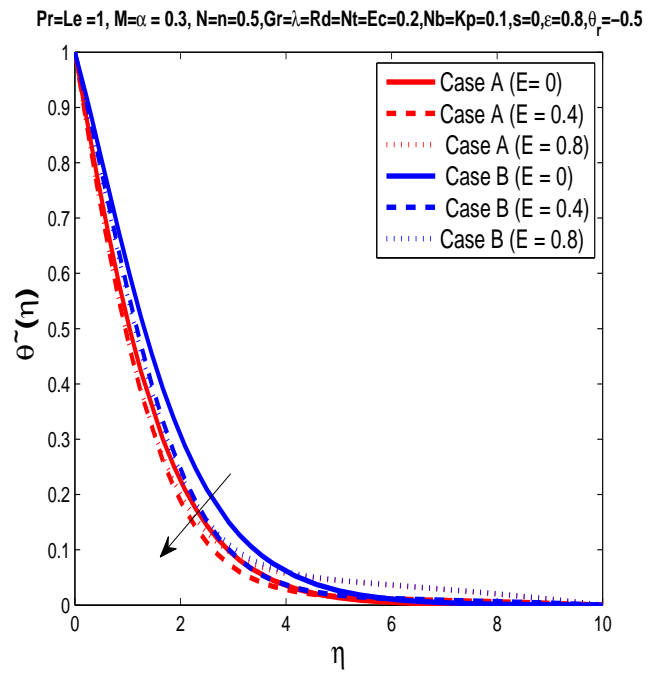


Figure 5.12: Temperature profile for different $E$.
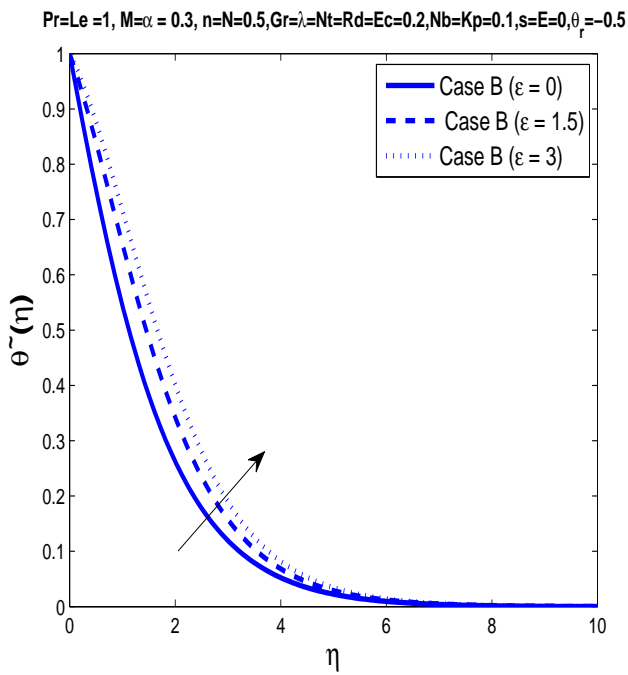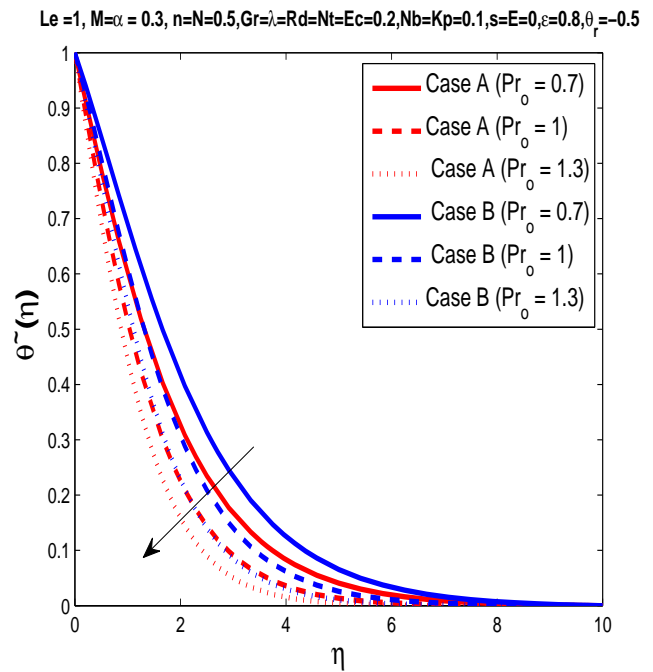


Figure 5.13: Temperature profile for different $\epsilon$.
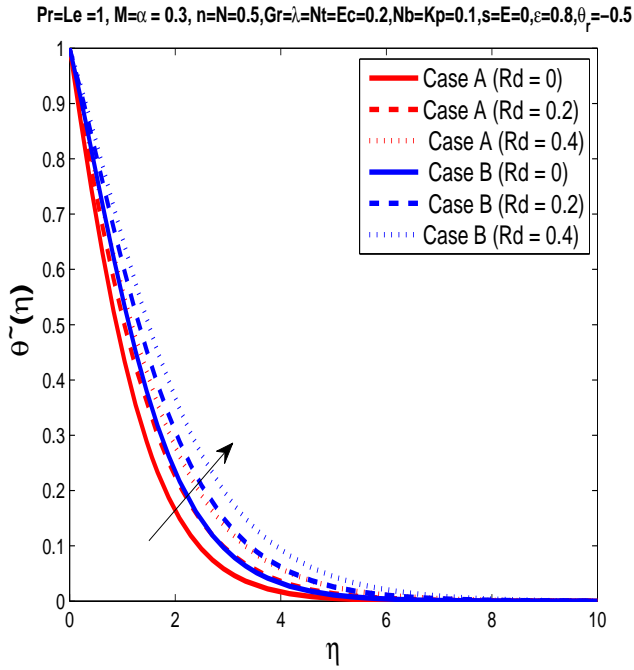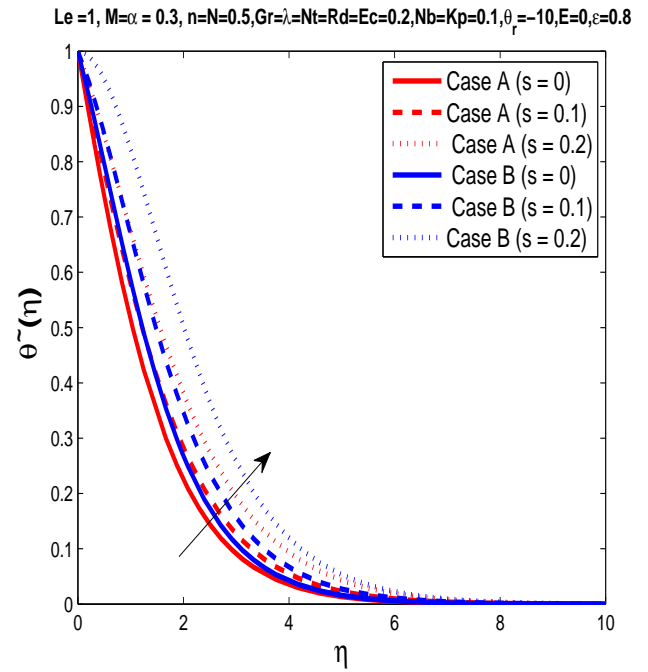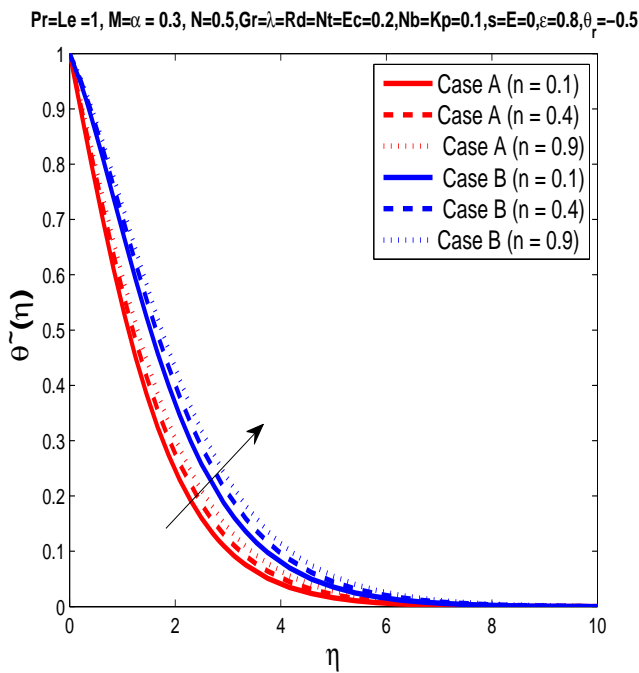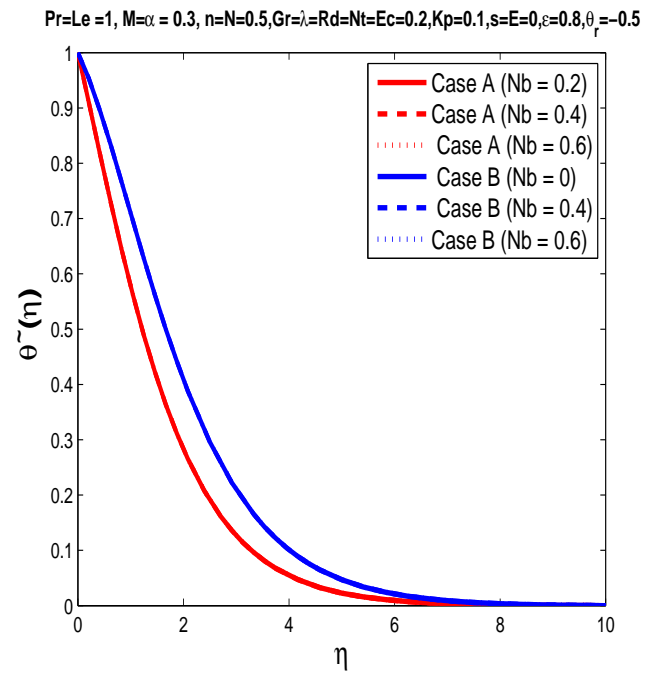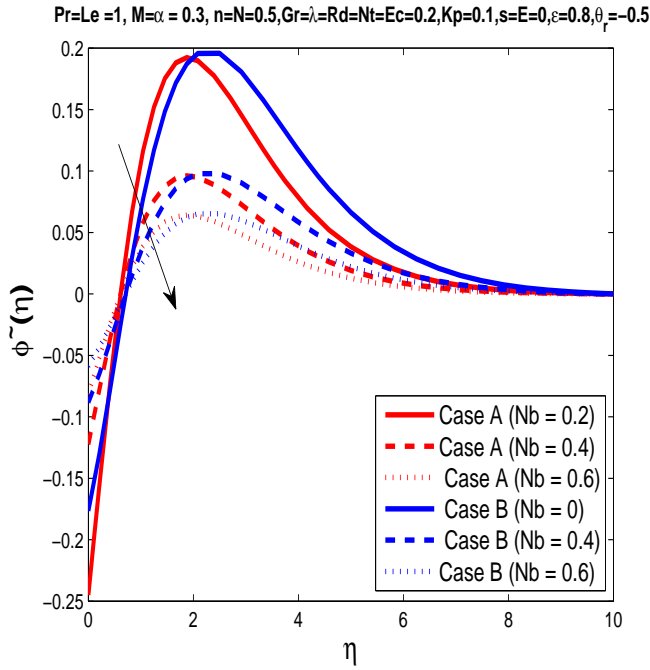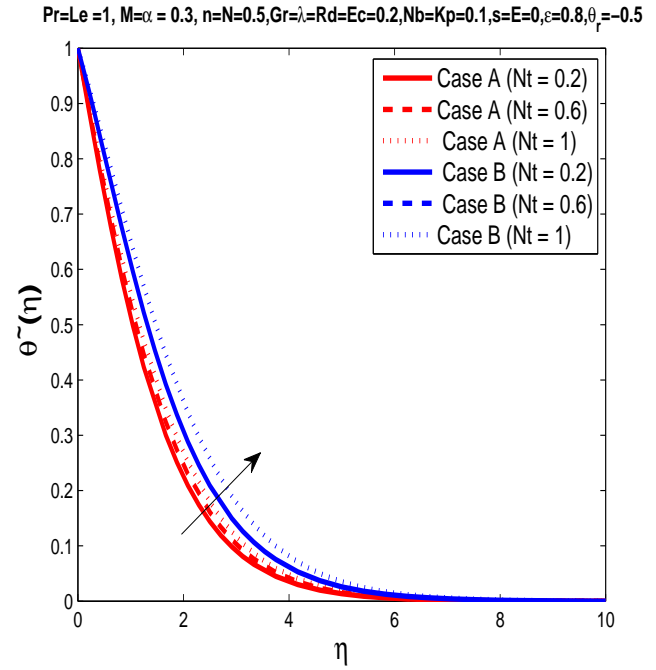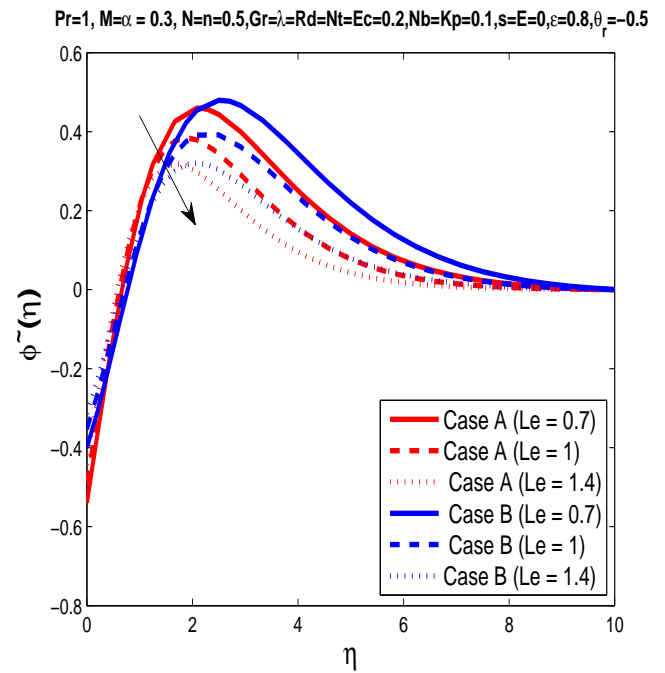


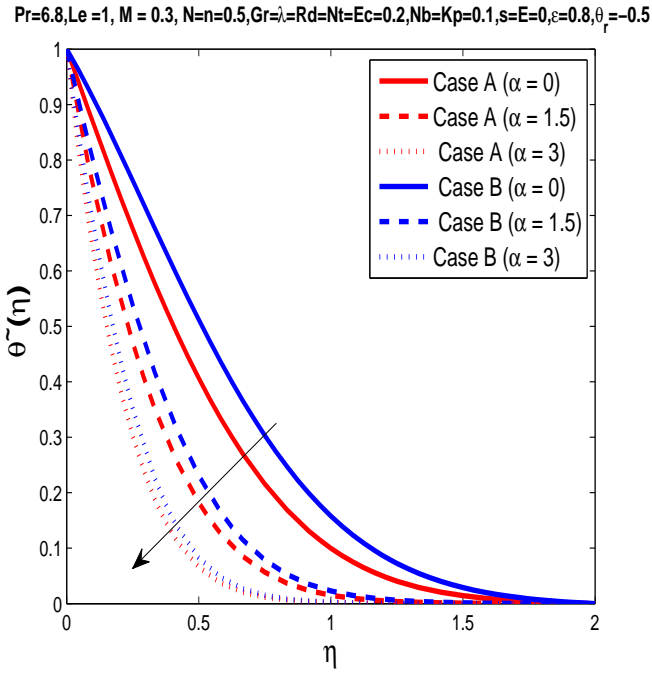Figure 5.14: Temperature profile for different $Pr_o$.

Figure 5.15: Temperature profile for different $Rd$.



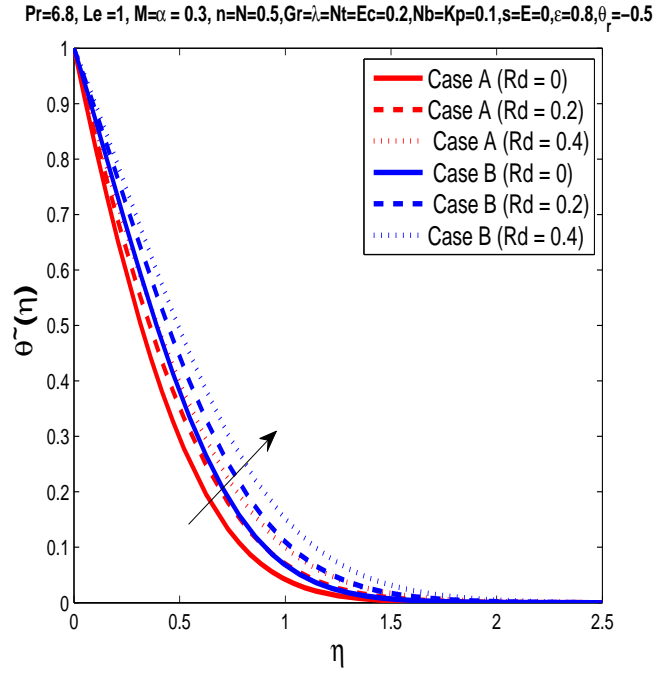Figure 5.16: Temperature profile for different $s$.



Figure 5.17: Temperature profile for different $n$.



Figure 5.18: Temperature profile for different $Nb$.

Figure 5.19: Concentration profile for different $Nb$.



Figure 5.20: Temperature profile for different $Nt$.
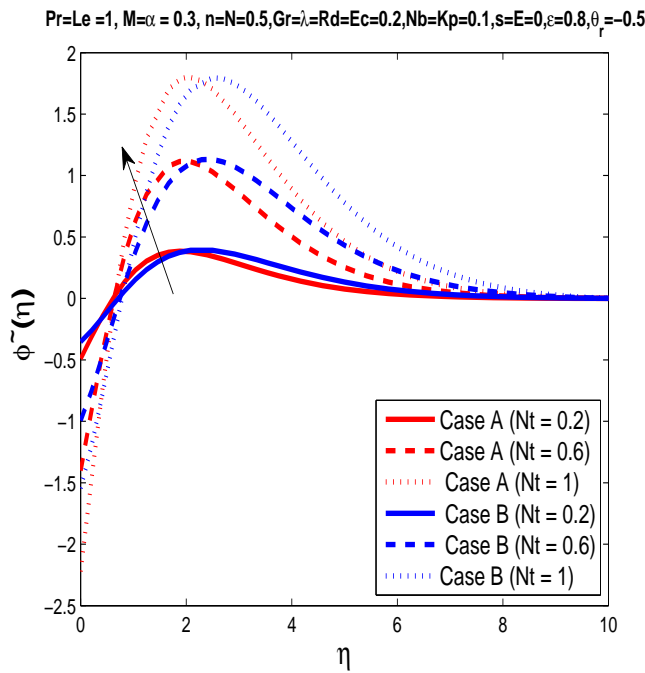


Figure 5.21: Concentration profile for different $Nt$.



Figure 5.22: Concentration profile for different $Le$.

Figure 5.23: Temperature profile for different $\alpha$.
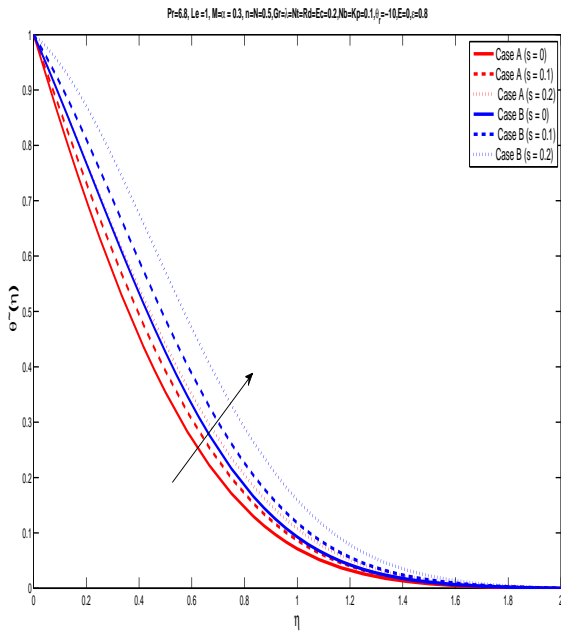


Figure 5.24: Temperature profile for different $Rd$.



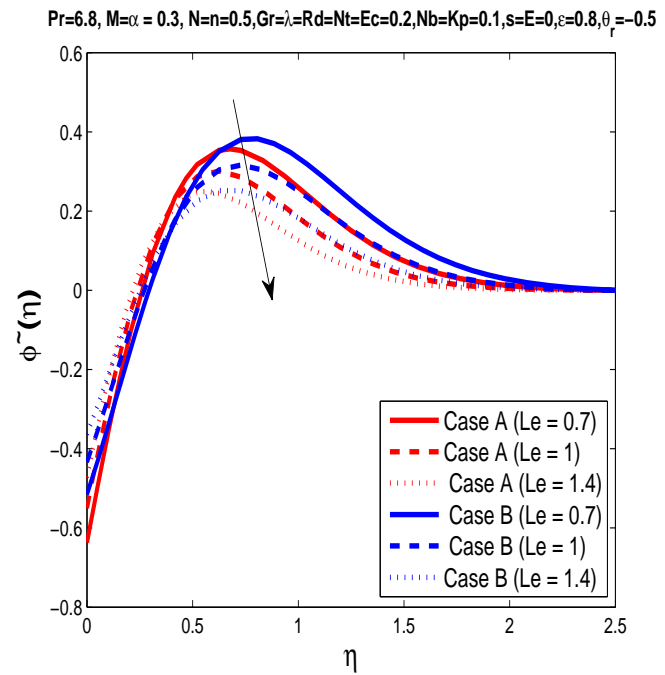Figure 5.25: Temperature profile for different $s$.



Figure 5.26: Concentration profile for different $Le$.
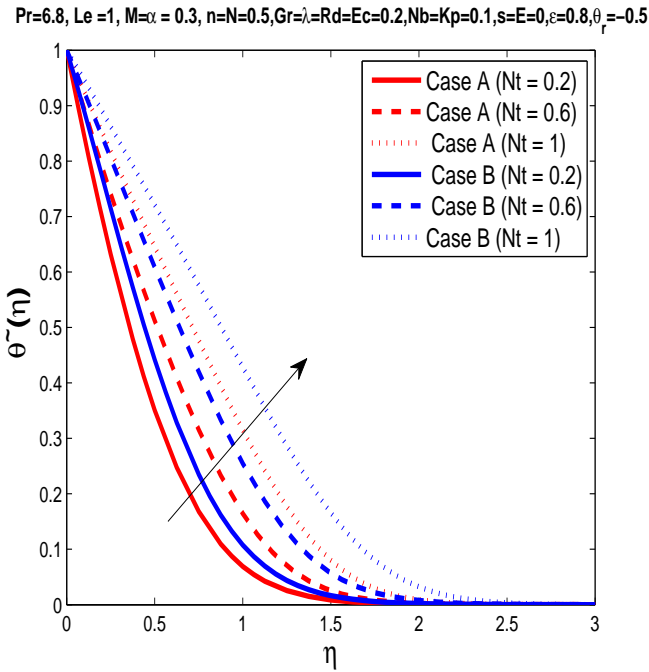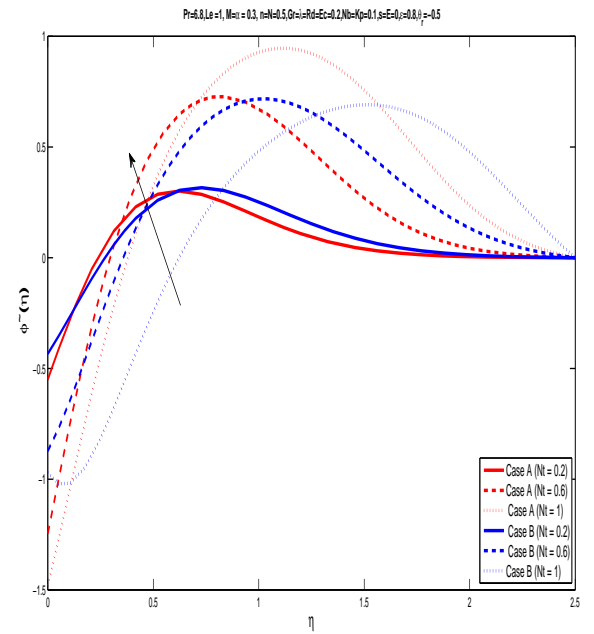
Figure 5.27: Temperature profile for different $Nt$.



Figure 5.28: Concentration profile for different $Nt$.
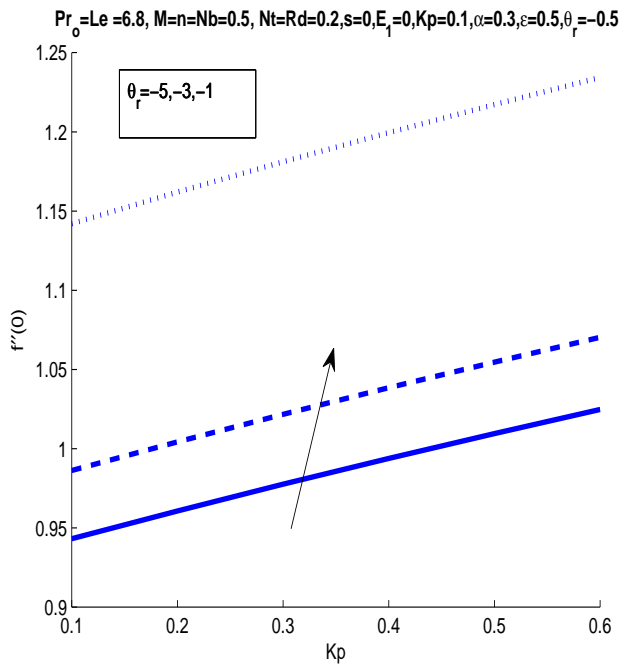


Figure 5.29: The skin friction coefficient with variations in $\theta_r$ and $Kp$.
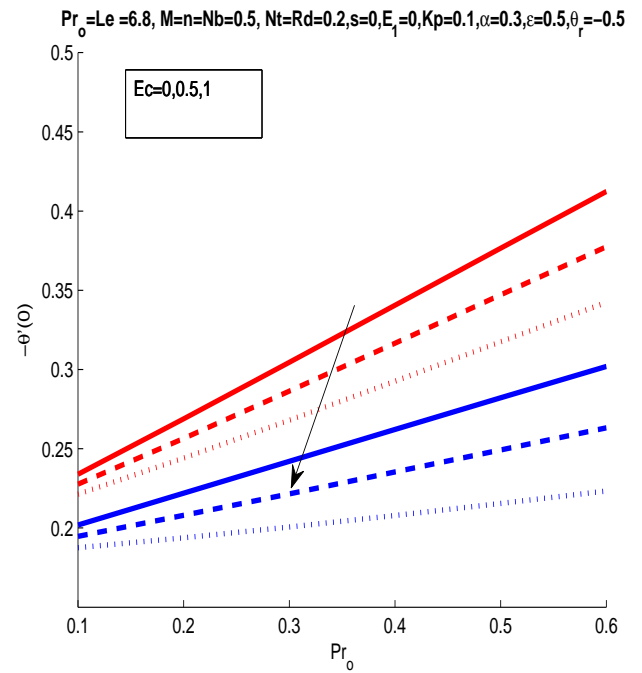


Figure 5.30: The local Nusselt number with variations in $Ec$ and $Pr_o$.
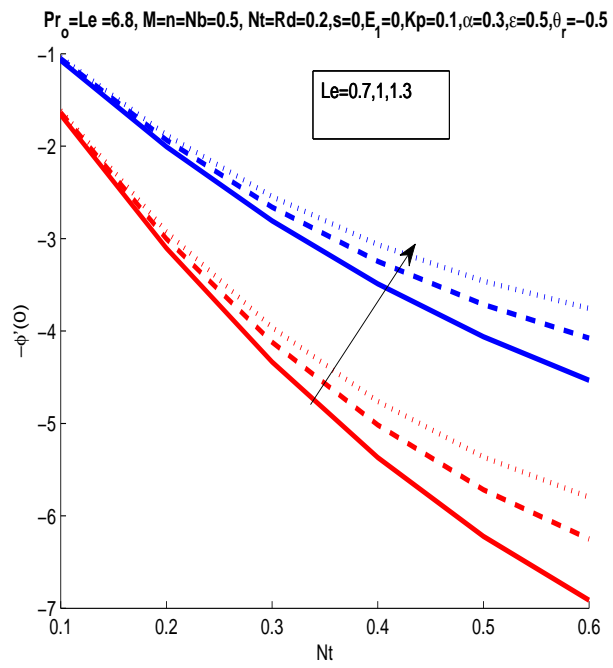
Figure 5.31: The sherwood number with variations in $Le$ and $Nt$ .

## 5.6    Conclusions

The present study gives the results of two dimensional EMHD Powell-Eyring nanofluid flow through an uneven non-linear stretched surface in a porous medium with variable thickness and variable liquid properties. The numerical solutions is obtained with the help of SFDM for constant fluid properties. However, $bvp4c$ is implemented for variable fluid properties. The key findings of the present study are as follows:

- Momentum boundary layer thickness is higher for $E$, $N$, $Gr$ whereas it is going down for $M$, $Kp$, $\alpha$ and $\theta_r$ (for variable properties only).

- Momentum boundary layer remains almost constant when we increase $n$ and $\lambda_1$.

- Thermal boundary layer thickness increases by increasing $Rd$, $\epsilon$, $s$, $n$ and $Nt$.

- Thermal boundary layer thickness lowers for $\alpha$, $E$ and $Pr_0$ whereas there is constant effect in thermal boundary layer when increasing in $Nb$.

- Concentration boundary layer thickness declines by increasing $Nt$ whereas increases by increasing $Nb$ and $Le$.

- Difference of the Cases A and B is seen with the help of graphs. Graphs show that boundary layer thickness of Case B is different when compared to Case A. Furthermore, the skin friction coefficient is higher for constant fluid properties when seen in comparison with variable properties. The same is observed for the local Nusselt number.

- Lastly, the accuracy of the SFDM has been observed when comparison is drawn with the literature.

# Chapter 6

# Unsteady Bio-Nanofluid Flow through a Stretching/ Shrinking Surface While Considering Chemical Reaction and Thermal Radiation

This chapter analyzed to explore the computational results of the unsteady, MHD, stagnation point, bio-nanofluid flow in a porous media with internal heat generation/absorption though a stretching and shrinking surface. The fundamental principles of the similarity transformations applied to the governing PDEs that leads to an ODEs. The transformed ODEs are numerically solved by the shooting algorithm implemented in MATLAB and verification is done from MATLAB built-in solver *bvp4c*. The numerical data produced for $C_{fx_1}$, the $Nu_{x_1}$ and $Sh_{x_1}$ are equated with available result and found to be in a close agreement. Impact of involved physical parameters on velocity, temperature, nanoparticles volume fraction and microorganisms distributions are scrutinized through graphs.It is analyzed that the wall resistance enhances for raising unsteady parameter $A$, magnetic parameter $M$ and porosity parameter $Kp$. In addition, we observe that the density of motile microorganisms profile enhances for a larger values of $Lb$ and $Pe$ while decreases for increasing values of an unsteady parameter $A$.

The sections division of chapter 6 is described below..

The introduction of the current chapter is presented in Section 6.1. Section 6.2 covers the problem formulation and governing equations. The numerical procedure is discussed in Section 6.3. Section 6.4 presents the numerical results through graphs. In Section 6.5 conclusion of the chapter is scrutinized.

## 6.1 Introduction

Raees et al. [141] recorded homotopy analysis method (HAM) solution for an unsteady bio-convection flow in a channel and showed that the velocity component decreases with the increase in time. Uddin et al. [142] discussed bio-convection nanofluid over a wavy surface with slip flow in application to nano-biofuel cells. Uddin et al. [143] investigated Stefan blowing with multiple slip effects in bioconvection. For finding similarity transformation they used Lie group analysis. Reddy and Naveen [144] reported results for activation energy and thermal radiation. Aziz et al. [145] discussed free convection flow in nanofluid with microorganism. They discovered that the bio-convection parameter effects heat transfer rate. Mutuku and Makinde [146] discussed hydromagnetic fluid flow in microorganism. Tausif et al. [147] presented multiple slip effects in the presence of microorganism. Ali et al. [148] discussed hybrid nanofluid with slip conditions for Jeffrey fluid. Mburu et al. [149] reported magnetic and thermal radiation effect over an inclined cylinder. In aforementioned literature studies, the chief emphasis has been made on various physical situations to find an in-depth understanding of physics but the route of bionanofluid along with other situations of unsteady effect in a free stream flow is mostly absent from the literature.

## 6.2 Problem Formulation

Assuming MHD, stagnation point, bio-nanofluid flow in the presence of thermal radiation, chemical reaction and internal heat generation/absorption adjacent to a stretching sheet with thermal radiation. A water based nanofluid containing nanoparticles and gyrotactic microorganisms is considered. It is assumed that the presence of nanoparticles have no affect on the swimming direction of microorganisms and on their swimming velocity. This assumptions holds only for less than 1% concentration of nanoparticles. The magnetic Reynolds number of

$$u_1 \rightarrow u_e, T_1 \rightarrow T_\infty, C_1 \rightarrow C_\infty, N_1 \rightarrow N_\infty, y_1 \rightarrow \infty$$
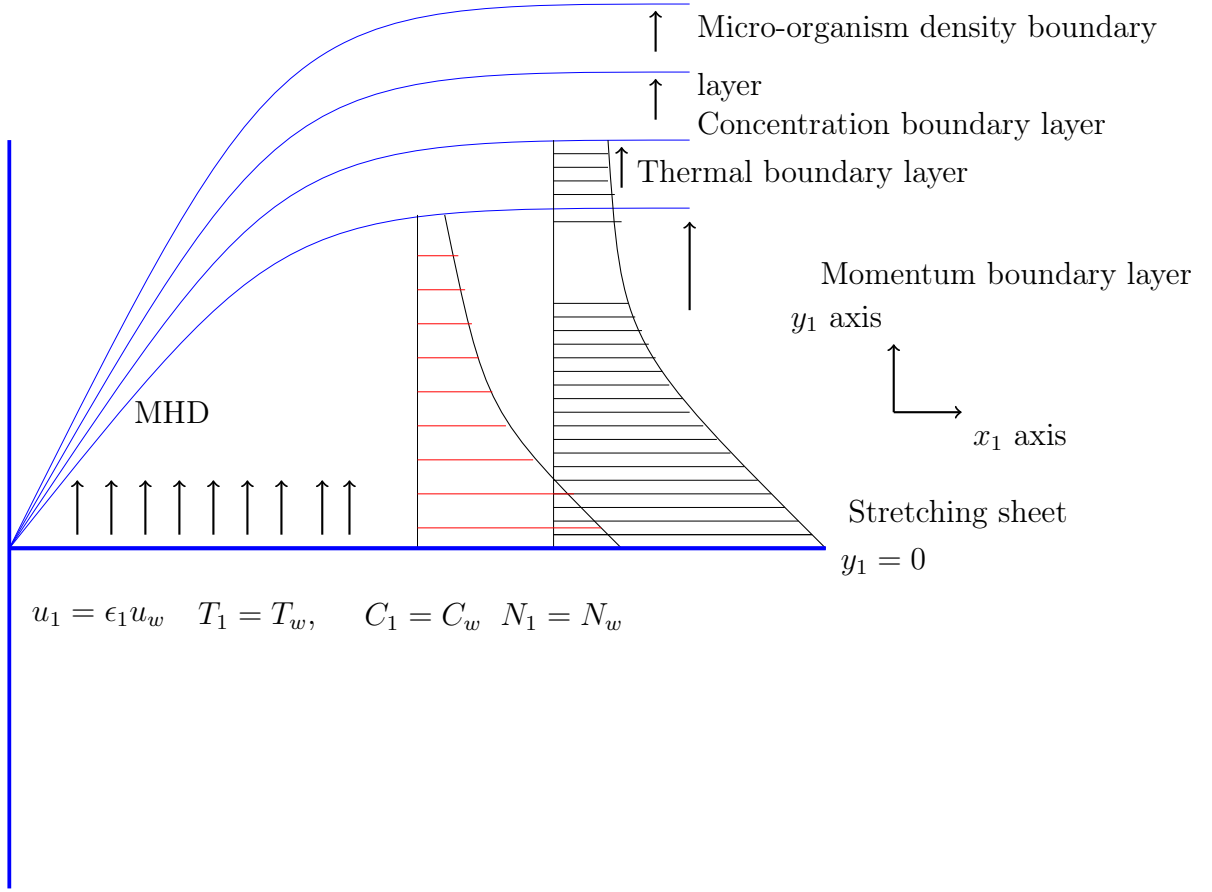


Figure 6.1: Geometry of the problem.

the flow is taken to be very small, so that induced magnetic field is presumed to be negligible. The applied magnetic field $\beta_o^2$ is taken along the normal to the sheet. $u_e = \epsilon_1 a x_1 (1 - A_1 t_1)^{-1}$ indicates the velocity stretching sheet for $\epsilon_1 > 0$ whereas it describes the velocity of shrinking sheet for $\epsilon_1 < 0$ while $\epsilon_1 = 0$ is an illustration of stationary sheet. The configuration of the flow is given in Fig. **??**.

Under the above assumptions, the governing model of flow reads [94], [93]:

$$\frac{\partial u_1}{\partial x_1} + \frac{\partial v_1}{\partial y_1} = 0, \tag{6.1}$$

$$\frac{\partial u_1}{\partial t_1} + u_1 \frac{\partial u_1}{\partial x_1} + v_1 \frac{\partial u_1}{\partial y_1} = u_e \frac{\partial u_e}{\partial x_1} + \frac{\partial u_e}{\partial t_1} + \nu_1 \frac{\partial^2 u_1}{\partial y_1^2} - \frac{\nu_1}{k^*}(u_1 - u_e) - \frac{\sigma B_o^2}{\rho_1}(u_1 - u_e), \tag{6.2}$$

$$\frac{\partial T_1}{\partial t_1} + u_1 \frac{\partial T_1}{\partial x_1} + v_1 \frac{\partial T_1}{\partial y_1} = \alpha_1 \frac{\partial^2 T_1}{\partial y_1^2} + \tau_1 (D_B \frac{\partial T_1}{\partial y_1} \frac{\partial C_1}{\partial y_1} + \frac{D_T}{T_\infty}(\frac{\partial T_1}{\partial y_1})^2) - \frac{1}{\rho_1 c_p} \frac{\partial q_r}{\partial y_1} + \frac{\mu_1}{\rho_1 c_p}(\frac{\partial u_1}{\partial y_1})^2)$$
$$+ \frac{(T_1 - T_\infty)Q}{\rho_1 c_p}, \tag{6.3}$$

$$\frac{\partial C_1}{\partial t_1} + u_1\frac{\partial C_1}{\partial x_1} + v_1\frac{\partial C_1}{\partial y_1} = D_B\frac{\partial^2 C_1}{\partial y_1^2} + \frac{D_T}{T_\infty}\frac{\partial^2 T_1}{\partial y_1^2} - (C_1 - C_\infty)K_c, \tag{6.4}$$

$$\frac{\partial N_1}{\partial t_1} + u_1\frac{\partial N_1}{\partial x_1} + v_1\frac{\partial N_1}{\partial y_1} + \frac{b_1 w_c}{C_w - C_\infty}\left(\frac{\partial}{\partial y_1}\left(N_1\frac{\partial C_1}{\partial y_1}\right)\right) = D_n\frac{\partial^2 N_1}{\partial y_1^2}. \tag{6.5}$$

while the boundary conditions corresponding to considered model is taken as,

$$t_1 \not< 0 : v_1 = 0, \qquad , u_1 = 0, \qquad T_1 = T_\infty, \qquad C_1 = C_\infty, \qquad N_1 = N_\infty,$$

$$t_1 > 0 : u_1 = \epsilon_1\, u_w(x_1,t_1) = \epsilon_1\, ax_1(1 - A_1t)^{-1}, \text{with}\ A_1t_1 \neq 1, \qquad v_1 = 0, \qquad T_1 = T_w,$$

$$C_1 = C_w, \qquad N_1 = N_w \quad \text{at} \quad y_1 = 0,$$

$$u = u_e(x_1,t_1) = ax_1(1 - A_1t_1)^{-1} \text{ with } A_1t_1 \neq 1, \qquad v_1 = 0, \qquad T_1 = T_\infty,$$

$$C_1 = C_\infty, \qquad N_1 = N_\infty \quad \text{as} \quad y_1 \longrightarrow \infty. \tag{6.6}$$

Introducing the similarity solutions as follows:

$$\eta = \sqrt{\frac{a}{\nu_1(1 - A_1t_1)}}y_1, \qquad \psi = \sqrt{\frac{a\nu_1}{1 - A_1t_1}}x_1 f(\eta), \qquad \theta(\eta) = \frac{T_1 - T_\infty}{T_w - T_\infty},$$

$$\phi(\eta) = \frac{C_1 - C_\infty}{C_w - C_\infty}, \qquad \chi(\eta) = \frac{N_1 - N_\infty}{N_w - N_\infty}. \tag{6.7}$$

By inserting Eq. (6.7) into Eqs. (6.1)-(6.5), we acquire the modified ODEs:

$$f''' + ff'' - f'^2 + 1 + A - A\left(f' + \frac{\eta}{2}f''\right) - (M + Kp)(f' - 1) = 0, \tag{6.8}$$

$$\left(1 + \frac{4}{3}Rd\right)\theta'' + Prf\theta' + Nb\theta'\phi' + Nt\theta'^2 + Pr\left(Ecf''^2 + s\theta - \frac{\eta}{2}\theta'A\right) = 0, \tag{6.9}$$

$$\phi'' + \frac{Nt}{Nb}\theta'' + LePrf\phi' - \frac{\eta}{2}LePrA\phi' - LePrKr\phi = 0, \tag{6.10}$$

$$\chi'' + LbPrf\chi' - Pe\left(\phi'\chi' + (\chi + \sigma_1)\phi''\right) - \frac{\eta}{2}LbPrA\chi' = 0. \tag{6.11}$$

Similarly, the relevant boundary conditions are:

$$f(\eta) = 0, \qquad f'(\eta) = \epsilon_1, \qquad \theta(\eta) = 1, \qquad \phi(\eta) = 1, \qquad \chi(\eta) = 1, \qquad \text{at} \qquad \eta = 0,$$

$$f(\eta) = 1, \qquad \theta(\eta) = 0, \qquad \phi(\eta) = 0, \qquad \chi(\eta) = 0, \qquad \text{as} \qquad \eta \to \infty. \tag{6.12}$$

we put the values as:

$A = \frac{A_1}{a}$, $Kp = \frac{\nu_1(1 - A_1t)}{ak^*}$ (Mijankwi et al. [159]), $M = \frac{\sigma B_o^2(1 - A_1t_1)}{\rho_1 a}$(Mijankwi et al. [159]),

$Pr = \frac{\nu_1}{\alpha}$, $Rd = \frac{4\sigma T_\infty^3}{k^* k_1}$, $Nb = \frac{\tau_1 D_B(C_w - C_\infty)}{\alpha_1}$, $Nt = \frac{\tau_1 D_T(T_w - T_\infty)}{T_\infty \alpha_1}$, $Ec = \frac{u_e^2}{c_p(T_w - T_\infty)}$ (Mijankwi et

al. [159]), $s = \frac{Q(1 - A_1t)}{a\rho_1 c_p}$, $Le = \frac{\alpha_1}{D_B}$, $Kr = \frac{K_c(1 - A_1t_1)}{a}$ (Mijankwi et al. [159]), $Lb = \frac{\alpha}{D_n}$ $Pe = \frac{bw_c}{D_n}$,

$\sigma_1 = \frac{N_\infty}{N_w - N_\infty}$

116

The physical quantities $C_{fx_1}$ (local skin friction), $Nu_{x_1}$ (local Nusselt number) , $Sh_{x_1}$ (local Sherwood number) and $Nn_{x_1}$ (local density number of motile microorganisms) presented as,

$$C_{fx_1} = \frac{\mu_1(\frac{\partial u_1}{\partial y_1})_{y_1=0}}{\rho_1 u_e^2}, \quad Nu_{x_1} = \frac{-kx_1(\frac{\partial T_1}{\partial y_1})_{y_1=0}}{k_1(T_w - T_\infty)}, \quad Sh_{x_1} = \frac{-D_B x_1(\frac{\partial C_1}{\partial y_1})_{y_1=0}}{D_B(C_w - C_\infty)},$$

$$Nn_{x_1} = \frac{-D_n x_1(\frac{\partial N_1}{\partial y_1})_{y_1=0}}{D_n(N_w - N_\infty)}. \quad (6.13)$$

Inserting Eq. (6.7) into Eq. () yields the following expressions:

$$Re_{x_1}^{1/2}C_{fx_1} = f''(0), \quad Re_{x_1}^{-1/2}Nu_{x_1} = -(1 + \frac{4}{3}Rd)\theta'(0), \quad Re_{x_1}^{-1/2}Sh_{x_1} = -\phi'(0),$$

$$Re_{x_1}^{-1/2}Nn_{x_1} = -\chi'(0). \quad (6.14)$$

## 6.3 Numerical Procedure

### 6.3.1 Shooting Method

The physical model of ODEs alongside boundary conditions quantitatively evaluated by the shooting algorithm implemented in MATLAB. The shooting approach involves two stages: Converting the BVP into an IVP and the higher-order ODEs into a system of first order ODEs. We employed Newton-Raphson approach in locating roots. The Runge-Kutta method is executed in determining the solution of the IVP. The system of first order ODEs reads as follows:

$$f = u_1, f' = u_2, f'' = u_3, f''' = u_3' = -u_1 u_3 + u_2^2 - 1 - A + A(u_2 + \frac{\eta}{2}u_3) + (M + Kp)(u_2 - 1),$$

$$u_4 = \theta, u_5 = \theta', \theta'' = u_5' = \frac{-1}{(1 + \frac{4}{3}Rd)}(Pru_1 u_5 + Nbu_5 u_7 + Ntu_5^2 + Pr(Ecu_3^2 + su_4 - \frac{\eta}{2}Au_5)),$$

$$u_6 = \phi, u_7 = \phi', \phi'' = u_7' = -\frac{N_t}{N_b}u_5' - LePru_1 u_7 + \frac{LePr\eta A}{2}u_7 + LePrKru_6,$$

$$u_8 = \chi, u_9 = \chi', \chi'' = u_9' = -LbPru_1 u_9 + Pe(u_7 u_9 + (u_8 + \sigma_1)u_7') + \frac{\eta}{2}LbPrAu_9.$$

The converted form of boundary conditions into an initial conditions for the shooting method is rewritten as,

$$u_1(0) = 0, \quad u_2(0) = \epsilon_1, \quad u_4(0) = 1, \quad u_6(0) = 1, \quad u_8(0) = 1, \quad u_3(0) = \tilde{\lambda}_1,$$

$$u_5(0) = \tilde{\lambda}_2, \quad u_7(0) = \tilde{\lambda}_3, \quad u_9(0) = \tilde{\lambda}_4.$$

Table 6.1: Comparison of $-f''(0)$, $-\theta'(0)$ and $-\phi'(0)$ when $\epsilon_1 = 1$, $Le = 2, M = Kp = A = Rd = Ec = s = Kr = Lb = Pe = 0, Nt = Nb = 0.5$ and $Pr = 1$.

|  | Ibrahim et al. [93] | Zaimi et al. [81] | Naganthran et al. [94] | Present result (Shooting Method) |
|---|---|---|---|---|
| $f''(0)$ | 0 | 0 | 0 | 0 |
| $-\theta'(0)$ | 0.4767 | 0.476737 | 0.476737 | 0.4767 |
| $-\phi'(0)$ | 1.0452 | 1.045154 | 1.045154 | 1.0452 |

### 6.3.2   *bvp4c*

Having found numerical results from the shooting method, we verify these results using MAT-LAB built-in solver *bvp4c* [105], [106]. The *bvp4c* is a collocation solver which uses Gauss-Lobatto points to compute accurate results. In *bvp4c* the first order system of ODEs remains the same as discussed in Section 3.1. However the boundary conditions implemented in MAT-LAB are as follows:

$$u_1(0) = 0, \quad u_2(0) = \epsilon_1, \quad u_4(0) = 1, \quad u_6(0) = 1, \quad u_8(0) = 1, \quad u_2(\infty) = 1,$$
$$u_4(\infty) = 0, \quad u_6(\infty) = 0, \quad u_8(\infty) = 0.$$

## 6.4   Results and Discussion

A summary of the current and the reported findings is seen with minimal disparity in Table 1. The data in Tables 2 and 3 shows computational results for the $C_{fx_1}$, $Nu_{x_1}$, the $Sh_{x_1}$ and $Nn_{x_1}$ obtained with shooting and *bvp4c* algorithm . In Table 2 it is revealed that $Cf_{x_1}$ increases with escalating values of $A$, $M$ and $Kp$. However, decreasing trend is seen in $Nu_{x_1}$ against $A$, $Rd$, $Nb$, $Nt$, $Ec$ and $s$. The local Nusselt number enhances for the increasing values of $Pr$. $Sh_{x_1}$ increases for higher values of $Pr$, $Rd$, $Nb$, $Ec$, $s$, $Le$ and $Kr$. The local Sherwood number decreases for higher values of $Nt$. $Nn_{x_1}$ shows decreasing trend for higher values of $A$ and $Nt$ is observed while increases by enhancing $Pr$, $Rd$, $Nb$, $Ec$, $s$, $Le$, $Kr$, $Lb$ and $Pe$.

In Figs. 6.2-6.3, we present velocity profile results against parameters $M$ and $Kp$ with $\epsilon_1 = -0.5, 0.5$ corresponding to a shrinking and stretching sheets. In both cases, the bound-

Table 6.2: **(Shooting Method)**Numerical values of $-f''(0), -\theta'(0),\ -\phi'(0)$ and $-\chi'(0)$ for several values of involved parameter $A$, $M$, $Kp$, $Pr$, $Rd$, $Nb$, $Nt$, $Ec$, $s$, $Le$, $Kr$, $Lb$, and $Pe$ where $\epsilon_1 = 0.5$ .

| $A$ | $M$ | $Kp$ | $Pr$ | $Rd$ | $Nb$ | $Nt$ | $Ec$ | $s$ | $Le$ | $Kr$ | $Lb$ | $Pe$ | S.M $-f''(0)$ | S.M. $-\theta'(0)$ | S.M. $-\phi'(0)$ | S.M $-\chi'(0)$ |
|---|---|---|---|---|---|---|---|---|---|---|---|---|---|---|---|---|
| 0.1 | 0.5 | 0.2 | 0.72 | 0.2 | 0.1 | 0.2 | 0.2 | 0.1 | 1 | 0.1 | 0.5 | 0.5 | 0.8364 | 0.4029 | 0.4109 | 0.5780 |
| 0.3 | | | | | | | | | | | | | 0.8576 | 0.3700 | 0.4109 | 0.5541 |
| 0.5 | | | | | | | | | | | | | 0.8784 | 0.3346 | 0.4121 | 0.5292 |
| 0.1 | 0.1 | 1 | 0.72 | 0.2 | 0.1 | 0.2 | 0.2 | 0.1 | 1 | 0.1 | 0.5 | 0.5 | 0.7749 | 0.4019 | 0.4082 | 0.5748 |
| | 0.3 | | | | | | | | | | | | 0.8062 | 0.4025 | 0.4095 | 0.5764 |
| | 0.5 | | | | | | | | | | | | 0.8364 | 0.4029 | 0.4108 | 0.5780 |
| 0.1 | 0.5 | 0 | 0.72 | 0.2 | 0.1 | 0.2 | 0.2 | 0.1 | 1 | 0.1 | 0.5 | 0.5 | 0.8062 | 0.4025 | 0.4095 | 0.5764 |
| | | 0.3 | | | | | | | | | | | 0.8512 | 0.4032 | 0.4115 | 0.5787 |
| | | 0.5 | | | | | | | | | | | 0.8799 | 0.4035 | 0.4127 | 0.5802 |
| 0.1 | 0.5 | 0.2 | 0.72 | 0.2 | 0.1 | 0.2 | 0.2 | 0.1 | 1 | 0.1 | 0.5 | 0.5 | 0.8364 | 0.4029 | 0.4108 | 0.5780 |
| | | | 1.0 | | | | | | | | | | 0.8364 | 0.4627 | 0.4919 | 0.6788 |
| | | | 1.3 | | | | | | | | | | 0.8364 | 0.5158 | 0.5681 | 0.7716 |
| 0.1 | 0.5 | 0.2 | 0.72 | 0 | 0.1 | 0.2 | 0.2 | 0.1 | 1 | 0.1 | 0.5 | 0.5 | 0.8364 | 0.4343 | 0.3812 | 0.5679 |
| | | | | 0.3 | | | | | | | | | 0.8364 | 0.3897 | 0.4232 | 0.5822 |
| | | | | 0.7 | | | | | | | | | 0.8364 | 0.3477 | 0.4611 | 0.5955 |
| 0.1 | 0.5 | 0.2 | 0.72 | 0.2 | 0.2 | 0.2 | 0.2 | 0.1 | 1 | 0.1 | 0.5 | 0.5 | 0.8364 | 0.3827 | 0.5386 | 0.6244 |
| | | | | | 0.5 | | | | | | | | 0.8364 | 0.3262 | 0.6138 | 0.6519 |
| | | | | | 0.7 | | | | | | | | 0.8364 | 0.2919 | 0.6272 | 0.6568 |
| 0.1 | 0.5 | 0.2 | 0.72 | 0.2 | 0.1 | 0.1 | 0.2 | 0.1 | 1 | 0.1 | 0.5 | 0.5 | 0.8364 | 0.4170 | 0.5116 | 0.6121 |
| | | | | | | 0.2 | | | | | | | 0.8364 | 0.4029 | 0.4108 | 0.5780 |
| | | | | | | 0.4 | | | | | | | 0.8364 | 0.3761 | 0.2685 | 0.5380 |
| 0.1 | 0.5 | 0.2 | 0.72 | 0.2 | 0.1 | 0.2 | 0.2 | 0.1 | 1 | 0.1 | 0.5 | 0.5 | 0.8364 | 0.4029 | 0.4108 | 0.5780 |
| | | | | | | | 0.4 | | | | | | 0.8364 | 0.3807 | 0.4518 | 0.5976 |
| | | | | | | | 0.7 | | | | | | 0.8364 | 0.3472 | 0.5132 | 0.6271 |
| 0.1 | 0.5 | 0.2 | 0.72 | 0.2 | 0.1 | 0.2 | 0.2 | 0 | 1 | 0.1 | 0.5 | 0.5 | 0.8364 | 0.4501 | 0.3345 | 0.5431 |
| | | | | | | | | 0.1 | | | | | 0.8364 | 0.4029 | 0.4108 | 0.5780 |
| | | | | | | | | 0.2 | | | | | 0.8364 | 0.3527 | 0.4916 | 0.6148 |
| 0.1 | 0.5 | 0.2 | 0.72 | 0.2 | | 0.2 | 0.2 | 0.1 | 0.7 | 0.1 | 0.5 | 0.5 | 0.8364 | 0.4066 | 0.2662 | 0.5221 |
| | | | | | | | | | 1 | | | | 0.8364 | 0.4029 | 0.4108 | 0.5780 |
| | | | | | | | | | 1.3 | | | | 0.8364 | 0.4005 | 0.5261 | 0.6242 |
| 0.1 | 0.5 | 0.2 | 0.72 | 0.2 | 0.1 | 0.2 | 0.2 | 0.1 | 1 | 0.1 | 0.5 | 0.5 | 0.8364 | 0.4029 | 0.4108 | 0.5780 |
| | | | | | | | | | | 0.4 | | | 0.8364 | 0.4007 | 0.6112 | 0.6658 |
| | | | | | | | | | | 0.8 | | | 0.8364 | 0.3984 | 0.8266 | 0.7617 |
| 0.1 | 0.5 | 0.2 | 0.72 | 0.2 | 0.1 | 0.2 | | 0.1 | 1 | 0.1 | 0.5 | 0.5 | 0.8364 | 0.4029 | 0.4108 | 0.5780 |
| | | | | | | | | | | | 1 | | 0.8364 | 0.4029 | 0.4108 | 0.7347 |
| | | | | | | | | | | | 2 | | 0.8364 | 0.4029 | 0.4108 | 0.9490 |
| | | | | | | | | | | 0.1 | 0.5 | 0.5 | 0.8364 | 0.4029 | 0.4108 | 0.5780 |
| | | | | | | | | | | | | 1 | 0.8364 | 0.4029 | 0.4108 | 0.7394 |
| | | | | | | | | | | | | 3 | 0.8364 | 0.4029 | 0.4108 | 1.4396 |

Table 6.3: **(BVP4C)** Numerical values of $-f''(0), -\theta'(0), -\phi'(0)$ and $-\chi'(0)$ for distinct $A$, $M$, $Kp$, $Pr$, $Rd$, $Nb$, $Nt$, $Ec$, $s$, $Le$, $Kr$, $Lb$, and $Pe$ where $\epsilon_1 = 0.5$
.

| | | | | | | | | | | | | | bvp4c | bvp4c. | bvp4c. | bvp4c |
|---|---|---|---|---|---|---|---|---|---|---|---|---|---|---|---|---|
| $A$ | $M$ | $Kp$ | $Pr$ | $Rd$ | $Nb$ | $Nt$ | $Ec$ | $s$ | $Le$ | $Kr$ | $Lb$ | $Pe$ | $-f''(0)$ | $-\theta'(0)$ | $-\phi'(0)$ | $-\chi'(0)$ |
| 0.1 | 0.5 | 0.2 | 0.72 | 0.2 | 0.1 | 0.2 | 0.2 | 0.1 | 1 | 0.1 | 0.5 | 0.5 | 0.8364 | 0.4029 | 0.4108 | 0.5780 |
| 0.3 | | | | | | | | | | | | | 0.8576 | 0.3700 | 0.4109 | 0.5541 |
| 0.5 | | | | | | | | | | | | | 0.8784 | 0.3346 | 0.4121 | 0.5292 |
| 0.1 | 0.1 | 1 | 0.72 | 0.2 | 0.1 | 0.2 | 0.2 | 0.1 | 1 | 0.1 | 0.5 | 0.5 | 0.7749 | 0.4019 | 0.4082 | 0.5748 |
| | 0.3 | | | | | | | | | | | | 0.8062 | 0.4025 | 0.4095 | 0.5764 |
| | 0.5 | | | | | | | | | | | | 0.8364 | 0.4029 | 0.4108 | 0.5780 |
| 0.1 | 0.5 | 0 | 0.72 | 0.2 | 0.1 | 0.2 | 0.2 | 0.1 | 1 | 0.1 | 0.5 | 0.5 | 0.8062 | 0.4025 | 0.4095 | 0.5764 |
| | | 0.3 | | | | | | | | | | | 0.8512 | 0.4032 | 0.4115 | 0.5787 |
| | | 0.5 | | | | | | | | | | | 0.8798 | 0.4035 | 0.4127 | 0.5801 |
| 0.1 | 0.5 | 0.2 | 0.72 | 0.2 | 0.1 | 0.2 | 0.2 | 0.1 | 1 | 0.1 | 0.5 | 0.5 | 0.8364 | 0.4029 | 0.4108 | 0.5780 |
| | | | 1.0 | | | | | | | | | | 0.8364 | 0.4627 | 0.4919 | 0.6788 |
| | | | 1.3 | | | | | | | | | | 0.8364 | 0.5158 | 0.5681 | 0.7717 |
| 0.1 | 0.5 | 0.2 | 0.72 | 0 | 0.1 | 0.2 | 0.2 | 0.1 | 1 | 0.1 | 0.5 | 0.5 | 0.8364 | 0.4343 | 0.3812 | 0.5679 |
| | | | | 0.3 | | | | | | | | | 0.8364 | 0.3897 | 0.4232 | 0.5822 |
| | | | | 0.7 | | | | | | | | | 0.8364 | 0.3477 | 0.4611 | 0.5955 |
| 0.1 | 0.5 | 0.2 | 0.72 | 0.2 | 0.2 | 0.2 | 0.2 | 0.1 | 1 | 0.1 | 0.5 | 0.5 | 0.8364 | 0.3827 | 0.5386 | 0.6244 |
| | | | | | 0.5 | | | | | | | | 0.8364 | 0.3262 | 0.6138 | 0.6519 |
| | | | | | 0.7 | | | | | | | | 0.8364 | 0.2919 | 0.6272 | 0.6568 |
| 0.1 | 0.5 | 0.2 | 0.72 | 0.2 | 0.1 | 0.1 | 0.2 | 0.1 | 1 | 0.1 | 0.5 | 0.5 | 0.8364 | 0.4170 | 0.5116 | 0.6121 |
| | | | | | | 0.2 | | | | | | | 0.8364 | 0.4029 | 0.4108 | 0.5779 |
| | | | | | | 0.4 | | | | | | | 0.8364 | 0.3761 | 0.2685 | 0.5380 |
| 0.1 | 0.5 | 0.2 | 0.72 | 0.2 | 0.1 | 0.2 | 0.2 | 0.1 | 1 | 0.1 | 0.5 | 0.5 | 0.8364 | 0.4029 | 0.4108 | 0.5779 |
| | | | | | | | 0.4 | | | | | | 0.8364 | 0.3807 | 0.4518 | 0.5976 |
| | | | | | | | 0.7 | | | | | | 0.8364 | 0.3472 | 0.5132 | 0.6271 |
| 0.1 | 0.5 | 0.2 | 0.72 | 0.2 | 0.1 | 0.2 | 0.2 | 0 | 1 | 0.1 | 0.5 | 0.5 | 0.8364 | 0.4501 | 0.3345 | 0.5431 |
| | | | | | | | | 0.1 | | | | | 0.8364 | 0.4029 | 0.4108 | 0.5779 |
| | | | | | | | | 0.2 | | | | | 0.8364 | 0.3527 | 0.4916 | 0.6148 |
| 0.1 | 0.5 | 0.2 | 0.72 | 0.2 | | 0.2 | 0.2 | 0.1 | 0.7 | 0.1 | 0.5 | 0.5 | 0.8364 | 0.4066 | 0.2662 | 0.5221 |
| | | | | | | | | | 1 | | | | 0.8364 | 0.4029 | 0.4108 | 0.5779 |
| | | | | | | | | | 1.3 | | | | 0.8364 | 0.4005 | 0.5261 | 0.6242 |
| 0.1 | 0.5 | 0.2 | 0.72 | 0.2 | 0.1 | 0.2 | 0.2 | 0.1 | 1 | 0.1 | 0.5 | 0.5 | 0.8364 | 0.4029 | 0.4108 | 0.5780 |
| | | | | | | | | | | 0.4 | | | 0.8364 | 0.4006 | 0.6112 | 0.6658 |
| | | | | | | | | | | 0.8 | | | 0.8364 | 0.3984 | 0.8266 | 0.7617 |
| 0.1 | 0.5 | 0.2 | 0.72 | 0.2 | 0.1 | 0.2 | | 0.1 | 1 | 0.1 | 0.5 | 0.5 | 0.8364 | 0.4029 | 0.4108 | 0.5780 |
| | | | | | | | | | | | 1 | | 0.8364 | 0.4029 | 0.4108 | 0.7347 |
| | | | | | | | | | | | 2 | | 0.8364 | 0.4029 | 0.4108 | 0.9490 |
| | | | | | | | | | | 0.1 | 0.5 | 0.5 | 0.8364 | 0.4029 | 0.4108 | 0.5780 |
| | | | | | | | | | | | | 1 | 0.8364 | 0.4029 | 0.4108 | 0.7394 |
| | | | | | | | | | | | | 3 | 0.8364 | 0.4029 | 0.4108 | 1.4396 |

ary layer thickness decreases.

Figs. 6.4-6.6 demonstrates the impact of $Nb$ on the temperature, nanoparticles concentration and the microorganisms distributions for the case of stretching sheet ($\epsilon_1 = -0.5$) and shrinking sheet ($\epsilon_1 = -0.5$), respectively. Fig. 6.4 gives an incremental thermal boundary layer thickness results as $Nb$ increases. The thermal boundary layer thickness for $Nb$ with stretching sheet is lower than the shrinking sheet. From Fig. 6.5, it is noticed that by increasing $Nb$ the concentration boundary layer thickness reduces in both stretching and shrinking sheet cases. Fig. 6.6 exhibits that for higher values of $Nb$ the density of motile microorganisms decreases. This decrease in density of motile microorganisms is higher in shrinking sheet case as compared to stretching sheet case.

The impact of $Nt$ on temperature, concentration and density of motile microorganisms can be seen in Fig. 6.7-6.9. Fig. 6.7 reveals that the thermal boundary layer thickness increases for lager values of $Nt$. Figs. 6.8 is not acceptable because theoretically, the concentration of the nanoparticles should be $< 1$. The concentration distribution for the shrinking case, as shown in fig. 6.8, portray values of the nanoparticles concentration greater than one, and this is due to the concentration overshoot along the shrinking surface which forms the backward flow that may disrupt the laminar flow. Fig. 6.9 indicates that the motile microorganisms increases by increasing $Nt$.

Fig. 6.10 depicts the behavior of $Rd$ on the temperature profile. We observe that by increasing radiation parameter thermal boundary layer thickness increases in both stretching and shrinking sheet cases.

Fig. 6.11 characterizes the influence of $Ec$ on temperature distribution. We conclude that increment in Eckert number enhances the temperature profile.

Fig. 6.12 scrutinizes the impact of $s$ on the temperature profile. It is seen that for higher values of $s$ magnify the temperature profile.

Fig. 6.13 examines the effect of $Pr$ on the temperature profile. We analyzed that enhancement in $Pr$ causes reduction in thermal boundary layer thickness.

Fig. 6.14 is drawn to perceive the impact of $Lb$ on the density of motile microorganisms profile. It is observed that higher values of $Lb$ lowers the boundary layer thickness of motile microorganisms profile.

Fig. 6.15 represents the influence of $Pe$ on microorganisms profile. It is validated the fact that increment in Peclet number causes reduction in motile microorganisms boundary layer thickness.

Fig. 6.16 and 6.17 portrays the impact of $Le$ and $Kr$ on concentration profile. It is analyzed that by increasing both the parameter $Le$ and $Kr$ the concentration boundary layer thins.

Fig. 6.18 depicts the the skin friction coefficient against $K_p$ with variations $A$ and $M$. The skin friction seems to increase with the porosity parameter and with the increasing values of $A$ and $M$.

Fig. 6.19 illustrates the impacts of $s$ and $Ec$ on local Nusselt number. The local Nusselt number increases for enhancing values of $M$.

Fig. 6.20 reflects the influences of $Kr$ and $Le$ on local Sherwood number. It is inspected that local Sherwood number shows improvement for higher values $Kr$.

Impact of $Pe$ and $Lb$ on density of motile microorganisms is demonstrated in fig. 6.21. It is perceived that by enhancing $Pe$ density of microorganisms increases.

Figure 6.2: Velocity profile $f\prime(\eta)$ for different $M$.



Figure 6.3: Velocity profile $f\prime(\eta)$ for different $Kp$.



Figure 6.4: Temperature profile $\theta(\eta)$ for different $Nb$.
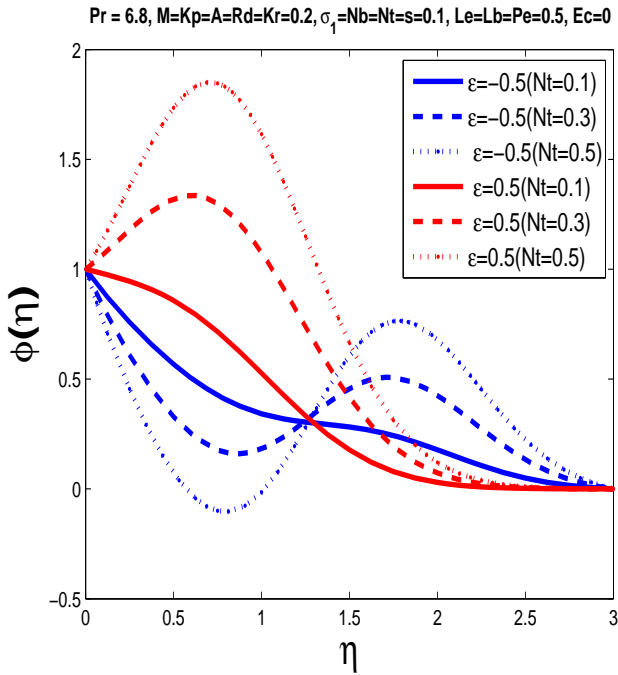


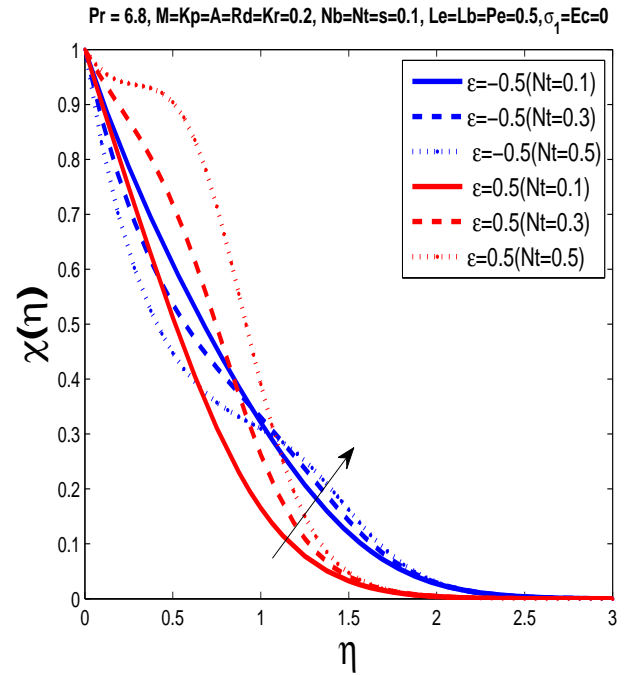Figure 6.5: Concentration profile $\phi(\eta)$ for different $Nb$.
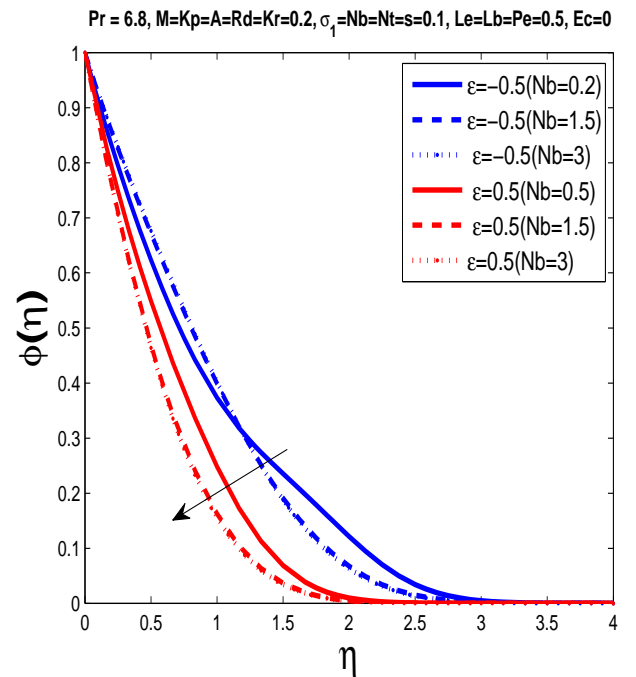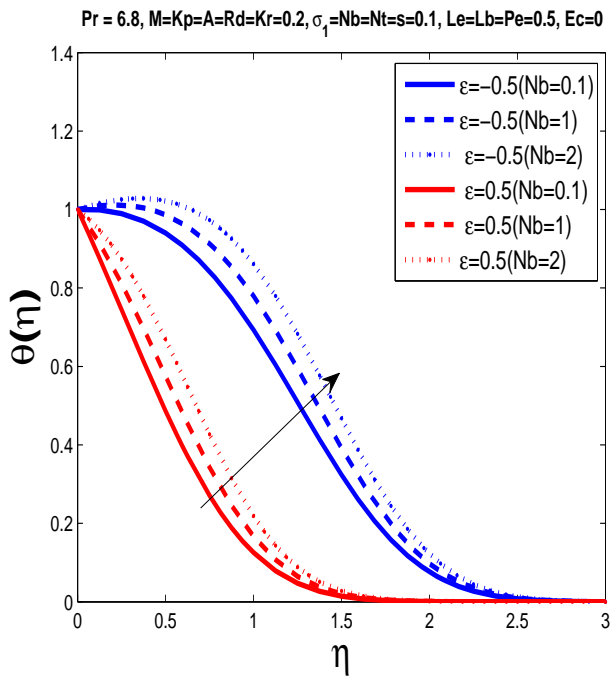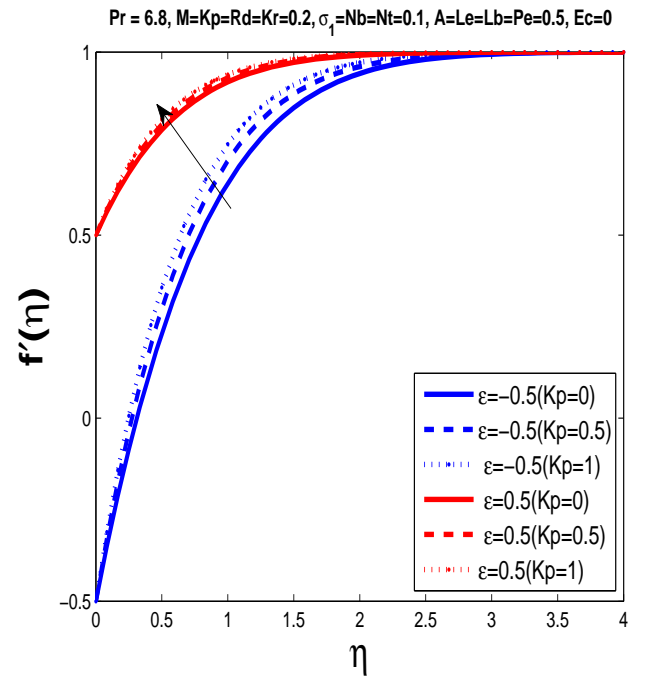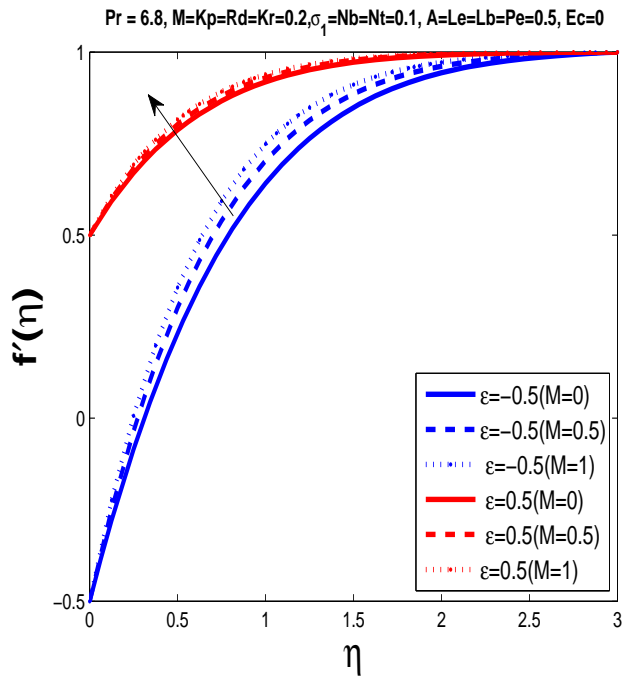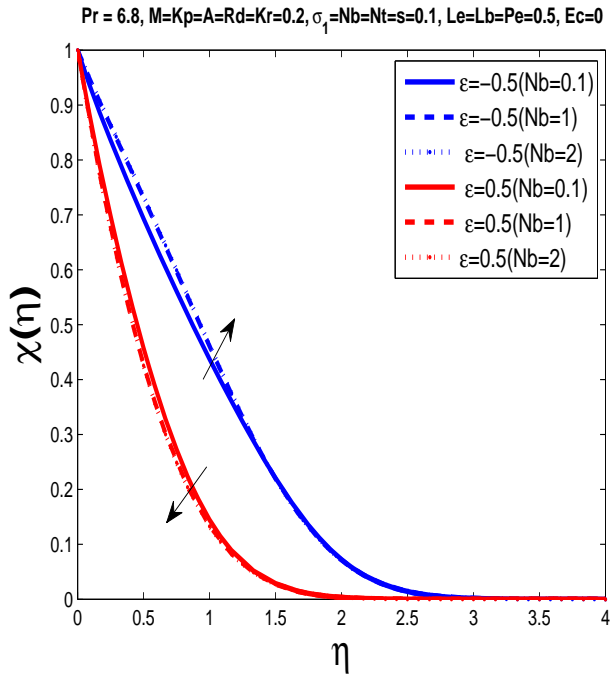
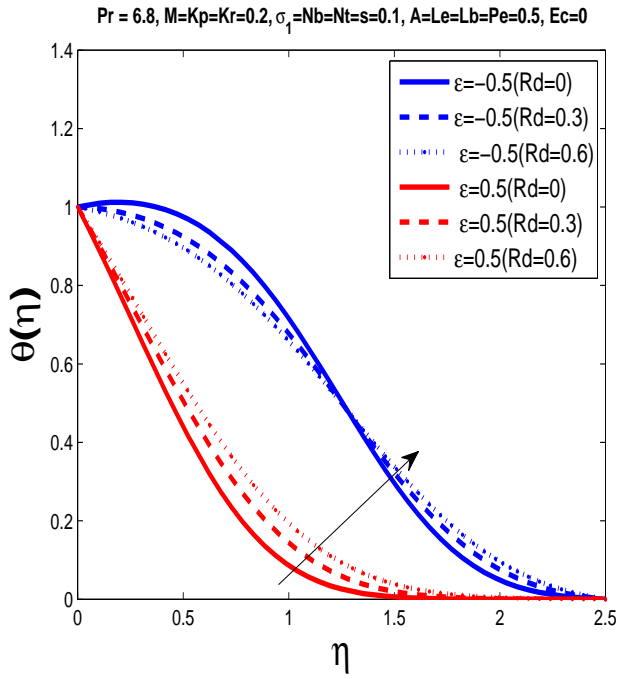Figure 6.6: Microorganisms profile $\chi(\eta)$ for different $Nb$.
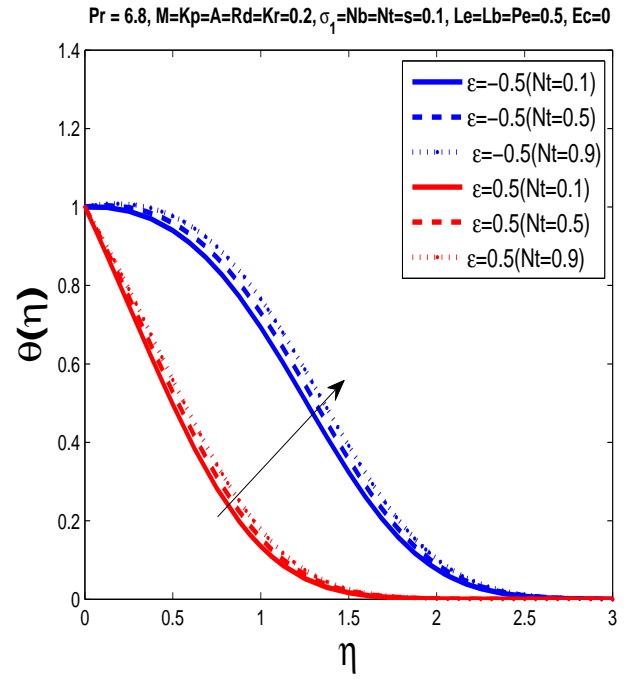


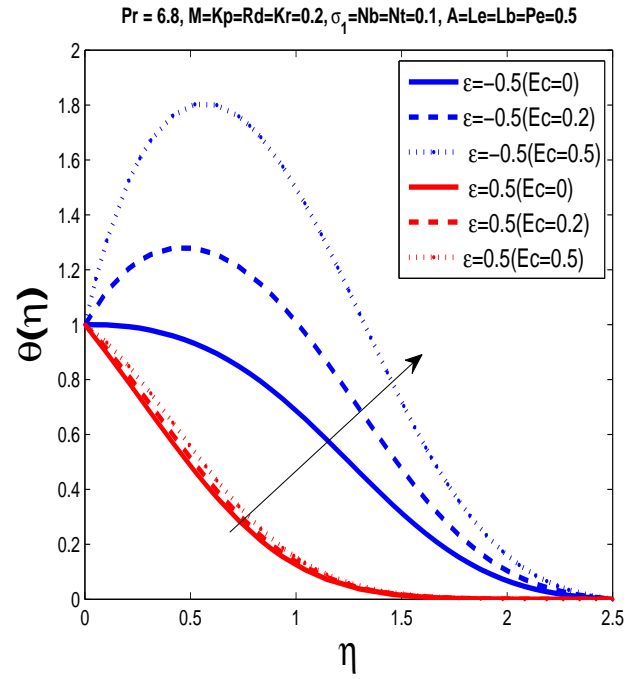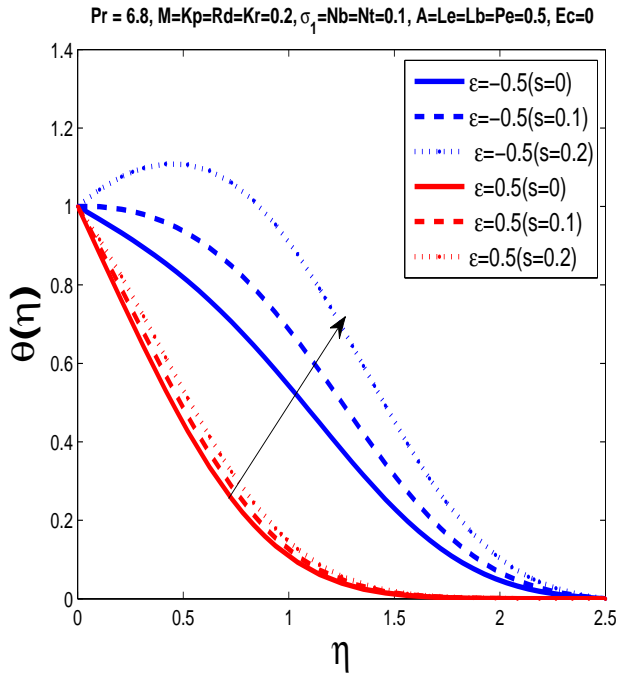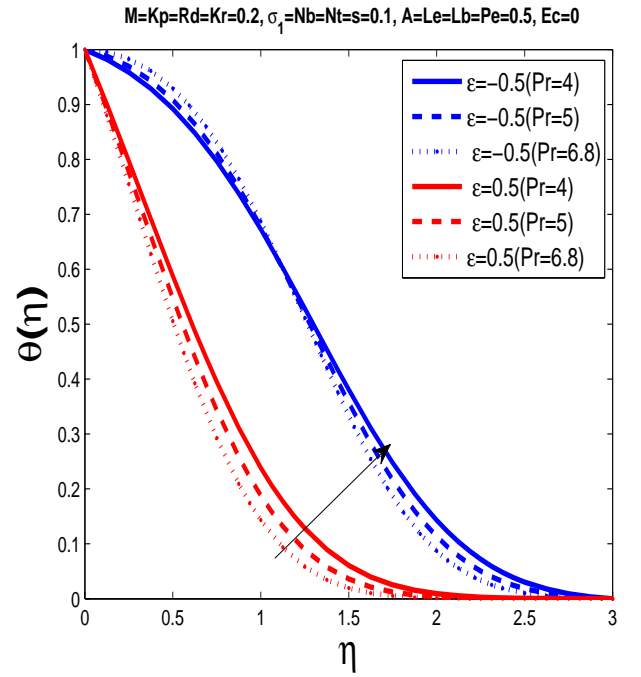Figure 6.7: Temperature profile $\theta(\eta)$ for different $Nt$.



Figure 6.8: Concentration profile $\phi(\eta)$ for different $Nt$.



Figure 6.9: Microorganisms profile $\chi(\eta)$ for different $Nt$.

Figure 6.10: Temperature profile $\theta(\eta)$ for different $Rd$.



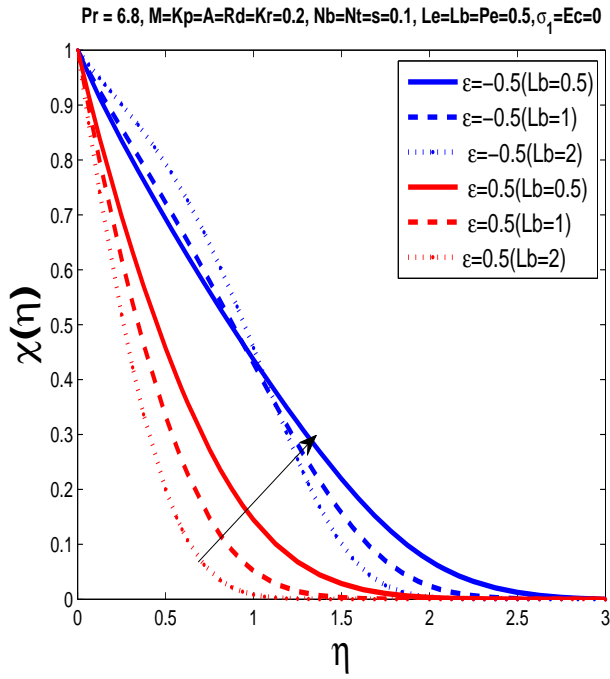Figure 6.11: Temperature profile $\theta(\eta)$ for different $Ec$.



Figure 6.12: Temperature profile $\theta(\eta)$ for different $s$.



Figure 6.13: Temperature profile $\theta(\eta)$ for different $Pr$.

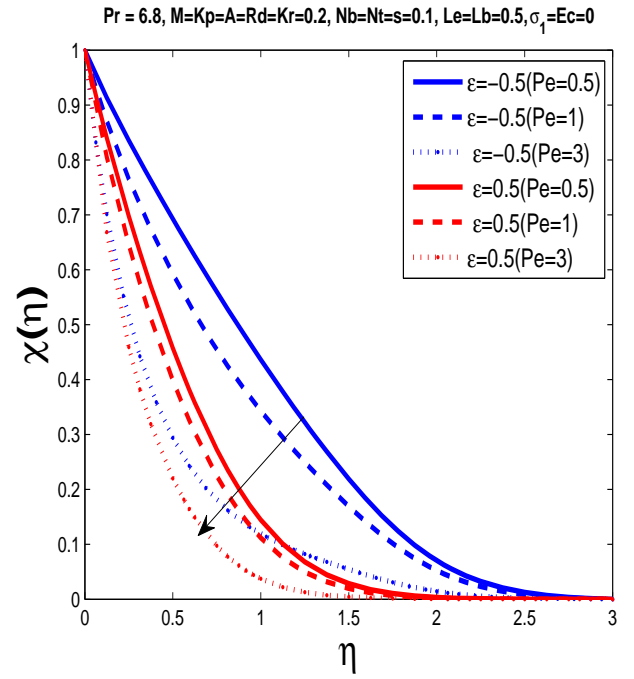Figure 6.14: Microorganisms profile $\chi(\eta)$ for different $Lb$.



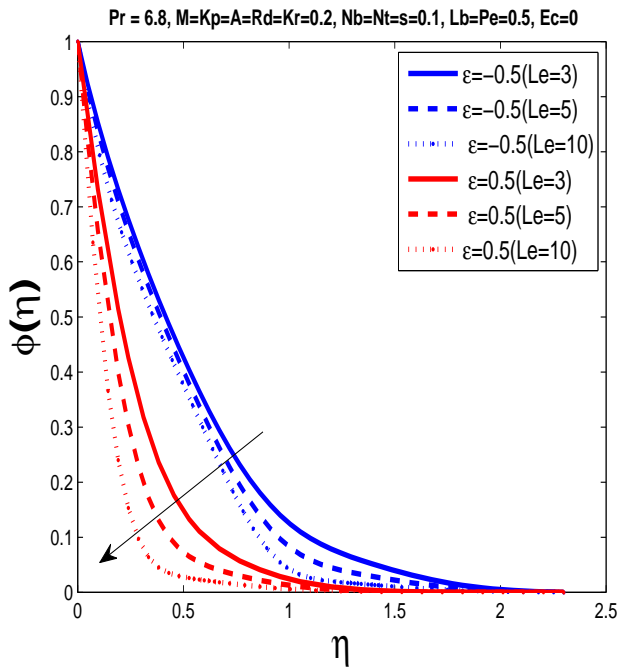Figure 6.15: Microorganisms profile $\chi(\eta)$ for different $Pe$.



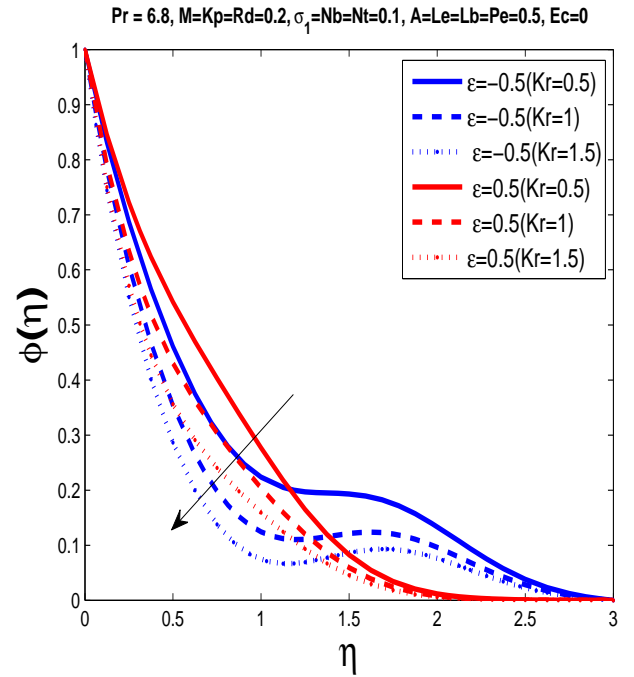Figure 6.16: Concentration profile $\phi(\eta)$ for different $Le$.



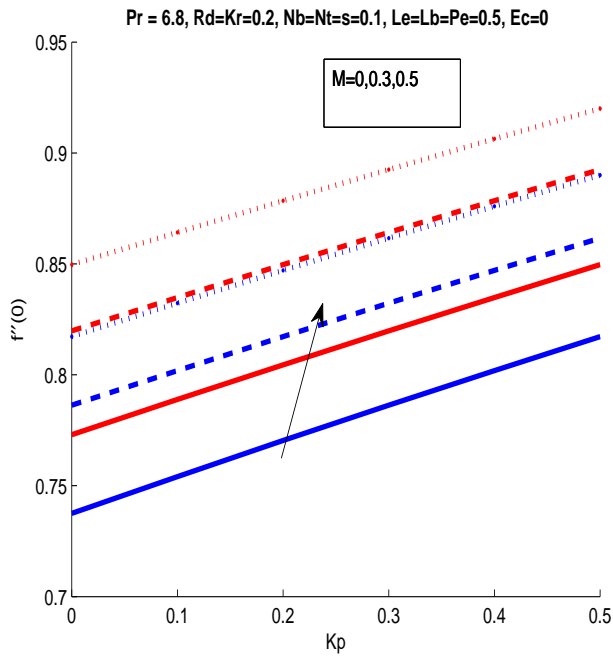Figure 6.17: Concentration profile $\phi(\eta)$ for different $Kr$.

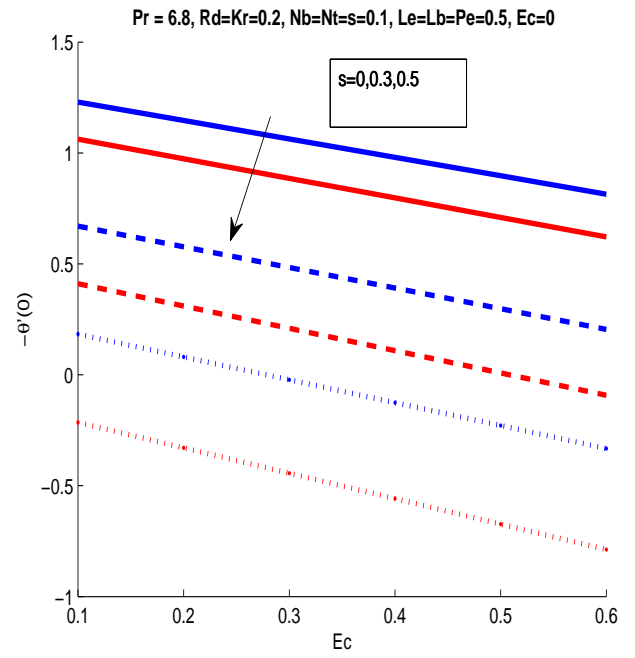Figure 6.18: The skin friction coefficient with variations in $M$ and $Kp$.



Figure 6.19: The local Nusselt number with variations in $s$ and $Ec$.
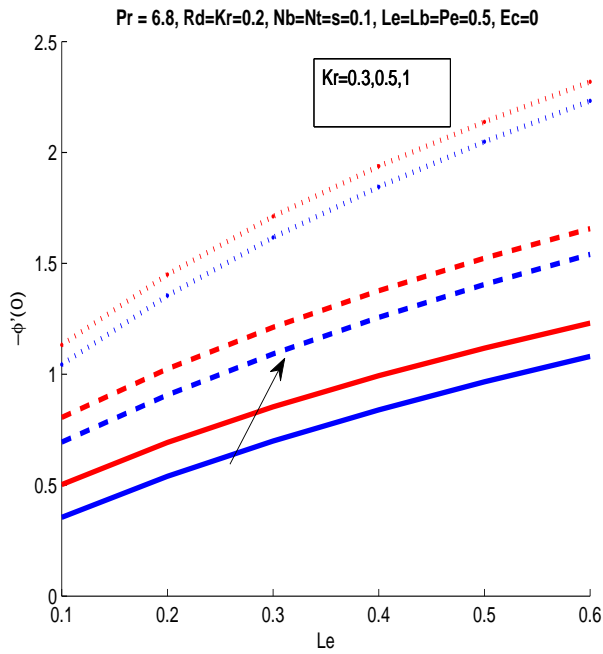


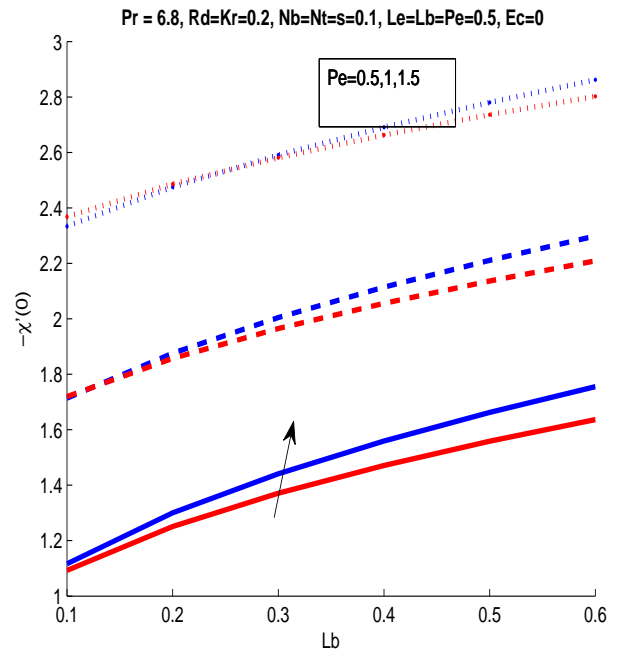Figure 6.20: The local Sherwood number with variations in $Kr$ and $Le$.



Figure 6.21: The density of motile microorganisms with variations in $Pe$ and $Lb$.

## 6.5   Conclusion

Current analysis focuses on the unsteady MHD stagnation point bio-nanofluid flow in a permeable medium with thermal radiation and chemical reaction into account over a stretching and shrinking sheet. The significant findings of the problem are summarized below:

- The skin friction coefficient enhances for higher values of unsteady parameter $A$, magnetic parameter $M$ and porosity parameter $Kp$.

- The increment in $Nb$, $Nt$, $Rd$, $Ec$, $s$ causes enhancement in thermal boundary layer thickness while higher values of $Pr$ causes reduction in thermal boundary layer thickness.

- The concentration boundary layer thickness increases for $Nt$ whereas it decreases for higher values of $Nb$, $Le$ and $Kr$.

- The increment of $Nb$, $Lb$ and $Pe$ reduces the density motile microorganisms while it increases for larger values of $Nt$.

- Different trends have been seen for boundary layer thickness through graphs. Graphs describe that boundary layer thickness is different in stretching sheet case when compared to shrinking sheet case.

# Chapter 7

# MHD Time Dependant Bio-Nanofluid Flow Past a Slippery Sheet While Considering Variable Thermo-Physical Properties

In this chapter, a theoretical model with a numerical solution is brought forward for a bio-nanofluid with varying fluid features over a slippery sheet. The PDEs involve temperature dependent quantities have been translated into ODEs by using dimensionless variables. It is followed by finding a numerical solution in adopting shooting method and *bvp4c*. To figure out the influence the graphs are plotted against various parameters for the velocity, temperature, concentration and microorganism curves. The boundary layer thickness of microorganism profile reduces with Schmidt number and Peclet number. In addition to adding radiative heat flux, we added heat generation, rate of chemical reaction, first order slip. By adding these parameters brought new aspects to the underlying profiles. Moreover, the obtained data of $cf_{x_1}$, $Nu_{x_1}$, $Sh_{x_1}$ and $Nn_{x_1}$ is tabulated against various parameters for the physical parameters. From the results, it is apparent that the $Nu_{x_1}$ decreases with enhancement in $Nb$ and $Nt$. The data obtained for physical parameters has a close agreement with the published one. Finally, the graphs for slip conditions are significantly different when the comparison is drawn with no-slip condition.

Chapter 7 is divided into following sections.

Section 7.1 gives the introduction of the chapter. In Section 7.2 problem formulation and governing equations of the problem is discussed. In Section 7.3 we presents the numerical procedure. Section 7.4 includes numerical results and graphs against pertinent parameters. In Section 7.5 we discuss the conclusion of the chapter.

## 7.1 Introduction

The thermal radiation with variable fluid properties is reported in [150]. They found that the skin friction coefficient increases with viscosity parameter. Anwar et al. [151] discussed MHD flow in a porous channel with generalized conditions. Fatumbi and Adeniyan [152] reported nonlinear thermal radiation in fluid flow with variable properties. Dandapat et al. [153] discussed thin film unsteady flow with variable fluid properties. Vajravelu and Prasad [154] discussed unsteady convective flow in a vertical surface with variable fluid properties. Shahsavar et al. [155] investigated the impact of variable fluid properties in hybrid nanofluid. Naganthran et al. [156] found results of stretching and shrinking sheet with variable fluid properties. They discussed dual solutions in this rotating disk. Salahuddin et al. [157] discussed variable fluid properties for viscoelastic fluid between two rotating plates. This study covers a variable thermophysical properties of bio-nanofluid with slip conditions taking into account. The viscosity of a fluid however, relies heavily on temperature than other on other factors. It comes out that the use of variable properties offers distinct effects on fluid flow motion.

## 7.2 Problem Development

The present theocratical model considers unsteady two-dimensional magnetohydrodynamic flow of an incompressible viscous nanofluid in the presence of a thermal radiation and internal heat generation/absorption over a stretching sheet with variable liquid characteristic. A water based nanofluid containing nanoparticles and grotactic microorganisms is considered. It is assumed that the presence of nanoparticles have no affect on the swimming direction of microorganisms and on their swimming velocity. This assumptions holds only for less than

1% concentration of nanoparticles. The applied magnetic field $\beta_o^2$ is taken along the normal to the surface. $U_w = ax_1(1 - A_1t_1)^{-1}$ is designated as stretching sheet velocity. In such cases, the model problem can be expressed asAmirson et al. [85]:

$$\frac{\partial u_1}{\partial x_1} + \frac{\partial v_1}{\partial y_1} = 0, \tag{7.1}$$

$$\frac{\partial u_1}{\partial t_1} + u_1\frac{\partial u_1}{\partial x_1} + v_1\frac{\partial u_1}{\partial y_1} = \frac{1}{\rho_\infty}\frac{\partial}{\partial y_1}\left(\mu_1(T_1)\frac{\partial u_1}{\partial y_1}\right) - \frac{\sigma\beta_o^2}{\rho_\infty}u_1 - \frac{\mu_1(T_1)}{\rho_\infty K^*}u_1, \tag{7.2}$$

$$\frac{\partial T_1}{\partial t_1} + u_1\frac{\partial T_1}{\partial x_1} + v_1\frac{\partial T_1}{\partial y_1} = \frac{1}{\rho_\infty c_p}\frac{\partial}{\partial y_1}\left(k_1(T_1)\frac{\partial T_1}{\partial y_1}\right) + \tau_1\left(D_B(c)\frac{\partial T_1}{\partial y_1}\frac{\partial C_1}{\partial y_1} + \frac{D_T}{T_\infty}\left(\frac{\partial T_1}{\partial y_1}\right)^2\right)$$

$$-\frac{1}{\rho_\infty c_p}\frac{\partial q_r}{\partial y_1} + \frac{\mu_1(T_1)}{\rho_\infty c_p}\left(\frac{\partial u_1}{\partial y_1}\right)^2 + \frac{(T_1 - T_\infty)Q}{\rho_\infty c_p} + \frac{\sigma B_o^2 u_1^2}{\rho_\infty c_p} + \frac{\mu_1(T_1)u_1^2}{c_p k^*}, \tag{7.3}$$

$$\frac{\partial C_1}{\partial t_1} + u_1\frac{\partial C_1}{\partial x_1} + v_1\frac{\partial C_1}{\partial y_1} = \frac{\partial}{\partial y_1}\left(D_B(C_1)\frac{\partial C_1}{\partial y_1}\right) + \frac{D_{T_1}}{T_\infty}\frac{\partial^2 T_1}{\partial y_1^2} - (C_1 - C_\infty)K_c, \tag{7.4}$$

$$\frac{\partial N_1}{\partial t_1} + u_1\frac{\partial N_1}{\partial x_1} + v_1\frac{\partial N_1}{\partial y_1} + \frac{b_1 w_c}{C_w - C_\infty}\left(\frac{\partial}{\partial y_1}\left(N_1\frac{\partial C_1}{\partial y_1}\right)\right) = \frac{\partial}{\partial y_1}\left(D_m(C_1)\frac{\partial N_1}{\partial y_1}\right). \tag{7.5}$$

The boundary conditions corresponding to considered model is taken as,

$$u_1 = U_w(x_1, t_1) + N^*\frac{\partial u_1}{\partial y_1}, \quad v_1 = 0, \quad T_1 = T_w(x_1, t_1) + D_1\frac{\partial T_1}{\partial y_1}, \quad C_1 = C_w, \quad N_1 = N_w, \quad \text{at } y_1 = 0,$$

$$u_1 \longrightarrow 0, \quad T_1 \longrightarrow T_\infty, \quad C_1 \longrightarrow C_\infty, \quad N_1 \longrightarrow N_\infty, \text{as} \quad y_1 \longrightarrow \infty. \tag{7.6}$$

The following dimensionless variables introduced to get the similarity solution of the governing equations

$$\eta = \sqrt{\frac{a}{\nu_1(1 - A_1t_1)}}y_1, \quad \psi = \sqrt{\frac{a\nu_1}{1 - A_1t_1}}x_1 f(\eta), \quad \theta(\eta) = \frac{T_1 - T_\infty}{T_w - T_\infty},$$

$$\phi(\eta) = \frac{C_1 - C_\infty}{C_w - C_\infty}, \quad \chi(\eta) = \frac{N_1}{N_w}. \tag{7.7}$$

By inserting Eq. (7.7) into Eqs. (7.1)-(7.5), we obtain the following modified ODEs:

$$\left(\frac{\mu(T)}{\mu_\infty}f''\right)' - f'^2 + ff'' - A\left(f' + \frac{\eta}{2}f''\right) - \left(M + Kp\left(\frac{\mu(T)}{\mu_\infty}\right)\right)f' = 0, \tag{7.8}$$

$$\left(\frac{k(T)}{k_\infty}\theta'\right)' + \frac{4}{3}Rd\theta'' + Nb\left(\frac{D_B(C)}{D_{B,\infty}}\right)\theta'\phi' + Nt\theta'^2 + Pr_\infty\left(f\theta' - \frac{\eta A}{2}\theta' + Ec\left(\frac{\mu(T)}{\mu_\infty}\right)f''^2\right.$$

$$\left. + MEcf'^2 + EcKp\left(\frac{\mu(T)}{\mu_\infty}\right)f'^2 + s\theta\right) = 0, \tag{7.9}$$

$$\left(\frac{D_B(C)}{D_{B,\infty}}\phi'\right)' + \frac{Nt}{Nb}\theta'' + Sc\left(f\phi' - \frac{A\eta}{2}\phi' - Kr\phi\right) = 0, \tag{7.10}$$

$$\left(\frac{D_m(C)}{D_{m,\infty}}\chi'\right)' + Sb\left(f\chi' - \frac{A\eta}{2}\chi'\right) - Pe(\phi'\chi' + \chi\phi'') = 0. \tag{7.11}$$

Using Eq. (7.7), the associated boundary conditions reduce as follows:

$$f(0) = 0, \quad f'(0) = 1 + \delta f''(0), \quad \theta(0) = 1 + \gamma\theta'(0), \quad \phi(0) = 1, \quad \chi(0) = 1,$$

$$f'(\infty) = 0, \quad \theta(\infty) = 0, \quad \phi(\infty) = 0, \quad \chi(\infty) = 0. \tag{7.12}$$

Amirsom et al. [107] expressed viscosity, thermal conductivity, nanoparticle and microorganisms diffusivities as a function of temperature with the following mathematical functions:

$$\mu_1(T_1) = \mu_\infty[1 + h_1(T_\infty - T_1)] = \mu_\infty(1 + h_2 - \theta(\eta)h_2),$$

$$k_1(T_1) = k_\infty[1 + h_3(T_\infty - T_1)] = k_\infty(1 + h_4\theta(\eta)),$$

$$D_B(C_1) = D_{B,\infty}[1 + h_5(C_1 - C_\infty)] = D_{B,\infty}(1 + h_6\phi(\eta)),$$

$$D_m(C_1) = D_{m,\infty}[1 + h_7(C_1 - C_\infty)] = D_{m,\infty}(1 + h_8\phi(\eta)). \tag{7.13}$$

Using above variable function defined in Eq. (7.13) in Eq. (7.8-7.11) we get

$$(1 + h_2 - h_2\theta)f''' - h_2\theta' f'' - f'^2 + ff'' - A(f' + \tfrac{\eta}{2}f'') -$$
$$(M + Kp(1 + h_2 - h_2\theta))f' = 0, \tag{7.14}$$

$$(1 + h_4\theta + \tfrac{4}{3}Rd)\theta'' + h_4\theta'^2 + Nb(1 + h_6\phi)\theta'\phi' + N_t\theta'^2 + Pr_\infty(f\theta' - \tfrac{A\eta}{2}\theta' + Ec(1 + h_2 - \theta h_2)f''^2$$
$$+MEcf'^2 + KpEc(1 + h_2 - h_2\theta)f'^2 + s\theta) = 0, \tag{7.15}$$

$$(1 + h_6\phi)\phi'' + h_6\phi'^2 + Sc(f\phi' - \tfrac{A\eta}{2}\phi' - Kr\phi) + \tfrac{Nt}{Nb}\theta'' = 0, \tag{7.16}$$

$$(1 + h_8\phi)\chi'' + h_8\phi'\chi' + Sb(f\chi' - \tfrac{A\eta}{2}\chi') - Pe(\phi'\chi' + \chi\phi'') = 0. \tag{7.17}$$

The parameters are defined by:

$A = \frac{A_1}{a}$, $Kp = \frac{\nu_\infty(1-A_1t_1)}{ak^*}$, $M = \frac{\sigma B_o^2(1-A_1t_1)}{\rho_\infty a}$, $Pr_\infty = \frac{\nu_\infty}{\alpha_\infty}$, $Rd = \frac{4\sigma T_\infty^3}{k_1 k_\infty}$, $Nb = \frac{\tau_1 D_{B,\infty}(C_w - C_\infty)}{\alpha_\infty}$,
$Nt = \frac{\tau_1 D_T(T_w - T_\infty)}{T_\infty \alpha}$, $Ec = \frac{u_w^2}{c_p(T_w - T_\infty)}$, $s = \frac{Q(1-A_1t_1)}{a}$, $Sc = \frac{\nu_\infty}{D_{B,\infty}}$, $K_r = K_c(1-A_1t_1)a$, $Sb = \frac{\nu_\infty}{D_{m,\infty}}$
$Pe = \frac{b_1 w_c}{D_{m,\infty}}$, $\delta = N_1(\frac{a}{\nu_\infty(1-A_1t)})^{\frac{1}{2}}$, $\gamma = D_1(\frac{a}{\nu_\infty(1-A_1t)})^{\frac{1}{2}}$.

Expressions for $C_{fx_1}$, $Nu_{x_1}$, $Sh_{x_1}$ and $Nn_{x_1}$ are,

$$C_{fx_1} = \frac{\mu_1(T_1)(\frac{\partial u_1}{\partial y_1})_{y_1=0}}{\rho_1 u_w^2}, \qquad Nu_{x_1} = \frac{-k_1(T_1)x(\frac{\partial T_1}{\partial y_1})_{y_1=0}}{k_1(T_1)(T_w - T_\infty)},$$

$$Sh_{x_1} = \frac{-D_{B,\infty}x_1(\frac{\partial C_1}{\partial y_1})_{y_1=0}}{D_{B,\infty}(C_w - C_\infty)}, \qquad Nn_{x_1} = \frac{-D_{m,\infty}x_1(\frac{\partial N_1}{\partial y_1})_{y_1=0}}{D_{m,\infty}N_w)}. \tag{7.18}$$

Inserting Eq. (7.7) into Eq. (7.18) yields the following expressions:

$$Re_{x_1}^{1/2}C_{fx_1} = -(1 + h_2\phi)f''(0), \qquad Re_{x_1}^{-1/2}Nu_{x_1} = -(1 + \frac{4}{3}Rd)\theta'(0),$$

$$Re_{x_1}^{-1/2}Sh_{x_1} = -\phi'(0), \qquad Re_{x_1}^{-1/2}Nn_{x_1} = -\chi'(0). \tag{7.19}$$

## 7.3 Numerical Process

### 7.3.1 Shooting Method

The transformed system of ODEs are solved numerically by employing shooting algorithm in MATLAB. To apply the shooting technique, we transformed the BVP into an IVP and reduce the higher order ODEs into a system of first order ODEs. We have applied Newton-Raphson method to locate the root. Finally, Runge-Kutta method of order five was implemented to determine the solution of IVP. The transformed system of first order ODEs are

$$f = v_1, f' = v_2, f'' = v_3, f''' = v_3' = \frac{1}{(1+h_2-y_4h_2)}(h_2v_5v_3 + v_2^2 - v_1v_3$$

$$A(v_2 + \frac{\eta}{2}v_3) + (M + Kp(1 + h_2 - h_2v_4)v_2),$$

$$v_4 = \theta, v_5 = \theta', \theta'' = v_5' = \frac{-1}{(1+h_4v_4+\frac{4}{3}Rd)}(h_4v_5^2 + Nb(1 + h_6v_6)v_5v_7 + Ntv_5^2$$

$$+Pr_\infty(v_1v_5 - \frac{\eta}{2}Av_5 + Ec(1 + h_2 - v_2v_4)v_3^2 + sv_4 + MEcv_2^2 + KpEc(1 + h_2 - h_2v_4)v_2^2)),$$

$$v_6 = \phi, v_7 = \phi', \phi'' = v_7' = \frac{-1}{(1+h_6v_6)}(\frac{N_t}{N_b}v_5' + h_6v_7^2 + Scv_1v_7 + \frac{Sc\eta A}{2}v_7 - ScKrv_6),$$

$$v_8 = \chi, v_9 = \chi', \chi'' = v_9' = \frac{-1}{(1+h_8v_6)}(h_8v_7v_9 - Sb(\frac{\eta A}{2}v_9 - v_1v_9) - Pe(v_7v_9 + v_8v_7')).$$

The results produced from the shooting method has been verified with the MATLAB built-in function *bvp4c*. The *bvp4c* is a collocation solved which computes solution of the boundary value problem. For details on *bvp4c* the reader is referred to [105].

## 7.4 Results and Discussion

Comparison of $-f''(0)$ is presented in Tables 1 and 2 with available literature. The obtained results shows good agreement.

The data in Table 3 shows computational results for the $Nu_{x_1}$, $Sh_{x_1}$ and $Nn_{x_1}$ obtained with the *bvp4c*. The local Nusselt number $Nu_{x_1}$ reduced against $Nb$, $Nt$, $Ec$, $s$ and $h_4$. The local Nusselt number enhances for the increasing values of $Pr_\infty$ and $Rd$. The local Sherwood number $Sh_{x_1}$ increases for higher values of $Nb$, $Nt$, $Sc$ and $Kr$. The local Sherwood number

Table 7.1: Comparison of surface resistance coefficient $-f''(0)$ for $M$ when $Pr_\infty = 1$ and $Kp = \delta = \gamma = h_2 = h_4 = h_6 = h_8 = 0$.

| $M$ | Hayat et al. [108] | Mabood and Mastroberardino [109] | Amirsom et al. [107] | shooting method | bvp4c |
|---|---|---|---|---|---|
| 0 | 1.0000 | 1.000008 | 1.0000002 | 1.0000 | 1.0001 |
| 1 | 1.41421 | 1.4142135 | 1.41422211 | 1.4142 | 1.4142 |
| 5 | 2.44948 | 2.4494897 | 2.4494901 | 2.4495 | 2.4495 |
| 10 | 3.31662 | 3.3166247 | 3.3166229 | 3.3166 | 3.3166 |
| 50 | 7.14142 | 7.1414284 | 7.1414279 | 7.1414 | 7.1414 |
| 100 | 10.04987 | 10.049875 | 10.049868 | 10.0499 | 10.0499 |
| 500 | 22.38302 | 22.383029 | 22.383031 | 22.3830 | 22.3830 |
| 1000 | 31.63858 | 31.638584 | 31.638578 | 31.6386 | 31.6386 |

decreases for higher values of mass diffusivity parameter $h_6$. For $Nn_{x_1}$ shows decreasing trend for higher values of mass diffusivity parameter $h_6$ and microorganisms diffusivity parameter $h_8$. While it is increasing for increasing values $Sb$ and $Pe$.

Figs. 7.1 and 7.2 displays the impacts of $M$ and $Kp$ on velocity profile with and without hydrodynamic slip. The boundary layer thickness reduces with an increasing values of $M$ and $Kp$.

Fig. 7.3 portrays the influences of $Pr_\infty$ on the temperature profile. It is noted that an enhancement in Prandtl number causes reduction in temperature distribution. The smaller values of $Pr_\infty$ corresponds to increase in thermal conductivities which causes reduction in a thermal boundary layer.

Fig. 7.4 depicts the influence of $Rd$ on the temperature profile. It is seen that an increment in $Rd$ elevates the temperature distribution.

Fig. 7.5 reports the impacts of $Ec$ on temperature distribution. It is evaluated that higher values of $Ec$ elevates the temperature of the fluid. For increasing values of $Ec$ kinetic energy enhances, which causes an increase in fluid temperature.

Table 7.2: Comparison of $-f''(0)$ for $\delta$ when $Pr_\infty = 1$ and $Kp = M = \gamma = h_2 = h_4 = h_6 = h_8 = 0$
.

| $\delta$ | Andersson [110] | Hamad et al. [111] | Amirsom et al. [107] | shooting method | bvp4c |
|------|------|------|------|------|------|
| 0 | 1.0000 | 1.00000000 | 1.00000000 | 1.0000 | 1.0001 |
| 0.1 | 0.8721 | 0.87208247 | 0.87204247 | 0.8721 | 0.8722 |
| 0.2 | 0.7764 | 0.77637707 | 0.77593307 | 0.7764 | 0.7765 |
| 0.5 | 0.5912 | 0.59119548 | 0.59119589 | 0.5912 | 0.5913 |
| 1.0 | 0.4302 | 0.43015970 | 0.43016000 | 0.4302 | 0.4303 |
| 2.0 | 0.2840 | 0.28397959 | 0.28398932 | 0.2840 | 0.2841 |
| 5.0 | 0.1448 | 0.14484019 | 0.14464015 | 0.1448 | 0.1449 |
| 10.0 | 0.0812 | 0.08124198 | 0.08124091 | 0.0812 | 0.0813 |
| 20.0 | 0.0438 | 0.04378834 | 0.04378790 | 0.0438 | 0.0439 |
| 50.0 | 0.0186 | 0.01859623 | 0.01857868 | 0.0186 | 0.0186 |
| 100.0 | 0.0095 | 0.00954997 | 0.00954677 | 0.0095 | 0.0096 |

Fig. 7.6 illustrates the impact of $s$ on the temperature distribution. It is observed that temperature of the fluid increase with an increment in heat generation parameter.

Fig. 7.7 examines the effect of temperature dependent thermal conductivity parameter $h_4$ on temperature profile. It is noted that the thickness thermal boundary layer rises by raising $h_4$.

Figs. 7.8 and 7.9 are plotted to perceive the consequences of $Nb$ on the temperature and concentration profiles. It is revealed that by increasing $Nb$ thermal boundary layer thickness rises while concentration boundary layer thickness decline.

Figs. 7.10 and 7.11 conveys the impacts of $Nt$ on temperature and nanoparticles volume fraction profiles. It is observed temperature and concentration profile grow up for escalating values of $Nt$.

Fig 7.12 portray the influence of $Kr$ on concentration profile. It is examined that rising

Table 7.3: Numerical values of $N_ux$, $S_hx$ and $N_nx$ for several values of involved parameter $Pr_\infty$, $Rd$, $Nb$, $Nt$, $Ec$, $s$, $Sc$, $Kr$, $Sb$, $Pe$, $h_2$, $h_4$, $h_6$, $h_8$ with $A = 0.1$, $M = 0.5$, $Kp = 0.2$, $\delta = 0$ and $\gamma = 1$ (bvp4c).

| | | | | | | | | | | | | | | bvp4c | bvp4c | bvp4c |
|---|---|---|---|---|---|---|---|---|---|---|---|---|---|---|---|---|
| $Pr_\infty$ | $Rd$ | $s$ | $Ec$ | $Nb$ | $Nt$ | $Sc$ | $Kr$ | $Sb$ | $Pe$ | $h_2$ | $h_4$ | $h_6$ | $h_8$ | $-(1+\frac{4}{3}Rd)\theta'(0)$ | $-\phi'(0)$ | $-\chi'(0)$ |
| 4 | 0.5 | 0.1 | 0.1 | 0.1 | 0.2 | 5 | 0.2 | 2 | 1 | 0.1 | 0.1 | 0.1 | 0.1 | 0.4578 | 1.6306 | 2.0202 |
| 5 | | | | | | | | | | | | | | 0.5132 | 1.6123 | 2.0097 |
| 6.8 | | | | | | | | | | | | | | 0.5745 | 1.5948 | 2.0020 |
| 6.8 | 1 | 0.1 | 0.1 | 0.1 | 0.2 | 5 | 0.2 | 2 | 1 | 0.1 | 0.1 | 0.1 | 0.1 | 0.7276 | 1.6018 | 2.0002 |
| | 1.5 | | | | | | | | | | | | | 0.8362 | 1.6165 | 2.0072 |
| | 2 | | | | | | | | | | | | | 0.9054 | 1.6330 | 2.0171 |
| 6.8 | 0.5 | 0 | 0.1 | 0.1 | 0.2 | 5 | 0.2 | 2 | 1 | 0.1 | 0.1 | 0.1 | 0.1 | 0.6771 | 1.4737 | 1.8969 |
| | | 0.1 | | | | | | | | | | | | 0.5745 | 1.5947 | 2.0020 |
| | | 0.2 | | | | | | | | | | | | 0.4183 | 1.7713 | 2.1544 |
| 6.8 | 0.5 | 0.1 | 0.1 | 0.1 | 0.2 | 5 | 0.2 | 2 | 1 | 0.1 | 0.1 | 0.1 | 0.1 | 0.5745 | 1.5947 | 2.0020 |
| | | | 0.15 | | | | | | | | | | | 0.4468 | 1.7580 | 2.1461 |
| | | | 0.2 | | | | | | | | | | | 0.3198 | 1.9198 | 2.2889 |
| 6.8 | 0.5 | 0.1 | 0.1 | 0.5 | 0.2 | 5 | 0.2 | 2 | 1 | 0.1 | 0.1 | 0.1 | 0.1 | 0.4974 | 1.6452 | 2.0171 |
| | | | | 1 | | | | | | | | | | 0.4000 | 1.6505 | 2.0179 |
| | | | | 1.5 | | | | | | | | | | 0.3040 | 1.6514 | 2.0170 |
| 6.8 | 0.5 | 0.1 | 0.1 | 0.1 | 1 | 5 | 0.2 | 2 | 1 | 0.1 | 0.1 | 0.1 | 0.1 | 0.5080 | 1.7646 | 2.3215 |
| | | | | | 1.5 | | | | | | | | | 0.4626 | 2.1563 | 2.7886 |
| | | | | | 2 | | | | | | | | | 0.4141 | 2.7811 | 3.4623 |
| 6.8 | 0.5 | 0.1 | 0.1 | 0.1 | 0.2 | 3 | 0.2 | 2 | 1 | 0.1 | 0.1 | 0.1 | 0.1 | 0.5780 | 1.1072 | 1.6118 |
| | | | | | | 5 | | | | | | | | 0.5745 | 1.5947 | 2.0020 |
| | | | | | | 10 | | | | | | | | 0.5712 | 2.4438 | 2.7096 |
| 6.8 | 0.5 | 0.1 | 0.1 | 0.1 | 0.2 | 5 | 0 | 2 | 1 | 0.1 | 0.1 | 0.1 | 0.1 | 0.5763 | 1.1491 | 1.6338 |
| | | | | | | | 0.5 | | | | | | | 0.5729 | 2.0765 | 2.4069 |
| | | | | | | | 1 | | | | | | | 0.5716 | 2.6584 | 2.9040 |
| 6.8 | 0.5 | 0.1 | 0.1 | 0.1 | 0.2 | 5 | 0.2 | 0.5 | 1 | 0.1 | 0.1 | 0.1 | 0.1 | 0.5745 | 1.5947 | 1.6129 |
| | | | | | | | | 1 | | | | | | 0.5745 | 1.5947 | 1.7596 |
| | | | | | | | | 3 | | | | | | 0.5745 | 1.5947 | 2.2000 |
| 6.8 | 0.5 | 0.1 | 0.1 | 0.1 | 0.2 | 5 | 0.2 | 2 | 0.5 | 0.1 | 0.1 | 0.1 | 0.1 | 0.5745 | 1.5947 | 1.3577 |
| | | | | | | | | | 1 | | | | | 0.5745 | 1.5947 | 2.0020 |
| | | | | | | | | | 3 | | | | | 0.5745 | 1.5947 | 4.6914 |
| 6.8 | 0.5 | 0.1 | 0.1 | 0.1 | 0.2 | 5 | 0.2 | 2 | 1 | 0.1 | 0.1 | 0.1 | 0.1 | 0.5745 | 1.5947 | 2.0020 |
| | | | | | | | | | | 0.5 | | | | 0.5573 | 1.6336 | 2.0454 |
| | | | | | | | | | | 0.9 | | | | 0.5386 | 1.6690 | 2.0830 |
| 6.8 | 0.5 | 0.1 | 0.1 | 0.1 | 0.2 | 5 | | 2 | 1 | 0.1 | 0.1 | 0.1 | 0.1 | 0.5745 | 1.5947 | 2.0020 |
| | | | | | | | | | | | 0.5 | | | 0.5493 | 1.6101 | 2.0127 |
| | | | | | | | | | | | 0.9 | | | 0.5258 | 1.6229 | 2.0213 |
| 6.8 | 0.5 | 0.1 | 0.1 | 0.1 | 0.2 | 5 | 0.2 | 2 | 1 | 0.1 | 0.1 | 0.1 | 0.1 | 0.5745 | 1.5947 | 2.0020 |
| | | | | | | | | | | | | 0.5 | | 0.5715 | 1.2788 | 1.7325 |
| | | | | | | | | | | | | 0.9 | | 0.5686 | 1.0845 | 1.5698 |
| 6.8 | 0.5 | 0.1 | 0.1 | 0.1 | 0.2 | 5 | 0.2 | 2 | 1 | 0.1 | 0.1 | 0.1 | 0.1 | 0.5745 | 1.5947 | 2.0020 |
| | | | | | | | | | | | | | 0.5 | 0.5745 | 1.5947 | 1.5143 |
| | | | | | | | | | | | | | 0.9 | 0.5745 | 1.5947 | 1.2232 |

values of $Kr$ results in decline of the concentration boundary layer.

Fig. 7.13 depicts the effects of $Sc$ on concentration distribution. We analyze that rise in $Sc$ causes reduction in concentration profile. As higher the Schmidt number means lower the mass diffusivity which is the reason of reduction in concentration boundary layer thickness.

Fig. 7.14 presents the influence of mass diffusivity parameter $h_6$ on concentration profile. We observed that rise in mass diffusivity parameter $h_6$ results an increase in concentration profile.

Fig. 7.15 describes the influence of $Pe$ on microorganisms profile. It is noticed that incremental values of $Pe$ causes reduction in motile microorganisms boundary layer thickness.

Fig. 7.16 investigates the effect of $Sb$ on the motile microorganisms profile. It is shown that rising values of $Sb$ lowers the boundary layer thickness of motile microorganisms profile.

Figs. 7.17 and 7.18 are drawn to perceive the effect of mass diffusivity parameter $h_6$ and microorganisms diffusivity parameter $h_8$. It is noted that increasing values of mass diffusivity parameter and microorganisms diffusivity parameter elevates the boundary layer thickness of motile microorganisms profile.

Influence of $Kp$ and $M$ on skin friction coefficient is illustrated in Fig. 7.19. It is noted that skin friction coefficient shows intensification for improving values of $Kp$.

Fig. 7.20 is drawn to see effects of $s$ and $Pr_o$. on local Nusselt number. It is noticed that local Nusselt number shows decrement for incremental values of $s$.

Fig. 7.21 illustrates the influence of $Sc$ and $Kr$ on local Sherwood number. It is analyzed that an increment in $Sc$ causes enhancement in local Sherwood number.

In Fig. 7.22, we presents the effects of $Sb$ and $Pe$ on density of motile microorganisms. It is observed that density of motile microorganisms increases by raising $Sb$.
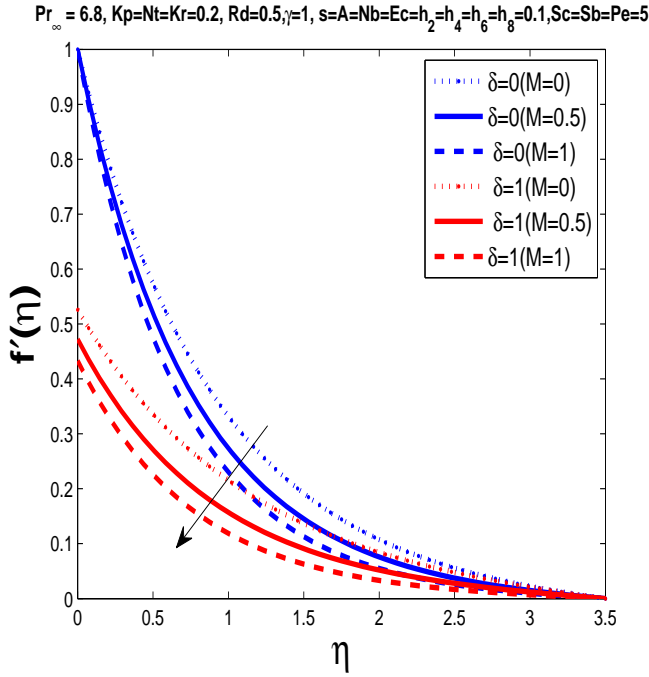


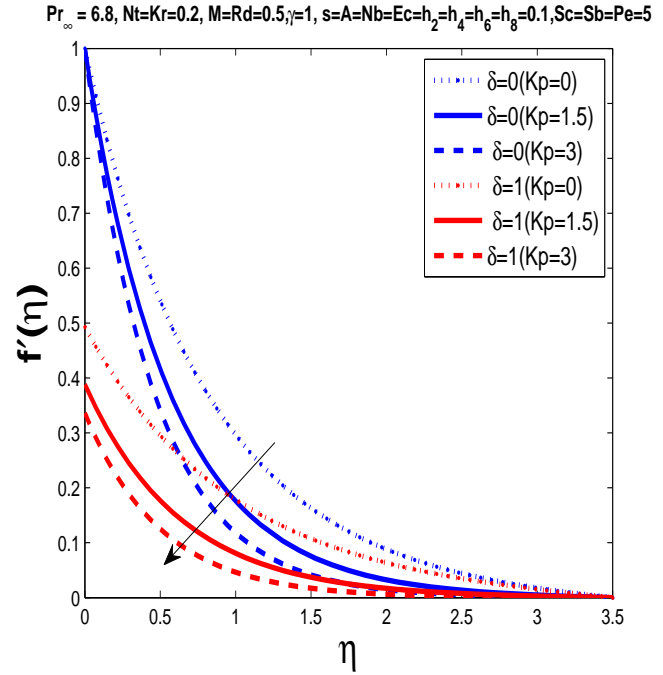Figure 7.1: Velocity profile $f'(\eta)$ for different $M$.



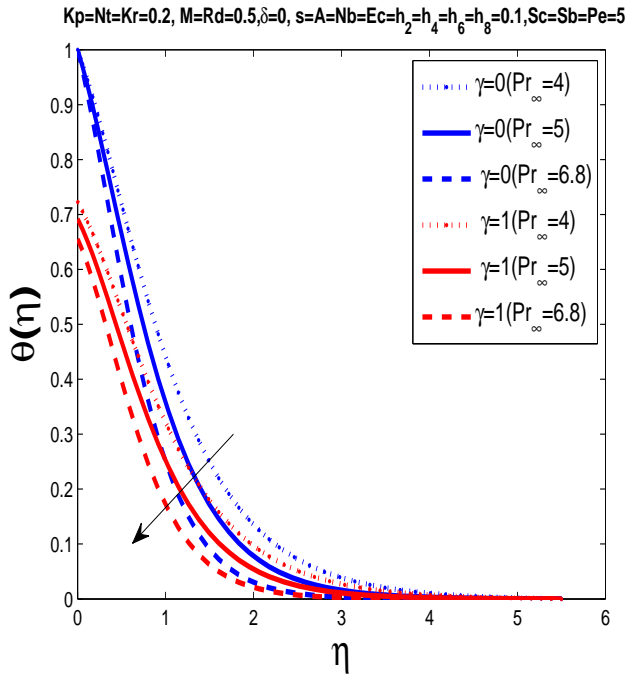Figure 7.2: Velocity profile $f'(\eta)$ for different $Kp$.



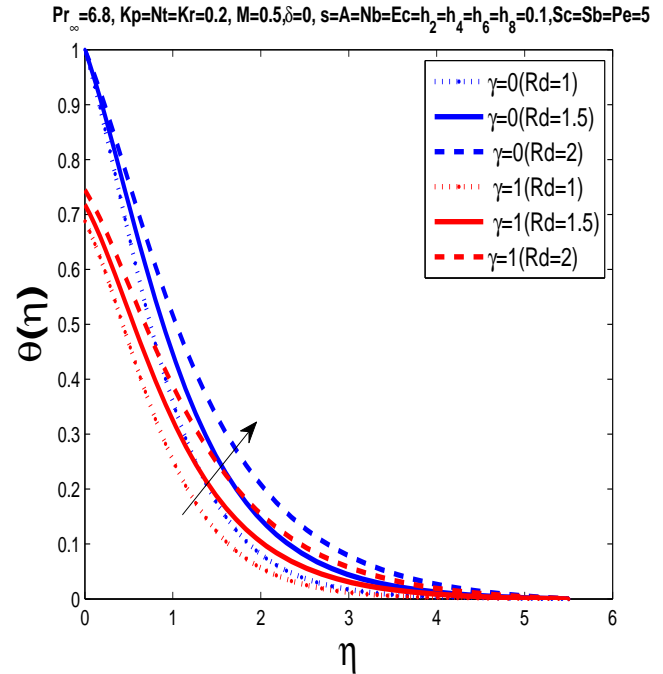Figure 7.3: Temperature profile $\theta(\eta)$ for different $Pr_\infty$.



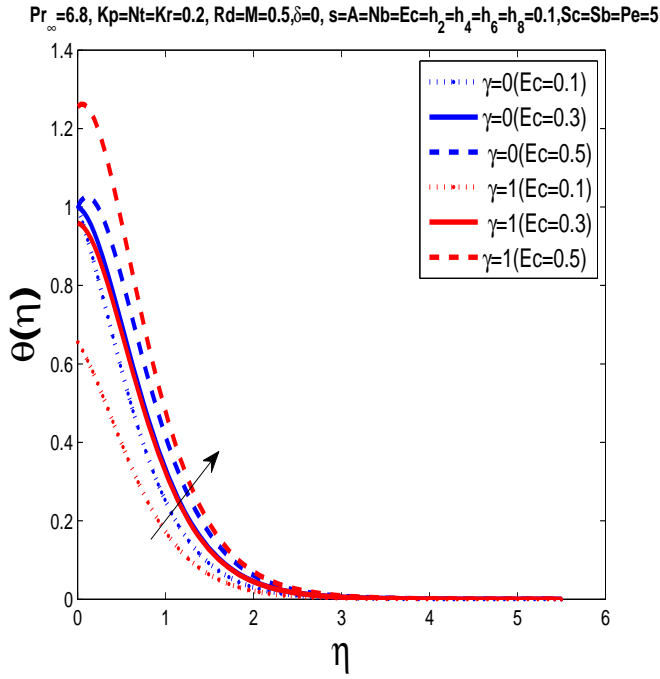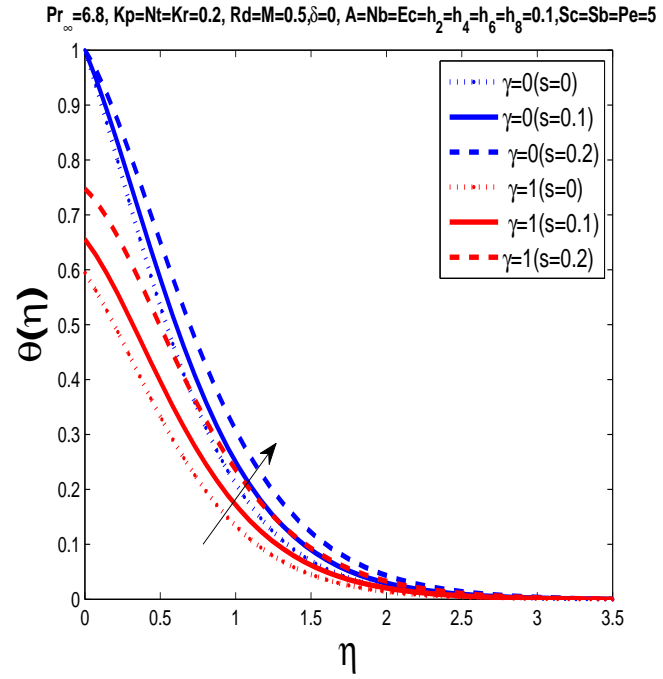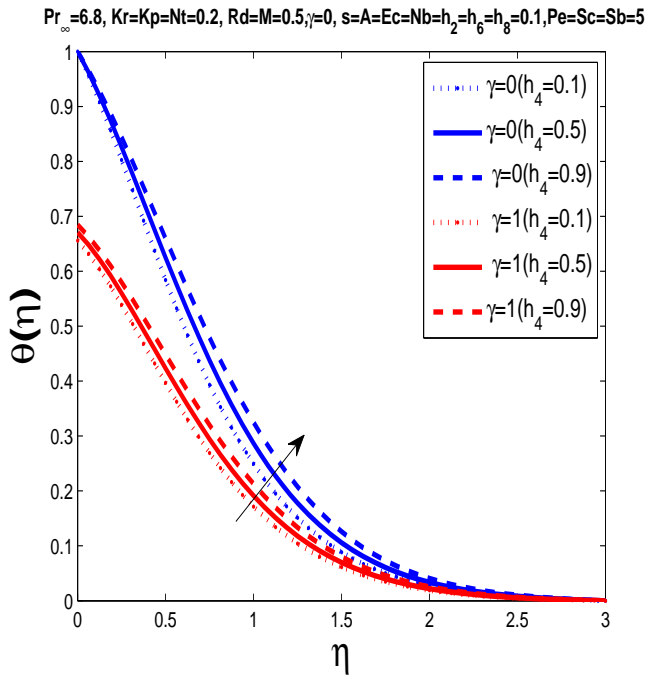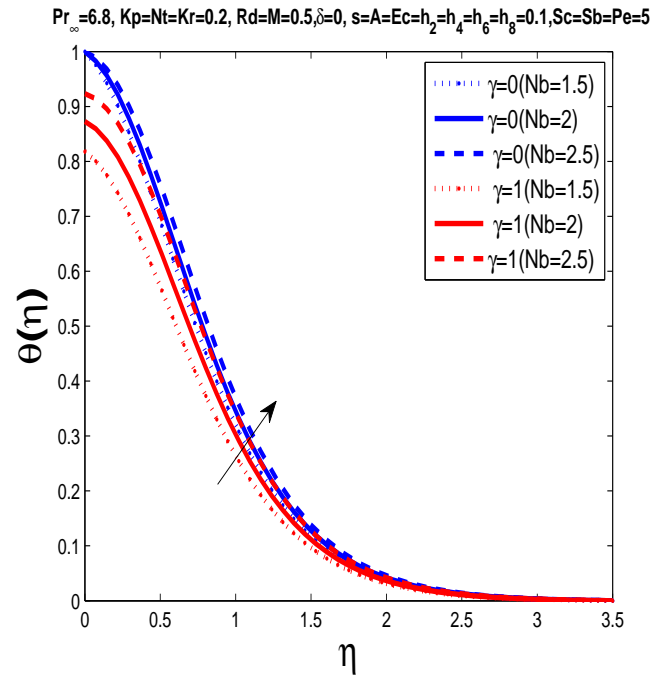Figure 7.4: Temperature profile $\theta(\eta)$ for different $Rd$.

$Pr_\infty=6.8$, Kp=Nt=Kr=0.2, Rd=M=0.5,$\delta$=0, s=A=Nb=Ec=$h_2$=$h_4$=$h_6$=$h_8$=0.1,Sc=Sb=Pe=5

Figure 7.5: Temperature profile $\theta(\eta)$ for different $Ec$.

Figure 7.6: Temperature profile $\theta(\eta)$ for different $s$.

Figure 7.7: Temperature profile $\theta(\eta)$ for different $h_4$.

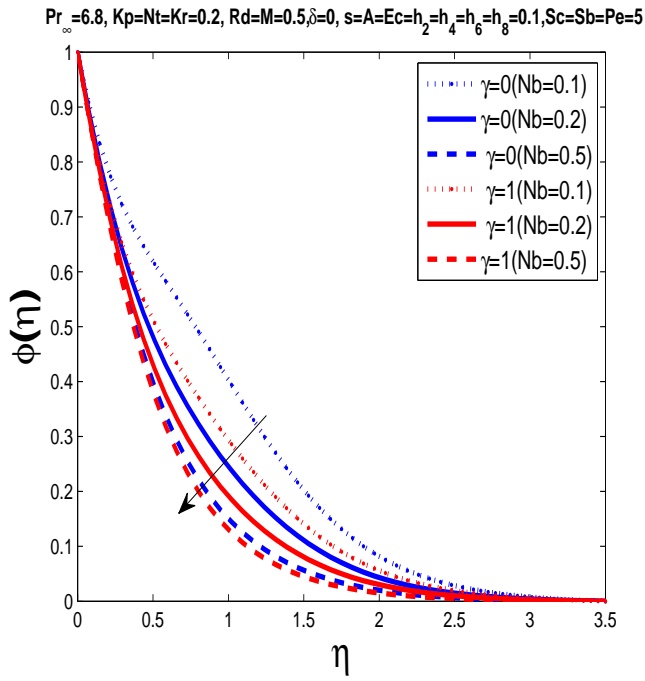Figure 7.8: Temperature profile $\theta(\eta)$ for different $Nb$.

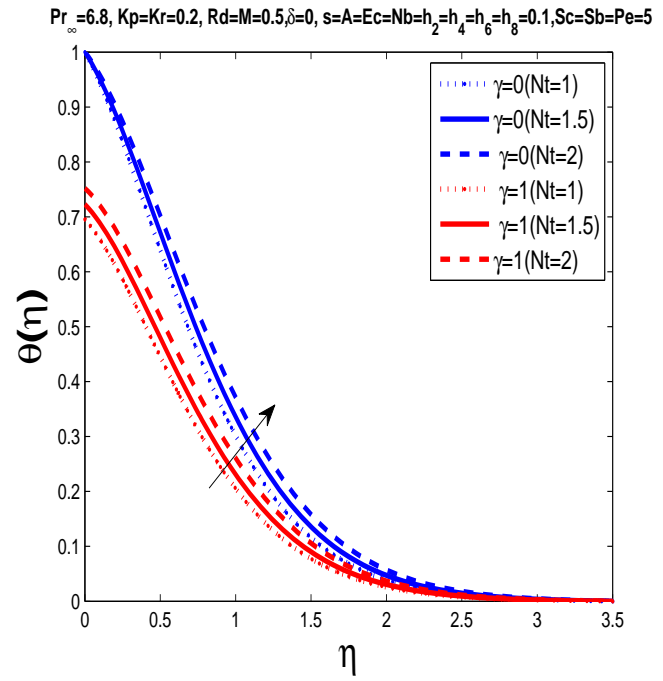Figure 7.9: Concentration profile $\phi(\eta)$ for different $Nb$.



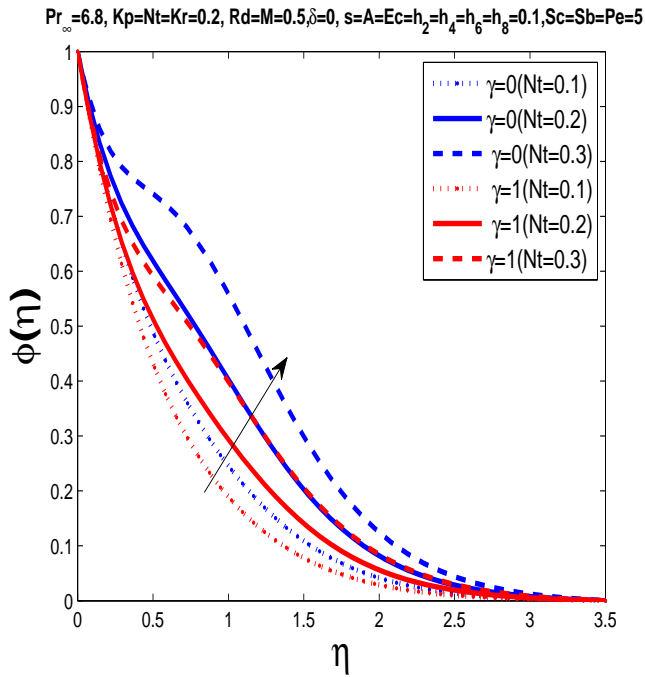Figure 7.10: Temperature profile $\theta(\eta)$ for different $Nt$.



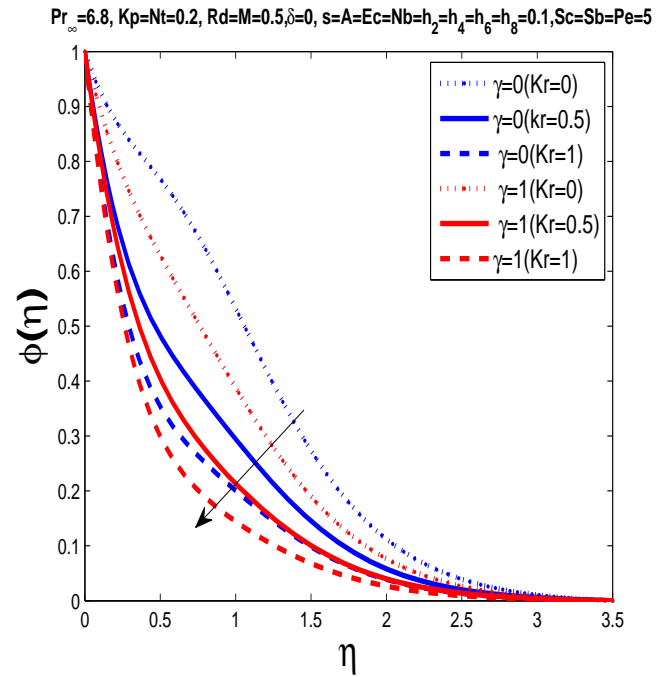Figure 7.11: Concentration profile $\phi(\eta)$ for different $Nt$.



Figure 7.12: Concentration profile $\phi(\eta)$ for different $Kr$.
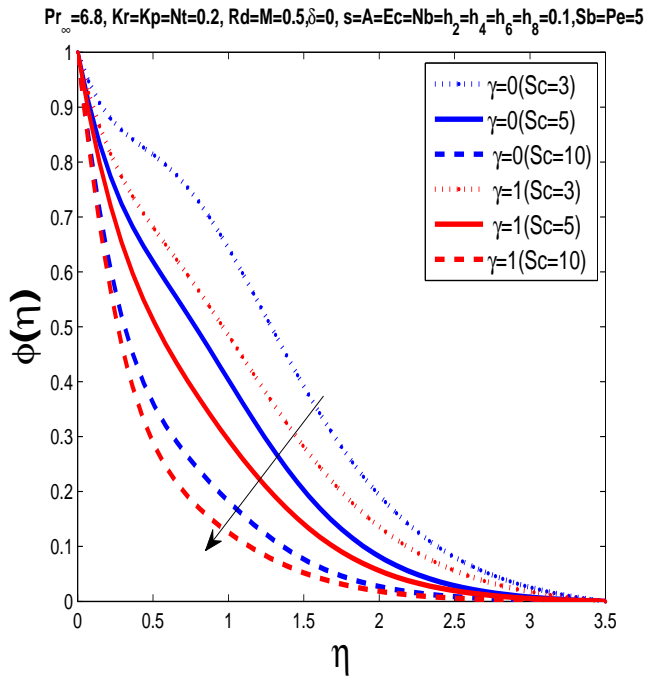
140

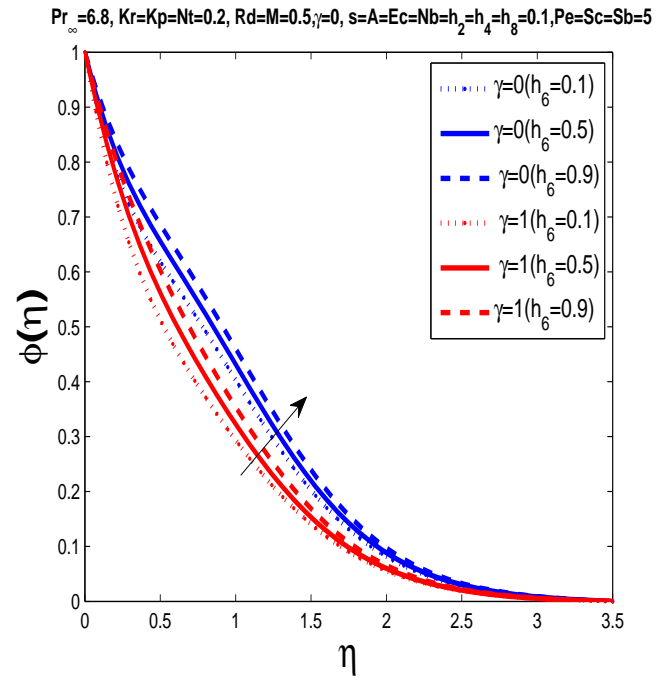Figure 7.13: Concentration profile $\phi(\eta)$ for different $Sc$.



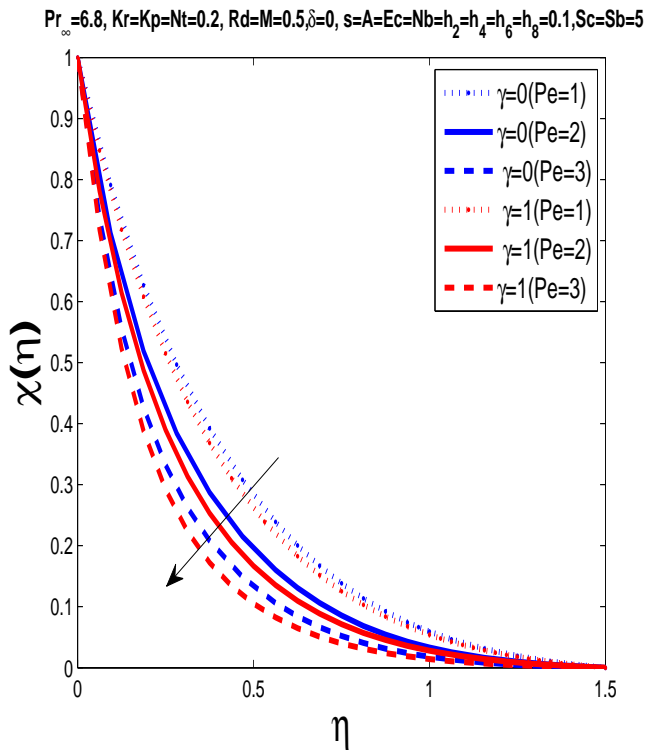Figure 7.14: Concentration profile $\phi(\eta)$ for different $h_6$.



Figure 7.15: Microorganisms profile $\phi(\eta)$ for different $Pe$.
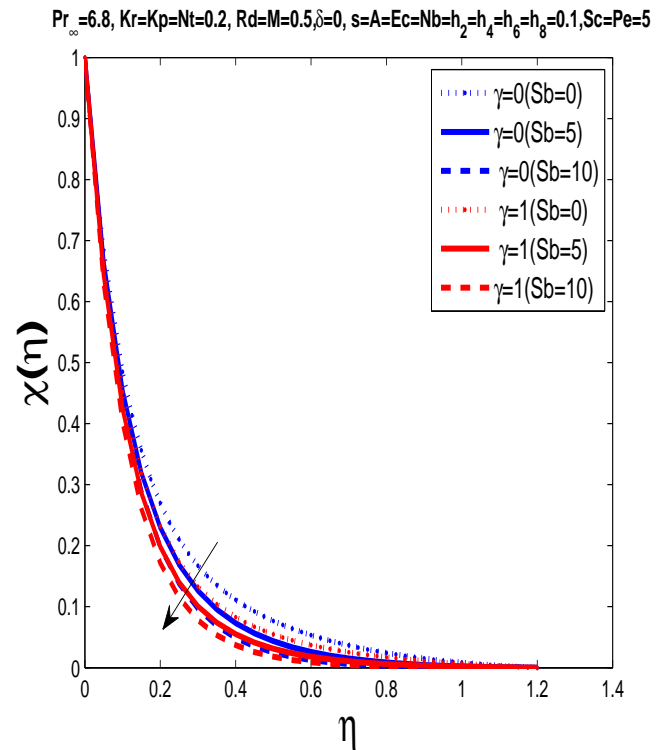


Figure 7.16: Microorganisms profile $\phi(\eta)$ for different $Sb$.
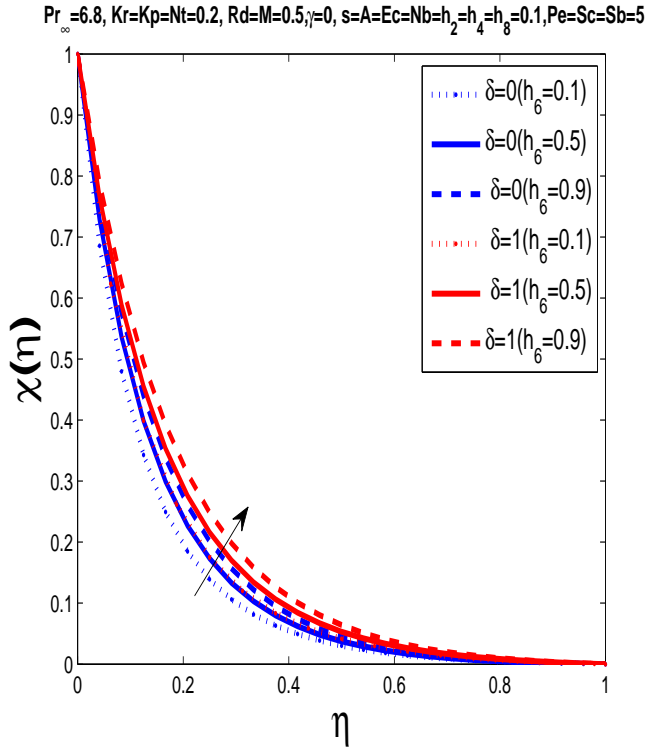
Figure 7.17: Microorganisms profile $\phi(\eta)$ for different $h_6$.
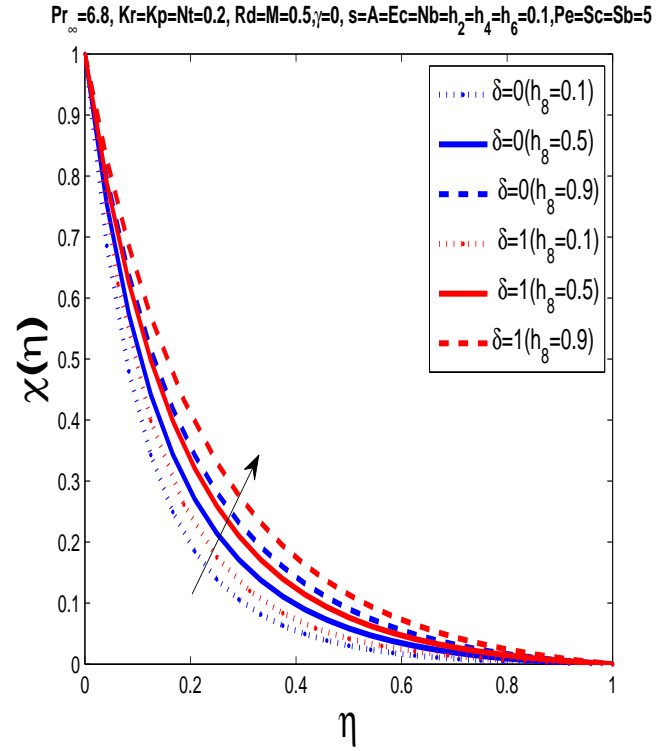


Figure 7.18: Microorganisms profile $\phi(\eta)$ for different $h_8$.
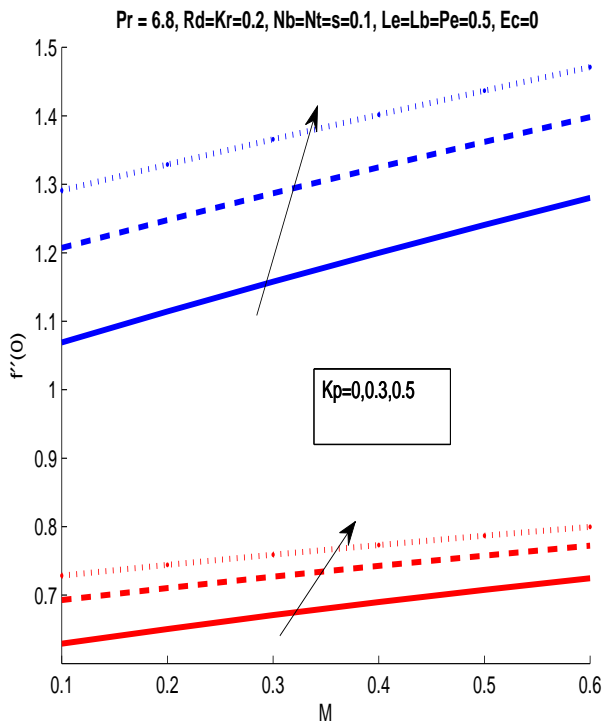


Figure 7.19: The skin friction coefficient with variations in $Kp$ and $M$.
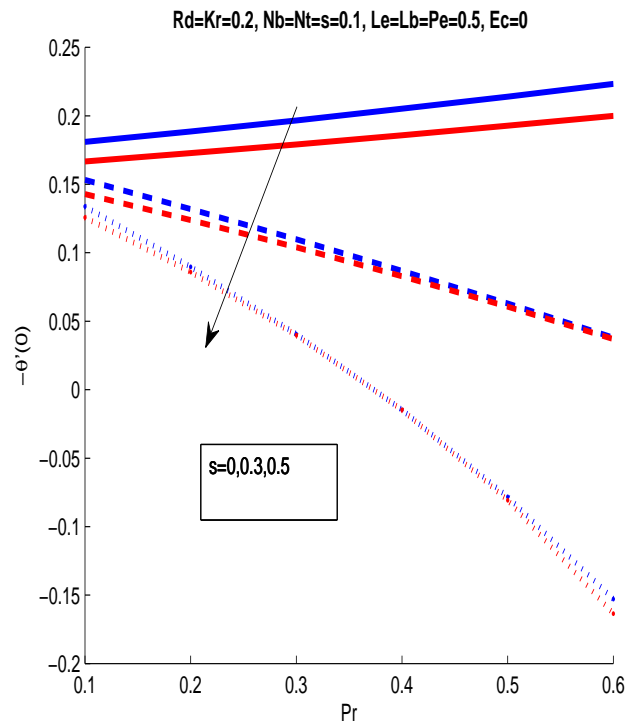


Figure 7.20: The local Nusselt number with variations in $s$ and $Pr$.
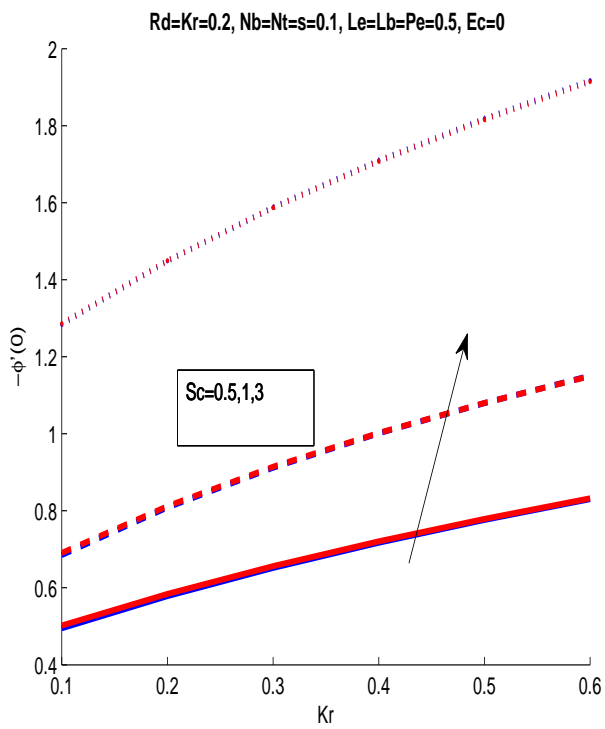
Figure 7.21: The local Sherwood number with variation in $Sc$ and $Le$.
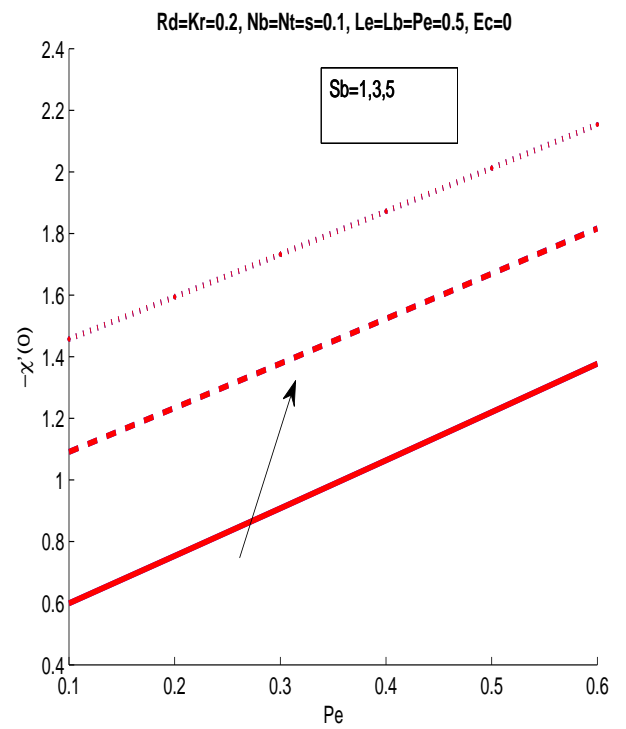


Figure 7.22: The density of motile microorganisms with variations in $Sb$ and $Pe$.

## 7.5  Conclusion

The focus of the chapter involves MHD unsteady flow of bio-nanofluid in a permeable medium with chemical reaction over a stretching surface with changeable thermo-physical properties. The notable findings of the problem are outlined below:

- The incremental values of $Nb$, $Nt$, $Rd$, $Ec$, $s$ magnify the thermal boundary layer thickness while rise in $Pr_\infty$ causes reduction in thermal boundary layer thickness.

- The concentration boundary layer thickness rises for $Nt$ and $h_6$ whereas it declines for higher values of the $Nb$, $Sc$ and $Kr$.

- The increment in $Sb$ and $Pe$ reduces the boundary layer thickness of motile microorganisms while motile microorganisms boundary layer shows inverse behavior for mass diffusivity parameter $h_6$ and microorganisms parameter $h_8$.

- Graph have been drawn with and without slip conditions. Difference can clearly be seen through graphs as the boundary layer thickness of slip condition is different when compare without slip flow case.

# Chapter 8

# Conclusions and Outlook

This chapter covers an overview of the study as well as suggestions for the future research. The research considered in this dissertation is focused on the numerical solution for MHD flow of nanofluid and bio-nanofluid over a stretching sheets with variable fluid properties.

Chapter 1 comprises the literature review and some basic definitions. In chapter 2, the governing equations for MHD boundary layer flow of nanofluid is presented first. We have solved the reduced ODEs by Shooting method. We found that momentum boundary layer reduces for incremental values of $M$ and $\theta_r$ while thermal boundary layer increases for higher values of $\epsilon$, $Nb$ and $Nt$.

Chapter 3 describes the MHD thermophoretic flow with variable fluid properties. In this chapter we established a comparison between constant and variable fluid properties. We reported that thermal boundary layer climbs up for rising values of $Rd$, $s$ and $\epsilon$ whereas momentum boundary layer thickness lowers down for higher values of $Kp$.

Chapter 4 explains the EMHD flow of nanofluid over a variable thickness stretching sheet considering changeable liquid properties. We applied the new numerical scheme, simplified finite difference method to solve the problem and made comparison of the established results with the *bvp4c* solver. We made comparison of constant and variable fluid properties in our study. We reports that momentum boundary layer grows higher for rising values of $E_1$ whereas

it decreases by raising $\theta_r$ and $Kp$.

In chapter 5, EMHD flow of powell-eyring flow of nanofluid with changeable liquid characteristics is considered. We apply simplified finite difference scheme and *bvp4c* method to solve the considered problem. We noted that skin friction coefficient is higher for constant fluid properties when compared with the variable fluid properties.

Chapter 6 explains the unsteady flow of bio-nanofluid over a stretching/ shrinking sheet. We solved the considered problem by Shooting method and compared the results with *bvp4c* method. We noticed that the skin friction coefficient intensifies for rising values of $A$, $Kp$ and $M$. Whereas increasing $Nb$, $Nt$ and $s$ results decrement in thermal boundary layer.

Chapter 7 describes the time dependent flow of bio-nanofluid over a stretching sheet with changeable thermo-physical properties. We found in our study that, the concentration boundary layer climbs up for $Nt$ and $h_6$ whereas it declines for incremental values of $Nb$, $Sc$ and $Kr$.

The work on incompressible flows can be further extended for compressible flows over a stretching sheet. We have only considered Buongiorno [96] model nanofluid flow but same work can be extended for others nanofluid flow as well. Moreover, the Keller-Box method can be developed to solve the boundary layer flows of incompressible and compressible flows. In future one can also use other numerical open source software chebfun.

## 8.1   Bibliography

# Bibliography

[1] Crane, Lawrence J. "Flow past a stretching plate." Zeitschrift für angewandte Mathematik und Physik ZAMP 21, no. 4 (1970): 645-647.

[2] Magyari, E., and B. Keller. "Heat and mass transfer in the boundary layers on an exponentially stretching continuous surface." Journal of Physics D: Applied Physics 32, no. 5 (1999): 577.

[3] Elbashbeshy, E. M. A. "Heat transfer over an exponentially stretching continuous surface with suction." Archives of Mechanics 53, no. 6 (2001): 643-651.

[4] Rajendar, Punnam, L. Anand Babu, and T. Vijaya Laxmi. "MHD Stagnation Point Flow and Heat Transfer Due to Nanofluid over Exponential Radiating Stretching Sheet." Global Journal of Pure and Applied Mathematics 13, no. 6 (2017): 1593-1610.

[5] Bachok, Norfifah, Anuar Ishak, and Ioan Pop. "Boundary layer flow and heat transfer with variable fluid properties on a moving flat plate in a parallel free stream." Journal of Applied Mathematics 2012 (2012).

[6] Hayat, T., M. Ijaz Khan, M. Waqas, A. Alsaedi, and T. Yasmeen. "Diffusion of chemically reactive species in third grade fluid flow over an exponentially stretching sheet considering magnetic field effects." Chinese Journal of Chemical Engineering 25, no. 3 (2017): 257-263.

[7] Pramanik, S. "Casson fluid flow and heat transfer past an exponentially porous stretching surface in presence of thermal radiation." Ain Shams Engineering Journal 5, no. 1 (2014): 205-212.

[8] Khan, Umar, Naveed Ahmed, Sheikh Irfan Ullah Khan, and Syed Tauseef Mohyud-din. "Thermo-diffusion effects on MHD stagnation point flow towards a stretching sheet in a nanofluid." Propulsion and Power Research 3, no. 3 (2014): 151-158.

[9] Isa, Siti Suzilliana Putri Mohamed, Norihan Md Arifin, and Umer Farooq. "The impact of slip conditions on magnetohydrodynamics radiating fluid beyond an exponentially extended sheet." In Journal of Physics: Conference Series, vol. 1039, no. 1, p. 012015. IOP Publishing, 2018.

[10] Mabood, F., S. M. Ibrahim, M. M. Rashidi, M. S. Shadloo, and Giulio Lorenzini. "Non-uniform heat source/sink and Soret effects on MHD non-Darcian convective flow past a stretching sheet in a micropolar fluid with radiation." International Journal of Heat and Mass Transfer 93 (2016): 674-682.

[11] Fang, Tiegang, Ji Zhang, and Yongfang Zhong. "Boundary layer flow over a stretching sheet with variable thickness." Applied Mathematics and Computation 218, no. 13 (2012): 7241-7252.

[12] Reddy, Srinivas, Kishan Naikoti, and Mohammad Mehdi Rashidi. "MHD flow and heat transfer characteristics of Williamson nanofluid over a stretching sheet with variable thickness and variable thermal conductivity." Transactions of A. Razmadze Mathematical Institute 171, no. 2 (2017): 195-211.

[13] Mukhopadhyay, Swati. "Slip effects on MHD boundary layer flow over an exponentially stretching sheet with suction/blowing and thermal radiation." Ain Shams Engineering Journal 4, no. 3 (2013): 485-491.

[14] Mabood, Fazle, W. A. Khan, and AI Md Ismail. "MHD boundary layer flow and heat transfer of nanofluids over a nonlinear stretching sheet: a numerical study." Journal of Magnetism and Magnetic Materials 374 (2015): 569-576.

[15] Reddy, Y. Dharmendar, V. Srinivasa Rao, and L. Anand Babu. "MHD boundary layer flow of nanofluid and heat transfer over a porous exponentially stretching sheet in presence of thermal radiation and chemical reaction with suction." International Journal of Mathematics Trends and Technology 47, no. 2 (2017): 87-100.

[16] Raju, C. S. K., N. Sandeep, V. Sugunamma, M. Jayachandra Babu, and JV Ramana Reddy. "Heat and mass transfer in magnetohydrodynamic Casson fluid over an exponentially permeable stretching surface." Engineering Science and Technology, an International Journal 19, no. 1 (2016): 45-52.

[17] Ibrahim, Wubshet, and Rizwan Ul Haq. "Magnetohydrodynamic (MHD) stagnation point flow of nanofluid past a stretching sheet with convective boundary condition." Journal of the Brazilian Society of Mechanical Sciences and Engineering 38, no. 4 (2016): 1155-1164.

[18] Akbar, Noreen Sher, S. Nadeem, R. Ul Haq, and Z. H. Khan. "Numerical solutions of Magnetohydrodynamic boundary layer flow of tangent hyperbolic fluid towards a stretching sheet." Indian journal of Physics 87, no. 11 (2013): 1121-1124.

[19] Mukhopadhyay, S., G. C. Layek, and Sk A. Samad. "Study of MHD boundary layer flow over a heated stretching sheet with variable viscosity." International journal of heat and mass transfer 48, no. 21-22 (2005): 4460-4466.

[20] Nadeem, Sohail, Rizwan Ul Haq, Noreen Sher Akbar, and Zafar Hayat Khan. "MHD three-dimensional Casson fluid flow past a porous linearly stretching sheet." Alexandria Engineering Journal 52, no. 4 (2013): 577-582.

[21] Zhang, Chaoli, Liancun Zheng, Xinxin Zhang, and Goong Chen. "MHD flow and radiation heat transfer of nanofluids in porous media with variable surface heat flux and chemical reaction." Applied Mathematical Modelling 39, no. 1 (2015): 165-181.

[22] Sheikholeslami, Mohsen, Mofid Gorji Bandpy, R. Ellahi, and Ahmad Zeeshan. "Simulation of MHD CuO-water nanofluid flow and convective heat transfer considering Lorentz forces." Journal of Magnetism and Magnetic Materials 369 (2014): 69-80.

[23] Patel, Harshad R. "Effects of heat generation, thermal radiation, and hall current on MHD Casson fluid flow past an oscillating plate in porous medium." Multiphase Science and Technology 31, no. 1 (2019).

[24] Farooq, Umer, Dianchen Lu, Shahzad Munir, Muhammad Ramzan, Muhammad Suleman, and Shahid Hussain. "MHD flow of Maxwell fluid with nanomaterials due to an exponentially stretching surface." Scientific reports 9, no. 1 (2019): 1-11.

[25] Ibrahim, Wubshet, and Ayele Tulu. "Magnetohydrodynamic (MHD) boundary layer flow past a wedge with heat transfer and viscous effects of nanofluid embedded in porous media." Mathematical Problems in Engineering 2019 (2019).

[26] Ali, Aamir, Kiran Shehzadi, M. Sulaiman, and Saleem Asghar. "Heat and mass transfer analysis of 3D Maxwell nanofluid over an exponentially stretching surface." Physica Scripta 94, no. 6 (2019): 065206.

[27] Raptis, Andreas, Christos Perdikis, and Harmindar S. Takhar. "Effect of thermal radiation on MHD flow." Applied Mathematics and computation 153, no. 3 (2004): 645-649.

[28] Devi, RLV Renuka, T. Poornima, N. Bhaskar Reddy, and S. Venkataramana. "Radiation and mass transfer effects on MHD boundary layer flow due to an exponentially stretching sheet with heat source." International Journal of Engineering and Innovative Technology 3, no. 8 (2014): 33-39.

[29] Mukhopadhyay, Swati. "Slip effects on MHD boundary layer flow over an exponentially stretching sheet with suction/blowing and thermal radiation." Ain Shams Engineering Journal 4, no. 3 (2013): 485-491.

[30] Ishak, Anuar. "MHD boundary layer flow due to an exponentially stretching sheet with radiation effect." Sains Malaysiana 40, no. 4 (2011): 391-395.

[31] Mabood, Fazle, W. A. Khan, and AI Md Ismail. "MHD flow over exponential radiating stretching sheet using homotopy analysis method." Journal of King Saud University-Engineering Sciences 29, no. 1 (2017): 68-74.

[32] Bidin, Biliana, and Roslinda Nazar. "Numerical solution of the boundary layer flow over an exponentially stretching sheet with thermal radiation." European journal of scientific research 33, no. 4 (2009): 710-717.

[33] Poornima, T., and N. Bhaskar Reddy. "Radiation effects on MHD free convective boundary layer flow of nanofluids over a nonlinear stretching sheet." Advances in Applied Science Research 4, no. 2 (2013): 190-202.

[34] Khalili, Noran Nur Wahida, Abdul Aziz Samson, Ahmad Sukri Abdul Aziz, and Zaileha Md Ali. "Chemical reaction and radiation effects on MHD flow past an exponentially stretching sheet with heat sink." In Journal of Physics: Conference Series, vol. 890, no. 1, p. 012025. IOP Publishing, 2017.

[35] Izadi, Mohsen, Mikhail A. Sheremet, S. A. M. Mehryan, Ioan Pop, Hakan F. Öztop, and Nidal Abu-Hamdeh. "MHD thermogravitational convection and thermal radiation of a micropolar nanoliquid in a porous chamber." International Communications in Heat and Mass Transfer 110 (2020): 104409.

[36] Daniel, Yahaya Shagaiya, Zainal Abdul Aziz, Zuhaila Ismail, and Faisal Salah. "Entropy analysis in electrical magnetohydrodynamic (MHD) flow of nanofluid with effects of thermal radiation, viscous dissipation, and chemical reaction." Theoretical and Applied Mechanics Letters 7, no. 4 (2017): 235-242.

[37] Muhammad, Taseer, Hassan Waqas, Shan Ali Khan, R. Ellahi, and Sadiq M. Sait. "Significance of nonlinear thermal radiation in 3D Eyring-Powell nanofluid flow with Arrhenius activation energy." Journal of Thermal Analysis and Calorimetry 143, no. 2 (2021): 929-944.

[38] Sohail, M., R. Naz, and Sara I. Abdelsalam. "On the onset of entropy generation for a nanofluid with thermal radiation and gyrotactic microorganisms through 3D flows." Physica Scripta 95, no. 4 (2020): 045206.

[39] Gireesha, B. J., G. Sowmya, M. Ijaz Khan, and Hakan F. Öztop. "Flow of hybrid nanofluid across a permeable longitudinal moving fin along with thermal radiation and natural convection." Computer methods and programs in biomedicine 185 (2020): 105166.

[40] Choi, S. US, and Jeffrey A. Eastman. Enhancing thermal conductivity of fluids with nanoparticles. No. ANL/MSD/CP-84938; CONF-951135-29. Argonne National Lab., IL (United States), 1995.

[41] Nield, D. A., and A. V. Kuznetsov. "The Cheng-Minkowycz problem for natural convective boundary-layer flow in a porous medium saturated by a nanofluid." International Journal of Heat and Mass Transfer 52, no. 25-26 (2009): 5792-5795.

[42] Khan, W. A., O. D. Makinde, and Z. H. Khan. "Non-aligned MHD stagnation point flow of variable viscosity nanofluids past a stretching sheet with radiative heat." International Journal of Heat and Mass Transfer 96 (2016): 525-534.

[43] Bachok, Norfifah, Anuar Ishak, and Ioan Pop. "Boundary layer stagnation-point flow and heat transfer over an exponentially stretching/shrinking sheet in a nanofluid." International Journal of Heat and Mass Transfer 55, no. 25-26 (2012): 8122-8128.

[44] Abu-Nada, Eiyad, Ziyad Masoud, Hakan F. Oztop, and Antonio Campo. "Effect of nanofluid variable properties on natural convection in enclosures." International Journal of Thermal Sciences 49, no. 3 (2010): 479-491.

[45] Malik, M. Y., M. Naseer, S. Nadeem, and Abdul Rehman. "The boundary layer flow of Casson nanofluid over a vertical exponentially stretching cylinder." Applied Nanoscience 4, no. 7 (2014): 869-873.

[46] Eid, Mohamed R. "Chemical reaction effect on MHD boundary-layer flow of two-phase nanofluid model over an exponentially stretching sheet with a heat generation." Journal of Molecular Liquids 220 (2016): 718-725.

[47] Gangaiah, T., N. Saidulu, and A. Venkata Lakshmi. "Magnetohydrodynamic flow of nanofluid over an exponentially stretching sheet in presence of viscous dissipation and chemical reaction." Journal of Nanofluids 7, no. 3 (2018): 439-448.

[48] Abel, M. Subhas, Mahantesh M. Nandeppanavar, and Veena Basanagouda. "Effects of Variable Viscosity, Buoyancy and Variable Thermal Conductivity on Mixed Convection Heat Transfer Due to an Exponentially Stretching Surface with Magnetic Field." Proceedings of the National Academy of Sciences, India Section A: Physical Sciences 87, no. 2 (2017): 247-256.

[49] Yousif, Majeed Ahmad, Hajar Farhan Ismael, Tehseen Abbas, and Rahmat Ellahi. "Numerical study of momentum and heat transfer of MHD Carreau nanofluid over an exponentially stretched plate with internal heat source/sink and radiation." Heat Transfer Research 50, no. 7 (2019).

[50] Ellahi, Rahmat, Ahmed Zeeshan, Farooq Hussain, and Tehseen Abbas. "Thermally charged MHD bi-phase flow coatings with non-Newtonian nanofluid and hafnium particles along slippery walls." Coatings 9, no. 5 (2019): 300.

[51] Ahmed, Zahid, Sohail Nadeem, Salman Saleem, and Rahmat Ellahi. "Numerical study of unsteady flow and heat transfer CNT-based MHD nanofluid with variable viscosity over a permeable shrinking surface." International Journal of Numerical Methods for Heat and Fluid Flow (2019).

[52] Nguyen-Thoi, Trung, M. M. Bhatti, Jagar A. Ali, Samir Mustafa Hamad, M. Sheikholeslami, Ahmad Shafee, and Rizwan-ul Haq. "Analysis on the heat storage unit through a Y-shaped fin for solidification of NEPCM." Journal of Molecular Liquids 292 (2019): 111378.

[53] Hayat, T., M. Bilal Ashraf, A. Alsaedi, and M. S. Alhothuali. "Soret and Dufour effects in three-dimensional flow of Maxwell fluid with chemical reaction and convective condition." International Journal of Numerical Methods for Heat and Fluid Flow (2015).

[54] Ramzan, M., Saba Inam, and S. A. Shehzad. "Three dimensional boundary layer flow of a viscoelastic nanofluid with Soret and Dufour effects." Alexandria Engineering Journal 55, no. 1 (2016): 311-319.

[55] Sravanthi, C. S. "Homotopy analysis solution of MHD slip flow past an exponentially stretching inclined sheet with Soret-Dufour effects." Journal of the Nigerian Mathematical Society 35, no. 1 (2016): 208-226.

[56] Zaidi, Syed Zulfiqar Ali, and Syed Tauseef Mohyud-Din. "Analysis of wall jet flow for Soret, Dufour and chemical reaction effects in the presence of MHD with uniform suction/injection." Applied Thermal Engineering 103 (2016): 971-979.

[57] Jain, Shalini, and Rakesh Choudhary. "Thermophoretic MHD flow and non-linear radiative heat transfer with convective boundary conditions over a non-linearly stretching sheet." arXiv preprint arXiv:1702.02039 (2017).

[58] Muhaimin, Ismoen, Ramasamy Kandasamy, Azme B. Khamis, and Rozaini Roslan. "Effect of thermophoresis particle deposition and chemical reaction on unsteady MHD mixed

convective flow over a porous wedge in the presence of temperature-dependent viscosity." Nuclear Engineering and Design 261 (2013): 95-106.

[59] Makinde, O. D., W. A. Khan, and Z. H. Khan. "Stagnation point flow of MHD chemically reacting nanofluid over a stretching convective surface with slip and radiative heat." Proceedings of the Institution of Mechanical Engineers, Part E: Journal of Process Mechanical Engineering 231, no. 4 (2017): 695-703.

[60] Rehman, Khalil Ur, Abid Ali Khan, M. Y. Malik, and O. D. Makinde. "Thermophysical aspects of stagnation point magnetonanofluid flow yields by an inclined stretching cylindrical surface: a non-Newtonian fluid model." Journal of the Brazilian Society of Mechanical Sciences and Engineering 39, no. 9 (2017): 3669-3682.

[61] Khan, W. A., O. D. Makinde, and Z. H. Khan. "Non-aligned MHD stagnation point flow of variable viscosity nanofluids past a stretching sheet with radiative heat." International Journal of Heat and Mass Transfer 96 (2016): 525-534.

[62] Ibrahim, Wubshet, and O. D. Makinde. "Magnetohydrodynamic stagnation point flow and heat transfer of Casson nanofluid past a stretching sheet with slip and convective boundary condition." Journal of Aerospace Engineering 29, no. 2 (2016): 04015037.

[63] Ibrahim, Wubshet, and O. D. Makinde. "Magnetohydrodynamic stagnation point flow of a power-law nanofluid towards a convectively heated stretching sheet with slip." Proceedings of the Institution of Mechanical Engineers, Part E: Journal of Process Mechanical Engineering 230, no. 5 (2016): 345-354.

[64] Bhatti, M. M., Rahmat Ellahi, A. Zeeshan, M. Marin, and N. Ijaz. "Numerical study of heat transfer and Hall current impact on peristaltic propulsion of particle-fluid suspension with compliant wall properties." Modern Physics Letters B 33, no. 35 (2019): 1950439.

[65] Nguyen-Thoi, Trung, M. M. Bhatti, Jagar A. Ali, Samir Mustafa Hamad, M. Sheikholeslami, Ahmad Shafee, and Rizwan-ul Haq. "Analysis on the heat storage unit through a Y-shaped fin for solidification of NEPCM." Journal of Molecular Liquids 292 (2019): 111378.

[66] Tlili, Iskander, M. M. Bhatti, Samir Mustafa Hamad, Azeez A. Barzinjy, M. Sheikholeslami, and Ahmad Shafee. "Macroscopic modeling for convection of Hybrid nanofluid with magnetic effects." Physica A: Statistical Mechanics and its Applications 534 (2019): 122136.

[67] Bhatti, M. M., Majeed A. Yousif, S. R. Mishra, and A. Shahid. "Simultaneous influence of thermo-diffusion and diffusion-thermo on non-Newtonian hyperbolic tangent magnetised nanofluid with Hall current through a nonlinear stretching surface." Pramana 93, no. 6 (2019): 1-10.

[68] Sheikholeslami, M. "New computational approach for exergy and entropy analysis of nanofluid under the impact of Lorentz force through a porous media." Computer Methods in Applied Mechanics and Engineering 344 (2019): 319-333.

[69] Sheikholeslami, M., Behnoush Rezaeianjouybari, Milad Darzi, Ahmad Shafee, Zhixiong Li, and Truong Khang Nguyen. "Application of nano-refrigerant for boiling heat transfer enhancement employing an experimental study." International Journal of Heat and Mass Transfer 141 (2019): 974-980.

[70] Sheikholeslami, M. "Numerical approach for MHD Al2O3-water nanofluid transportation inside a permeable medium using innovative computer method." Computer Methods in Applied Mechanics and Engineering 344 (2019): 306-318.

[71] Xue, Qing-Zhong. "Model for effective thermal conductivity of nanofluids." Physics letters A 307, no. 5-6 (2003): 313-317.

[72] Yu, W., and S. U. S. Choi. "The role of interfacial layers in the enhanced thermal conductivity of nanofluids: a renovated Maxwell model." Journal of Nanoparticle Research 5, no. 1 (2003): 167-171.

[73] Yu, W., and S. U. S. Choi. "The role of interfacial layers in the enhanced thermal conductivity of nanofluids: a renovated Hamilton-Crosser model." Journal of Nanoparticle Research 6, no. 4 (2004): 355-361.

[74] https://tfaws.nasa.gov/TFAWS10/Proceedings/Interdisciplinary/Debjyoti%20Banerjee.pdf

[75] Wang, Xiang-Qi, and Arun S. Mujumdar. "Heat transfer characteristics of nanofluids: a review." International Journal of Thermal Sciences 46, no. 1 (2007): 1-19.

[76] Pedley, T. J., N. A. Hill, and John O. Kessler. "The growth of bioconvection patterns in a uniform suspension of gyrotactic micro-organisms." Journal of Fluid Mechanics 195 (1988): 223-237.

[77] Khan, W. A., and O. D. Makinde. "MHD nanofluid bioconvection due to gyrotactic microorganisms over a convectively heat stretching sheet." International Journal of Thermal Sciences 81 (2014): 118-124.

[78] Kuznetsov, A. V., A. A. Avramenko, and P. Geng. "Analytical investigation of a falling plume caused by bioconvection of oxytactic bacteria in a fluid saturated porous medium." International Journal of Engineering Science 42, no. 5-6 (2004): 557-569.

[79] Mutuku, Winifred Nduku, and Oluwole Daniel Makinde. "Hydromagnetic bioconvection of nanofluid over a permeable vertical plate due to gyrotactic microorganisms." Computers and Fluids 95 (2014): 88-97.

[80] Naganthran, Kohilavani, Md Faisal Md Basir, Sayer Obaid Alharbi, Roslinda Nazar, Anas M. Alwatban, and Iskander Tlili. "Stagnation point flow with time-dependent bio-nanofluid past a sheet: Richardson extrapolation technique." Processes 7, no. 10 (2019): 722.

[81] Zaimi, Khairy, Anuar Ishak, and Ioan Pop. "Stagnation-point flow toward a stretching/shrinking sheet in a nanofluid containing both nanoparticles and gyrotactic microorganisms." Journal of heat transfer 136, no. 4 (2014).

[82] Ali, F., and A. Zaib. "Unsteady flow of an Eyring-Powell nanofluid near stagnation point past a convectively heated stretching sheet." Arab Journal of Basic and Applied Sciences 26, no. 1 (2019): 215-224.

[83] Zeng, L., and T. J. Pedley. "Distribution of gyrotactic micro-organisms in complex three-dimensional flows. Part 1. Horizontal shear flow past a vertical circular cylinder." Journal of Fluid Mechanics 852 (2018): 358-397.

[84] Shah, Nehad Ali, Asiful H. Seikh, Iskander Tlili, Khadim Shah, Rana Muhammad Shabbir, Mohammad Rahimi-Gorji, and Nabeel Alharthi. "Natural convection of bio-nanofluid between two vertical parallel plates with damped shear and thermal flux." Journal of Molecular Liquids 296 (2019): 111575.

[85] Amirsom, Nur Ardiana, Md Uddin, Md Faisal Md Basir, Ali Kadir, and O. Anwar Bég. "Computation of melting dissipative magnetohydrodynamic nanofluid bioconvection with second-order slip and variable thermophysical properties." Applied Sciences 9, no. 12 (2019): 2493.

[86] Khdher, Abdolbaqi Mohammed, Nor Azwadi Che Sidik, Wan Azmi Wan Hamzah, and Rizalman Mamat. "An experimental determination of thermal conductivity and electrical conductivity of bio glycol based Al2O3 nanofluids and development of new correlation." International Communications in Heat and Mass Transfer 73 (2016): 75-83.

[87] Zhang, Lijun, Muhammad Mubashir Bhatti, Rahmat Ellahi, and Efstathios E. Michaelides. "Oxytactic microorganisms and thermo-bioconvection nanofluid flow over a porous Riga plate with Darcy-Brinkman-Forchheimer medium." Journal of Non-Equilibrium Thermodynamics 45, no. 3 (2020): 257-268.

[88] Atif, S. M., S. Hussain, and M. Sagheer. "Magnetohydrodynamic stratified bioconvective flow of micropolar nanofluid due to gyrotactic microorganisms." AIP Advances 9, no. 2 (2019): 025208.

[89] Zhang, Tianping, Sami Ullah Khan, Muhammad Imran, Iskander Tlili, Hassan Waqas, and Nasir Ali. "Activation energy and thermal radiation aspects in bioconvection flow of rate-type nanoparticles configured by a stretching/shrinking disk." Journal of Energy Resources Technology 142, no. 11 (2020).

[90] Li, Yurong, Hassan Waqas, Muhammad Imran, Umar Farooq, Fouad Mallawi, and Iskander Tlili. "A numerical exploration of modified second-grade nanofluid with motile microorganisms, thermal radiation, and Wu's slip." Symmetry 12, no. 3 (2020): 393.

[91] Alwatban, Anas M., Sami Ullah Khan, Hassan Waqas, and Iskander Tlili. "Interaction of Wu's slip features in bioconvection of Eyring Powell nanoparticles with activation energy." Processes 7, no. 11 (2019): 859.

[92] Wang, Ying, Hassan Waqas, Madeeha Tahir, Muhammad Imran, and Chahn Yong Jung. "Effective Prandtl aspects on bio-convective thermally developed magnetized tangent hyperbolic nanoliquid with gyrotactic microorganisms and second order velocity slip." IEEE Access 7 (2019): 130008-130023.

[93] Ibrahim, Wubshet, Bandari Shankar, and Mahantesh M. Nandeppanavar. "MHD stagnation point flow and heat transfer due to nanofluid towards a stretching sheet." International journal of heat and mass transfer 56, no. 1-2 (2013): 1-9.

[94] Naganthran, Kohilavani, Md Faisal Md Basir, Sayer Obaid Alharbi, Roslinda Nazar, Anas M. Alwatban, and Iskander Tlili. "Stagnation point flow with time-dependent bionanofluid past a sheet: Richardson extrapolation technique." Processes 7, no. 10 (2019): 722.

[95] Shampine, Lawrence F., Jacek Kierzenka, and Mark W. Reichelt. "Solving boundary value problems for ordinary differential equations in MATLAB with bvp4c." Tutorial notes 2000 (2000): 1-27.

[96] Buongiorno, Jacopo. "Convective transport in nanofluids." (2006): 240-250.

[97] Hayat, T., S. A. Shehzad, M. Qasim, and A. Alsaedi. "Mixed convection flow by a porous sheet with variable thermal conductivity and convective boundary condition." Brazilian Journal of Chemical Engineering 31, no. 1 (2014): 109-117.

[98] Reddy, N. Bhaskar, T. Poornima, and P. Sreenivasulu. "Influence of variable thermal conductivity on MHD boundary layer slip flow of ethylene-glycol based Cu nanofluids over a stretching sheet with convective boundary condition." International Journal of Engineering Mathematics 10 (2014): 1-10.

[99] Na, Tsung Yen, ed. Computational methods in engineering boundary value problems. Academic press, 1980.

[100] Thomas, Llewellyn. "Elliptic problems in linear differential equations over a network: Watson scientific computing laboratory." Columbia Univ., NY (1949).

[101] White, F.M. Fluid mechanics . McGraw-Hill, New York, NY., 10020, 366-76 (2003).

[102] Irfan, Muhammad, Muhammad Asif Farooq, and Tousif Iqra. "A new computational technique design for EMHD nanofluid flow over a variable thickness surface with variable liquid characteristics." Frontiers in Physics 8 (2020): 66.

[103] Na, Tsung Yen, ed. Computational methods in engineering boundary value problems. Academic press, 1980.

[104] Thomas, Llewellyn Hilleth. "Elliptic problems in linear difference equations over a network." Watson Sci. Comput. Lab. Rept., Columbia University, New York 1 (1949).

[105] Kierzenka, Jacek, and Lawrence F. Shampine. "A BVP solver based on residual control and the Maltab PSE." ACM Transactions on Mathematical Software (TOMS) 27, no. 3 (2001): 299-316.

[106] Kierzenka, Jacek, and Lawrence F. Shampine. "A BVP solver that controls residual and error." JNAIAM J. Numer. Anal. Ind. Appl. Math 3, no. 1-2 (2008): 27-41.

[107] Amirsom, Nur Ardiana, Md Uddin, Md Faisal Md Basir, Ali Kadir, and O. Anwar Bég. "Computation of melting dissipative magnetohydrodynamic nanofluid bioconvection with second-order slip and variable thermophysical properties." Applied Sciences 9, no. 12 (2019): 2493.

[108] Hayat, T., Q. Hussain, and T. Javed. "The modified decomposition method and Padé approximants for the MHD flow over a non-linear stretching sheet." Nonlinear Analysis: Real World Applications 10, no. 2 (2009): 966-973.

[109] Mabood, Fazle, and Antonio Mastroberardino. "Melting heat transfer on MHD convective flow of a nanofluid over a stretching sheet with viscous dissipation and second order slip." Journal of the Taiwan Institute of Chemical Engineers 57 (2015): 62-68.

[110] Andersson, Helge I. "Slip flow past a stretching surface." Acta Mechanica 158, no. 1 (2002): 121-125.

[111] Hamad, M. A. A., Md J. Uddin, and AI Md Ismail. "Investigation of combined heat and mass transfer by Lie group analysis with variable diffusivity taking into account hydrodynamic slip and thermal convective boundary conditions." International Journal of Heat and Mass Transfer 55, no. 4 (2012): 1355-1362.

[112] Andersson, Helge I., and Jan B. Aarseth. "Sakiadis flow with variable fluid properties revisited." International Journal of Engineering Science 45, no. 2-8 (2007): 554-561.

[113] Mohammed Ibrahim, S., and K. Suneetha. "Effects of heat generation and thermal radiation on steady MHD flow near a stagnation point on a linear stretching sheet in porous medium and presence of variable thermal conductivity and mass transfer." Journal of Computational and Applied Research in Mechanical Engineering (JCARME) 4, no. 2 (2015): 133-144.

[114] Makinde, O. D., Fazle Mabood, W. A. Khan, and M. S. Tshehla. "MHD flow of a variable viscosity nanofluid over a radially stretching convective surface with radiative heat." Journal of Molecular Liquids 219 (2016): 624-630.

[115] Elbashbeshy, E. M. A., and M. A. A. Bazid. "The effect of temperature-dependent viscosity on heat transfer over a continuous moving surface." Journal of Physics D: Applied Physics 33, no. 21 (2000): 2716.

[116] Poply, Vikas, Phool Singh, and A. K. Yadav. "A study of temperature-dependent fluid properties on MHD free stream flow and heat transfer over a non-linearly stretching sheet." Procedia Engineering 127 (2015): 391-397.

[117] Prasad, K. V., K. Vajravelu, and P. S. Datti. "The effects of variable fluid properties on the hydro-magnetic flow and heat transfer over a non-linearly stretching sheet." International Journal of Thermal Sciences 49, no. 3 (2010): 603-610.

[118] Sharif, Razia, M. Asif Farooq, and Asif Mushtaq. "Magnetohydrodynamic study of variable fluid properties and their impact on nanofluid over an exponentially stretching sheet." Journal of Nanofluids 8, no. 6 (2019): 1249-1259.

[119] Murugesan, Thiagarajan, and M. Dinesh Kumar. "Effects of thermal radiation and heat generation on hydromagnetic flow of nanofluid over an exponentially stretching sheet in

a porous medium with viscous dissipation." World Scientific News 128, no. 2 (2019): 130-147.

[120] Reddy, M. Gnaneswara. "Effects of Thermophoresis, Viscous Dissipation and Joule Heating on Steady MHD Flow over an Inclined Radiative Isothermal Permeable Surface with Variable Thermal Conductivity." Journal of Applied Fluid Mechanics 7, no. 1 (2014).

[121] Swain, K., S. K. Parida, and G. C. Dash. "MHD heat and mass transfer on stretching sheet with variable fluid properties in porous medium." AMSE Journals, Modelling B 86, no. 3 (2017): 706-726.

[122] Ali, Liaqat, Saeed Islam, Taza Gul, Ali Saleh Alshomrani, Ilyas Khan, and Aurangzeb Khan. "Magnetohydrodynamics thin film fluid flow under the effect of thermophoresis and variable fluid properties." AIChE Journal 63, no. 11 (2017): 5149-5158.

[123] Irfan, M. "Study of Brownian motion and thermophoretic diffusion on non-linear mixed convection flow of Carreau nanofluid subject to variable properties." Surfaces and Interfaces 23 (2021): 100926.

[124] Ogunseye, Hammed Abiodun, Sulyman Olakunle Salawu, Yusuf Olatunji Tijani, Mustapha Riliwan, and Precious Sibanda. "Dynamical analysis of hydromagnetic Brownian and thermophoresis effects of squeezing Eyring-Powell nanofluid flow with variable thermal conductivity and chemical reaction." Multidiscipline Modeling in Materials and Structures (2019).

[125] Khan, Waris, Muhammad Idress, Taza Gul, Muhammad Altaf Khan, and Ebenezer Bonyah. "Three non-Newtonian fluids flow considering thin film over an unsteady stretching surface with variable fluid properties." Advances in Mechanical Engineering 10, no. 10 (2018): 1-17.

[126] Khan, Noor Saeed, Taza Gul, Saeed Islam, and Waris Khan. "Thermophoresis and thermal radiation with heat and mass transfer in a magnetohydrodynamic thin-film second-grade fluid of variable properties past a stretching sheet." The European Physical Journal Plus 132, no. 1 (2017): 1-20.

[127] Hayat, T., M. Farooq, A. Alsaedi, and Falleh Al-Solamy. "Impact of Cattaneo-Christov heat flux in the flow over a stretching sheet with variable thickness." AIP Advances 5, no. 8 (2015): 087159.

[128] Hayat, T., M. Ijaz Khan, M. Farooq, A. Alsaedi, M. Waqas, and Tabassam Yasmeen. "Impact of CattaneoŬChristov heat flux model in flow of variable thermal conductivity fluid over a variable thicked surface." International Journal of Heat and Mass Transfer 99 (2016): 702-710.

[129] Khader, M. M., and Ahmed M. Megahed. "Numerical solution for boundary layer flow due to a nonlinearly stretching sheet with variable thickness and slip velocity." The European Physical Journal Plus 128, no. 9 (2013): 1-7.

[130] Daniel, Yahaya Shagaiya, Zainal Abdul Aziz, Zuhaila Ismail, and Faisal Salah. "Thermal stratification effects on MHD radiative flow of nanofluid over nonlinear stretching sheet with variable thickness." Journal of Computational Design and Engineering 5, no. 2 (2018): 232-242.

[131] Daniel, Yahaya Shagaiya, Zainal Abdul Aziz, Zuhaila Ismail, and Faisal Salah. "Impact of thermal radiation on electrical MHD flow of nanofluid over nonlinear stretching sheet with variable thickness." Alexandria Engineering Journal 57, no. 3 (2018): 2187-2197.

[132] Seth, G. S., and P. K. Mandal. "Analysis of electromagnetohydrodynamic stagnation point flow of nanofluid over a nonlinear stretching sheet with variable thickness." Journal of Mechanics 35, no. 5 (2019): 719-733.

[133] Qayyum, Sajid, Tasawar Hayat, and Ahmed Alsaedi. "Chemical reaction and heat generation/absorption aspects in MHD nonlinear convective flow of third grade nanofluid over a nonlinear stretching sheet with variable thickness." Results in Physics 7 (2017): 2752-2761.

[134] Hayat, T., M. Farooq, A. Alsaedi, and Z. Iqbal. "Melting heat transfer in the stagnation point flow of PowellŬEyring fluid." Journal of Thermophysics and Heat Transfer 27, no. 4 (2013): 761-766.

[135] Jalil, Mudassar, and Saleem Asghar. "Flow and heat transfer of powell-eyring fluid over a stretching surface: A lie group analysis." Journal of Fluids Engineering 135, no. 12 (2013).

[136] Mushtaq, Ammar, Meraj Mustafa, Tasawar Hayat, Mahmood Rahi, and Ahmed Alsaedi. "Exponentially stretching sheet in a Powell-Eyring fluid: numerical and series solutions." Zeitschrift für Naturforschung A 68, no. 12 (2013): 791-798.

[137] Javed, Tariq, Nasir Ali, Zaheer Abbas, and Muhammad Sajid. "Flow of an Eyring-Powell non-Newtonian fluid over a stretching sheet." Chemical Engineering Communications 200, no. 3 (2013): 327-336.

[138] Mustafa, M., M. Nawaz, T. Hayat, and A. Alsaedi. "MHD boundary layer flow of second-grade nanofluid over a stretching sheet with convective boundary conditions." Journal of Aerospace Engineering 27, no. 4 (2014): 04014006.

[139] Motsumi, T. G., and O. D. Makinde. "Effects of thermal radiation and viscous dissipation on boundary layer flow of nanofluids over a permeable moving flat plate." Physica Scripta 86, no. 4 (2012): 045003.

[140] Hayat, T., Ikram Ullah, A. Alsaedi, and M. Farooq. "MHD flow of Powell-Eyring nanofluid over a non-linear stretching sheet with variable thickness." Results in Physics 7 (2017): 189-196.

[141] Raees, Ammarah, Hang Xu, and Shi-Jun Liao. "Unsteady mixed nano-bioconvection flow in a horizontal channel with its upper plate expanding or contracting." International Journal of Heat and Mass Transfer 86 (2015): 174-182.

[142] Uddin, M. J., W. A. Khan, S. R. Qureshi, and O. Anwar Bég. "Bioconvection nanofluid slip flow past a wavy surface with applications in nano-biofuel cells." Chinese Journal of Physics 55, no. 5 (2017): 2048-2063.

[143] Uddin, Md Jashim, M. N. Kabir, and O. Anwar Bég. "Computational investigation of Stefan blowing and multiple-slip effects on buoyancy-driven bioconvection nanofluid flow with microorganisms." International Journal of Heat and Mass Transfer 95 (2016): 116-130.

[144] RamReddy, Ch, and P. Naveen. "Analysis of activation energy and thermal radiation on convective flow of a power-law fluid under convective heating and chemical reaction." Heat TransferŮAsian Research 48, no. 6 (2019): 2122-2154.

[145] Aziz, A., W. A. Khan, and I. Pop. "Free convection boundary layer flow past a horizontal flat plate embedded in porous medium filled by nanofluid containing gyrotactic microorganisms." International Journal of Thermal Sciences 56 (2012): 48-57.

[146] Mutuku, Winifred Nduku, and Oluwole Daniel Makinde. "Hydromagnetic bioconvection of nanofluid over a permeable vertical plate due to gyrotactic microorganisms." Computers and Fluids 95 (2014): 88-97.

[147] Sk, Md Tausif, Kalidas Das, and Prabir Kumar Kundu. "Multiple slip effects on bioconvection of nanofluid flow containing gyrotactic microorganisms and nanoparticles." Journal of Molecular Liquids 220 (2016): 518-526.

[148] Ali, Aamir, S. Saleem, Sana Mumraiz, Anber Saleem, M. Awais, and DN Khan Marwat. "Investigation on TiO 2-Cu/H 2 O hybrid nanofluid with slip conditions in MHD peristaltic flow of Jeffrey material." Journal of Thermal Analysis and Calorimetry 143, no. 3 (2021): 1985-1996.

[149] Mburu, Zachariah Mbugua, Sabyasachi Mondal, and Precious Sibanda. "Numerical study on combined thermal radiation and magnetic field effects on entropy generation in unsteady fluid flow past an inclined cylinder." Journal of Computational Design and Engineering 8, no. 1 (2021): 149-169.

[150] Das, K. "Impact of thermal radiation on MHD slip flow over a flat plate with variable fluid properties." Heat and Mass Transfer 48, no. 5 (2012): 767-778.

[151] Anwar, Talha, Poom Kumam, Dumitru Baleanu, Ilyas Khan, and Phatiphat Thounthong. "Radiative heat transfer enhancement in MHD porous channel flow of an Oldroyd-B fluid under generalized boundary conditions." Physica Scripta 95, no. 11 (2020): 115211.

[152] Fatunmbi, E. O., and A. Adeniyan. "Nonlinear thermal radiation and entropy generation on steady flow of magneto-micropolar fluid passing a stretchable sheet with variable properties." Results in Engineering 6 (2020): 100142.

[153] Dandapat, B. S., B. Santra, and K. Vajravelu. "The effects of variable fluid properties and thermocapillarity on the flow of a thin film on an unsteady stretching sheet." International Journal of Heat and Mass Transfer 50, no. 5-6 (2007): 991-996.

[154] Vajravelu, K., K. V. Prasad, and Chiu-On Ng. "Unsteady convective boundary layer flow of a viscous fluid at a vertical surface with variable fluid properties." Nonlinear Analysis: Real World Applications 14, no. 1 (2013): 455-464.

[155] Shahsavar, Amin, Ali Godini, Pouyan Talebizadeh Sardari, Davood Toghraie, and Hamzeh Salehipour. "Impact of variable fluid properties on forced convection of Fe 3 O 4/CNT/water hybrid nanofluid in a double-pipe mini-channel heat exchanger." Journal of Thermal Analysis and Calorimetry 137, no. 3 (2019): 1031-1043.

[156] Naganthran, Kohilavani, Meraj Mustafa, Ammar Mushtaq, and Roslinda Nazar. "Dual solutions for fluid flow over a stretching/shrinking rotating disk subject to variable fluid properties." Physica A: Statistical Mechanics and its Applications 556 (2020): 124773.

[157] Salahuddin, T., Maryam Arshad, Nazim Siddique, and I. Tlili. "Change in internal energy of viscoelastic fluid flow between two rotating parallel plates having variable fluid properties." Indian Journal of Physics (2020): 1-11.

[158] Hayat, T., Tehseen Abbas, M. Ayub, M. Farooq, and A. Alsaedi. "Flow of nanofluid due to convectively heated Riga plate with variable thickness." Journal of Molecular Liquids 222 (2016): 854-862.

[159] Mjankwi, Musa Antidius, Verdiana Grace Masanja, Eunice W. Mureithi, and Makungu NgŠoga James. "Unsteady MHD flow of nanofluid with variable properties over a stretching sheet in the presence of thermal radiation and chemical reaction." International Journal of Mathematics and Mathematical Sciences 2019 (2019).

[160] Rao, Jakkula Anand, Gandamalla Vasumathi, and Jakkula Mounica. "Joule heating and thermal radiation effects on MHD boundary layer flow of a nanofluid over an exponentially stretching sheet in a porous medium." World Journal of Mechanics 5, no. 09 (2015): 151.